# Diiminopyridine Complexes of Ti, Zr and Hf

By Naser Rahimi

A thesis submitted to the Faculty of Graduate Studies of The University of Manitoba in partial fulfilment of the requirements for the degree of

**Doctor of Philosophy**

Department of Chemistry

University of Manitoba

Winnipeg, MB, Canada, R3T 2N2

To my beloved parents

for their endless sacrifices

# Abstract

This thesis focuses on the electronic and chemical noninnocence of diiminepyridine (DIP) ligand in its group IV metals complexes.

A series of mono- and dialkyl titanium complexes of DIP were synthesized and the oxidation state of the metal and the ligand were characterized by a combination of techniques such as nuclear magnetic resonance spectroscopy, X-ray diffraction, X-ray photoelectron spectroscopy and density functional theory. It was elucidated that the unpaired electron in (DIP)$TiCl_3$ is mostly residing in the metal *d* orbital giving a $Ti^{III}$. Interestingly, one electron reduction of (DIP)$TiCl_3$ to (DIP)$TiCl_2$ led into oxidation of $Ti^{III}$ to $Ti^{IV}$, subsequently reduction of $DIP^0$ to $DIP^{2-}$. The two dialkyl titanium complexes (DIP)$TiMe_2$ and (DIP)$Ti(CH_2SiMe_3)_2$ was shown to be stable at elevated temperature. Variable temperature (VT) $^1$H-NMR of the former exhibited a thermal population of the triplet state while the latter displayed a normal dynamic behavior.

The formation of (DIP)$ZrCl_4$ was accompanied by a yellow precipitate, but (DIP)$HfCl_4$ stayed in solution. This difference in solubility could very well be due to formation of six-coordinate ionic $[(DIP)HfCl_3]^+Cl^-$. In contrast to (DIP)$TiCl_3$, attempts to manufacture (DIP)$MCl_3$ (M: Zr, Hf) were unsuccessful. Although, (DIP)$ZrCl_2$ could also be made in coordinating solvents, formation of (DIP)$HfCl_2$ proved to be problematic and it was only obtained in toluene. Similar to titanium complexes, all reduced zirconium and hafnium complexes contain dianionic chelates. The solid-state structure of (DIP)$ZrCl_2$ was shown to be a dimer whereas its hafnium counterpart was a monomer. This difference was obvious in their VT-NMR spectra. While broadened, their spectra exhibited a pattern similar to their titanium counterpart at room temperature. Upon cooling the samples, the signals of (DIP)$HfCl_2$ became sharper and splitting emerged while the signals of (DIP)$ZrCl_2$ merged

into the baseline and new peaks indicating a new complex with left-right asymmetry appeared.

Attempts to use the reducing power of the two electrons which reside in the π system of the ligand in (DIP)$TiCl_2$ failed. However, its zirconium and hafnium counterparts broke C-Cl bond in $CH_2Cl_2$ instantly. In one example, (DIP)$TiMe_2$ reacted with PhHN-NHPh and furnished a titanium imido/amido complex.

Furthermore, a unique H-shift isomerization of the ligand was observed in several cases. Alkylation of (DIP)$MCl_2$ (M: Ti, Hf) using LiR or RMgX in excess resulted in formation of (DIP+H/-H)$MR_2$, in which one H atom has been transferred from one imine methyl to the other imine carbon. (DIP)$ZrCl_2$ underwent the same isomerization on standing whereas it was not observed in (DIP)$TiCl_2$.

When the DIP ligand with various sizes of N-aryl fragments was reacted with $MBn_4$ (M: Zr, Hf), two benzyl groups migrated to the imine carbons which formed a mixture of $C_s$ and $C_2$ isomers. In contradiction of the previously reported alkylated DIP ligands, heating either of the pure isomers led into $C_s/C_2$ isomerization rather than transfer of benzyl groups to the pyridine ring. In one example, reaction of a $C_2$ isomer of zirconium with TEMPO led into replacement of one benzyl group with a TEMPO molecule. Further heating did not result isomerization.

# Acknowledgements

I am grateful to numerous people who have provided support, guidance and encouragement during my PhD. First, I would like to thank my advisor, Dr. Peter Budzelaar, for the great opportunity to do a PhD under his supervision. I admire his wide knowledge and vast experience in the field of organometallic chemistry, but also, I appreciate his patience and kindness during the past five years. He always inspired me to improve my research abilities and work ethically.

I would like to thank my committee members Dr. Phil Hultin, Dr. Georg Schreckenbach, Dr. Johan van Lierop and Dr. Geoffrey Tranmer for their helpful comments. I appreciate Dr. Hultin for helping me to improve my writing and presentation skills. Also, I thank to Dr. Schreckenbach for his help with computational chemistry.

Also, I want to show my appreciation to other faculty members and technicians of the Chemistry Department. Dr. David Herbert helped me with doing X-ray crystallography and was always welcoming to answer my questions. I acknowledge Dr. Kirk Marat and Dr. David Davidson and Mr. Mark Cooper (Geology Department) who were always available to help me with my VT-NMR experiments and X-ray analysis, respectively. I would also like to thank Dr. Bieringer's, Dr. Herbert's and Dr. Nemykin's lab members for their help.

Thanks to my amazing lab members Eric Cuthbert, Nan Zang and Dr. Gurmeet S. Bindra for creating a great atmosphere in the lab. They helped me countless times with my experiments and data interpretations.

I sincerely thank to my best friend Ms. Mahlagha Bahrami Shehni for her endless encouragement and support. Last not the least, I am grateful to my beloved parents and siblings, who have always supported me in every aspect of my life.

# Table of Contents

ABSTRACT III

ACKNOWLEDGEMENTS V

TABLE OF CONTENTS VI

LIST OF FIGURES XI

LIST OF SCHEMES XVI

LIST OF TABLES XVIII

CONTRIBUTIONS OF OTHER AUTHORS XIX

LIST OF ABBREVIATIONS XX

1 INTRODUCTION 1

1.1 Noninnocent Ligands 1

1.2 Types of noninnocent behaviour 3

1.3 Diiminopyridine ligands 5

1.3.1 Background 5

1.3.2 Synthesis 9

1.3.3 Steric properties 13

1.3.4 Electronic factors 15

1.4 DIP: Ligand-centered reactions 19

1.5 DIP complexes of metal halides 22

1.6 Stabilization of low-valent metals 23

1.7 Low-valent DIP complexes: electronic structures 26

1.8 Applications of DIP complexes 29

1.9 Chemical Reactivity of DIP ligands 31

1.10 Metal-ligand cooperation 32

1.11 Simpler ligands: α-Diimines 33

1.12 DIP Complexes in Polymerization 35

1.13 Polymerization Mechanism: Late Transition Metals 37

1.14 Characterization Techniques 38

1.14.1 NMR 38

1.14.2 NMR Spectroscopy of dynamic systems 40

1.14.3 EPR 43

1.14.4 XRD 43

1.14.5 XPS 45

1.15 Alternative technique 47

1.15.1 High energy X-ray 47

1.16 Organization of the thesis 48

1.17 References 50

2 SYNTHESIS AND CHARACTERIZATION OF MONO- AND DIALKYL DIIMINOPYRIDINE TITANIUM(II) COMPLEXES 60

2.1 Authorship Consideration 60

2.2 Abstract 60

2.3 Introduction 61

2.4 Results and Discussion 63

2.4.1 EPR 65

2.4.2 X-ray Structural Characterization 68

2.4.3 XPS 75

2.4.4 NMR 76

2.4.5 DFT 78

2.5 Conclusions 80

2.6 Experimental Section 81

2.7 References 88

3 REACTIVITY OF DIIMINOPYRIDINE TI COMPLEXES 98

3.1 ABSTRACT 98

3.2 INTRODUCTION 99

3.3 RESULTS AND DISCUSSION 101

3.3.1 Attempted redox chemistry of 2- 4 101

3.3.2 X-ray Structural Characterization of 5-8 105

3.3.3 Reactions with amides and alkoxides 110

3.3.4 X-ray Structural Characterization of 10-14 115

3.3.5 XPS 121

3.4 Conclusions 122

3.5 Experimental 123

3.6 References 131

4 SYNTHESIS AND CHARACTERIZATION OF DIIMINOPYRIDINE ZR AND HF COMPLEXES 136

4.1 ABSTRACT 136

4.2 INTRODUCTION 137

4.3 RESULTS AND DISCUSSION 139

4.3.1 X-ray Structural Characterization 148

4.3.2 Alkyl Migration 158

4.3.3 X-ray structures of benzyl derivatives. 162

4.4 Conclusions 166

4.5 Experimental Section 167

4.6 References 181

5 CONCLUSIONS AND OUTLOOK 187

5.1 Conclusions 187

5.2 Outlook 190

5.3 References 194

6 SUPPORTING INFORMATION 196

# List of Figures

Figure 1.1. Unambiguous oxidation states with innocent ligands ..... 1

Figure 1.2. Examples of noninnocent ligands ..... 2

Figure 1.3. Ambiguous oxidation state involving a noninnocent ligand ..... 3

Figure 1.4. DIP ligand with 2,6-disubstituted aryl groups ..... 5

Figure 1.5. Orientation of imine arms a) in the free DIP ligand and b) in a transition metal complex ..... 6

Figure 1.6. Different symmetries deriving from different substitution patterns at the aryl groups ..... 7

Figure 1.7. DIP binding modes through N atoms ..... 8

Figure 1.8. Ionic bis(2,6-dialdiminopyridine)$Fe^{+2}$ complex ..... 8

Figure 1.9. Sterics of the imine R′groups and the bulky phenyl rings ..... 13

Figure 1.10. Influence of DIP sterics on the complex geometry ..... 14

Figure 1.11. (DIP)M and $(DIP)_2M$ complexes ..... 15

Figure 1.12. Bond elongation and contraction in the DIP ligand upon accepting electrons ..... 15

Figure 1.13. Positions which could influence on the electronics of the ligand ..... 18

Figure 1.14. Complexes with EWG and EDG on the DIP ligand ..... 18

Figure 1.15. DIP ligand dimerization ..... 22

Figure 1.16. A few examples of stabilization by DIP of low-valent metals ..... 24

Figure 1.17. A few representative DIP metal alkyl complexes ..... 26

Figure 1.18. Electronic structures of the low valent DIP complexes ..... 28

Figure 1.19. Electronic structure of (DIP)AlX ..... 29

Figure 1.20. Influence of ligand steric properties on polymerization ..... 36

Figure 1.21. Proposed active sites for (DIP)M (M = Co, Fe) polymerization catalysts ..... 38

Figure 1.22. Proton spin states in the presence of a magnetic field.....39

Figure 1.23. The nuclear magnetic resonance process; v = $\omega$.....40

Figure 1.24. Berry pseudorotation in trigonal bipyramidal geometry of $Fe(CO)_5$.....42

Figure 1.25. An illustration of the Bragg's law.....44

Figure 1.26. A schematic view of an XPS analysis.....46

Figure 2.1. $^{R}$DIP ligand.....62

Figure 2.2. Experimental and simulated X-band EPR spectrum of **1** recorded at 20 K using a frozen solution of **1** in $CH_2Cl_2$ (~0.1 M $[(^nBu)_4N]PF_6$ was added). Experimental parameters: frequency = 9.362511 GHz, modulation amplitude = 4 Gauss, microwave power = 0.632 mW.....65

Figure 2.3. Spin density plots of **1**.....67

Figure 2.4. Solid-state structure of **1**. Hydrogens and ethyl $CH_3$ carbons are omitted for clarity.....68

Figure 2.5. Solid-state structure of **2**. Hydrogens and ethyl $CH_3$ carbons are omitted for clarity.....69

Figure 2.6. Solid-state structure of **3a**. Hydrogens and ethyl $CH_3$ carbons are omitted for clarity.....71

Figure 2.7. Solid-state structure of **3b**. Hydrogens and ethyl $CH_3$ carbons are omitted for clarity.....71

Figure 2.8. Solid-state structure of **3c**. Hydrogens and ethyl $CH_3$ carbons are omitted for clarity.....72

Figure 3.1. Formally low-valent main group and transition metal complexes of DIP.....99

Figure 3.2. VT $^1$H NMR (500 MHz) study of **6** in $d_8$-toluene (the black dot indicates solvent).....103

Figure 3.3. $^1$H-NMR (500 MHz) spectrum of **8** in $d_6$-benzene.....105

Figure 3.4. a) Molecular structure of **5**. Hydrogens and ethyl $CH_3$ carbons are omitted for clarity. b) Numbered molecular structure of **5**. Aryl rings are omitted for clarity .....106

Figure 3.5. Molecular structure of **6**. Hydrogens and ethyl $CH_3$ carbons are omitted for clarity .....107

Figure 3.6. Molecular structure of **7**. Hydrogens and ethyl $CH_3$ carbons are omitted for clarity .....109

Figure 3.7. Molecular structure of **8**. Hydrogens and ethyl $CH_3$ carbons are omitted for clarity .....110

Figure 3.8. $^1$H NMR (500 MHz) spectrum of **16** in $d_6$-benzene.....114

Figure 3.9. Molecular structure of **10**. Hydrogens and ethyl $CH_3$ carbons are omitted for clarity .....115

Figure 3.10. Molecular structure of **12**. Hydrogens and ethyl $CH_3$ carbons are omitted for clarity .....115

Figure 3.11. Two views of the molecular structure of **11**. Hydrogens and ethyl carbons are omitted for clarity .....118

Figure 3.12. Molecular structure of **13**. Hydrogens and ethyl $CH_3$ carbons are omitted for clarity .....120

Figure 3.13. Molecular structure of **14**. Hydrogens and ethyl $CH_3$ carbons are omitted for clarity .....121

Figure 4.1. $^R$DIP ligand.....137

Figure 4.2. Possible alkylation positions in DIP ligand.....138

Figure 4.3. $^1$H-NMR spectra of a) **4** at 25 °C and b) **5** at -5 °C (in toluene-$d_8$). (*) one molecule of toluene in the crystal lattice of **5**.....142

Figure 4.4. $^1$H-NMR spectrum of **4** in toluene-$d_8$ at -55 °C. (*) molecules of toluene in the crystal lattice of **4**.....143

Figure 4.5. $^{1}$H-NMR spectrum of the mixture of **4**, **4'** and **4"** in benzene-$d_6$ .....144

Figure 4.6. $^{1}$H-NMR spectra of a) **5'** and b) **5"** in toluene-$d_8$. (*) toluene solvent peak .....146

Figure 4.7. $^{1}$H NMR (500 MHz; toluene-$d_8$) spectrum of **5"** after 5 days in solution, showing hydrogen atom migration and loss.....147

Figure 4.8. Molecular structure of **1** [($^{Et}$DIP)$ZrCl_4$]. Hydrogens and ethyl $CH_3$ carbons are omitted for clarity .....149

Figure 4.9. Molecular structure of **3** [($^{Et}$DIP)$ZrCl_2$(THF)]. Hydrogens and ethyl $CH_3$ carbons are omitted for clarity.....151

Figure 4.10. Molecular structure of **4** [($^{Et}$DIP)$ZrCl_2$]$_2$. Hydrogens and ethyl $CH_3$ carbons are omitted for clarity. Only one of three crystallographically independent dimeric units shown. .....151

Figure 4.11. Molecular structure of **4-$Et_2O$** [($^{Et}$DIP)$ZrCl_2$($Et_2O$)]. Hydrogens and ethyl $CH_3$ carbons are omitted for clarity.....152

Figure 4.12. Molecular structure of **4"-$Et_2O$** [($^{Et}$DIP-2H)$ZrCl_2$($Et_2O$)]. Hydrogens and ethyl $CH_3$ carbons are omitted for clarity .....152

Figure 4.13. Molecular structure of **5** [($^{Et}$DIP)$HfCl_2$]. Hydrogens and ethyl $CH_3$ carbons are omitted for clarity .....153

Figure 4.14. Molecular structure of **5"** [($^{Et}$DIP)Hf($CH_2SiMe_3$)$_2$]. Hydrogens and ethyl $CH_3$ carbons are omitted for clarity.....153

Figure 4.15. Molecular structure of **6** [($^{Et}$DIP-2H)$HfCl_2$($Et_2O$)]. Hydrogens and ethyl $CH_3$ carbons are omitted for clarity.....155

Figure 4.16. Molecular structure of **7** [($^{Et}$DIP-H)$ZrCl_3$]. Hydrogens and ethyl $CH_3$ carbons are omitted for clarity .....156

Figure 4.17. Molecular structure of **8** [($^{Et}$DIP-H)$HfCl_3$]. Hydrogens and ethyl $CH_3$ carbons are omitted for clarity .....157

Figure 4.18. Molecular structure of **9-$C_s$**. Hydrogens are omitted for clarity.....163

Figure 4.19. Molecular structure of **10-$C_2$**. Hydrogens and ethyl carbons are omitted for clarity .....163

Figure 4.20. Molecular structure of **10-$C_s$**. Hydrogens and $CH_3$ carbons are omitted for clarity .....164

Figure 4.21. Molecular structure of **13**. Hydrogens and ethyl carbons are omitted for clarity .....164

Figure 4.22. Molecular structure of **14**. Hydrogens and ethyl $CH_3$ carbons are omitted for clarity .....165

Figure 5.1. Modification of $^{Et}$DIP to $^{iPr}$PhDIP.....191

# List of Schemes

Scheme 1.1. Promotion of the Lewis acidity of the metal center by a noninnocent ligand..... 3

Scheme 1.2. The role of a noninnocent ligand as an electron source..... 4

Scheme 1.3. Using redox active Tyrosine radical in oxidation of alcohols..... 4

Scheme 1.4. Formation of nitrene as a noninnocent ligand..... 5

Scheme 1.5. Typical DIP synthetic procedure..... 9

Scheme 1.6. Substitution at the pyridine 4-position.....10

Scheme 1.7. Substitutions at the pyridine ring.....11

Scheme 1.8. Synthetic methods for more variations of the ligand.....11

Scheme 1.9. Synthesis of DIP ligand bearing C-aryl imine arms.....12

Scheme 1.10. Synthesis of DIP ligand bearing C-alkoxy imine arms.....12

Scheme 1.11. Electron reservoir feature of DIP in stabilization of iron complexes.....17

Scheme 1.12. DIP ligand dehydrogenation.....19

Scheme 1.13. DIP ligand dimerization.....20

Scheme 1.14. Homolysis vs migration.....20

Scheme 1.15. Treatment of $ZnR_2$ with DIP ligand.....21

Scheme 1.16. Reaction of $MX_n$ with DIP.....22

Scheme 1.17. Alkylation/reduction of (DIP)$CoCl_2$.....25

Scheme 1.18. Single and double bond cleavages.....30

Scheme 1.19. Selective anti-Markovnikov alkene hydrosilylation.....31

Scheme 1.20. DIP-based reaction.....32

Scheme 1.21. Metal-ligand cooperation.....33

Scheme 1.22. Application of α-Diimine nickel complexes in hydrosilylation of olefins.....34

Scheme 1.23. Noninnocent character of iminopyridine ligand.....35

Scheme 2.1. Synthesis of Ti(III) and Ti(II) complexes .....64

Scheme 3.1. Synthesis of ($^{Et}$DIP)TiCl$_2$ and ($^{Et}$DIP)TiR$_2$ .....100

Scheme 3.2. Attempted redox chemistry involving **2** and **4a** .....101

Scheme 3.3. Possible mechanism for formation of **7** .....104

Scheme 3.4. Treatment of **2** with varying size bases.....111

Scheme 3.5. Reaction of $^{t}$BuOK with ($^{Et}$DIP)TiCl$_3$.....113

Scheme 3.6. Reaction of **4b** with TEMPO.....114

Scheme 3.7. Probable mechanism for formation of **11**.....119

Scheme 3.8. Possible mechanism for formation of **13**.....121

Scheme 4.1. Synthesis of Zr(IV), Hf(IV), Hf(II) and Zr(II) Complexes .....140

Scheme 4.2. Isomerization of **5"** on standing .....146

Scheme 4.3. Synthesis of **7** and **8** via C-Cl bond cleavage and bases .....148

Scheme 4.4. Synthesis of Zr and Hf complexes with a doubly benzylated ligand.....159

Scheme 4.5. Isomerization of pure isomers over heating .....160

Scheme 4.6. Treatment of **10-C$_2$** with 2 equivalents of TEMPO .....161

Scheme 4.7. Synthesis of the bis chelate complex **14** .....161

# List of Tables

Table 1.1. DIP bond lengths modifications....16

Table 1.2. Synthesized DIP complexes of main group and transition metals....23

Table 2.1. Experimental and DFT calculated EPR parameters of **1**....66

Table 2.2. Selected Bond lengths for ($^{Et}$DIP)Ti complexes....68

Table 2.3. Selected Bond lengths for ($^{Et}$DIP)Ti$R_2$ complexes....74

Table 2.4. Ti $2p_{3/2}$ binding energy from XPS....75

Table 3.1. Selected bond lengths (Å) for ($^{Et}$DIP)Ti complexes....107

Table 3.2. Selected bond lengths (Å) for ($^{Et}$DIP)Ti complexes....116

Table 3.3. Bond length comparison between IP ligand and DIP in **11**....118

Table 3.4. Ti $2p_{3/2}$ Binding energies....122

Table 4.1. Selective bond lengths (Å) for ($^{Et}$DIP)Zr and Hf complexes....149

Table 4.2. Selected bond lengths (Å) for (DIP-H)M$Cl_3$ complexes....157

Table 4.3. Selective bond lengths (Å) for ($^{R}$DBAP)Zr and Hf complexes....162

Table 5.1. (DIP)M chemical shifts at room temperature....188

# Contributions of other Authors

1) Prof. Peter H. M. Budzelaar did most of the DFT calculations in Chapter 2. Also, he solved crystal structures with disorders in this thesis.
2) Dr Kirk Marat and Dr. David D. Davidson did the low-temperature NMR experiments in Chapters 2 and 4.
3) Dr. David E. Herbert and Mr. Mark Cooper helped me with doing single-crystal X-ray diffraction measurements.
4) Dr. Kevin McEleney (Manitoba Institute for Materials) did the XPS analysis in Chapter 2 and 3.

# List of Abbreviations

| | |
|---|---|
| ADF | Amsterdam Density Functional |
| B3-LYP | Adiabatic connection method using Becke (1998) exchange functional and Lee-Yang-Parr correlation functional |
| Bn | Benzyl |
| BP86 | Gradient corrected method using Becke 88 exchange functional and Perdew 86 correlation functional |
| DCM | Dichloromethane |
| DFT | Density Functional Theory |
| DME | Dimethoxyethane |
| DMF | Dimethylformamide |
| DMSO | Dimethyl sulfoxide |
| EAN | Effective Atomic Number |
| EPR | Electron Paramagnetic Resonance |
| Et | Ethyl |
| $Et_2O$ | Diethyl ether |
| EtOH | Ethanol |
| HOMO | Highest occupied molecular orbital |
| $^{i}Pr_2O$ | Diisopropyl ether |
| $KC_8$ | Potassium graphite |
| LUMO | Lowest unoccupied molecular orbital |
| MAO | Methylaluminoxane |
| Me | Methyl |
| MeOH | Methanol |
| MO | Molecular orbital |

| | |
|---|---|
| NMR | Nuclear Magnetic Resonance |
| $^{n}$Bu | n-butyl |
| PCET | Proton Coupled Electron Transfer |
| PTSA | *p*-toluenesulfonic Acid |
| SOMO | Singly occupied molecular orbital |
| $^{t}$Bu | tert-butyl |
| TEMPO | 2,2,6,6-Tetramethylpiperidine 1-oxyl |
| THF | Tetrahydrofuran |
| TPSSh | Functional (10% Hartree Fock exchange) by Tao-Perdew-Staroverov-Scuseria |
| TZVP | Triple Zeta Valence Plus Polarization |
| VT-NMR | Variable temperature- Nuclear Magnetic Resonance |
| XPS | X-ray Photoelectron Spectroscopy |
| XRD | X-ray Diffraction |

# 1 Introduction

## 1.1 Noninnocent Ligands

Every element in the periodic table has its own characteristic chemistry. Within the chemistry of a single element, different oxidation states are associated with different types of reactions and different physical (spectroscopic, magnetic, etc) properties. Thus, the metal oxidation state is an important descriptor of a coordination complex or organometallic compound. In Werner type complexes, assignment of the formal oxidation state is straightforward. Ligands are classified as neutral (L type) and negatively charged (X type), and by considering the overall charge of the complex, the oxidation state of the metal center can easily be assigned. For example, in Figure 1.1 the oxidation states of Co and Fe are +3 and +2, respectively.

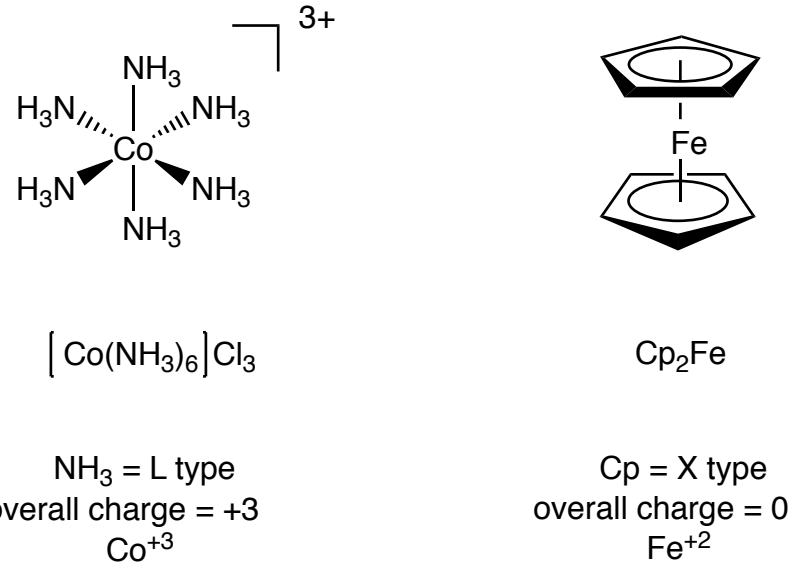


Figure 1.1. Unambiguous oxidation states with innocent ligands

There are ligands which introduce uncertainty in the oxidation state assignment. In 1966, Jorgensen classified ligands as “innocent” and “noninnocent” (redox active).[1] Noninnocent

ligands have low-lying empty orbitals that can accept electrons, or high-lying occupied orbitals that can donate electrons. A few typical noninnocent ligands are shown in Figure 1.2.

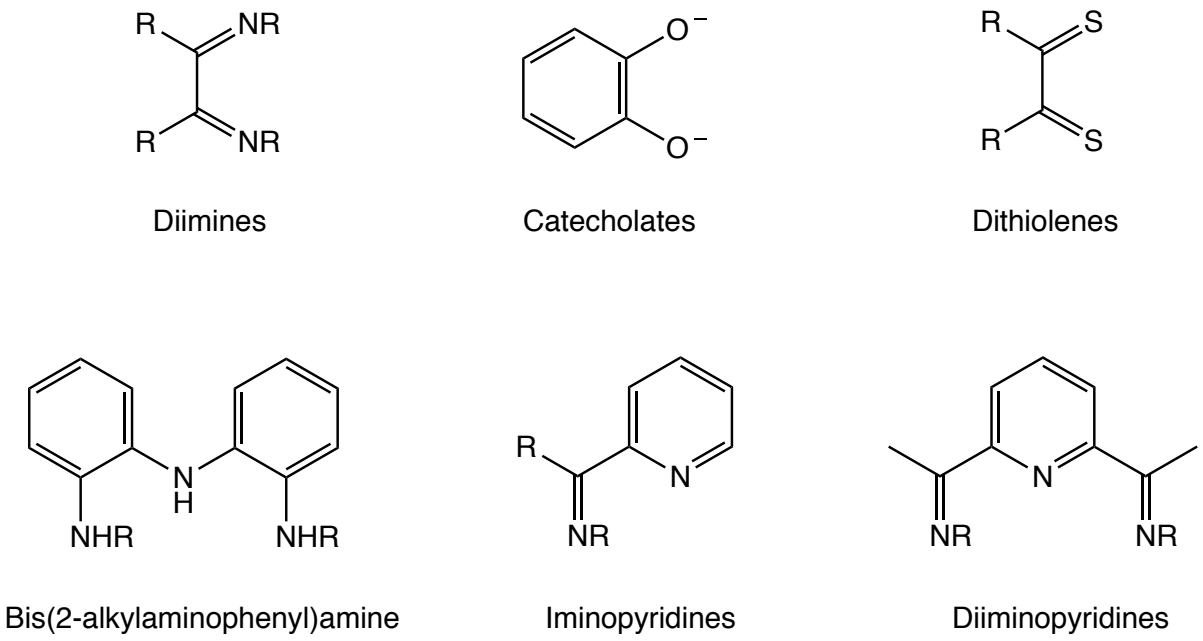


Figure 1.2. Examples of noninnocent ligands

It should be noted that noninnocence is also a question of degree: relative to a very strongly reducing metal many ligands show "noninnocent" behaviour. The term "noninnocence" is more general than "redox-active" and also covers ligands that undergo chemical modification while bound to a metal ("chemical noninnocence").

The formal oxidation state of the metal in complexes with noninnocent ligands can be deceptive, since it can differ from the spectroscopic ("real") oxidation state. Below, the formal oxidation state of Ni is 0 but the "real" oxidation state, assigned by various characterization techniques, is closer to +2 (Figure 1.3).[2]

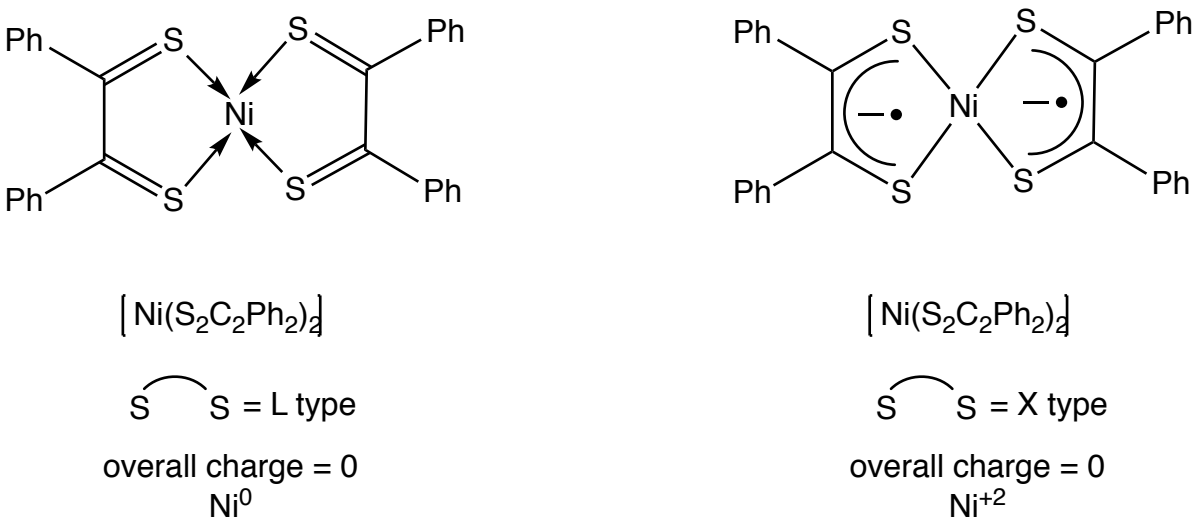


Figure 1.3. Ambiguous oxidation state involving a noninnocent ligand

## 1.2 Types of noninnocent behaviour

In catalysis, noninnocent ligands actively participate in redox processes. This is in contrast to the classical behavior of a transition metal complex in which redox reactions occurs at the metal and the ligands play spectator roles. Redox-active ligands play their active roles by accepting/delivering electrons to the metal center or contributing directly in substrate bond making/breaking in a metal-ligand cooperative fashion. The former could happen in different ways. In the example shown in Scheme 1.1, the noninnocent ligand at Ir undergoes oxidation, thus increasing the Lewis acidity of the iridium center and facilitating successive reactions.[3]

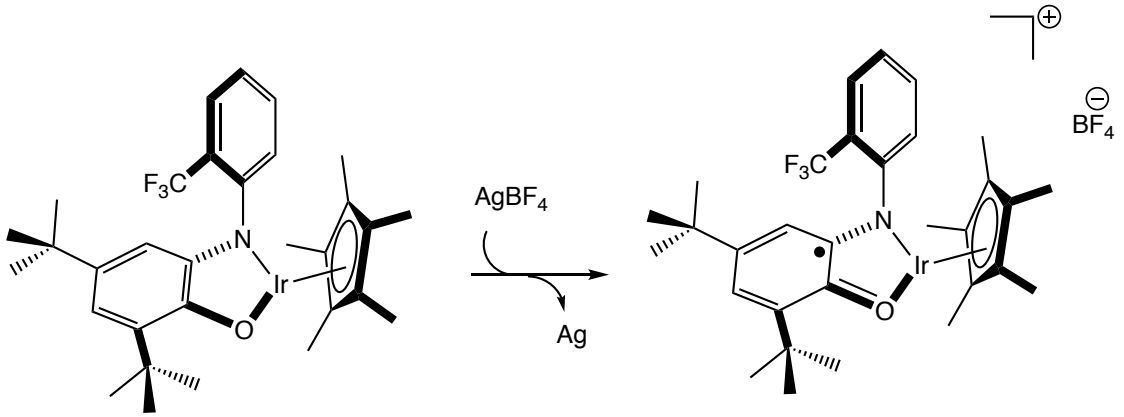


Scheme 1.1. Promotion of the Lewis acidity of the metal center by a noninnocent ligand

The "electron-reservoir" feature of the noninnocent ligand allows the metal to send electrons to the ligand or to accept electrons from it. This allows the complex as a whole to undergo redox type reactions while keeping the metal center in its preferred oxidation state (Scheme 1.2).[4]

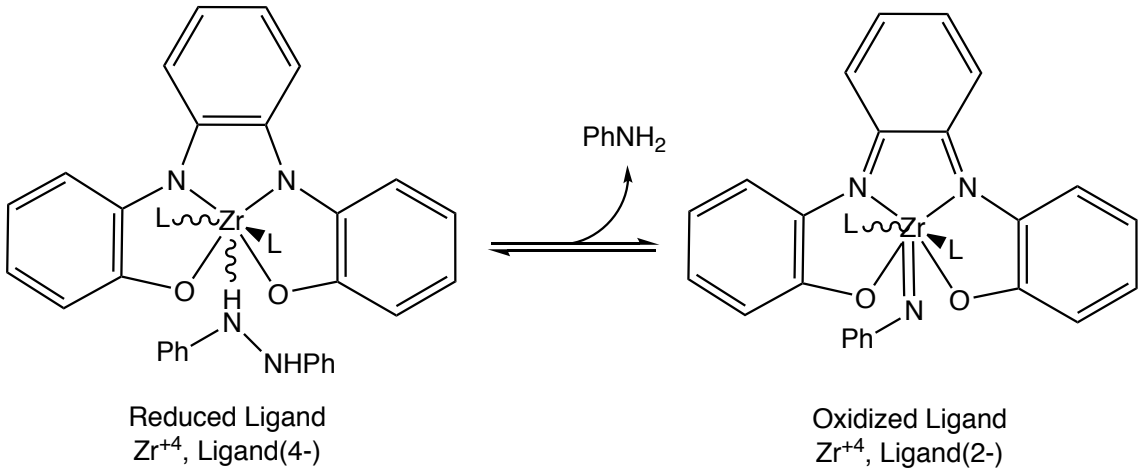


Scheme 1.2. The role of a noninnocent ligand as an electron source

Apart from or in addition to being redox-active, ligands can also be "chemically noninnocent" as mentioned above. Formation of a ligand-radical in a redox process could lead to substrate activation in a metal-ligand cooperative manner (Scheme 1.3).[5]

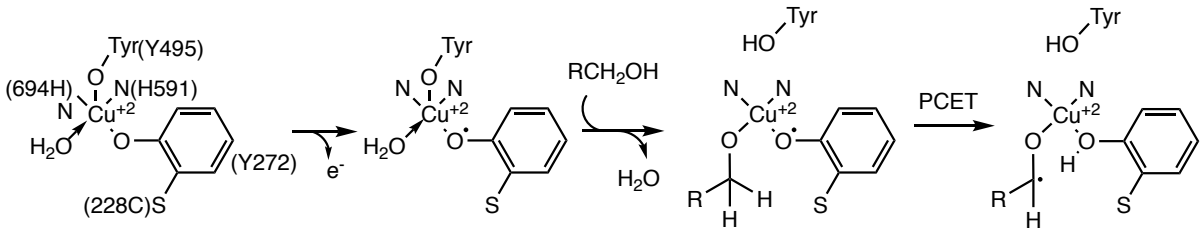


Scheme 1.3. Using redox active Tyrosine radical in oxidation of alcohols

On occasion, a substrate in a chemical process gets activated and then acts as a noninnocent ligand (Scheme 1.4).[6]

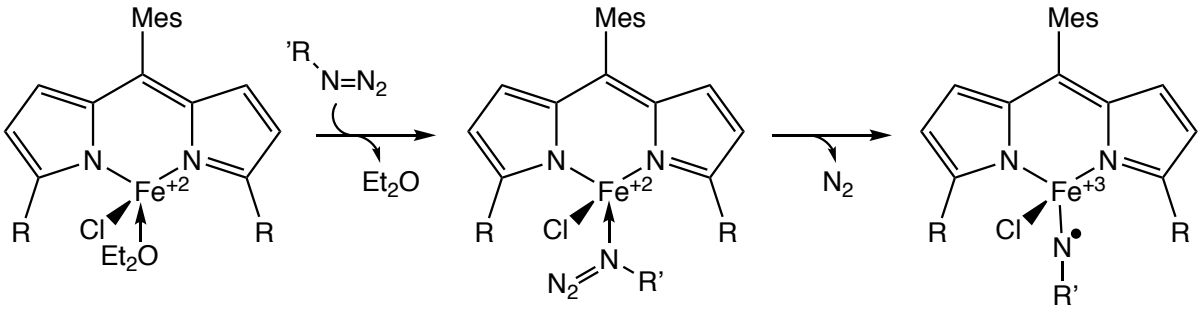


Scheme 1.4. Formation of nitrene as a noninnocent ligand

Dissociation of the $Et_2O$ molecule followed by coordination of the organic azide is accompanied by liberation of one molecule of dinitrogen. The substrate functions as a noninnocent ligand while keeping the iron in its preferred oxidation state and further reactivity happens at the R-N radical moiety.

# 1.3 Diiminopyridine ligands

## 1.3.1 Background

This thesis is focused on the chemistry of diiminopyridine (DIP) ligands bound to group IV transition metals. In particular, we are interested in DIP ligands bearing 2,6-disubstituted aryl groups at the imine nitrogens ($^{R}$DIP ligands) (Figure 1.4).

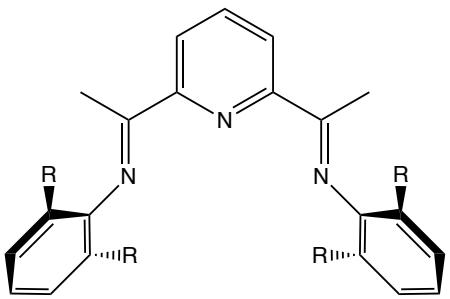


Figure 1.4. DIP ligand with 2,6-disubstituted aryl groups

The DIP ligand has a conjugated system of π bonds which is responsible for its noninnocent character.

In the solid state, the free ligand has both imine arms coplanar with the central pyridine ring[7] and pointing away from it, thus minimizing the steric hindrance of the bulky aryl rings (Figure 1.5a). This is unlike the conformation in complexes with transition metals, where imine arms are located parallel to each other to form a tridentate ligand (Figure 1.5b).

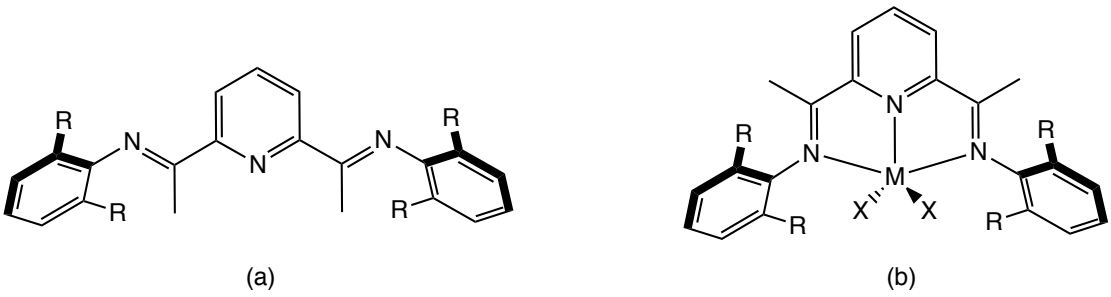


Figure 1.5. Orientation of imine arms a) in the free DIP ligand and b) in a transition metal complex

The highest possible symmetry of a DIP ligand in a complex is $C_{2v}$. Assuming the metal center introduces no further asymmetry, this occurs when the two phenyl rings at the imine nitrogens have two identical substituents at their 2,6-positions. Different substituents at these positions may further reduce the symmetry to $C_2$, $C_s$ and $C_1$ (Figure 1.6).

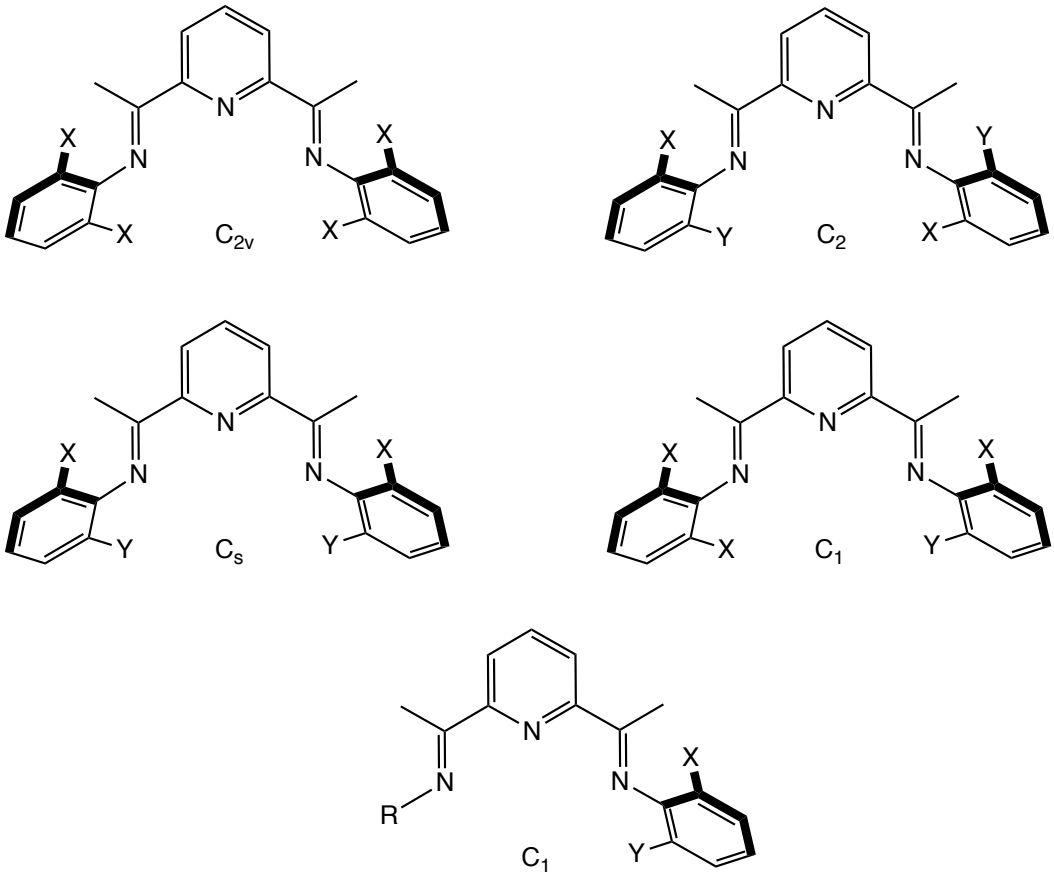


Figure 1.6. Different symmetries deriving from different substitution patterns at the aryl groups

NMR resonances due to the X/Y substituents "report" on the symmetry of the complex. In complexes of $^{Et}$DIP (a ligand often used in this work) the methylene protons are inequivalent (diastereotopic) due to hindered rotation around the N-Ar bonds.

While the DIP ligand normally acts as terdentate ligand (N1-N2-N3 coordination), bidentate (N1-N2) and N1-N2-C coordination modes have on occasion been observed with some main group metals (Figure 1.7).[8]

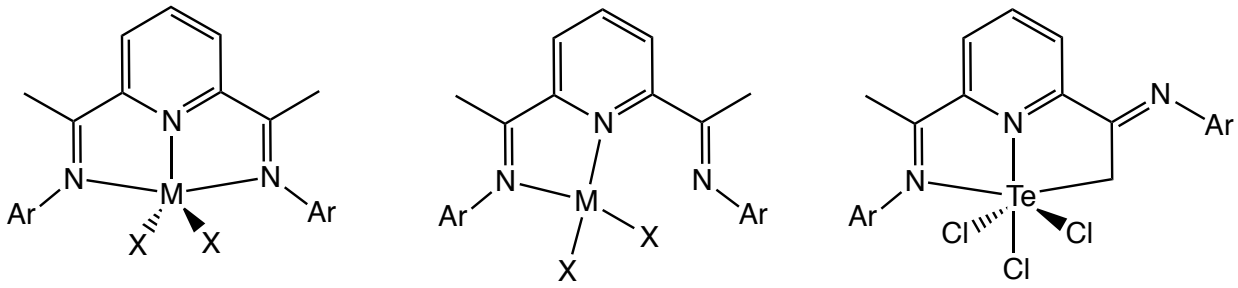


Figure 1.7. DIP binding modes through N atoms

In 1956, Stoufer reported the first series of 2,6-dialdiminepyridinedihydrazone complexes of $Fe^{+2}$, $Co^{+2}$ and $Ni^{+2}$. Shortly after, variations of the ligand with different small groups at the imine nitrogens were synthesized. It was reported that such ligands give bis chelate complexes (Figure 1.8).

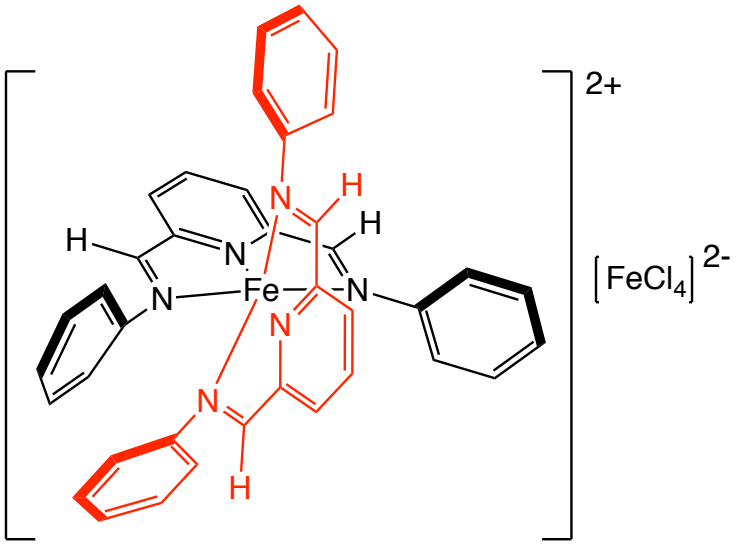


Figure 1.8. Ionic bis(2,6-dialdiminopyridine)$Fe^{+2}$ complex

Krumholz and Figgins[9], independently, carried out spectroscopic studies. Curry et al. extended the complexation of DIP ligands by replacing the aldimine side arms with ketimines and reported $Fe^{+2}$, $Co^{+2}$, $Ni^{+2}$ and $Cu^{+2}$ complexes. There were a number of reports on DIP complexes of late metals, but not much was reported on their reactivity until cobalt and iron

complexes were found to be active in olefin polymerization.[10] After that, many chemists have conducted research on DIP complexes in combination with main group elements, transition metals and lanthanides, and have discovered not only surprising chemistry but also interesting applications.[11]

### 1.3.2 Synthesis

DIP ligands can easily be synthesized based on a classical condensation reaction where 2,6-diacetyl pyridine reacts with excess alkyl or aryl amine and a catalytic amount of acid, e.g. using PTSA in refluxing toluene (Scheme 1.5), or formic acid in refluxing methanol.[10a]

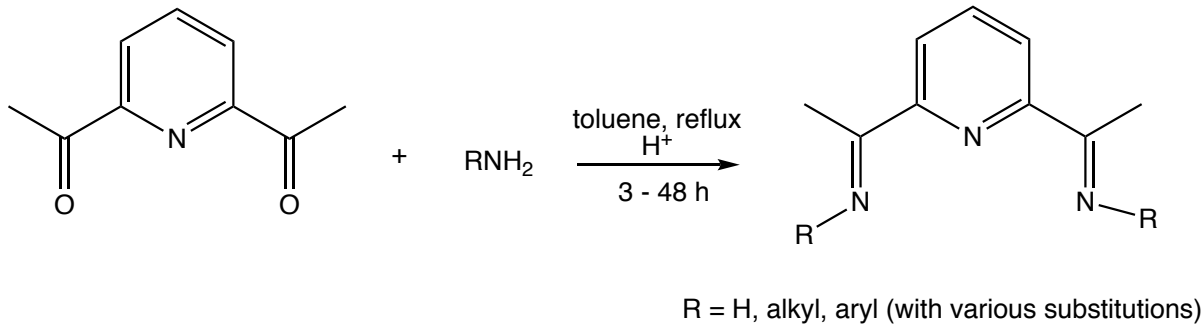


Scheme 1.5. Typical DIP synthetic procedure

Cámpora and co-workers have reported modification of the DIP ligand at pyridine C4 by addition/re-aromatization using $MnR_2$ complexes (Scheme 1.6).[12]

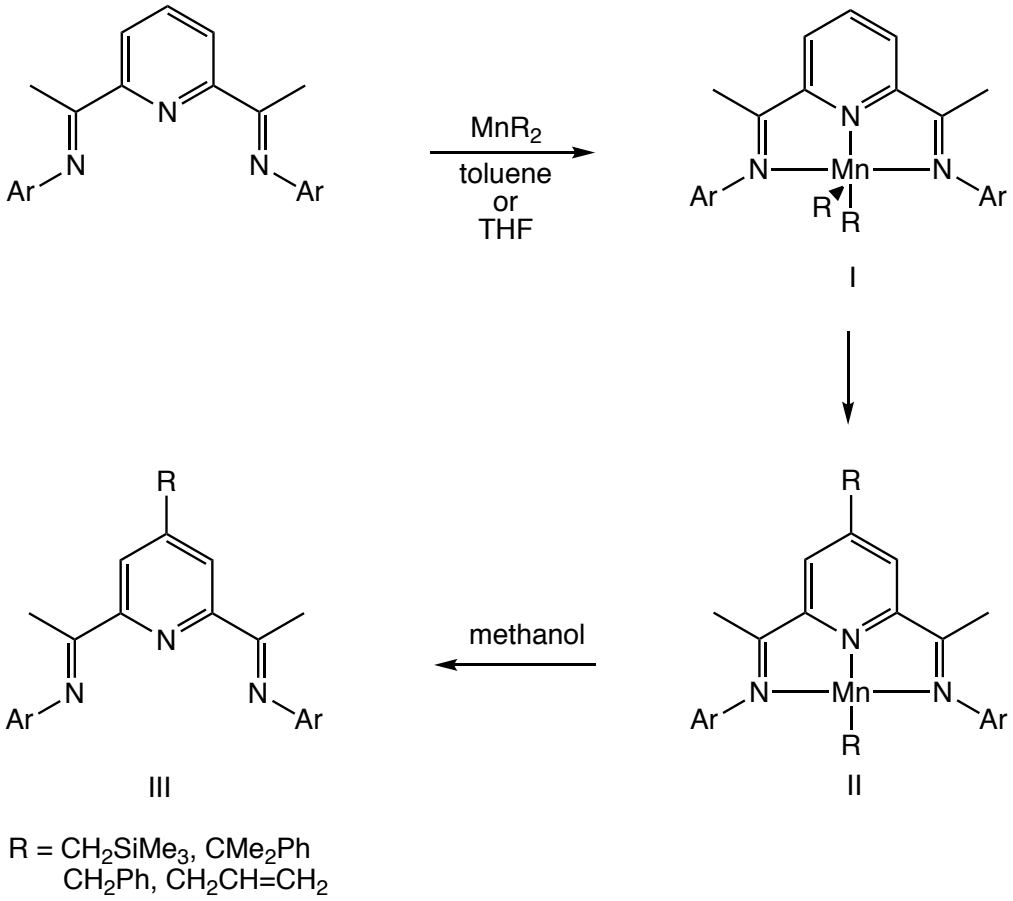


Scheme 1.6. Substitution at the pyridine 4-position

After formation of I, one of the R groups migrates to C2 of the pyridine ring. Upon heating, the R group shifts to C3 and finally to C4. By losing a H atom, the ligand undergoes rearomatization and gives II. Methanolysis of II leads into formation of C4-alkylated DIP ligand.

More variations of DIP ligands can be synthesized by treatment of amines with 4-substituted analogues of 2,6-diformyl- or 2,6-diacetylpyridines (Scheme 1.7 and Scheme 1.8).

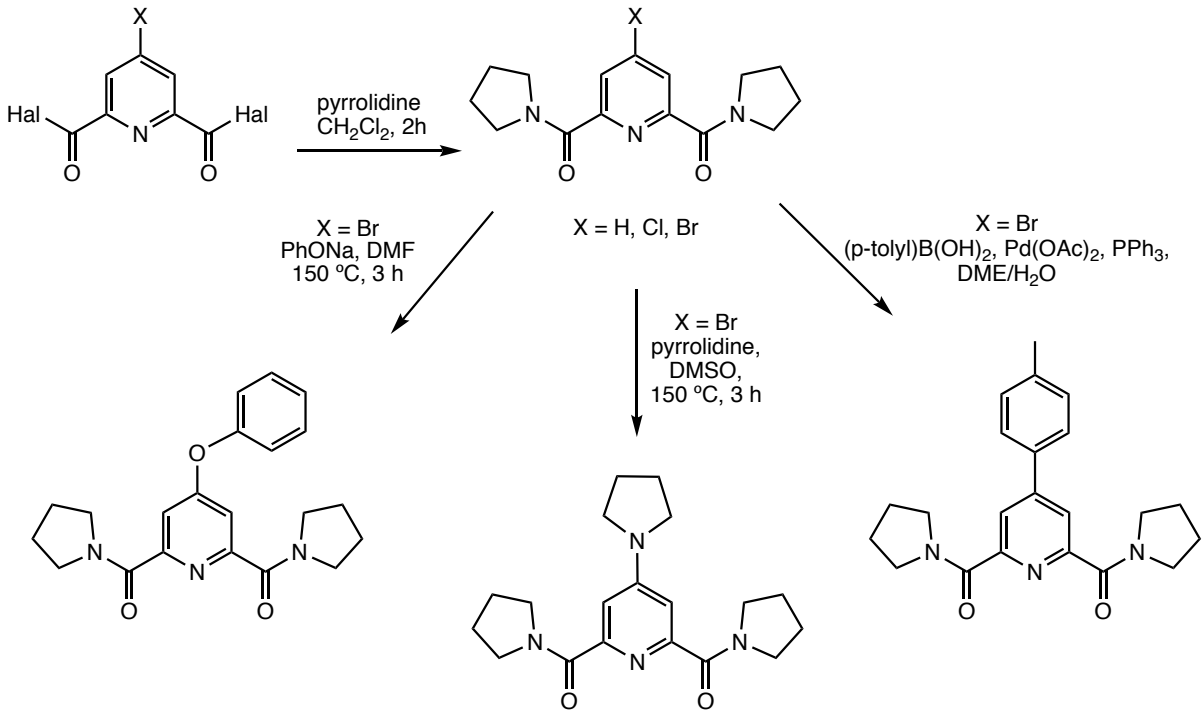


Scheme 1.7. Substitutions at the pyridine ring

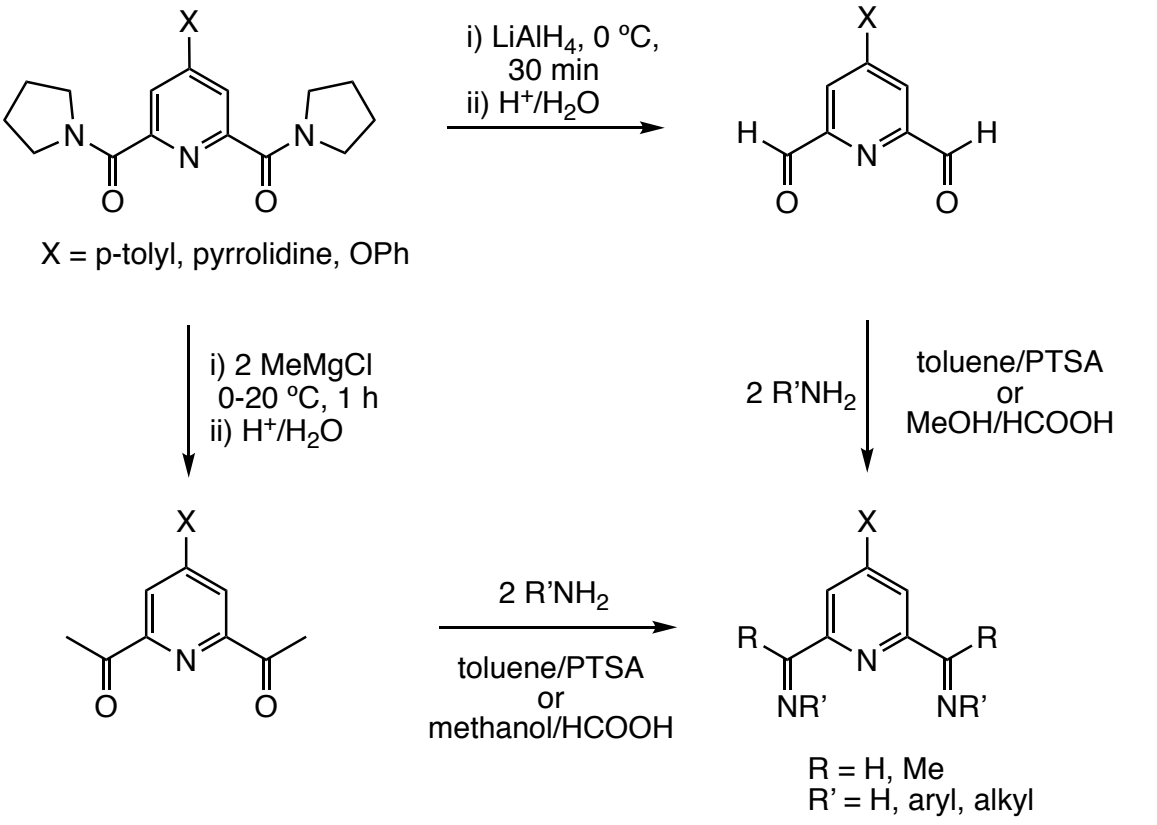


Scheme 1.8. Synthetic methods for more variations of the ligand

To avoid probable dehydrogenation of methyl imines in chemical reactions, or to have bulkier substituents at imine groups, one can use ligands having phenyl or alkoxy groups instead; their synthesis is shown in Scheme 1.9 and Scheme 1.10, respectively.[13]

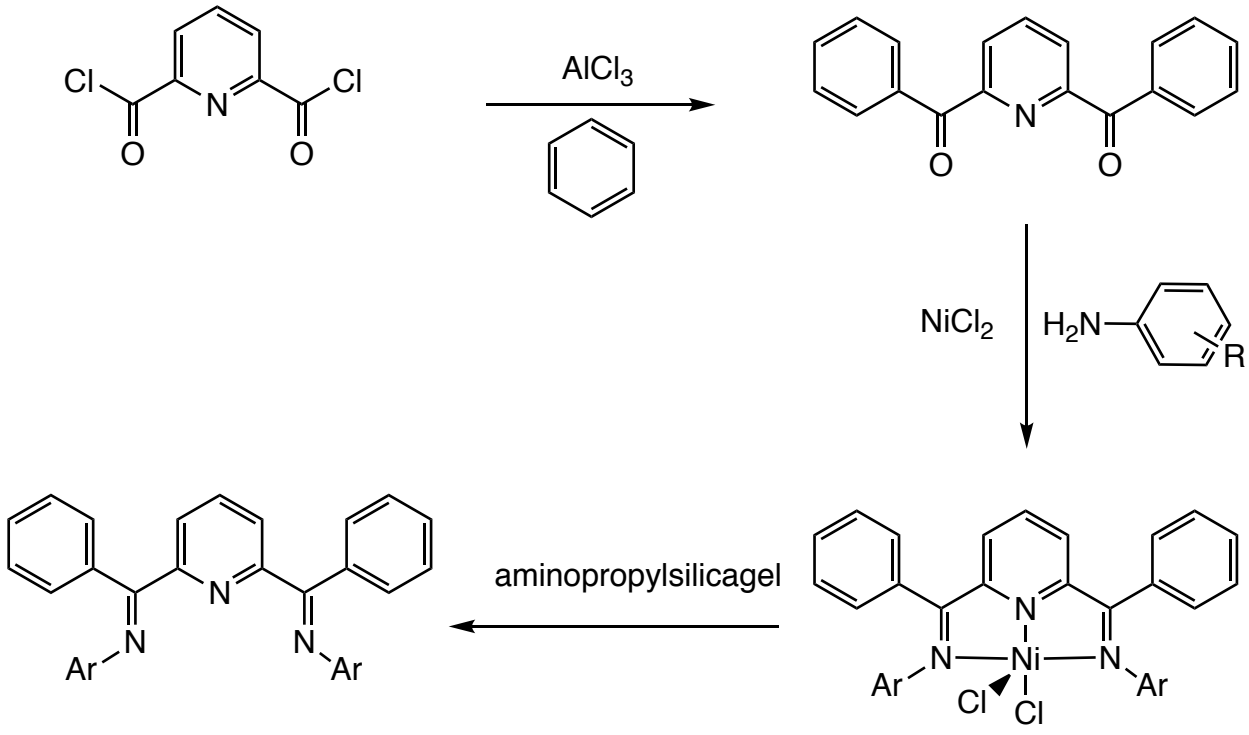


Scheme 1.9. Synthesis of DIP ligand bearing C-aryl imine arms

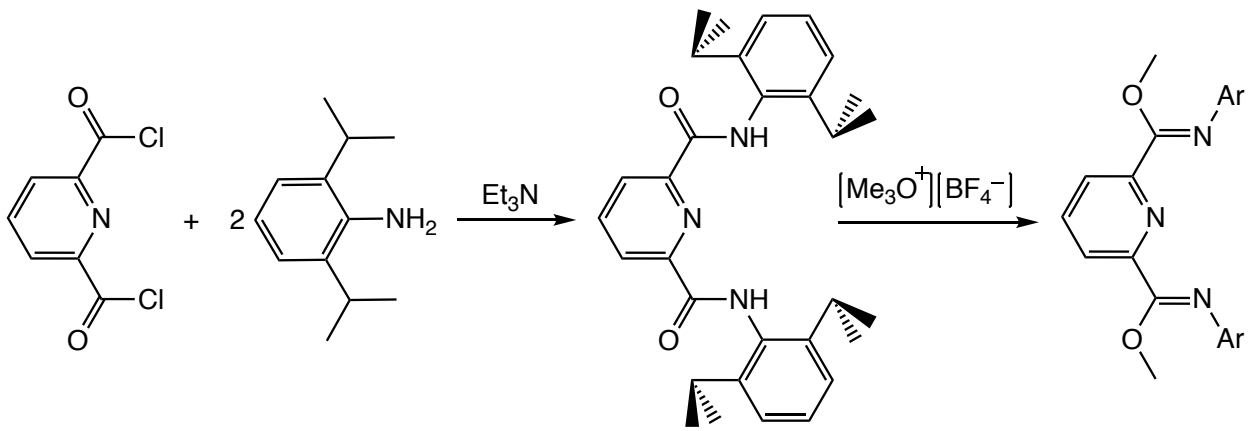


Scheme 1.10. Synthesis of DIP ligand bearing C-alkoxy imine arms

It should be noted that DIP ligands with bulky *t*-butyl groups at the imine side arms have been made. Since the ligands become too bulky they will not go on a metal.[14]

### 1.3.3 Steric properties

The $^{R}$DIP ligands we focus on are rather bulky due to the presence of 2,6-disubstitued aryl groups at the imine nitrogens. They take up far more space, in particular also above and below the DIP NNN plane, than most other 6e-donors would.

As a consequence, the metal in DIP complexes is usually unable to fulfill the EAN rule, which makes complexes of these ligands reactive. On the other hand, the aryl groups also offer some steric shielding, protecting the metal against attack from above and below the MNNN plane. Thus, it is not surprising that tuning of the size of these 2,6-substituents is often the key to optimizing performance (Figure 1.9).

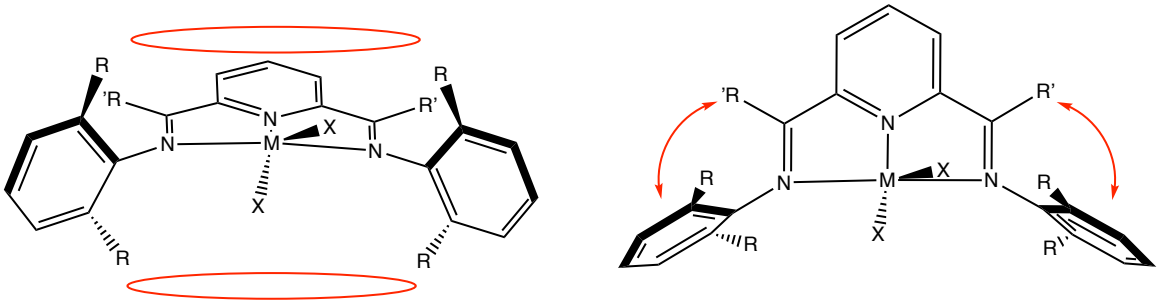


Figure 1.9. Sterics of the imine R′ groups and the bulky phenyl rings

The clash between the imine methyl (or bulkier) groups and the substituents at the 2,6-position on the N-aryl rings results in keeping the aryl rings perpendicular to the plane of the molecule and increases rigidity. This increases steric hindrance above and below the metal center. Replacing the bulky imino fragments with smaller groups reduces the clash which allows rotation about N-aryl bonds. All this affects the geometry around the metal center. For

example, replacing a diketimino pyridine with a dialdimino pyridine ligand in a Ni complex results in geometry modification of the complex (Figure 1.10).[15]

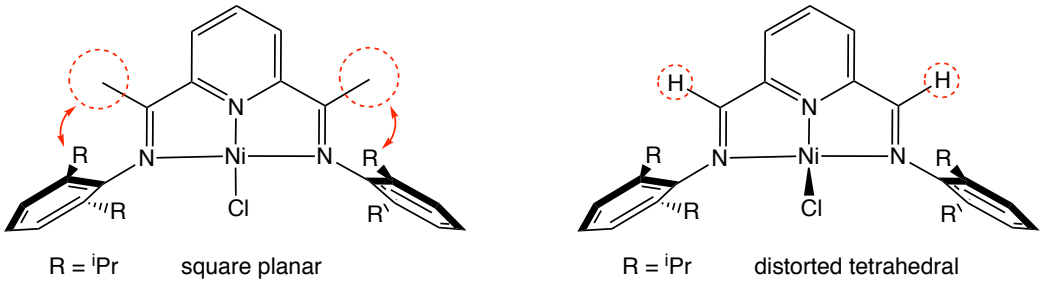


| | | |
|---|---|---|
| Dihedral angles (º): | ~ 86 | ~ 60 |
| N-Ni-Cl (º): | ~ 179 | ~ 162 |

Figure 1.10. Influence of DIP sterics on the complex geometry

Steric factors seem to control the stoichiometry of formation of DIP complexes. For "small" ligands (alkyl or 2,6-unsubstituted aryl at N) one usually obtains bis(ligand) complexes $(DIP)_2M$ in a reduction reaction. Whenever the N-aryl groups are 2,6-disubstituted with anything larger than F, complexation seems to stop at mono(ligand) complexes $(DIP)MX_n$ (Figure 1.11).[16]

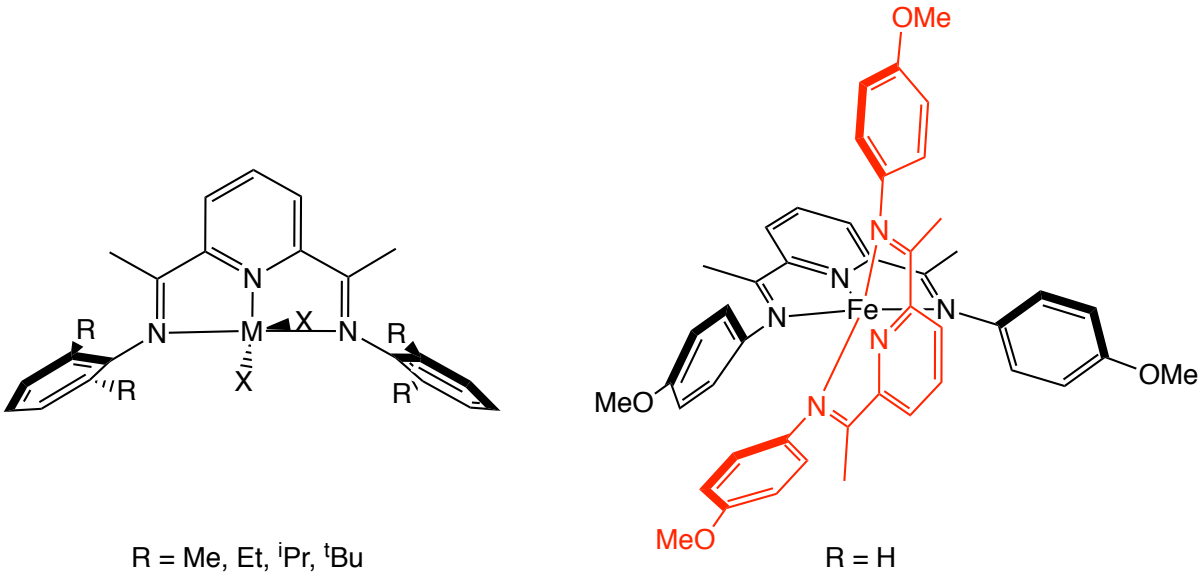


Figure 1.11. (DIP)M and $(DIP)_2M$ complexes

### 1.3.4 Electronic factors

The DIP pyridine ring and its two imine side arms form a highly π-conjugated system which can accommodate up to three electrons in its two low-lying π* orbitals in redox reactions (the N-aryl groups hardly participate because they are perpendicular to the NNN plane). Electron transfer from metal to ligand results in the population of the ligand π* orbitals which leads to elongation of C=N and contraction of $C_{imine}$-$C_{py}$ (Figure 1.12).

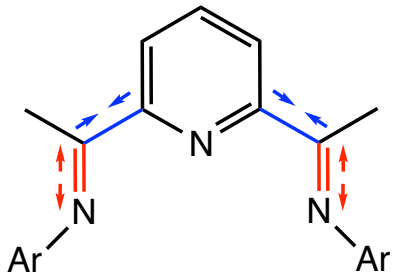


Figure 1.12. Bond elongation and contraction in the DIP ligand upon accepting electrons

The magnitude of the bond length changes highly depends on the number of transferred electrons, apparently in a nonlinear fashion (Table 1.1).[17]

Table 1.1. DIP bond lengths modifications

| | av C=N | av $C_{imine}$-$C_{py}$ |
|---|---|---|
| 0e transfer | 1.280 | 1.493 |
| 1e transfer | 1.330 | 1.437 |
| 2e transfer | 1.337 | 1.425 |

This noninnocent behavior of the DIP ligand can stabilize the metal center in an unusually low formal oxidation state, leading to ambiguity about the "real" oxidation states of both the DIP ligand and the metal center. For example, successive reduction of ($^{iPr}$DIP)$FeCl_2$ resulted in formation of a diamagnetic formally low-valent iron$^0$ dinitrogen complex (Scheme 1.11).[18]

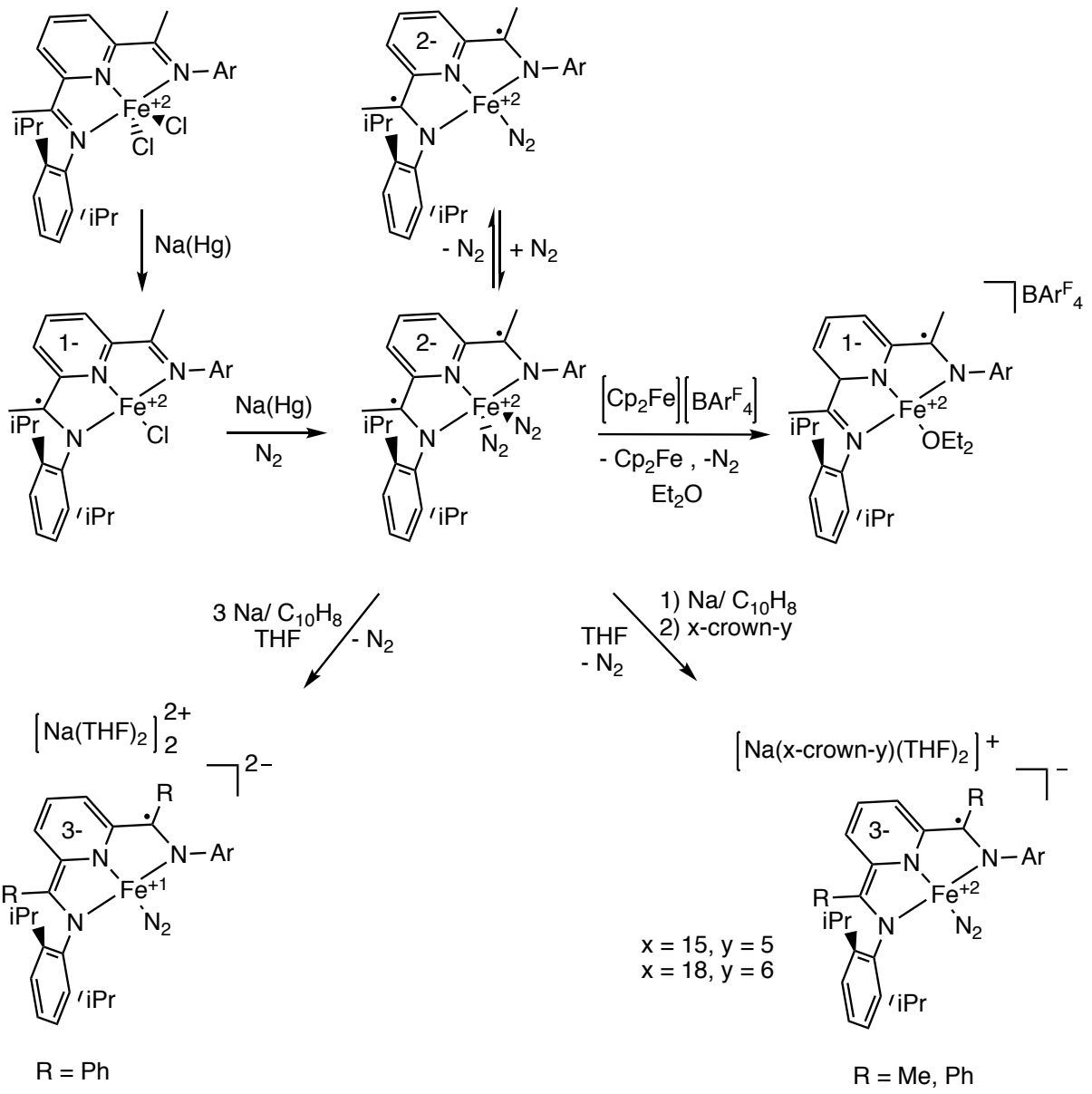


Scheme 1.11. Electron reservoir feature of DIP in stabilization of iron complexes

Bond lengths determined by X-ray crystallography of the DIP ligand suggested a reduced chelate with two electrons and an intermediate-spin state iron center. The diamagnetic ground state may arise from antiferromagnetic coupling between the two parallel electrons on the chelate and two electrons with opposite spins in iron 3*d* orbitals. Further reduction of this complex resulted in formation of a trianionic DIP ligand still bound to $Fe^{+2}$. Finally, with ligand modification, the fourth reduction step leads into reduction of the metal center and

formation of an $Fe^{+1}$ complex. It should be noted that the dianionic chelate in $(DIP^{2-})Fe^{+2}(N_2)$ undergoes ligand oxidation instead of oxidation of the iron center.

Substitutions at N-aryl moieties, located perpendicular to the plane of the ligand in a complex, would not make prominent changes in electronic structure of the DIP ligands. But any electron withdrawing or electron donating groups in the plane of the DIP ligand, as shown in Figure 1.13, alters the donating and accepting properties of the chelate considerably.

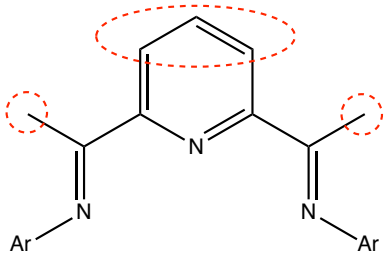


Figure 1.13. Positions which could influence on the electronics of the ligand

Chirik and co-workers have studied the effect of electron withdrawing (EWG) and electron donating groups (EDG) at the pyridine 4-position of the DIP ligand (Figure 1.14).[19]

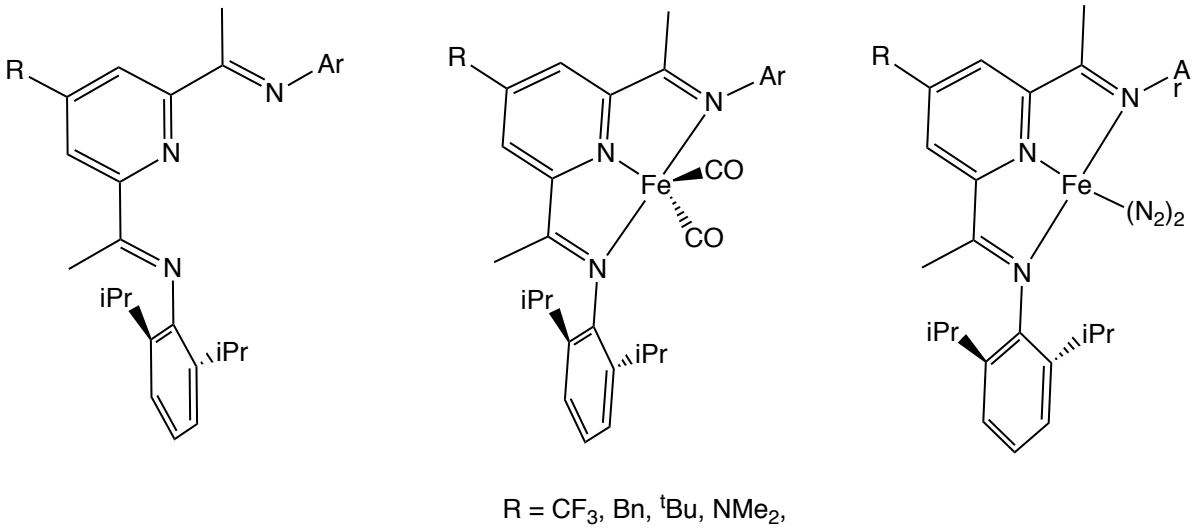


Figure 1.14. Complexes with EWG and EDG on the DIP ligand

In the free ligands, as well as the iron complexes, 4-$CF_3$-$^{iPr}$DIP ligand has the lowest reduction potential. In contrast, as expected, 4-$NMe_2$-$^{iPr}$DIP is the most challenging to reduce.

## 1.4 DIP: Ligand-centered reactions

In addition to accepting electrons in redox processes, as demonstrated above (see Scheme 1.11), the DIP ligand participates in other types of chemical reactions. These reactions usually lead to interruption of the conjugated π system of the ligand either at the pyridine ring or the imine side arms. One consequence is that the modified ligand is less effective at accepting further electrons. The most common types of DIP ligand-centered reactions are:

1) Dehydrogenation of a methylimine side arm

The imine methyl groups appear to be moderately acidic, at least in complexes containing "innocent" DIP ligands, so dehydrogenation (or sometimes loss of a hydrogen atom?) is a relatively common reaction (Scheme 1.12).

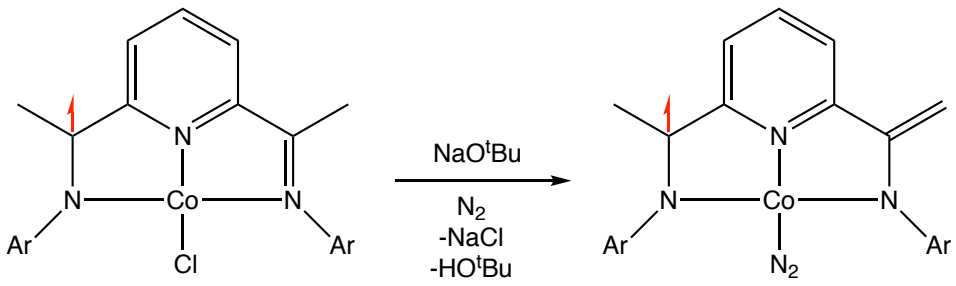


Scheme 1.12. DIP ligand dehydrogenation

It should be noted that the singly dehydrogenated DIP ligand can still accommodate two electrons in its iminopyridine moiety.

2) Depending on the metal center, a dehydrogenated DIP ligand complex often undergoes dimerization (Scheme 1.13):[11b]

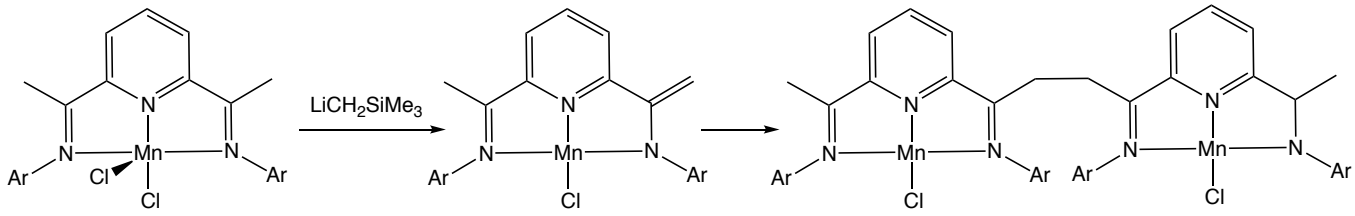


Scheme 1.13. DIP ligand dimerization

This phenomenon "revives" the π system of the ligand and allows the newly formed complex to undergo further redox chemistry.

3) Transfer of an alkyl or hydride to a C or N atom of the ligand backbone.[20]

Alkylated DIP ligands have often been observed in the reaction of alkylating agents (LiR, $MgR_2$, $AlR_3$) with (DIP)M halide complexes. The first step is likely to be substitution of halide by alkyl. It is believed that the accepting feature of the ligand facilitates the M-C bond cleavage (homolysis), producing an organic radical. Depending on factors which have not been fully elucidated, this radical can be released into the solvent (leading to overall 1*e* reduction of the complex),[21] or be transferred to a C or N atom of the DIP backbone. The location to which the alkyl group transfers also varies (Scheme 1.14).

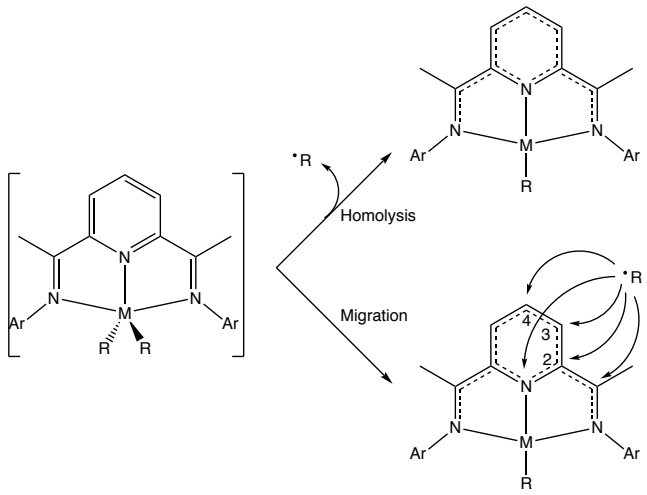


Scheme 1.14. Homolysis vs migration

M-C bond homolysis has mostly been observed for transition metals but the alkyl migration happens for both main group and transition metals. The destination of the transferred alkyl is highly dependent to the type of alkyl, the metal center and the steric properties of the ligand. Alkyl migration in the reaction of $MnR_2$ (R = allyl, benzyl, $CH_2CMe_2Ph$, $CH_2SiMe_3$) with DIP ligands has been exploited in a one-pot selective and direct alkylation of position 4 of the pyridine ring (see Scheme 1.6).

Diorganozinc compounds ($ZnR_2$, R = benzyl or allyl) react with DIP ligands to form 4-benzyl or 4-allyl 1,4-dihydropyridinate complexes.[22] In contrast to Mn complexes, no stepwise alkyl migration can be observed by NMR monitoring of reactions of the $ZnR_2$ fragments with DIP and the final products do not tend to undergo aromatization. Hence, the dihydropyridinato complexes are the most thermodynamically stable in case of zinc. Unexpectedly, when R = $CH_2SiMe_3$ or $CH_2CMe_2Ph$ the expected intermediate complex [(DIP)$ZnR_2$] does not form (Scheme 1.15).

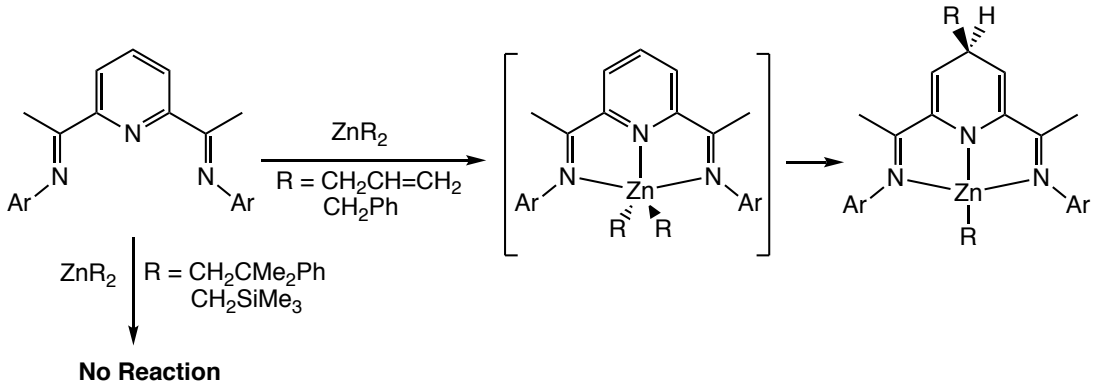


Scheme 1.15. Treatment of $ZnR_2$ with DIP ligand

4) After alkylation at the 4-position, dimerization (of a type different from the above) has been observed for both main group and transition metals (Figure 1.15):[11b, 23]

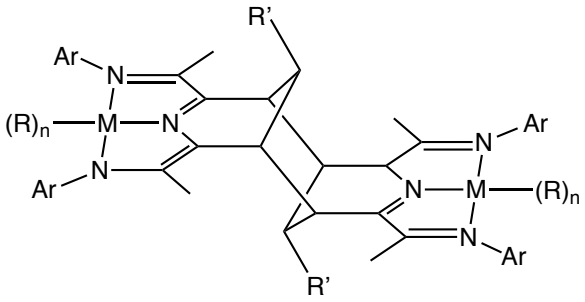


M = Al; n = 2, R = $^{i}$Bu, R' = H
M = Cr; n = 1, R = R' = Bn

Figure 1.15. DIP ligand dimerization

## 1.5 DIP complexes of metal halides

Almost all variations of DIP ligand have been combined with first-row transition metal halides to form relevant complexes. For bulky DIP variations (2,6-disubstituted aryl at N), they are easily synthesized using a 1:1 ratio of the metal halide and the DIP ligand in a range of coordinating and non-coordinating solvents such as THF, acetonitrile, acetone, toluene and *n*-butanol at room temperature (Scheme 1.16).

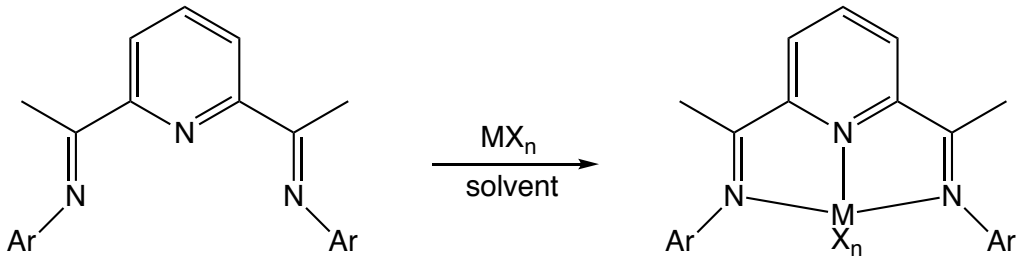


Scheme 1.16. Reaction of $MX_n$ with DIP

Some complexes with second- and third-row metals have also been prepared, but their reactivity has not been explored as extensively.

A series of representative (DIP)$MX_n$ (n = 2, 3, 4) complexes is presented in Table 1.2.

Table 1.2. Synthesized DIP complexes of main group and transition metals

| Entry | $MX_n$/solvent | Entry | $MX_n$/solvent |
|---|---|---|---|
| 1 | $(THF)_3ScCl_3$/toluene[18a] | 11 | $CoCl_2$/THF[24] |
| 2 | $(THF)_3TiCl_3$/THF[17] | 12 | $NiCl_2$ /$CH_3CN$ or THF[25] |
| 3 | $(THF)_3VCl_3$/THF[26] | 13 | $PdCl_2$/EtOH[27] |
| 4 | $(THF)_2CrCl_2$/toluene[28] | 14 | $CuCl_2$/MeOH[29] |
| 5 | $(THF)_3CrCl_3$/acetone[13a] | 15 | $ZnCl_2$/THF[30] |
| 6 | $(THF)_3MoCl_3$/toluene[31] | 16 | $CdCl_2$. 2.5 $H_2O$/ $CH_3CN$[32] |
| 7 | $(THF)_2MnCl_2$/toluene[33] | 17 | $HgCl_2$/$CH_3CN$[34] |
| 8 | $FeCl_2$/*n*-butanol[35] | 18 | $SnBr_2$/toluene-hexane[36] |
| 9 | $GaI_3$/toluene[37] | 19 | $GeCl_2$/DCM[38] |
| 10 | $RuCl_3$/(EtOH:$H_2O$)[39] | 20 | $Re(CO)_5Cl$/toluene[40] |

## 1.6 Stabilization of low-valent metals

In the late 90's, Gibson and Brookhart independently discovered that DIP complexes of $Co^{+2}$ and $Fe^{+2}$ are very active in olefin oligomerization and polymerization.[10] This discovery sparked detailed research in DIP properties and elucidated unexpected facts about their reactivity and their functions in various fields.

Low-valent DIP complexes of primarily first-row transition metals (V,[41] Cr,[28] Mn,[42] Co,[11a] Fe,[18a] Ni,[15c, 43] Cu[44]), but also heavier metals (Mo[45]) and main group metals (Al,[46] Ge[38]) have been synthesized and their electronic structures have been studied experimentally and computationally (Figure 1.16).

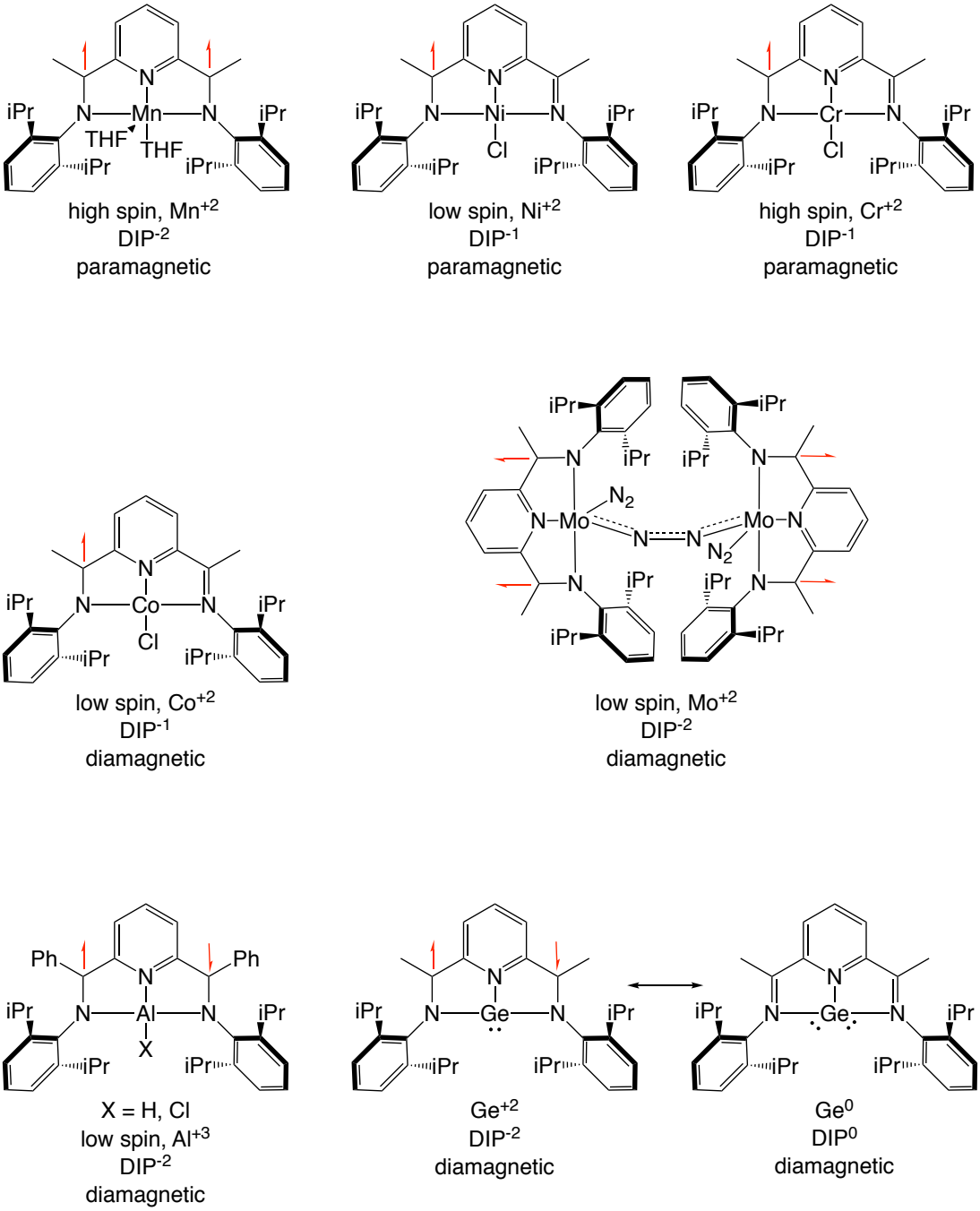


Figure 1.16. A few examples of stabilization by DIP of low-valent metals

Often, the aim of such studies has been to establish whether redox events are ligand- or metal-based.

Usually, alkylation of metal halide complexes of DIP is accompanied by reduction of the ligand. It is proposed that the noninnocent character of the ligand weakens the freshly formed M-C bond by accepting one electron involved in the bond. This leads to easy M-C bond cleavage and release of the alkyl group, most likely as a radical, into the solution (Scheme 1.17).[11c]

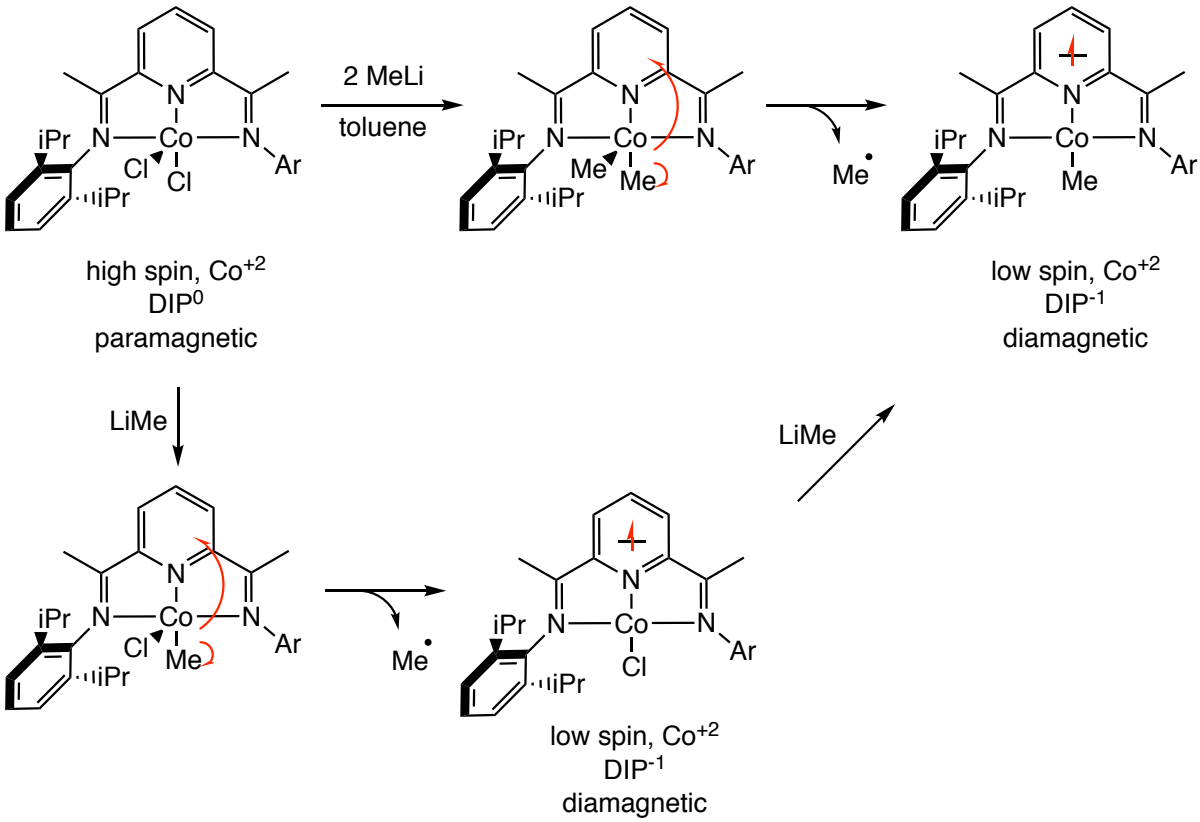


Scheme 1.17. Alkylation/reduction of (DIP)$CoCl_2$

To avoid any unwanted ligand-based reactions, the alkylation of DIP metal halides complexes is often conducted at lower temperatures in non-coordinating solvents.

Because of the prominence of M-C bonds in many catalytic reactions, and the ability of DIP ligands to stabilize low-valent metal complexes, many metal-alkylated DIP complexes with different metals have been synthesized (Figure 1.17).[11a, 12]

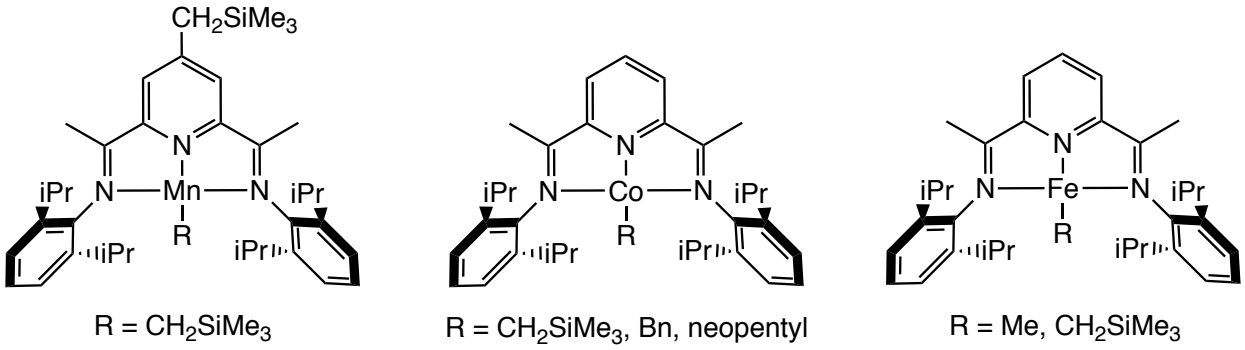


Figure 1.17. A few representative DIP metal alkyl complexes

They have been used in reactions such as hydrogenation,[47] cyclization[11d] and C-C coupling.[11c]

## 1.7 Low-valent DIP complexes: electronic structures

Several electronic structures are conceivable for reduced complexes of DIP. In this thesis, we are mainly concerned with interpreting the molecular electronic structures. Specifically, for reduced complexes the issues are:

- Where are the added electrons (on ligand, on metal, or both)?
- In cases where there is more than one electron, how are they coupled to each other?

Figure 1.18 shows some reasonable-looking electronic structure alternatives for formally $M^{+3}$, $M^{+2}$, $M^{+1}$ and $M^{0}$ complexes.

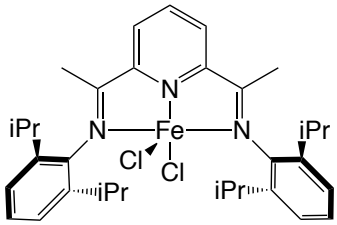


high spin, $Fe^{+2}$
$DIP^{0}$
S = 2

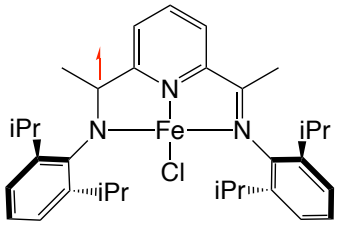


high spin, $Fe^{+2}$
$DIP^{-1}$
S = 3/2

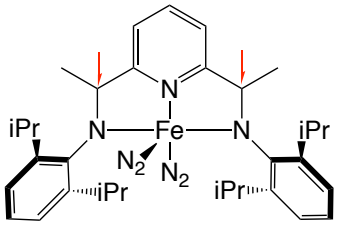


intermediate spin, $Fe^{+2}$
$DIP^{-2}$
S = 0

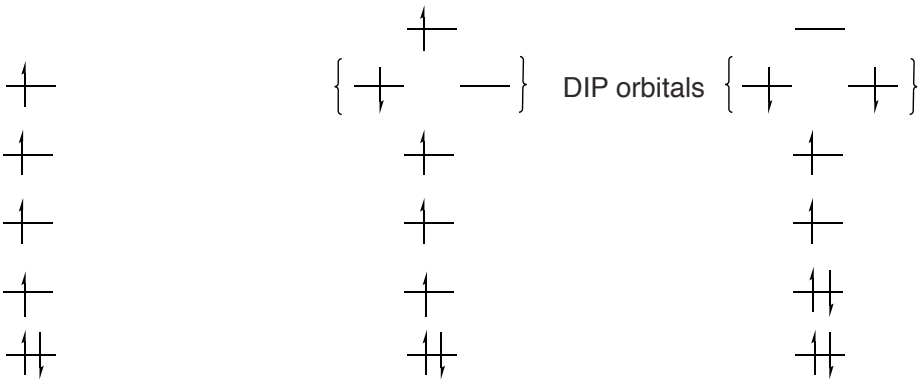


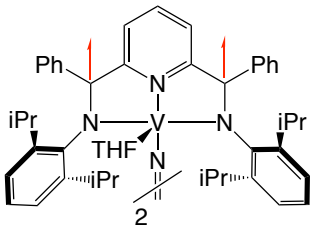


high spin, $V^{+3}$
$DIP^{-2}$
S = 2

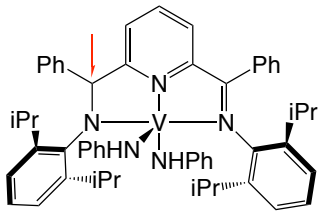


high spin, $V^{+3}$
$DIP^{-1}$
S = 1/2

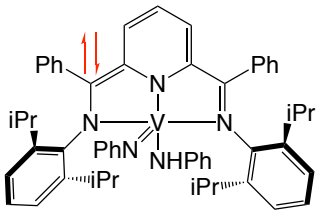


$V^{+5}$
$DIP^{-2}$
S = 0

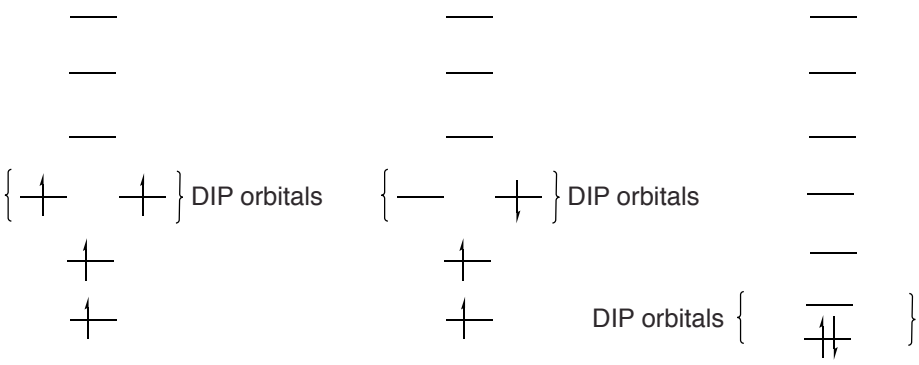

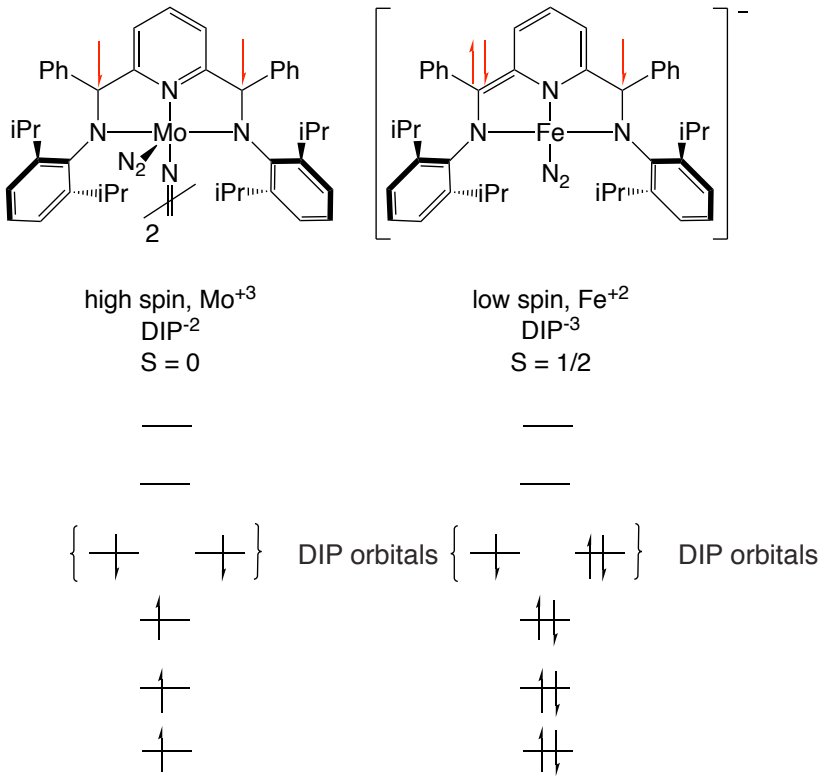


Figure 1.18. Electronic structures of the low valent DIP complexes

In complexes with mono- or dianionic ligands, depending on the system (mostly metal and oxidation state), antiferromagnetic coupling between ligand and metal unpaired electrons may stabilize the product. For example, the precursor complex ($^{iPr}$DIP)$FeCl_2$ is high spin ($d^6$, $S_{Fe} = 2$) with a neutral $DIP^0$.[18a] The electronic structure of the one-electron reduced complex ($^{iPr}$DIP)FeCl is best described as a high spin $Fe^{+2}$ ($d^6$, $S_{Fe} = 2$), antiferromagnetically coupled to a monoanionic $DIP^-$ ($S_{DIP} = ½$). Similarly, in the two-electron reduced complex ($^{iPr}$DIP)$Fe(N_2)_2$, an intermediate spin $Fe^{+2}$ ($d^6$, $S_{Fe} = 1$), antiferromagnetically couples to a triplet diradical $DIP^{2-}$ ($S_{DIP} = 1$). As a result, the complex appears to be diamagnetic. More examples are shown in Figure 1.18.

In another example in Figure 1.19, two-electron reduction of ($^{iPr}$PhDIP)$AlCl_3$ gives ($^{iPr}$PhDIP)AlCl in which the ligand is dianionic, $DIP^{-2}$.

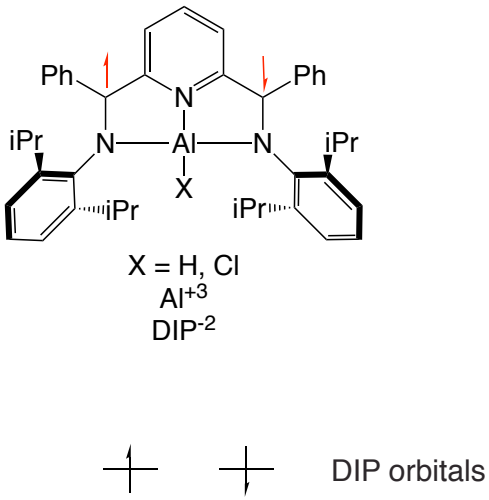


Figure 1.19. Electronic structure of (DIP)AlX

In this complex, the Al center is +3 ($S_{Al}$ = 0) and the two electrons in the ligand π∗ orbitals are antiferromagnetically coupled, ($S_{DIP}$ = 0).[46b]

## 1.8 Applications of DIP complexes

Low-valent first row transition metal complexes stabilized by DIP ligands have found a number of applications. This is mainly because of the electron reservoir properties of the DIP ligand which enables the ligand to be either a source or a sink for electrons.

In a study of DIP vanadium complexes,[11e] (DIP)$VCl_3$ was reduced under an atmosphere of $N_2$ which resulted in $N_2$ fixation and reduction to a dianionic DIP ligand. The reducing power of the electrons residing in the ligand π system was sufficient to break single and double bonds in azobenzene, molecular oxygen and $S_8$ (Scheme 1.18).

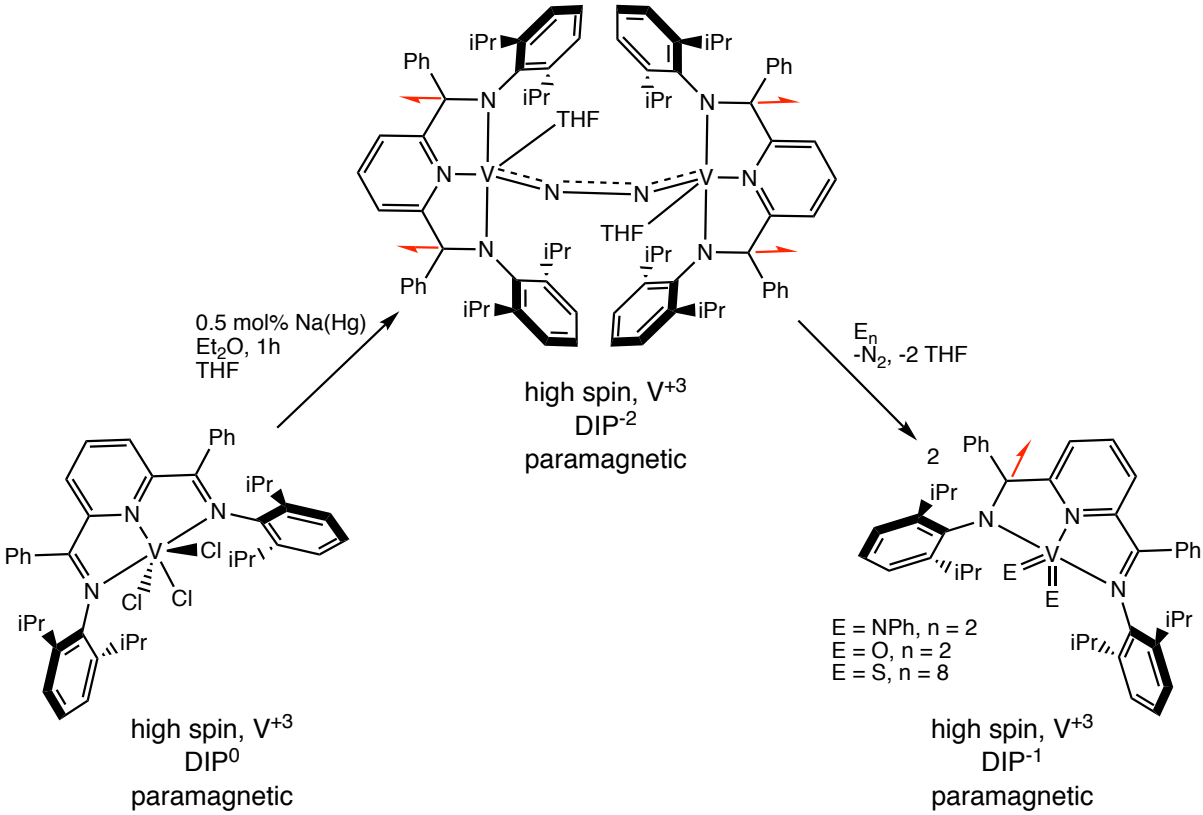


Scheme 1.18. Single and double bond cleavages

The two-electron reduced DIP iron dinitrogen complex has been shown to be highly active in a variety of catalytic reactions such as hydrogenation,[11f, 18a] hydrosilylation[11f, 48] and cycloaddition of dienes.[11d] A representative example of selective anti-Markovnikov alkene hydrosilylation using tertiary silanes under mild conditions is shown in Scheme 1.19.

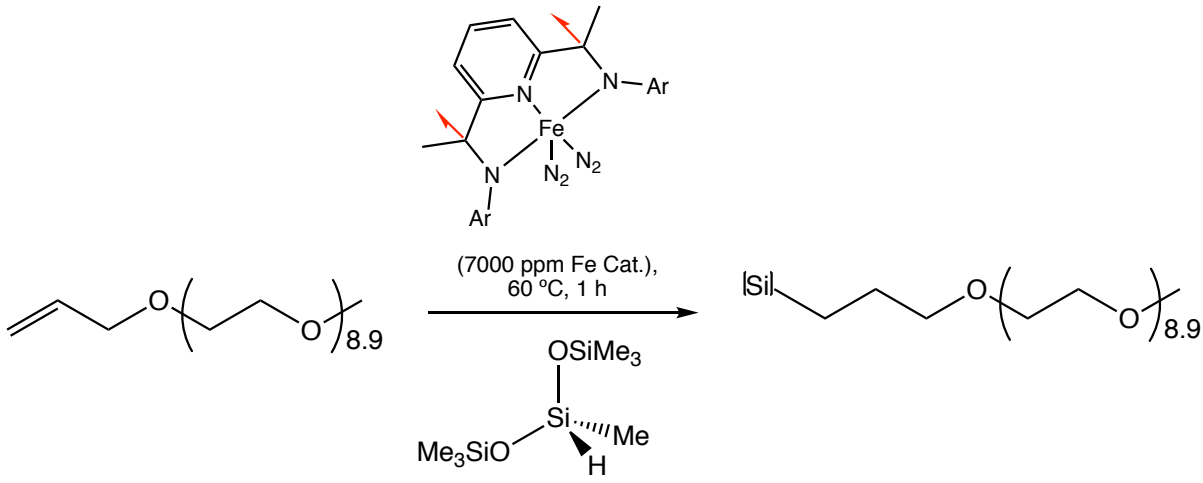


Scheme 1.19. Selective anti-Markovnikov alkene hydrosilylation

Addition of silicon hydride (Si-H) to olefins (C=C bond) is one of the largest-scale industrial applications of homogeneous catalysis. For years, complexes of precious metals (Pt and Rh) have been used for such important conversions. Despite their widespread use, precious metals are rare and toxic which makes the production costly. Earth-abundant metal catalysts, such as DIP iron dinitrogen complexes, were shown to be good candidates to replace precious metals, although the high oxygen sensitivity of reduced complexes can be a problem.

## 1.9 Chemical Reactivity of DIP ligands

In addition to electron transfer, DIP complexes undergo other types of chemical reactions. Dehydrogenation and alkylation were mentioned above. Another interesting example, observed with a low-valent nickel complex, is ligand oxidation to an amide (Scheme 1.20) involving C-C bond cleavage.[15b]

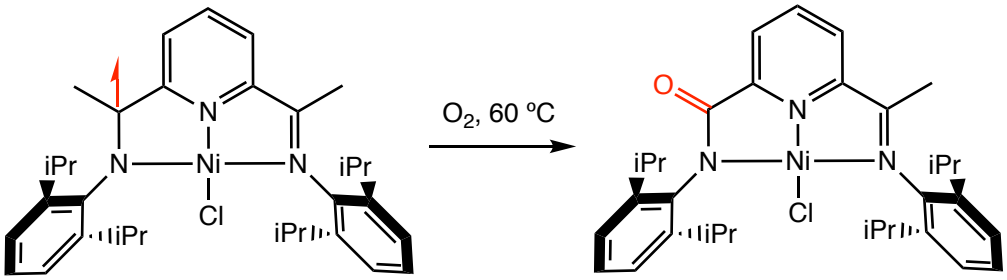


Scheme 1.20. DIP-based reaction

The mechanism is unknown, but it seems reasonable to assume that unpaired electron density at the imine carbon would be a factor activating the ligand for attack by $O_2$.

## 1.10Metal-ligand cooperation

The cooperative effect between the DIP ligand and the metal center is not restricted to transition metals. In a reaction between a doubly reduced aluminum complex and aniline, one of the imine nitrogens in the ligand gets protonated and the anilide that is produced coordinates to the Al center. One molecule of hydrogen as one of the products is released and the conjugated π system of the ligand is revived (Scheme 1.21).[46b]

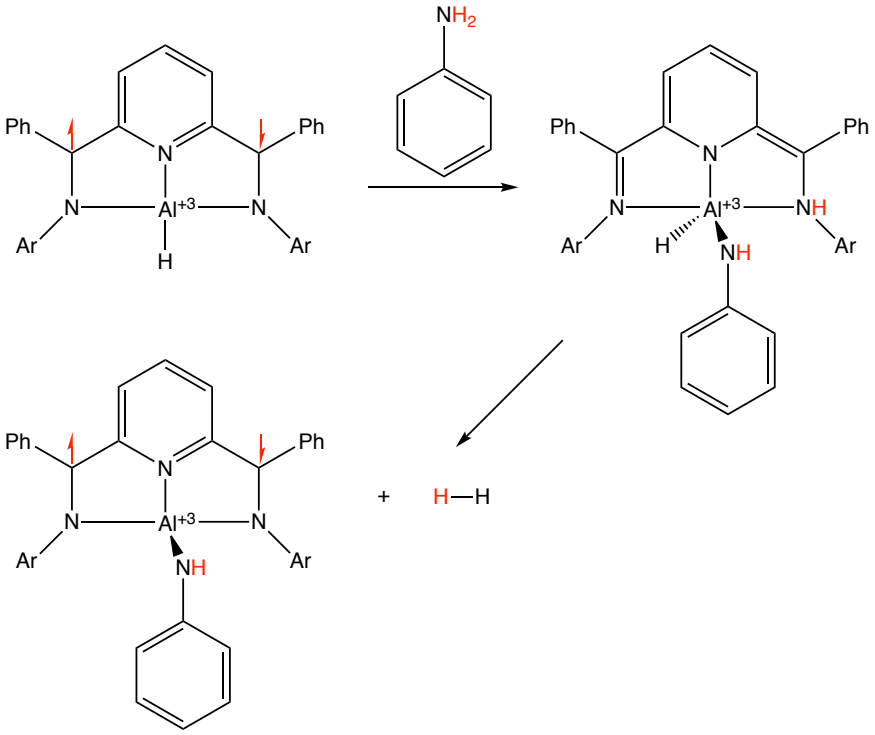


Scheme 1.21. Metal-ligand cooperation

## 1.11 Simpler ligands: α-Diimines

The α-diimine ligand can be viewed as "half" a DIP ligand, or as the bidentate analog of tridentate DIP. It has a less extended π system and can accept two electrons in its single low-lying π* orbital. Like in DIP ligands, 2,6-disubstituted aryl groups at N would be approximately perpendicular to the plane of the molecule and have minimal electronic effects on the active site of the molecule. α-Diimine ligands have been used to stabilize many first-row transition metals in unusually low formal oxidation states. An interesting application is the catalytic activity of an α-diimine nickel complex in the hydrosilylation of olefins (Scheme 1.22).[49]

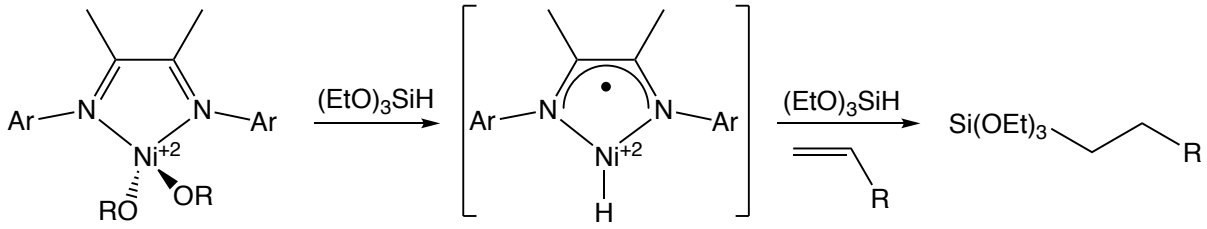


Scheme 1.22. Application of α-Diimine nickel complexes in hydrosilylation of olefins

The noninnocent character of the α-diimine ligand plays a crucial role in this conversion by stabilizing the formally $Ni^{+1}$ active species.

Iminopyridine is another bidentate analog of DIP, a hybrid of aromatic 2,2′-bipyridine and α-diimine. An example of its noninnocent behavior is the stabilization of aluminium complexes in which the reduction exclusively happens at the ligand rather than the metal center (Scheme 1.23).[50]

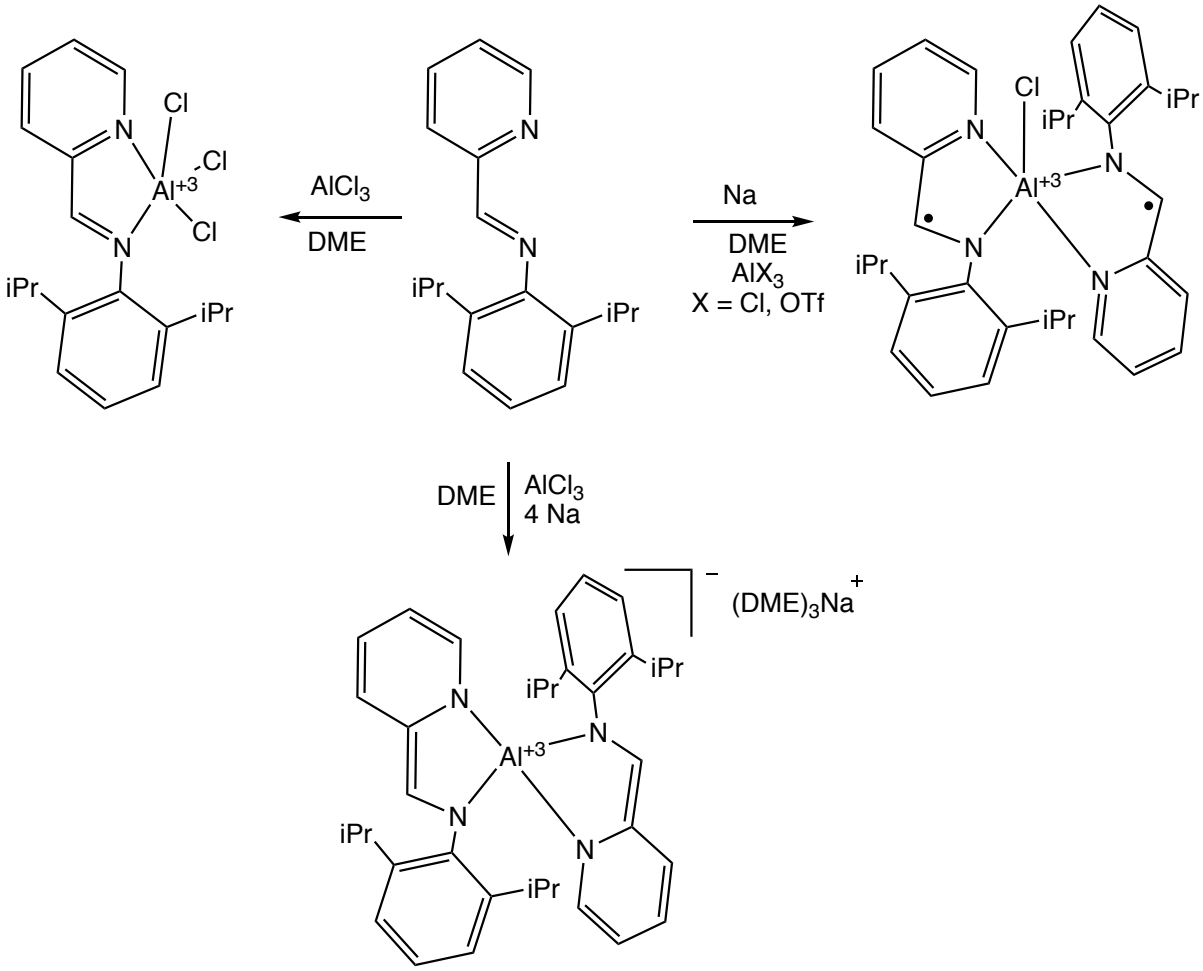


Scheme 1.23. Noninnocent character of iminopyridine ligand

## 1.12 DIP Complexes in Polymerization

Combinations of the variations of the DIP ligand with almost all of the first-row transition metals (Ti-Cu) have been tested in olefin oligomerization and polymerization. Brookhart and Gibson, in their first independent reports on the activity of DIP complexes of iron and cobalt in polymerization of ethene and propene, showed that the steric hindrance of the ligand at the N-aryl groups plays a prominent role in determining polymer molecular weight.[10] They showed unprecedented activities for those metals, in some case as high as those of the most efficient metallocenes. Reduction of the size of the phenyl substituents facilitates termination reactions. For example, DIP iron complexes bearing only a single *o*-alkyl substituent at each

N-aryl group are good catalysts for ethene oligomerization and acetylene cyclotrimerization. Analogous complexes with bulkier substituents at both *ortho* positions are effective at catalyzing acetylene and ethene polymerization (Figure 1.20).

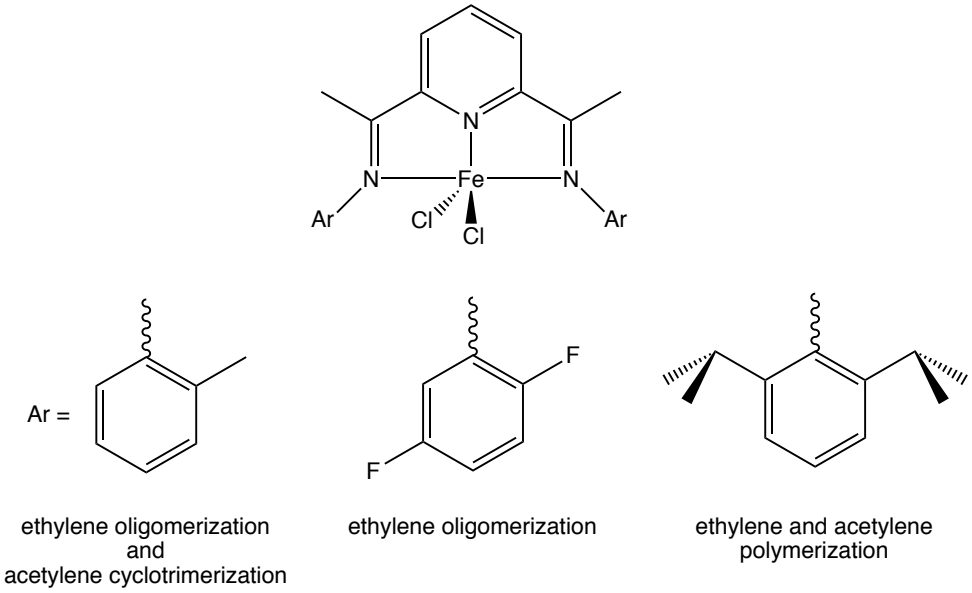


Figure 1.20. Influence of ligand steric properties on polymerization

Unfortunately, the activity of DIP complexes of late transition metals with moderate size substituents at the phenyl groups diminishes at elevated temperatures, and the molecular weights of the products decrease. This has been ascribed to a variety of chain termination processes (including β-elimination and C-H bond activation of the N-aryl substituent) as well as to reduced solubility of ethene at higher temperature.[51, 52] Various strategies towards more robust catalysts have been explored, such as having a single bulky substituent at one imine nitrogen. Catalysts have been heterogenized on $MgCl_2$, calcosilicate and carbon nanotubes to good effect.

Generally, iron complexes are more active than cobalt complexes but with iron complexes products with a wider range of molecular weights are produced. DIP complexes of nickel are

much less active and mainly oligomers are generated. Among the first-row transition metals, manganese showed no activity. $Cr^{+3}$-based precatalysts are promising because they show single-site character and encouraging thermal stability. $V^{+3}$ complexes have displayed high activity but exhibit multi-site behaviour, particularly at elevated temperatures. Calderazzo and co-workers showed that the activity of the bulky DIP complexes of $Ti^{+4}$ and $Zr^{+4}$ in polymerization reactions is the same order of magnitude as $TiCl_4$ and $ZrCl_4$.[53] They attributed this behavior to a bidentate rather than a tridentate coordination mode of the ligand. This change in coordination is ascribed to the weak imine nitrogen interaction with early transition metals and the neutral charge of the chelate. Ligands with smaller N-aryl fragments display high activity in branched polymerization.

DIP complexes have shown to be promising catalysts for ethene polymerization but less effective in promoting oligomerization. Also, they are less active catalysts for the polymerization and oligomerization of propene compared to ethene. Overall, both the choice of the metal and the specific variation of the DIP ligand play significant roles in the catalytic activity and the nature of the products (polymers vs oligomers).

## 1.13 Polymerization Mechanism: Late Transition Metals

Since polymerization is not very relevant to this thesis work, it will not be discussed in detail here. Neutral (DIP)FeR and (DIP)CoR complexes without added activators are inactive (although (DIP)CoR is active in olefin hydrogenation catalysis).[47] Gibson has repeatedly suggested involvement of $Fe^{+3}$ active species in iron catalysis,[51, 54] and a computational study based on this assumption produced results compatible with experiment.[55] However, one would expect easy reduction of $Fe^{+3}$ to $Fe^{+2}$ or lower by Al alkyls. More complicated species containing Al alkyl or MAO units have also been proposed[56] but proving their involvement in

catalysis is not easy. At present, the simplest and most natural assumption seems to be that of a (DIP)$MR^+$ active species (Figure 1.21).[57]

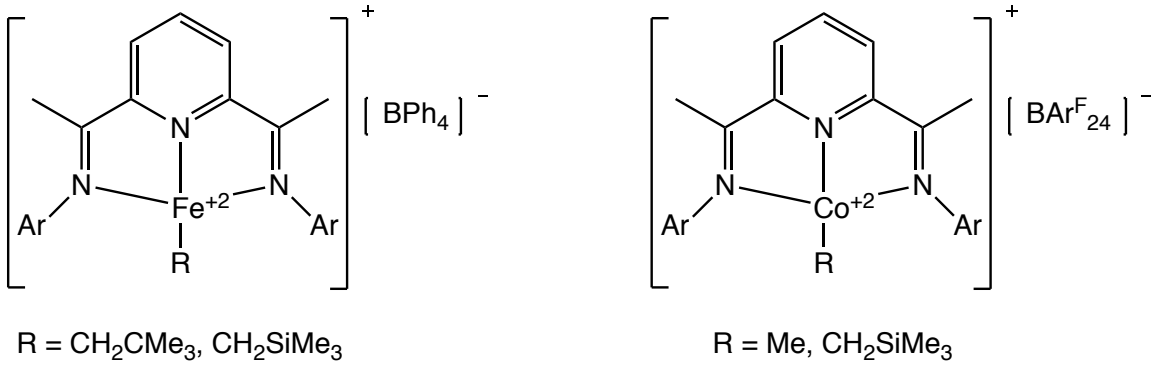


Figure 1.21. Proposed active sites for (DIP)M (M = Co, Fe) polymerization catalysts

## 1.14 Characterization Techniques

As mentioned above, the non-innocence character of the DIP ligand in a complex makes the oxidation states of both the metal and the ligand ambiguous. Hence, a combination of techniques is necessary to elucidate the molecular and electronic structure of the synthesized complexes of DIP ligands. In this thesis, a variety of spectroscopic techniques such as NMR, EPR, XPS and XRD have been used.

### 1.14.1 NMR

NMR spectroscopy is a frequently used technique in determination of organic and organometallic compounds. This technique provides information about the number of magnetically different atoms and their immediate environment of the type being analyzed. It allows to study the dynamic behavior of compounds in solution, inter- and intramolecular interactions and chemical exchanges happening in the solution. In addition, mixtures of compounds and their ratios, and existence of any impurities in the whole sample can be

obtained by an NMR experiment. The nuclei with a property called *spin* are active in NMR. Generally, a nucleus which possesses an odd mass number, odd atomic number, or both has quantized spin angular momenta and magnetic moments. Nuclei such as $^{1}H$, $^{2}H$, $^{13}C$, $^{17}O$, $^{19}F$ and $^{14}N$ possess spin ($I \neq 0$) and the number of allowed spin states can be calculated by $2I+1$.[58]

A spinning hydrogen nucleus, as a positively charged particle, generates a magnetic moment (μ). In the absence of an external magnetic field, hydrogen nuclei take equally +1/2 and -1/2 spin. However, in an applied magnetic field a hydrogen nucleus may have a +1/2 or -1/2 spin and μ in the two cases are in the opposite directions (Figure 1.22).

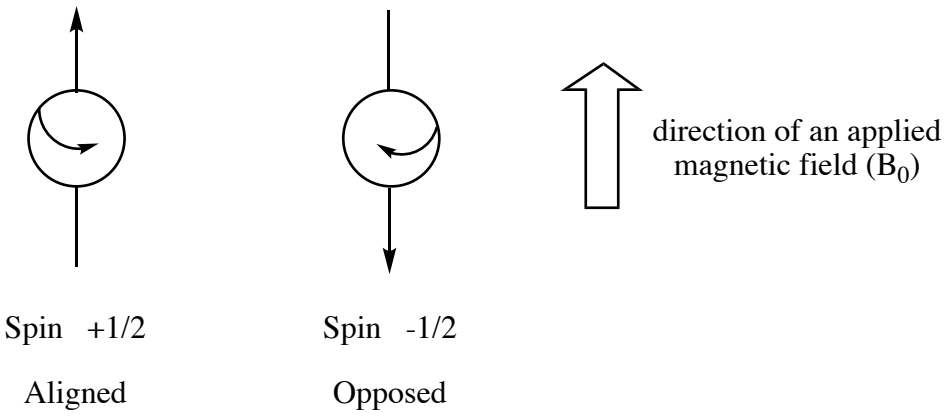


Figure 1.22. Proton spin states in the presence of a magnetic field.

There is the energy gap E= hν between the two spin states in the external magnetic field. Since the gap is small the thermal energy at room temperature is enough to populate both spin states. However, the population of the lower state is in slight excess, proportional to the magnitude of the applied magnetic field.

In the presence of the magnetic field, the nucleus starts to precess about its spin axis with angular frequency ω, known as *Larmor frequency*. This generates an electric field of the

same frequency. If the frequency of the electric field component of the radiation matches the Larmor frequency, the two fields can couple, and the energy will be transferred to the nucleus which cause the spin flip of those excess spins in the lower energy state (Figure 1.23). This process is called resonance. The NMR signal will be recorded when the spin returns to the lower energy state through relaxation processes.

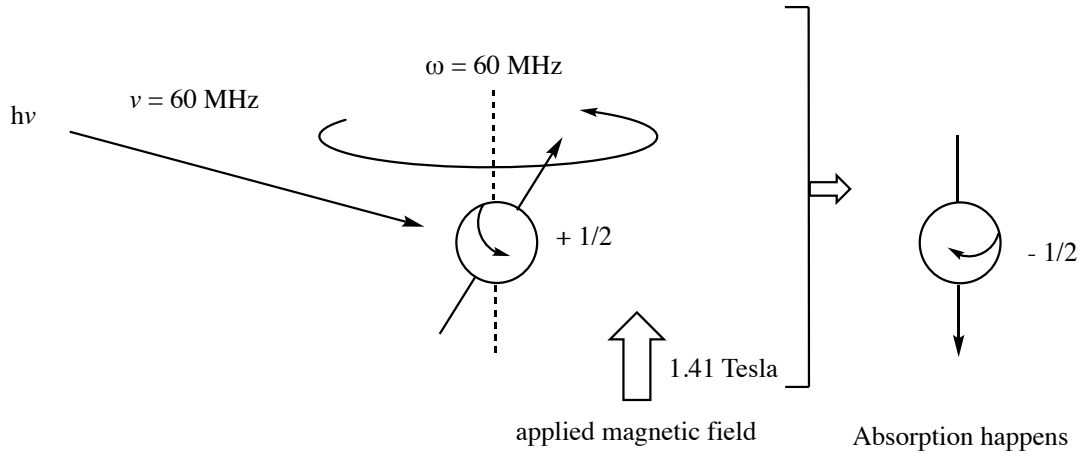


Figure 1.23. The nuclear magnetic resonance process; $\nu = \omega$.

## 1.14.2 NMR Spectroscopy of dynamic systems

NMR is one of the most important characterization techniques used in the present study. One particularly interesting application is in the study of dynamic (fluxional) systems.[59] Dynamic behavior can be observed in fluxional molecules in which some or all of the atoms swap between symmetry-equivalent (or symmetry-inequivalent) positions. Generally, line-broadening, field and temperature dependency and a too simple or too complicated spectrum for an expected structure can be indications for a dynamic process. In a fluxional molecule, alternative structures or conformations usually interconvert at a rate comparable to the NMR timescale and the frequency differences between relevant peaks in the NMR spectrum. The

spectrum is temperature-dependent because the rate of interconversion varies with temperature.

For any dynamic process, there are three important temperature regions. At a sufficiently low temperature, the system is said to be at the "slow exchange limit". In this situation, spectra will display distinct signals for the various species undergoing exchange. This is the case when (for a simple system of two exchanging nuclei):

$\kappa = 1/t \ll \pi\Delta\upsilon/\sqrt{2}$

$\kappa$ = the exchange rate ($s^{-1}$)

t = the exchange time (s)

$\Delta\upsilon$ = the NMR chemical shift separation of peaks ($s^{-1}$)

Spectra recorded at high temperature can be assigned to the “fast exchange limit” where a weighted average resonance is observed for the exchanging partners. In this case the rate constant is much larger than the relevant shift difference:

$\kappa \gg \pi\Delta\upsilon/\sqrt{2}$

In between those two limits, at a temperature called the coalescence temperature the appearance of the spectrum modifies from those two separate signals (at low temperature) to that of a single, flat-topped signal. At this temperature:

$\kappa \approx \pi\Delta\upsilon/\sqrt{2}$

It should be noted here that for a molecule having several exchanging groups there normally is not a single coalescence temperature. Instead, every exchanging pair has its own coalescence point. In any case, the rate at the coalescence point can be used to derive a free energy of activation for the process via the classical transition state theory expression:

$$k = (k_B T/h) \exp(-\Delta G^{\dagger}/RT)$$

It is also possible to extract rates as a function of temperature through fitting of simulated to observed spectra. Rates obtained this way can be used in an Arrhenius plot (ln (k/T) vs 1/T) to obtain separate values for the enthalpy and entropy of activation.

One of the famous examples[60] of fluxional molecules is iron pentacarbonyl ($Fe(CO)_5$) with trigonal bipyramidal geometry which undergoes dynamics through Berry pseudorotation.[61] In this pseudorotation, the two axial carbonyls exchange with two equatorial ones, re-forming the starting compound with the same symmetry (Figure 1.24).

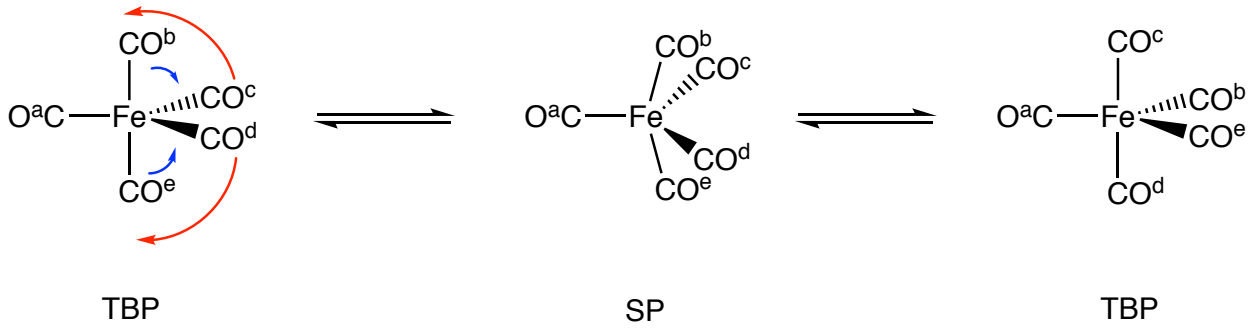


Figure 1.24. Berry pseudorotation in trigonal bipyramidal geometry of $Fe(CO)_5$

At lower temperatures, two signals (in a 2:3 ratio) are observed by $^{13}$C-NMR, whereas at elevated temperatures only one signal can be observed.

### 1.14.3 EPR

EPR spectroscopy has a limited use compared to NMR spectroscopy as it is used to analyze paramagnetic compounds. In contrast to some other techniques such as fluorescence which may give indirect evidence of free radicals, EPR detects unpaired electrons unambiguously. The technique provides information about the environment of the unpaired electron since interactions of the magnetic fields of the neighboring nuclei with the magnetic field of the unpaired electron give valuable information about the environment of the electron and identity of the compound.[62]

In EPR, electron transitions are detected in an applied magnetic field rather than nuclear transitions in NMR. Like a proton, an electron has a spin, which gives it magnetic moment and by spinning about its axis generates a magnetic field which is much greater than a proton. By supplying an external magnetic field, the electron spins rotate align or opposite to the direction of the magnetic field which lead into two distinct energy levels. As in NMR, there will be a slight excess of electrons in the lower level parallel to the direction of the external magnetic field. When a specific strength of the applied magnetic field is exactly match with the fixed frequency of microwave absorption will happen. The transition between these two levels is measured and recorded as a signal.

### 1.14.4 XRD

In this thesis, X-ray crystallography has been used to characterize the three-dimensional structures of many synthesized titanium, zirconium and hafnium complexes. This technique is one of the important tools in determination of the oxidation state of the metal and the ligand by measuring the bond lengths around the metal and within the ligand. In addition, X-

ray crystallography elucidates the geometry around the metal center and identifies the nature of the complex (ionic or neutral, monomer or dimer).

A diffractometer is equipped with an X-ray (electromagnetic wave) source such as copper (1.54 Å) or molybdenum (0.71 Å), a goniometer to hold the crystal and a detector to record the scattered beams with various intensities and angles. When an incident X-ray beam hits the atoms in the single crystal, it diffracts in many specific directions. Primarily, scattering happens through the atoms′ electrons. This phenomenon as known as an elastic scattering since the energy of the scattered beam equals to the energy of the incoming beam. Although, most of scattered beams cancel each other out via destructive interference, those beams in a few specific directions add up constructively (constructive interference) based on the Bragg′s law[63] (Figure *1.25*):

$$2d \sin \theta = n\lambda$$

where $d$ is the space between lattice planes, $\theta$ is the incident beam angle, $n$ is an integer and $\lambda$ is the wavelength of the beam.

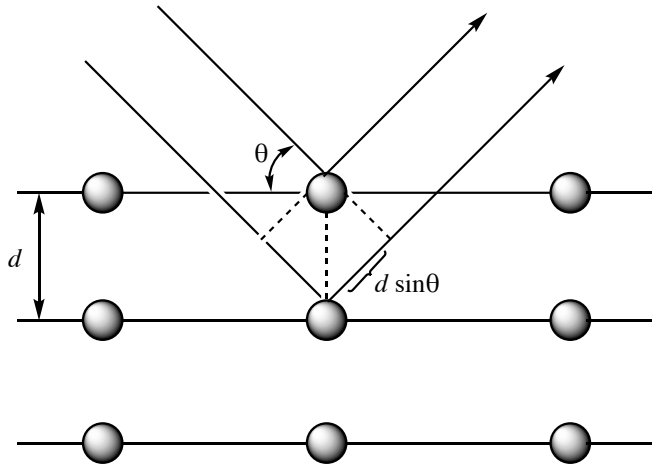


Figure 1.25. An illustration of the Bragg's law.

By rotating the crystal using the goniometer, all orientations of the sample are exposed to the X-ray beam. Each orientation has its specific diffraction image containing thousands of reflections. As the crystal is slowly rotated, the diffraction image in that specific angle disappears and a new diffraction image for the new angle appears. All the reflections intensities in each image will be recorded. Peak intensity has a direct correlation with the atoms′ electron density (the higher the electron density, the more intense the reflection peak). When the data collection is finished, using the mathematical method of Fourier Transform, the two-dimensional images are converted into a three-dimensional model of the density of electrons in the crystal. These data are used to produce and refine a model of arrangement of atoms in the crystal.

### 1.14.5 XPS

In contrast to the above mentioned techniques, in which the whole sample is needed for analysis, in the XPS technique only the surface of the sample is analyzed. An XPS spectrum is attained by irradiating of the X-ray beams at the surface of the sample being analyzed while concurrently measuring the kinetic energy and number of electrons that escape from the top 0-12 nm of the sample.[64] Since the energy of an X-ray with specific wavelength is known ($E_{photon}$) and the kinetic energies of the emitted electrons ($E_{kinetic}$) are measured, the binding energy of each electron can be achieved by:

$$E_{binding} = E_{photon} - (E_{kinetic} + \phi)$$

where $\phi$ is work function dependent on both material and the spectrometer. A schematic view of the XPS analysis is shown in Figure 1.26.

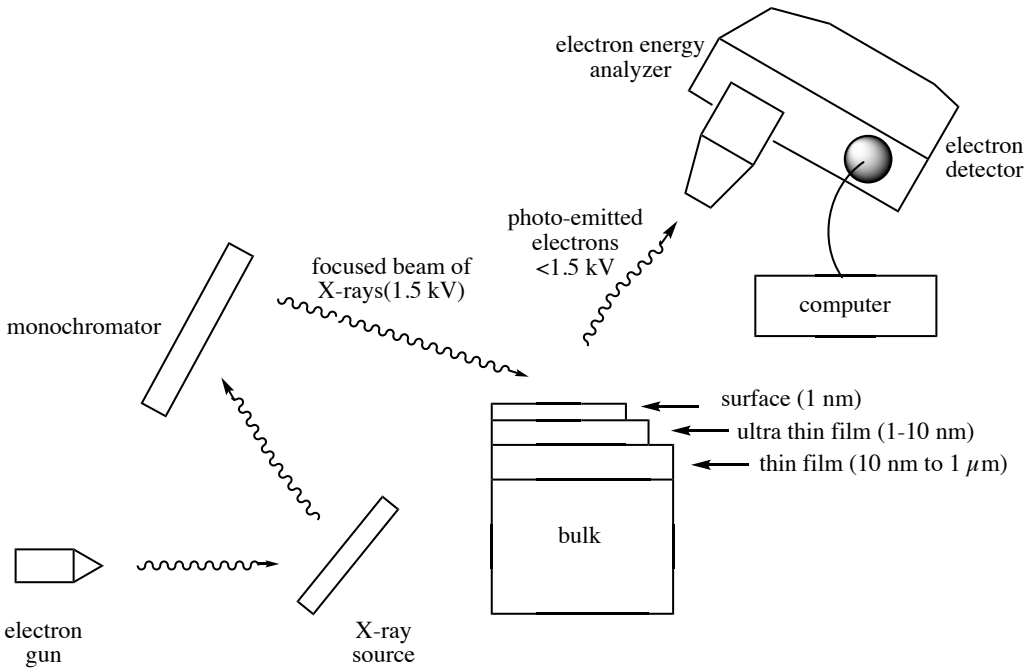


Figure 1.26. A schematic view of an XPS analysis.

Thus, an XPS spectrum is a plot of the number of detected electrons versus the binding energy of the detected electrons. Each element has a characteristic set of XPS signals with characteristic binding energies which directly identify the element in or on the surface of the sample. These characteristic signals are because of the electronic configuration within the element and the number of detected electrons in each signal directly gives the amount of that element on the surface. At the beginning of many XPS analysis, a wide scan (low energy resolution) is done to discover the types and amounts of elements and their binding energies on the top surface of the sample. Then, a narrow scan (high energy resolution) is done to detect the electronic and chemical states of atoms and measure each layer′s thickness.

XPS is routinely used to analyze organic and inorganic compounds, catalysts, metal alloys, paints, woods, polymers, glasses, and etc. This technique is capable to determine:

- Electronic states of elements and the amount of those elements within the top 1-12 nm of the surface

- Chemical states of one or more elements and their bonding environment
- Contamination, if any exists, on the top surface
- Thickness of one or two thin layers (1-8 nm)
- Empirical formula of the surface of the sample

## 1.15 Alternative technique

### 1.15.1 High energy X-ray

High-energy X-rays (HEX-rays) have typical energies of 30–1000 keV , about one order of magnitude higher than conventional X-rays (and well into gamma-ray energies over 120 keV).[65] They have the benefit of large penetration depth into substances which makes them useful as an analysis method for thick samples and mm-sized samples. Where oxidation happens only on the surface, use of HEX-rays allows an in-air sample environment and operation. Applying HEX-rays, even under heavy and compressed sample environment, highest resolution single crystal characterization can be achieved by using triple axis diffractometry and reciprocal space mapping. There are several advantageous of HEX-rays (100-300 KeV) over the conventional hard X-rays (5-20 KeV):

- High penetration into materials
- Up to ten times smaller curvature of the Ewald sphere compare to that in the low energy case which permits whole regions to be mapped in a reciprocal lattice.
- Access to high-energy spectroscopic levels, both electronic and nuclear
- Trivial polarization consequences because of relative small scattering angles

The scope of applications of HEX-rays is broad. Only a few of them are listed below:

- Structure of metals, liquids and ceramics can be investigated. Phase transitions, recrystallization, twinning and domain formation can be monitored in an experiment.
- In situ studies of materials which undergo chemical changes in chemical environments (e.g. electrodes in batteries)
- Thick layers can be analyzed where classical reflectometry experiments are not useful.
- Where conventional X-rays are only used for near-surface regions due to limited penetration, bulk studies in single crystals can be done by HEX-rays.
- Deformation, phase transition or annealing can be studied as a function of time.

While this approach looks promising, no HEX-ray studies of diiminopyridine complexes have been reported so far.

## 1.16 Organization of the thesis

This thesis begins with an introduction chapter in which the background of the DIP ligand, its role in various chemical reactions and the reactivity of its complexes are provided. In Chapter 2, the synthesis, electronic structure and NMR study of a series of mono- and dialkyl complexes of titanium of DIP is presented. Chapter 3 is about the reactivity of the synthesized titanium complexes and a few examples of the ligand-based reactions have been reported. Exploring the noninnocence character of the DIP ligand in combination with zirconium and hafnium is collected in Chapter 4. The reactivity of DIP with tetra alkyl zirconium and hafnium has been discussed in the same chapter. Outlook and conclusions are provided in Chapter 5. The CIF files of the crystal structures have been collected in one file. It is mentioned in Chapter 6 that it is uploaded to MSpace. The last chapter, Chapter 7, is the

supporting information (SI) which consist of all the $^{1}H$- and $^{13}C$-NMR data for the synthesized complexes.

## 1.17 References


1. Jørgensen, C. K., Differences between the four halide ligands, and discussion remarks on trigonal-bipyramidal complexes, on oxidation states, and on diagonal elements of one-electron energy. *Coord. Chem. Rev.* **1966,** *1* (1), 164-178.

2. Eisenberg, R.; Gray, H. B., Noninnocence in Metal Complexes: A Dithiolene Dawn. *Inorg. Chem.* **2011,** *50* (20), 9741-9751.

3. Ringenberg, M. R.; Kokatam, S. L.; Heiden, Z. M.; Rauchfuss, T. B., Redox-Switched Oxidation of Dihydrogen Using a Non-Innocent Ligand. *J. Am. Chem. Soc.* **2008,** *130* (3), 788-789.

4. Heyduk, A. F.; Zarkesh, R. A.; Nguyen, A. I., Designing Catalysts for Nitrene Transfer Using Early Transition Metals and Redox-Active Ligands. *Inorg. Chem.* **2011,** *50* (20), 9849-9863.

5. Que Jr, L.; Tolman, W. B., Biologically inspired oxidation catalysis. *Nature* **2008,** *455*, 333.

6. King, E. R.; Hennessy, E. T.; Betley, T. A., Catalytic C−H Bond Amination from High-Spin Iron Imido Complexes. *J. Am. Chem. Soc.* **2011,** *133* (13), 4917-4923.

7. Agrifoglio, G.; Reyes, J.; Atencio, R.; Briceño, A., 2,6-Bis[1-(2-isopropyl-phenyl-imino)-ethyl]-pyridine. *Acta Crystallogr. Sect. Sect. E: Struct. Rep. Online* **2008,** *64* (Pt 1), o28-o29.

8. (a) Orrell, K. G.; Osborne, A. G.; Šik, V.; Webba da Silva, M., Stereochemically non-rigid transition metal complexes of 2,6-bis[(1-phenylimino) ethyl]pyridine (BIP) part 1. Dynamic NMR studies of [M(C6F5) 2(BIP)] (M = PdII or PtII). *J. Organomet. Chem.* **1997,** *530* (1), 235-246; (b) Reeske, G.; Cowley, A. H., Direct reactions of tellurium tetrahalides with chelating nitrogen ligands. Trapping of TeI2 by a 1,2-bis(arylimino)acenaphthene (aryl-

BIAN) ligand and C-H activation of an [small alpha],[small alpha][prime or minute]-diiminopyridine (DIMPY) ligand. *Chem. Commun.* **2006,** (46), 4856-4858.

9. Figgins, P. E.; Busch, D. H., Complexes of Iron(II), Cobalt(II) and Nickel(II) with Biacetyl-bis-methylimine, 2-Pyridinal-methylimine and 2,6-Pyridindial-bis-methylimine. *J. Am. Chem. Soc.* **1960,** *82* (4), 820-824.

10. (a) Small, B. L.; Brookhart, M.; Bennett, A. M. A., *J. Am. Chem. Soc.* **1998,** *120*, 4049; (b) J. P. Britovsek, G.; C. Gibson, V.; J. McTavish, S.; A. Solan, G.; J. P. White, A.; J. Williams, D.; J. P. Britovsek, G.; S. Kimberley, B.; J. Maddox, P., Novel olefin polymerization catalysts based on iron and cobalt. *Chem. Commun.* **1998,** (7), 849-850.

11. (a) Kooistra, T. M.; Knijnenburg, Q.; Smits, J. M. M.; Horton, A. D.; Budzelaar, P. H. M.; Gal, A. W., Olefin Polymerization with [{bis(imino)pyridyl}CoIICl2]: Generation of the Active Species Involves CoI. *Angew. Chem. Int. Ed.* **2001,** *40* (24), 4719-4722; (b) Sugiyama, H.; Aharonian, G.; Gambarotta, S.; Yap, G. P. A.; Budzelaar, P. H. M., Participation of the α,α‘-Diiminopyridine Ligand System in Reduction of the Metal Center during Alkylation. *J. Am. Chem. Soc.* **2002,** *124* (41), 12268-12274; (c) Zhu, D.; Korobkov, I.; Budzelaar, P. H. M., Radical Mechanisms in the Reaction of Organic Halides with Diiminepyridine Cobalt Complexes. *Organometallics* **2012,** *31* (10), 3958-3971; (d) Hoyt, J. M.; Schmidt, V. A.; Tondreau, A. M.; Chirik, P. J., Iron-catalyzed intermolecular [2+2] cycloadditions of unactivated alkenes. *Science* **2015,** *349* (6251), 960-963; (e) Milsmann, C.; Turner, Z. R.; Semproni, S. P.; Chirik, P. J., Azo N□N Bond Cleavage with a Redox-Active Vanadium Compound Involving Metal–Ligand Cooperativity. *Angew. Chem. Int. Ed.* **2012,** *51* (22), 5386-5390; (f) Tondreau, A. M.; Atienza, C. C. H.; Weller, K. J.; Nye, S. A.; Lewis, K. M.; Delis, J. G. P.; Chirik, P. J., Iron Catalysts for Selective Anti-Markovnikov Alkene Hydrosilylation Using Tertiary Silanes. *Science* **2012,** *335* (6068), 567-570.

12. Cámpora, J.; Pérez, C. M.; Rodríguez-Delgado, A.; Naz, A. M.; Palma, P.; Álvarez, E., Selective Alkylation of 2,6-Diiminopyridine Ligands by Dialkylmanganese Reagents: A "One-Pot" Synthetic Methodology. *Organometallics* **2007,** *26* (4), 1104-1107.

13. (a) Esteruelas, M. A.; López, A. M.; Méndez, L.; Oliván, M.; Oñate, E., Preparation, Structure, and Ethylene Polymerization Behavior of Bis(imino)pyridyl Chromium(III) Complexes. *Organometallics* **2003,** *22* (3), 395-406; (b) Smit, T. M.; Tomov, A. K.; Gibson, V. C.; White, A. J. P.; Williams, D. J., Dramatic Effect of Heteroatom Backbone Substituents on the Ethylene Polymerization Behavior of Bis(imino)pyridine Iron Catalysts. *Inorg. Chem.* **2004,** *43* (21), 6511-6512.

14. Steves, J. E.; Kennedy, M. D.; Chiang, K. P.; Kassel, W. S.; Dougherty, W. G.; Dudley, T. J.; Zubris, D. L., Synthesis of a bulky bis(imino)pyridine compound: a methodology for systematic variation of steric bulk and energetic implications for metalation. *Dalton Trans.* **2009,** (7), 1214-1222.

15. (a) Reed, B. R.; Stoian, S. A.; Lord, R. L.; Groysman, S., The aldimine effect in bis(imino)pyridine complexes: non-planar nickel(i) complexes of a bis(aldimino)pyridine ligand. *Chem. Commun.* **2015,** *51* (30), 6496-6499; (b) Manuel, T. D.; Rohde, J.-U., Reaction of a Redox-Active Ligand Complex of Nickel with Dioxygen Probes Ligand-Radical Character. *J. Am. Chem. Soc.* **2009,** *131* (43), 15582-15583; (c) Zhu, D.; Thapa, I.; Korobkov, I.; Gambarotta, S.; Budzelaar, P. H. M., Redox-Active Ligands and Organic Radical Chemistry. *Inorg. Chem.* **2011,** *50* (20), 9879-9887.

16. Wile, B. M.; Trovitch, R. J.; Bart, S. C.; Tondreau, A. M.; Lobkovsky, E.; Milsmann, C.; Bill, E.; Wieghardt, K.; Chirik, P. J., Reduction Chemistry of Aryl- and Alkyl-Substituted Bis(imino)pyridine Iron Dihalide Compounds: Molecular and Electronic Structures of [(PDI)2Fe] Derivatives. *Inorg. Chem.* **2009,** *48* (9), 4190-4200.

17. Rahimi, N.; de Bruin, B.; Budzelaar, P. H. M., Balance between Metal and Ligand Reduction in Diiminepyridine Complexes of Ti. *Organometallics* **2017,** *36* (17), 3189-3198.

18. (a) Bart, S. C.; Lobkovsky, E.; Chirik, P. J., Preparation and Molecular and Electronic Structures of Iron(0) Dinitrogen and Silane Complexes and Their Application to Catalytic Hydrogenation and Hydrosilation. *J. Am. Chem. Soc.* **2004,** *126* (42), 13794-13807; (b) Tondreau, A. M.; Stieber, S. C. E.; Milsmann, C.; Lobkovsky, E.; Weyhermüller, T.; Semproni, S. P.; Chirik, P. J., Oxidation and Reduction of Bis(imino)pyridine Iron Dinitrogen Complexes: Evidence for Formation of a Chelate Trianion. *Inorg. Chem.* **2013,** *52* (2), 635-646.

19. Darmon, J. M.; Turner, Z. R.; Lobkovsky, E.; Chirik, P. J., Electronic Effects in 4-Substituted Bis(imino)pyridines and the Corresponding Reduced Iron Compounds. *Organometallics* **2012,** *31* (6), 2275-2285.

20. Scott, J.; Gambarotta, S.; Korobkov, I.; Budzelaar, P. H. M., Metal versus Ligand Alkylation in the Reactivity of the (Bis-iminopyridinato)Fe Catalyst. *J. Am. Chem. Soc.* **2005,** *127* (37), 13019-13029.

21. Zhu, D.; Janssen, F. F. B. J.; Budzelaar, P. H. M., (Py)2Co(CH2SiMe3)2 As an Easily Accessible Source of "CoR2". *Organometallics* **2010,** *29* (8), 1897-1908.

22. Sandoval, J. J.; Palma, P.; Alvarez, E.; Rodriguez-Delgado, A.; Campora, J., Dibenzyl and diallyl 2,6-bisiminopyridinezinc(ii) complexes: selective alkyl migration to the pyridine ring leads to remarkably stable dihydropyridinates. *Chem. Commun.* **2013,** *49* (60), 6791-6793.

23. Knijnenburg, Q.; Smits, J. M. M.; Budzelaar, P. H. M., Reaction of the Diimine Pyridine Ligand with Aluminum Alkyls: An Unexpectedly Complex Reaction. *Organometallics* **2006,** *25* (4), 1036-1046.

24. Tellmann, K. P.; Gibson, V. C.; White, A. J. P.; Williams, D. J., Selective Dimerization/Oligomerization of α-Olefins by Cobalt Bis(imino)pyridine Catalysts Stabilized by Trifluoromethyl Substituents: Group 9 Metal Catalysts with Productivities Matching Those of Iron Systems. *Organometallics* **2005,** *24* (2), 280-286.

25. Antonov, A. A.; Semikolenova, N. V.; Zakharov, V. A.; Zhang, W.; Wang, Y.; Sun, W.-H.; Talsi, E. P.; Bryliakov, K. P., Vinyl Polymerization of Norbornene on Nickel Complexes with Bis(imino)pyridine Ligands Containing Electron-Withdrawing Groups. *Organometallics* **2012,** *31* (3), 1143-1149.

26. Reardon, D.; Conan, F.; Gambarotta, S.; Yap, G.; Wang, Q., Life and Death of an Active Ethylene Polymerization Catalyst. Ligand Involvement in Catalyst Activation and Deactivation. Isolation and Characterization of Two Unprecedented Neutral and Anionic Vanadium(I) Alkyls. *J. Am. Chem. Soc.* **1999,** *121* (40), 9318-9325.

27. Dayan, O.; Doĝan, F.; Kaya, İ.; Çetinkaya, B., Palladium(II) Complexes Containing 2,6-Bis(Imino)Pyridines: Synthesis, Characterization, Thermal Study, and Catalytic Activity in Suzuki Reactions. *Synthesis and Reactivity in Inorganic, Metal-Organic, and Nano-Metal Chemistry* **2010,** *40* (5), 337-344.

28. Vidyaratne, I.; Scott, J.; Gambarotta, S.; Duchateau, R., Reactivity of Chromium Complexes of a Bis(imino)pyridine Ligand: Highly Active Ethylene Polymerization Catalysts Carrying the Metal in a Formally Low Oxidation State. *Organometallics* **2007,** *26* (13), 3201-3211.

29. Shaban, S. Y.; Ramadan, A. M.; van Eldik, R., Structural and catalytic aspects of copper(II) complexes containing 2,6-bis(imino)pyridyl ligands. *J. Coord. Chem.* **2012,** *65* (14), 2415-2431.

30. Chen, J.; Huang, Y.; Li, Z.; Zhang, Z.; Wei, C.; Lan, T.; Zhang, W., Syntheses of iron, cobalt, chromium, copper and zinc complexes with bulky bis(imino)pyridyl ligands and

their catalytic behaviors in ethylene polymerization and vinyl polymerization of norbornene. *J. Mol. Catal. A: Chem.* **2006,** *259* (1), 133-141.

31. Margulieux, G. W.; Turner, Z. R.; Chirik, P. J., Synthesis and Ligand Modification Chemistry of a Molybdenum Dinitrogen Complex: Redox and Chemical Activity of a Bis(imino)pyridine Ligand. *Angew. Chem. Int. Ed.* **2014,** *53* (51), 14211-14215.

32. Fan, R.-Q.; Chen, H.; Wang, P.; Yang, Y.-L.; Yin, Y.-B.; Hasi, W., Syntheses, structures, and luminescent properties of Zn(II) and Cd(II) complexes: 3-D supramolecules based on 2,6-bis(imino)pyridine ligands constructed by hydrogen bonding interactions. *J. Coord. Chem.* **2010,** *63* (9), 1514-1530.

33. Reardon, D.; Aharonian, G.; Gambarotta, S.; Yap, G. P. A., Mono- and Zerovalent Manganese Alkyl Complexes Supported by the α,α‘-Diiminato Pyridine Ligand: Alkyl Stabilization at the Expense of Catalytic Performance. *Organometallics* **2002,** *21* (5), 786-788.

34. Fan, R.; Yang, Y.; Yin, Y.; Hasi, W.; Mu, Y., Syntheses and Structures of Blue-Luminescent Mercury(II) Complexes with 2,6-Bis(imino)pyridyl Ligands. *Inorg. Chem.* **2009,** *48* (13), 6034-6043.

35. Schmidt, R.; Welch, M. B.; Knudsen, R. D.; Gottfried, S.; Alt, H. G., N,N,N-Tridentate iron(II) and vanadium(III) complexes: Part I. Synthesis and characterization. *J. Mol. Catal. A: Chem.* **2004,** *222* (1), 9-15.

36. Jurca, T.; Hiscock, L. K.; Korobkov, I.; Rowley, C. N.; Richeson, D. S., The tipping point of the inert pair effect: experimental and computational comparison of In(i) and Sn(ii) bis(imino)pyridine complexes. *Dalton Trans.* **2014,** *43* (2), 690-697.

37. Baker, R. J.; Jones, C.; Kloth, M.; Mills, D. P., The reactivity of gallium(i) and indium(i) halides towards bipyridines, terpyridines, imino-substituted pyridines and bis(imino)acenaphthenes. *New J. Chem.* **2004,** *28* (2), 207-213.

38. Chu, T.; Belding, L.; van der Est, A.; Dudding, T.; Korobkov, I.; Nikonov, G. I., A Coordination Compound of Ge0 Stabilized by a Diiminopyridine Ligand. *Angew. Chem. Int. Ed.* **2014,** *53* (10), 2711-2715.

39. Garza-Ortiz, A.; Maheswari, P. U.; Siegler, M.; Spek, A. L.; Reedijk, J., Ruthenium(III) Chloride Complex with a Tridentate Bis(arylimino)pyridine Ligand: Synthesis, Spectra, X-ray Structure, 9-Ethylguanine Binding Pattern, and In Vitro Cytotoxicity. *Inorg. Chem.* **2008,** *47* (15), 6964-6973.

40. Jurca, T.; Chen, W.-C.; Michel, S.; Korobkov, I.; Ong, T.-G.; Richeson, D. S., Solid-State Thermolysis of a fac-Rhenium(I) Carbonyl Complex with a Redox Non-Innocent Pincer Ligand. *Chemistry – A European Journal* **2013,** *19* (13), 4278-4286.

41. Vidyaratne, I.; Gambarotta, S.; Korobkov, I.; Budzelaar, P. H. M., Dinitrogen Partial Reduction by Formally Zero- and Divalent Vanadium Complexes Supported by the Bis-iminopyridine System. *Inorg. Chem.* **2005,** *44* (5), 1187-1189.

42. Russell, S. K.; Bowman, A. C.; Lobkovsky, E.; Wieghardt, K.; Chirik, P. J., Synthesis and Electronic Structure of Reduced Bis(imino)pyridine Manganese Compounds. *Eur. J. Inorg. Chem.* **2012,** *2012* (3), 535-545.

43. Reed, B. R.; Yousif, M.; Lord, R. L.; McKinnon, M.; Rochford, J.; Groysman, S., Coordination Chemistry and Reactivity of Bis(aldimino)pyridine Nickel Complexes in Four Different Oxidation States. *Organometallics* **2017,** *36* (3), 582-593.

44. Cheung, P. M.; Berger, R. F.; Zakharov, L. N.; Gilbertson, J. D., Square planar Cu(I) stabilized by a pyridinediimine ligand. *Chem. Commun.* **2016,** *52* (22), 4156-4159.

45. Margulieux, G. W.; Bezdek, M. J.; Turner, Z. R.; Chirik, P. J., Ammonia Activation, H2 Evolution and Nitride Formation from a Molybdenum Complex with a Chemically and Redox Noninnocent Ligand. *J. Am. Chem. Soc.* **2017,** *139* (17), 6110-6113.

46. (a) Sherbow, T. J.; Carr, C. R.; Saisu, T.; Fettinger, J. C.; Berben, L. A., Insight into Varied Reaction Pathways for O–H and N–H Bond Activation by Bis(imino)pyridine Complexes of Al(III). *Organometallics* **2016,** *35* (1), 9-14; (b) Myers, T. W.; Berben, L. A., Aluminum–Ligand Cooperative N–H Bond Activation and an Example of Dehydrogenative Coupling. *J. Am. Chem. Soc.* **2013,** *135* (27), 9988-9990.

47. Monfette, S.; Turner, Z. R.; Semproni, S. P.; Chirik, P. J., Enantiopure C1-Symmetric Bis(imino)pyridine Cobalt Complexes for Asymmetric Alkene Hydrogenation. *J. Am. Chem. Soc.* **2012,** *134* (10), 4561-4564.

48. Lam, Y. C.; Nielsen, R. J.; Goddard, W. A.; Dash, A. K., The mechanism for catalytic hydrosilylation by bis(imino)pyridine iron olefin complexes supported by broken symmetry density functional theory. *Dalton Trans.* **2017,** *46* (37), 12507-12515.

49. Pappas, I.; Treacy, S.; Chirik, P. J., Alkene Hydrosilylation Using Tertiary Silanes with α-Diimine Nickel Catalysts. Redox-Active Ligands Promote a Distinct Mechanistic Pathway from Platinum Catalysts. *ACS Catalysis* **2016,** *6* (7), 4105-4109.

50. Myers, T. W.; Kazem, N.; Stoll, S.; Britt, R. D.; Shanmugam, M.; Berben, L. A., A Redox Series of Aluminum Complexes: Characterization of Four Oxidation States Including a Ligand Biradical State Stabilized via Exchange Coupling. *J. Am. Chem. Soc.* **2011,** *133* (22), 8662-8672.

51. Britovsek, G. J. P.; Bruce, M.; Gibson, V. C.; Kimberley, B. S.; Maddox, P. J.; Mastroianni, S.; McTavish, S. J.; Redshaw, C.; Solan, G. A.; Strömberg, S.; White, A. J. P.; Williams, D. J., Iron and Cobalt Ethylene Polymerization Catalysts Bearing 2,6-Bis(Imino)Pyridyl Ligands: Synthesis, Structures, and Polymerization Studies. *J. Am. Chem. Soc.* **1999,** *121* (38), 8728-8740.

52. Tempel, D. J.; Johnson, L. K.; Huff, R. L.; White, P. S.; Brookhart, M., Mechanistic Studies of Pd(II)−α-Diimine-Catalyzed Olefin Polymerizations1. *J. Am. Chem. Soc.* **2000,** *122* (28), 6686-6700.

53. Calderazzo, F.; Englert, U.; Pampaloni, G.; Santi, R.; Sommazzi, A.; Zinna, M., Bis(arylimino)pyridine derivatives of Group 4 metals: preparation, characterization and activity in ethylene polymerization. *Dalton Trans.* **2005,** (5), 914-922.

54. Britovsek, G. J. P.; Clentsmith, G. K. B.; Gibson, V. C.; Goodgame, D. M. L.; McTavish, S. J.; Pankhurst, Q. A., The nature of the active site in bis(imino)pyridine iron ethylene polymerisation catalysts. *Catal. Commun.* **2002,** *3* (5), 207-211.

55. Raucoules, R.; de Bruin, T.; Raybaud, P.; Adamo, C., Evidence for the Iron(III) Oxidation State in Bis(imino)pyridine Catalysts. A Density Functional Theory Study. *Organometallics* **2008,** *27* (14), 3368-3377.

56. Bryliakov, K. P.; Semikolenova, N. V.; Zakharov, V. A.; Talsi, E. P., Active Intermediates of Ethylene Polymerization over 2,6-Bis(imino)pyridyl Iron Complex Activated with Aluminum Trialkyls and Methylaluminoxane. *Organometallics* **2004,** *23* (22), 5375-5378.

57. (a) Hojilla Atienza, C. C.; Milsmann, C.; Lobkovsky, E.; Chirik, P. J., Synthesis, Electronic Structure, and Ethylene Polymerization Activity of Bis(imino)pyridine Cobalt Alkyl Cations. *Angew. Chem. Int. Ed.* **2011,** *50* (35), 8143-8147; (b) Tondreau, A. M.; Milsmann, C.; Patrick, A. D.; Hoyt, H. M.; Lobkovsky, E.; Wieghardt, K.; Chirik, P. J., Synthesis and Electronic Structure of Cationic, Neutral, and Anionic Bis(imino)pyridine Iron Alkyl Complexes: Evaluation of Redox Activity in Single-Component Ethylene Polymerization Catalysts. *J. Am. Chem. Soc.* **2010,** *132* (42), 15046-15059.

58. Macomber, R. S., *A Complete Introduction to Modern NMR Spectroscopy*. John Wiley & Sons: New York: 1998; p 382.

59. Jackman, L. M.; Cotton, F. A., *Dynamic Nuclear Magnetic Resonance Spectroscopy*. Academic press, Inc.: 1975; p 660.

60. Hanson, B. E.; Whitmire, K. H., Exchange of axial and equatorial carbonyl groups in pentacoordinate metal carbonyls in the solid state. The variable temperature magic angle spinning carbon-13 NMR spectroscopy of iron pentacarbonyl, [Ph3PNPPh3][HFe(CO)4], and [NEt4][HFe(CO)4]. *J. Am. Chem. Soc.* **1990,** *112* (3), 974-977.

61. Berry, R. S., Correlation of Rates of Intramolecular Tunneling Processes, with Application to Some Group V Compounds. *The Journal of Chemical Physics* **1960,** *32* (3), 933-938.

62. (a) Gordy, W., *Theory and Applications of Electron Spin Resonance*. John Wiley & Sons: New York: 1980; (b) Eaton, G. R.; Eaton, S. S.; Barr, D. P.; Weber, R. T., Quantitative EPR. Springer-Verlag: Wien, New York: 2010.

63. Ladd, M.; Palmer, R., Structure Determination by X-ray Crystallography. 4th ed.; Kluwer Academic/Plenum Publishers: New York: 2003.

64. Andrade, J. D., X-ray Photoelectron Spectroscopy (XPS). In *Surface and Interfacial Aspects of Biomedical Polymers*, Andrade, J. D., Ed. Springer, Boston, MA: 1985.

65. Liss, K.-D.; Bartels, A.; Schreyer, A.; Clemens, H., High-Energy X-Rays: A tool for Advanced Bulk Investigations in Materials Science and Physics. *Textures and Microstructures* **2003,** *35* (3-4), 219-252.

# 2 Synthesis and Characterization of Mono- and Dialkyl Diiminopyridine Titanium(II) Complexes

This work is published as ″Balance between metal and ligand reduction in diiminopyridine complexes of Ti″ *Organometallics*, 2017, *36* (17), pp 3189-3198.

## 2.1 Authorship Consideration

Naser Rahimi was responsible for synthesizing and characterizing the mono- and dialkyl Titanium complexes of the DIP ligand and doing theoretical investigations with the help of Prof. Peter H. M. Budzelaar. The XPS and EPR analysis have been done by Dr. K. McEleney (Manitoba Institute for Materials) and Prof. B. de Bruin (U. of Amsterdam, the Netherlands), respectively. The preliminary draft of the paper was prepared by Naser Rahimi which was modified into its publication format by Prof. Budzelaar.

## 2.2 Abstract

Reaction of diiminopyridine ligand $^{Et}$DIP (2,6-$Et_2$-$C_6H_3N$=CMe)$_2C_5H_3N$) with $TiCl_3$.$(THF)_3$ gave the corresponding Ti(III) complex ($^{Et}$DIP)$TiCl_3$ (**1**). Reduction of **1** with 1 equivalent of $KC_8$ or Na/Hg produced the formally Ti(II) complex ($^{Et}$DIP)$TiCl_2$ (**2**). From this, ($^{Et}$DIP)TiClR complexes (R = Me (**3a**), $CH_2Si(CH_3)_3$ (**3b**), Ph (**3c**)) were obtained by addition of 1 equivalent of LiR. Similarly, dialkylated complexes ($^{Et}$DIP)$TiR_2$ (R = Me (**4a**), $CH_2Si(CH_3)_3$ (**4b**)) were obtained with 2 equivalents of LiR. All of the new complexes were characterized by single crystal X-ray diffraction. EPR studies indicate that complex **1** is best regarded as a true Ti(III) complex with an "innocent" DIP ligand. Complexes **2**-**5** are all diamagnetic. In contrast to DIP complexes of the late transition metals Fe and Co, new complexes **2**-**4** show strong upfield $^1$H NMR shifts for the pyridine protons. Based on this and

the imine C=N and $C_{imine}$-$C_{py}$ bond lengths, a description involving Ti(IV) and a di-anionic ligand seems most appropriate, and DFT calculations support this interpretation. VT-NMR studies of **4a** suggest a small and temperature-dependent thermal population of a triplet state, and indeed calculations indicate that **4a** has the lowest singlet-triplet energy difference of the systems studied.

## 2.3 Introduction

The main claim to fame for Ti catalysis of olefin polymerization undoubtedly is the Ziegler-Natta[1] catalyst. In addition, important classes of Ti(III) and (IV) complexes have been developed mainly for copolymerization of α-olefins and styrenes with ethylene,[2] polymerization of 1-hexene in a "living" fashion,[3] polymerization of styrene to syndiotactic polymer,[4] and polymerization of ethylene with extraordinarily high activity at high temperatures.[5] These advances have encouraged synthetic chemists to make titanium catalysts including an extensive range of ancillary ligands, containing for instance cyclopentadienyl (Cp) ligands with pendant neutral donor groups,[6] isocyanide ligands,[7] *β*-diketiminates,[8] and mixed cyclopentadienyl-alkoxide ligands.[9]

Following the report by Wilkinson,[10] researchers have made a variety of Ti(IV), (III) and (II) complexes containing Cp and indenyl groups.[11]

The group of Stephan has made the diamagnetic complex $[CpClTi(\mu\text{-}NP(^{i}Pr)_3)]_2$ in which neighbouring titanium(III) centers are antiferromagnetically coupled.[12] Using benzamidinates, Arnold *et.al.* made titanium(IV) and (III) complexes and illustrated their reactivities.[13] A stable Ti(III) alkyl complex of this type of ligand, $[PhC(NSiMe_3)_2]_2TiMe$, showed a Ti-C-H acute angle comparing to the other two hydrogens indicating an agostic interaction with the metal center.[13]

It seems that chemistry of Ti has not been well explored in combination with redox-active ligands. Redox-active ligands have drastically expanded the role of ligands in organometallic

chemistry and catalysis. Instead of a more standard ligand just sitting there and maybe be a bit bulky, or a bit electron-withdrawing, a redox-active ligand can actively participate in the chemistry of its complexes. It can function as an electron reservoir, allowing increased electronic flexibility within the coordination sphere of the metal. This flexibility introduces ambiguity in the oxidation state of the central metal atom. For example, in complexes of the 2,6-diiminopyridine ligand with both main group metals and transition metals, the ligand is typically counted as neutral, whereas in reality it can accept up to three electrons in its extended π-system.[14] These "stored electrons" can be used to break carbon-halogen bonds and even form carbon-carbon bonds via non-traditional mechanisms.[15] The combination of an inexpensive first-row transition metal with a DIP ligand has on occasion resulted in chemistry more typical of the noble metals.[16]

For the particular case of $^{R}$DIP ligands (Figure 2.1), complexes with elements V,[17] Cr,[18] Mn,[19] Fe,[14] Co[20] and Ni[21] have been extensively explored, and examples of both "innocent" and "noninnocent" ligand roles have been established.

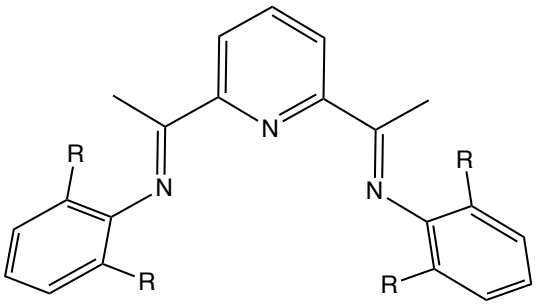


Figure 2.1. $^{R}$DIP ligand

There is, however, only a single paper mentioning Ti complexes, and characterization of the complexes reported there is rather incomplete.[22] We were interested in exploring DIP complexes of Ti with low formal oxidation states (III and II) to investigate how the balance between metal and ligand centered reduction works out. Ti(IV) is the dominant oxidation

state of titanium. In its complexes Ti(IV) tends to be strongly acidic. As mentioned above, such complexes are active in olefin polymerization and epoxidation catalysis. Ti(III) is somewhat less common but by no means rare. It is a moderate reductant. The most prominent example of Ti(III) reactivity is in heterogeneous Ziegler-Natta olefin polymerization catalysis. Finally, Ti(II) is much rarer and is a strong reductant. Characteristic reactions include activation of dinitrogen[23] and the McMurry coupling of ketones and sterically hindered alkenes along with aromatic heterocycles,[24] respectively. The issue we want to explore is whether formally low-valent complexes like (DIP)$TiX_3$ and (DIP)$TiX_2$ contain a reduced ligand and/or a reduced metal and how this affects reactivity. A series of mono- and dialkyl titanium complexes of DIP have been synthesized and characterized by a combination of NMR spectroscopy, single crystal X-ray diffraction, XPS and elemental analysis. Furthermore, the real oxidation state of the central metal and the DIP ligand has been investigated.

## 2.4 Results and Discussion

Synthesis of the formally Ti(II) complexes of $^{Et}$DIP ligand is demonstrated in Scheme 2.1. Synthesis of Ti(III) and Ti(II) complexes

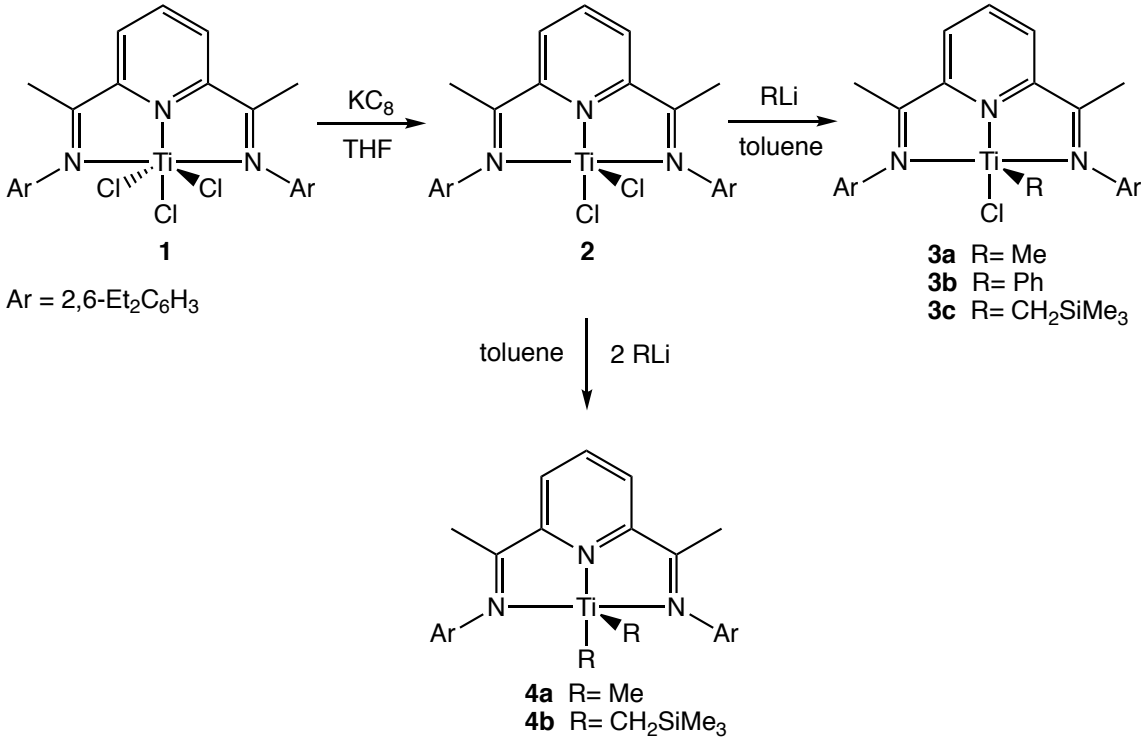


Scheme 2.1. Synthesis of Ti(III) and Ti(II) complexes

Under an atmosphere of $N_2$, slow addition of a solution of $^{Et}$DIP to a solution of $TiCl_3(THF)_3$, both in THF, yielded dark green crystals of paramagnetic **1**. This complex is very poorly soluble in most solvents, and we did not obtain meaningful $^1$H NMR spectra. Recrystallization of **1** was not satisfactory, but slow diffusion between carefully layered solutions of $^{Et}$DIP and $TiCl_3(THF)_3$ directly produced needle-shaped crystals suitable for X-ray diffraction.

Reduction of **1** with 1 equivalent $KC_8$ (or Na/Hg) resulted in diamagnetic dark green **2**. This complex is much more soluble than **1** and could be fully characterized.

Treatment of **2** with one equivalent of the LiR (R = Me, $CH_2SiMe_3$, Ph) in toluene afforded the corresponding titanium(II) monoalkyl-monohalide complexes **3a-3c**. They were characterized by elemental analysis, NMR spectroscopy, and also by X-ray diffraction.

Reaction of two equivalents of LiR (R = Me or $CH_2Si(CH_3)_3$) with **2** in toluene under an atmosphere of $N_2$ gave the corresponding complexes ($^{Et}$DIP)$TiR_2$ (**4a** and **4b**).

### 2.4.1 EPR

The solubility of **1** in $CH_2Cl_2$ was sufficient for EPR studies ($CH_2Cl_2$ glass) which confirm the presence of a single unpaired electron (Figure 2.2).

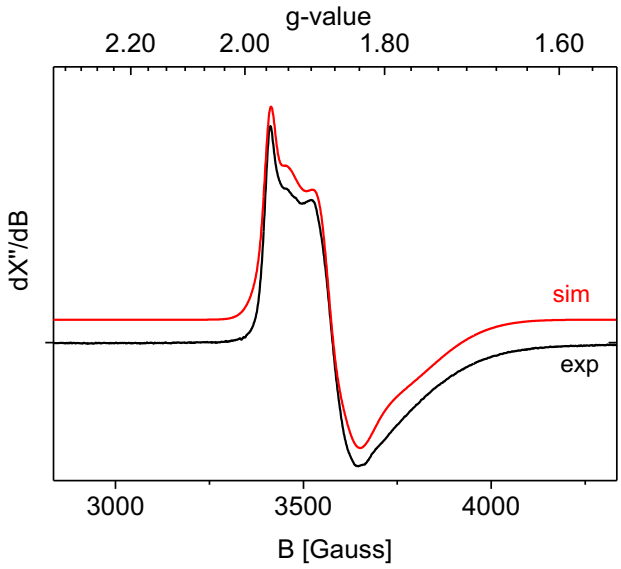


Figure 2.2. Experimental and simulated X-band EPR spectrum of **1** recorded at 20 K using a frozen solution of **1** in $CH_2Cl_2$ (~0.1 M $[(^nBu)_4N]PF_6$ was added). Experimental parameters: frequency = 9.362511 GHz, modulation amplitude = 4 Gauss, microwave power = 0.632 mW.

The X-band EPR spectrum of a crystalline sample of **1** was recorded in frozen dichloromethane. This solvent gives a poor glass, and hence often leads to aggregation behavior and preferred orientation effects of the paramagnetic solutes. Indeed, in pure $CH_2Cl_2$ the EPR spectrum of **1** is very broad and highly asymmetric. Unfortunately, this is also the only solvent in which **1** is reasonably soluble (even mixtures of $CH_2Cl_2$ and other solvents

like MeTHF result in very poor solubilities). In an attempt to prevent such preferred orientation/aggregation effects due to poor glass formation we added $[(^nBu)_4N]PF_6$ to the solution. The EPR spectrum of this frozen mixture (see Figure 2.2) is indeed sharper (showing overall identical peak positions as the spectrum in pure $CH_2Cl_2$). However, some aggregation/preferred orientation effects remain, and as a result a satisfactory simulation of the experimental spectrum could only be obtained assuming the presence of two species (ratio ~ 1:4) with very similar g-tensors, but differing widely in their linewidth parameters. This behavior is best ascribed to remaining 'bad glass' effects. The rhombicity of the g-tensor and significant deviations of the g-values from $g_e$ (2.0023) due to substantial spin-orbit effects signifies that the unpaired electron of **1** is predominantly metal centered, in agreement with the intra-ligand metrics showing an essentially unreduced $^{Et}$DIP ligand in the X-ray structure of **1**.

The DFT calculated g-tensors of **1** (X-ray and B3-LYP optimized geometries) are in reasonable agreement with the experimental values, showing a similar rhombicity, although the absolute experimental values are somewhat lower than those calculated (Table 2.1).

Table 2.1. Experimental and DFT calculated EPR parameters of **1**

| | $g_x$ | $g_y$ | $g_z$ | $W_x$ | $W_y$ | $W_z$ |
|---|---|---|---|---|---|---|
| Experimental ('species 1'; 80%) | 1.938 | 1.855 | 1.761 | 49 | 51 | 152 |
| Experimental ('species 2'; 20%) | 1.958 | 1.875 | 1.778 | 15 | 25 | 102 |
| | | | | | | |
| DFT (ADF) X-ray geometry | 1.986 | 1.954 | 1.826 | - | - | - |
| DFT (ORCA) X-ray geometry | 1.988 | 1.967 | 1.858 | - | - | - |
| | | | | | | |
| DFT (ADF) b3-lyp geometry | 1.974 | 1.951 | 1.910 | - | - | - |
| DFT (ORCA) | 1.981 | 1.955 | 1.920 | - | - | - |

| b3-lyp geometry | | | | | | |
|---|---|---|---|---|---|---|
| | | | | | | |
| DFT (ADF) BP86 geometry | 1.994 | 1.987 | 1.948 | - | - | - |
| DFT (ORCA) BP86 geometry | 1.994 | 1.986 | 1.944 | - | - | - |

It seems the experimental spin density distribution is perhaps a bit stronger localized on the metal as compared to the DFT studies showing some delocalization of spin density over the metal and the ligand (

Figure *2.3*).

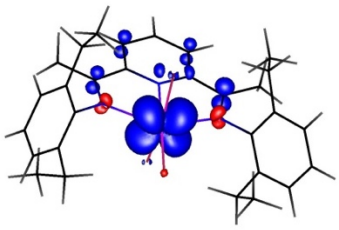

Spin density plot (b3-lyp, def2-TZVP optimized)

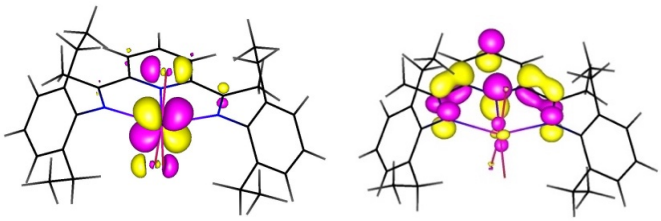

SOMO (left) and LUMO (right) plots (b3-lyp, def2-TZVP optimized)

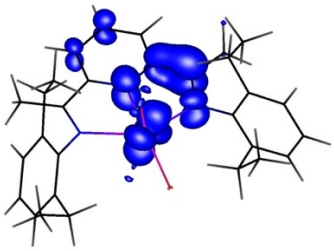

Spin density plot (BP86, def2-TZVP optimized)

Figure 2.3. Spin density plots of **1**

## 2.4.2 X-ray Structural Characterization

The solid-state structure of **1** is shown in Figure 2.4. Table 2.2 contains the most relevant bond lengths and structural parameter ($\tau$)[25] for this and subsequent complexes.

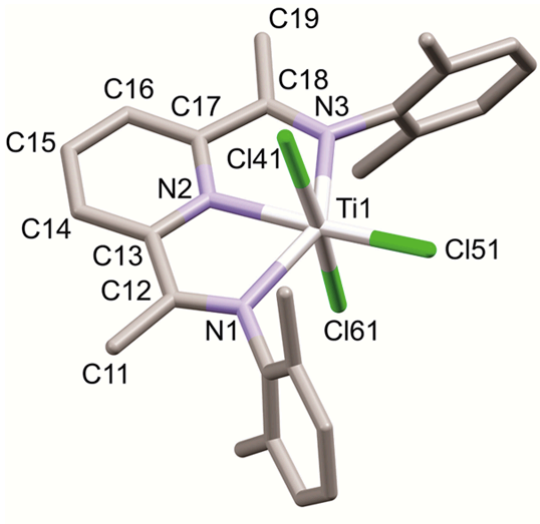


Figure 2.4. Solid-state structure of **1**. Hydrogens and ethyl $CH_3$ carbons are omitted for clarity

Table 2.2. Selected Bond lengths for ($^{Et}$DIP)Ti complexes

| | **1** | **2** | **3a** | **3c** |
|---|---|---|---|---|
| Ti1-N1 | 2.202(3) | 2.107(5) | 2.040(2) | 2.1546(18) |
| Ti1-N2 | 2.160(3) | 1.971(4) | 1.9719(18) | 1.9712(18) |
| Ti1-N3 | 2.219(3) | 2.094(5) | 2.1390(19) | 2.0409(19) |
| Ti1-X41 | 2.4155(11) | 2.279(2) | 2.108(3) | 2.102(2) |
| Ti1-X51 | 2.2543(13) | 2.268(2) | 2.2997(10) | 2.2976(6) |
| Ti1-X61 | 2.3422(12) | | | |
| N1-C12 | 1.297(5) | 1.327(7) | 1.360(3) | 1.317(3) |
| C12-C13 | 1.459(6) | 1.411(8) | 1.398(3) | 1.429(3) |
| C17-C18 | 1.471(5) | 1.414(9) | 1.424(3) | 1.392(3) |
| C18-N3 | 1.298(4) | 1.333(7) | 1.3 26(3) | 1.370(3) |
| $\tau$ | | 0.37 | 0.49 | 0.54 |

The geometry around titanium in **1** is best described as distorted octahedral. The complex deviates considerably from ideal $C_{2v}$ symmetry by having one apical chloride atom (Cl41) tilted towards the pyridine ring of the $^{Et}$DIP ligand, resulting in an N2-Ti-Cl41 angle of 79° (c.f. N2-Ti-Cl61 93°). The titanium atom is also displaced out of the N1-N2-N3 plane of the DIP ligand by 0.142 Å. The bond distances in the solid-state structure of **1** indicate a neutral ligand. Ti-N (2.160(3)-2.219(3) Å), $C_{imine}$-$C_{py}$ (1.459(6)-1.471(5) Å) and imine (1.297(5)-1.298(4) Å) bonds distances are in the range of the other observed DIP complexes with neutral ligands (DIP$^{(0)}$: av C=N: 1.280 Å; av $C_{imine}$-$C_{py}$: 1.493 Å).[26]

Previously reported,[12] typical $Ti^{III}$-Cl and $Ti^{IV}$-Cl bond lengths are ~2.38 (Å) and ~2.31 (Å), respectively. In complex **1**, the average Ti-Cl bond length of ~2.34 Å suggests a situation somewhere between Ti(III) and Ti(IV). This is all consistent with the EPR results mentioned above.

The solid-state structure of **2** is shown in Figure 2.5 and selected bond lengths are included in Table 2.2.

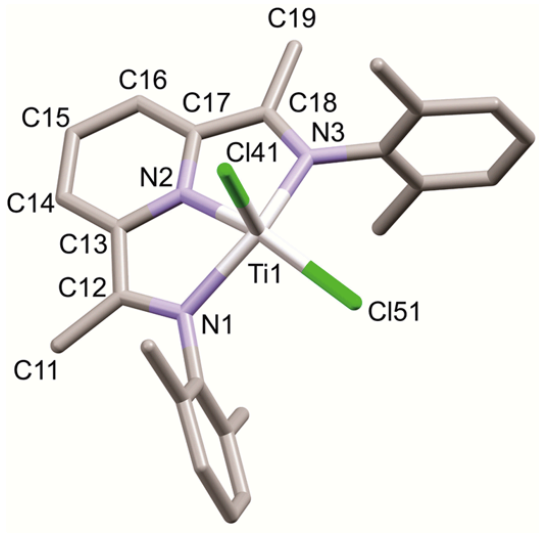


Figure 2.5. Solid-state structure of **2**. Hydrogens and ethyl $CH_3$ carbons are omitted for clarity

The geometry about titanium in complex **2** is best described as distorted square pyramidal, with one Cl atom occupying the apical position. The titanium center and the basal Cl atom are displaced out of the N1-N2-N3 plane by 0.677 and 0.248 Å, respectively. The geometric preference for a square pyramidal (SP) over a trigonal bipyramidal (TBP) geometry is most likely due to steric reasons. In a hypothetical $C_{2v}$-symmetrical TBP structure, both Cl atoms would be much closer to the ethyl substituents on the aryl "arms" of the ligand.

Different from **1**, the elongation of the imine double bonds in **2** is characteristic for electron density transfer to the π-system of the ligand. Also, $C_{imine}$-$C_{py}$ and Ti-N bond contractions are significant in **2** for the same reason. The Ti-Cl bonds in **2** (Ti-Cl: 2.268(2), 2.279(2)) are much shorter than previously reported for authentic $Ti^{II}$ complexes (Ti-Cl: ~2.4- 2.5 Å )[10, 27] and more typical of $Ti^{IV}$-Cl complexes (~2.31 Å ).[12]

The geometry around the titanium atom in **3a** is best defined as distorted square pyramidal, with the methyl group occupying the apical position. The structure is very similar to that of **2**; the preference of the methyl group for an apical position might be due to its larger *trans* influence. The Ti and Cl atoms are displaced from the N1-N2-N3 plane by 0.634 Å and 0.439 Å, respectively. The structures of **3b** and **3c** are similar to those of **2** and **3a**, again showing an SP structure with the organic group occupying the apical position. The alkyl group in **3b** has occupied the apical position likely due to both its larger *trans* effect and steric reasons. The trimethylsilyl group is oriented away from ethyl substituents on the phenyl rings (because of the low-quality structure, we avoid analyzing of the bond lengths of **3b** in detail). All three compounds **3a**-**3c** show upfield shifts for the pyridine protons, slightly more pronounced than in **2**. Solid state structures of **3a**, **3b** and **3c** are shown in Figure 2.6, Figure 2.7 and Figure 2.8, respectively, and the related bond lengths for **3a** and **3c** are summarized in Table 2.2.

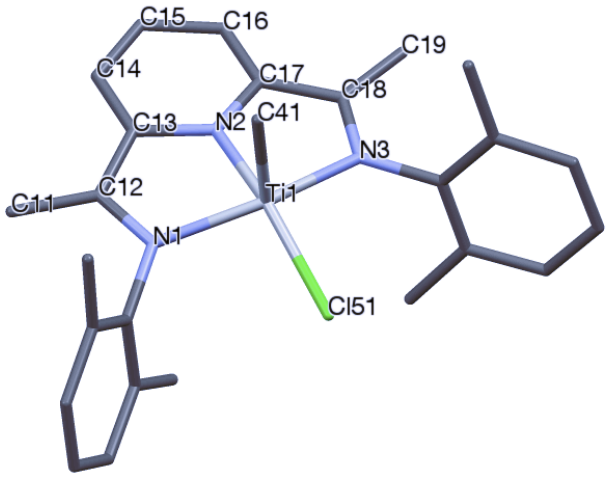


Figure 2.6. Solid-state structure of **3a**. Hydrogens and ethyl $CH_3$ carbons are omitted for clarity

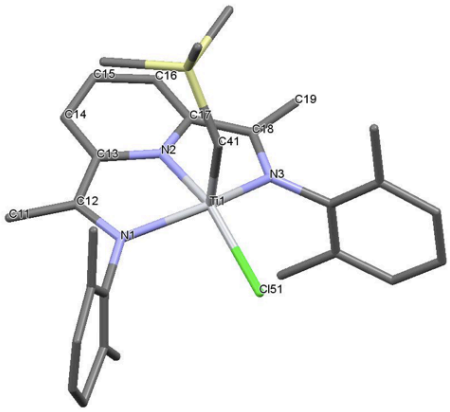


Figure 2.7. Solid-state structure of **3b**. Hydrogens and ethyl $CH_3$ carbons are omitted for clarity

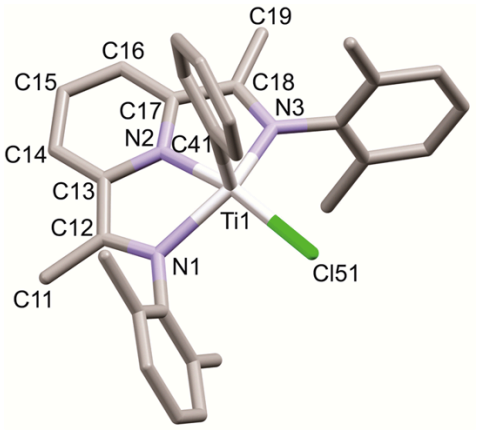


Figure 2.8. Solid-state structure of **3c**. Hydrogens and ethyl $CH_3$ carbons are omitted for clarity

Replacing the Cl ligand in apical position in **2** with a methyl group in **3a** has produced further electron transfer to the π-system of the ligand. This is reflected in further elongation of the C=N bonds and contraction of the Ti-N and $C_{imine}$-$C_{py}$ bond. The Ti-Cl bond is somewhat longer than the basal Ti-Cl bond in **2**, which might be due to stronger electron donation from the methyl group to the Ti centre in **3a**. Changes in bond lengths are accompanied by small changes in N-Ti-N bond angles. It should be noted that in **3a** changes in bond lengths are not happening in a symmetric fashion. Half of the $^{Et}$DIP ligand is more contracted (Ti1-N1: 2.040(2) Å, C12-C13: 1.398(3) Å) and elongated (C12-N1: 1.360(3) Å) relative to the bonds in another half of the ligand (Ti1-N3: 2.1390(13) Å, C18-N3: 1.326(3) Å, C17-C18: 1.424(3) Å). As observed in **2**, the Ti-Cl bond distance (2.2997(10) Å) in **3a** is shorter than that in $Ti^{II}$ complexes of innocent ligands. The Ti-C bonds in **3** and **4** (2.077-2.112 Å) seems to be shorter than those in literature $Ti^{II}$-Me[28] (2.219(2) Å) and closer to $Ti^{IV}$-Me[29] (2.121(7)Å) complexes.

The geometry about the titanium in **3c** is best described as distorted square pyramidal with one Cl ligand occupying the fourth site of the basal plane while the phenyl group is placed in the apical position. The titanium center and the basal Cl ligand are displaced 0.597 and 0.431

Å out of the plane described by N1-N2-N3 of the $^{Et}$DIP ligand, respectively. The phenyl group in the apical site is rotated by 25° away from its most symmetric orientation, likely to prevent undesirable interactions with ethyl substituents on the phenyl rings perpendicular to the plane of the molecule; the effective $C_s$ symmetry of the NMR spectrum shows that this tilting is dynamic in solution. It seems that steric forces play important roles in preferring the square pyramidal over pseudo trigonal bipyramid in **3c**. As observed in **3a**, the solid-state structure of **3c** illustrates the same asymmetric deformation pattern in the ligand backbone (Ti1-N1: 2.1546(18) Å, C12-N1: 1.317(3) Å, C12-C13: 1.429(3) Å, Ti1-N3: 2.0409(19) Å, C18-N3: 1.370(3) Å, C17-C18: 1.392(3) Å. Also, in **3c**, the Ti-Cl bond length (Ti-Cl: 2.2976(6) Å) is shorter than expected for $Ti^{II}$ but compatible with $Ti^{IV}$. The Ti-C bond length (2.102(2)Å) is also in the range expected for $Ti^{IV}$.

The molecular structures of **4a** and **4b** are shown in Figure 2.9 and Figure 2.10 and their bond lengths and structural parameters are collected in Table 2.3.

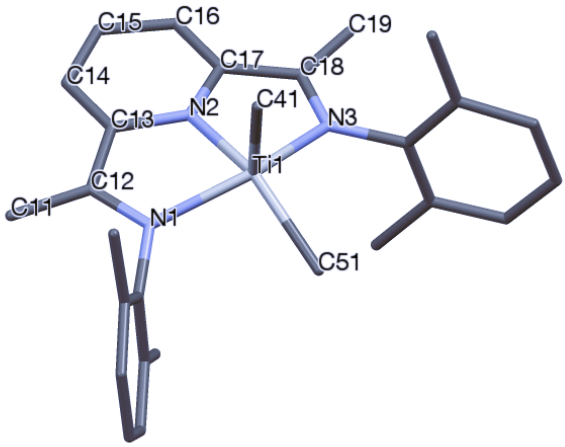


Figure 2.9. Solid-state structure of **4a**. Hydrogens and ethyl $CH_3$ carbons are omitted for clarity

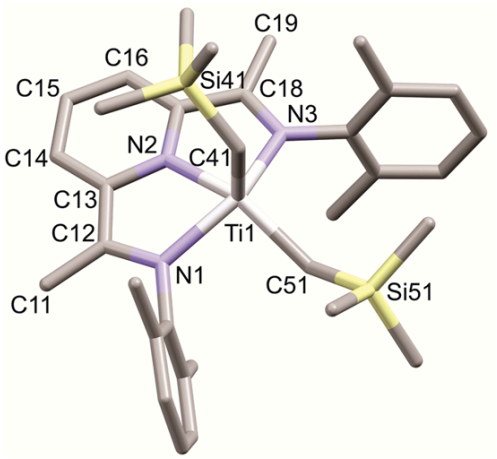


Figure 2.10. Solid-state structure of **4b**. Hydrogens and ethyl $CH_3$ carbons are omitted for clarity

Table 2.3. Selected Bond lengths for ($^{Et}$DIP)Ti$R_2$ complexes

| | **4a** | **4b** |
|---|---|---|
| Ti1-N1 | 2.059(2) | 2.119(3) |
| Ti1-N2 | 1.990(2) | 2.014(3) |
| Ti1-N3 | 2.122(2) | 2.089(3) |
| Ti1-X41 | 2.112(3) | 2.077(3) |
| Ti1-X51 | 2.109(3) | 2.093(3) |
| N1-C12 | 1.355(3) | 1.347(4) |
| C12-C13 | 1.386(4) | 1.418(5) |
| C17-C18 | 1.421(4) | 1.404(5) |
| C18-N3 | 1.339(4) | 1.355(4) |
| τ | 0.51 | 0.48 |

The geometries of **4a** and **4b** are again distorted square pyramidal, with basal and apical alkyl groups. As in **2** and **3**, the titanium center in **4b** is displaced by 0.572 Å out of the plane defined by N1-N2-N3; the basal carbon is located *below* this plane by 0.174 Å. In **4b**, the apical $CH_2SiMe_3$ group folds over the pyridine ring of the DIP ligand, while the equatorial one extends more or less in the molecular plane away from the pyridine ring. In this conformation, both alkyl groups minimize their interactions with the ligand Et groups and with each other.

### 2.4.3 XPS

X-ray photoelectron spectroscopy is one of the most direct techniques for establishing the oxidation state of a metal atom. While the exact binding energies of core orbitals vary somewhat depending on the precise nature of the ligands around the metal, different oxidation states are typically associated with distinct ranges of the binding energy. Table 2.4 presents the Ti $2p_{3/2}$ binding energies of the complexes measured, together with relevant reference data.

Table 2.4. Ti $2p_{3/2}$ binding energy from XPS

| complex | binding energy (eV) |
|---|---|
| **$TiO_2$** | 458.8 |
| **$TiCl_3$** | 457.8 |
| **TiO** | 454.7 |
| **1** | 457.7 |
| **2** | 458.7 |
| **3b** | 458.4 |
| **3c** | 458.6 |
| **4a** | 458.4 |
| **4b** | 458.4 |

Parent complex **1** has a binding energy of 457.7 eV typical of Ti(III) complexes such as $Ti_2O_3$ and $TiCl_3$.[30] Reduction of **1** by removal of a chloride leads to complex **2**, which might be expected to have a Ti(II) center. However, its observed binding energy is 458.7 eV, typical of Ti(IV)[30-31] rather than Ti(II), which would be observed around 454.7 eV.[31-32] Alkylation to give **3** or **4** results in a very small decrease of the Ti 2p binding energy, which remains in the range typical of Ti(IV). The XPS data thus agree with the formulation of **1** as containing $(DIP^{(0)})Ti^{III}$ and indicate the "more reduced" complexes **2**−**4** actually contain Ti in a higher oxidation state: $(DIP^{2-})Ti^{IV}$.

### 2.4.4 NMR

The sharp $^{1}H$ and $^{13}C$ NMR spectra confirm the diamagnetic nature of **2**. It has effective $C_{2v}$ symmetry in solution, indicating fast inversion of the SP structure. Interestingly, in contrast to DIP complexes of late transition metals such as cobalt[15] and iron[16b], the pyridine hydrogens of **2** are shifted strongly upfield, appearing as a doublet of 2H for py H3/5 at 5.92 ppm and a triplet of 1H for py H4 at 5.03 ppm. The shift of the imine methyl groups is "normal", in contrast to that observed for low-valent Co and Fe complexes.

Preferring the pseudo square pyramidal geometry rather than pseudo trigonal bipyramidal is most likely because of avoiding unfavorable interaction of R ligands with ethyl groups. The $^{1}H$ NMR spectra of ($^{Et}$DIP)TiClR compounds showed *m*- and *p*-py hydrogens shifted strongly upfield in agreement with the large amount of electron density transferred from the metal center into the π-system of the ligand. The *m*-py hydrogens appeared as a doublet at 5.89, 5.98 and 5.72 ppm for **3a**, **3b** and **3c**, respectively. Also, the *p*-py hydrogens emerged as a triplet at 5.20, 5.27 and 5.04 ppm for **3a**, **3b** and **3c**, respectively. The trend in shielding of the hydrogens on the pyridine ring could be related to the Ti-C bond strength. Since the phenyl ligand is attached with a $sp^2$ carbon it makes a stronger bond relative to the other ligands coordinated with a $sp^3$ C. The $CH_3$ group causes less steric hindrance than $CH_2SiMe_3$ which might also lead to stronger bonding. Thus, these stronger interactions may result in increased electron density transfer to the π-system of the $^{Et}$DIP ligand. The NMR spectra of these complexes consistently showed two magnetically inequivalent ethyl groups on the NAr rings demonstrating that in solution apical and equatorial ligands bound to Ti do not switch positions: the number of peaks in the NMR spectra of **3a**, **3b** and **3c** indicates effective $C_s$ symmetry in solution.

Unlike for **2** and **3a-3c**, the NMR spectra of **4a** and **4b** are both temperature dependent, but in rather different ways. The spectrum of **4b** shows strongly broadened resonances for the alkyl

groups. On cooling to -40 °C the signals decoalesced to show two inequivalent $CH_2SiMe_3$ groups; heating to +85 °C resulted in coalescence to a single set of $CH_2SiMe_3$ resonances and effective $C_{2v}$ symmetry. Evidently the "inversion" of the SP structure is much more difficult for **4b** than for **2**. This is perhaps not surprising: in addition to a simple canting of the $TiR_2$ unit, 180° rotations around both Ti-$CH_2$ bonds are required, and these should be strongly hindered by the ligand side arms.

The room-temperature spectrum of **4a** also shows a rather broad resonance for the $TiMe_2$ unit. However, cooling does not result in decoalescence, nor does heating cause any sharpening. Rather, the chemical shift of the $TiMe_2$ signal changes by about 1.5 ppm over the temperature range from -40 to +80 °C, while the remaining signals are much less affected (Figure 2.11). Also, the linewidth of the $TiMe_2$ resonance increases somewhat at higher temperatures.

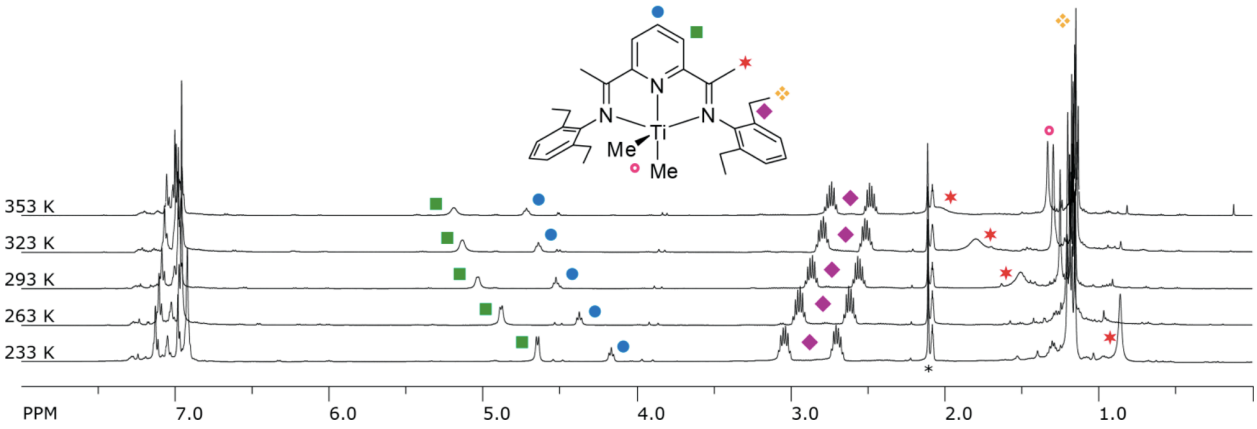


Figure 2.11. Variable Temperature $^1$H NMR of complex **4a**

Over the whole temperature range, the remaining ligand signals are consistent with effective $C_{2v}$ symmetry. Thus, we believe the most reasonable explanation for the imine methyl broadening is the presence of a small (<1%) and temperature-dependent amount of triplet (Et DIP)$TiMe_2$ in equilibrium with the dominant singlet species, similar to e.g. the situation

reported by Autschbach for bissemiquinone complexes of ruthenium.[33] Figure 2.12 shows the chemical shift change of TiMe hydrogens in **4a** as a function of temperature.

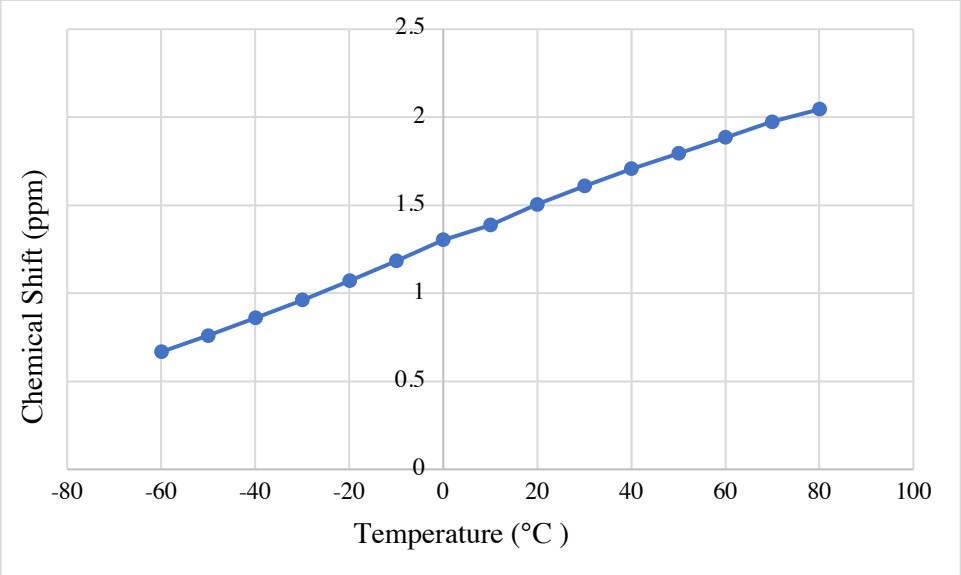


Figure 2.12. Chemical shift of C*H*$_3$C=N hydrogens in **4a** vs temperature

## 2.4.5 DFT

The geometries and electronic structures of **1-4b** have been studied with density functional theory (DFT) (TPSSh, TZVP, Turbomole). Solid-state structures were used as the initial guess while ethyl aryl groups were replaced with methyl substituents. The optimized geometry of **1** (C=N: 1.345-1.356 (Å); $C_{imine}$-$C_{py}$: 1.416-1.421 (Å)) is in good agreement with the experimental data (C=N: 1.312-1.351 (Å); $C_{imine}$-$C_{py}$: 1.411-1.427 (Å)) obtained by crystallography.

A spin density plot of **1** (<$S^2$>= 0.7591) is illustrated in Figure 2.13. The unpaired electron is mostly residing in the metal *d* orbital and partly in the π* of the ligand. This is consistent with EPR and XPS results for **1**.

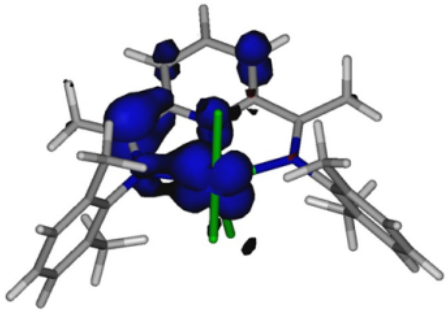

Figure 2.13. Spin density of **1**

HOMO and LUMO orbitals of **2** and **4a** are presented in Figure 2.14.

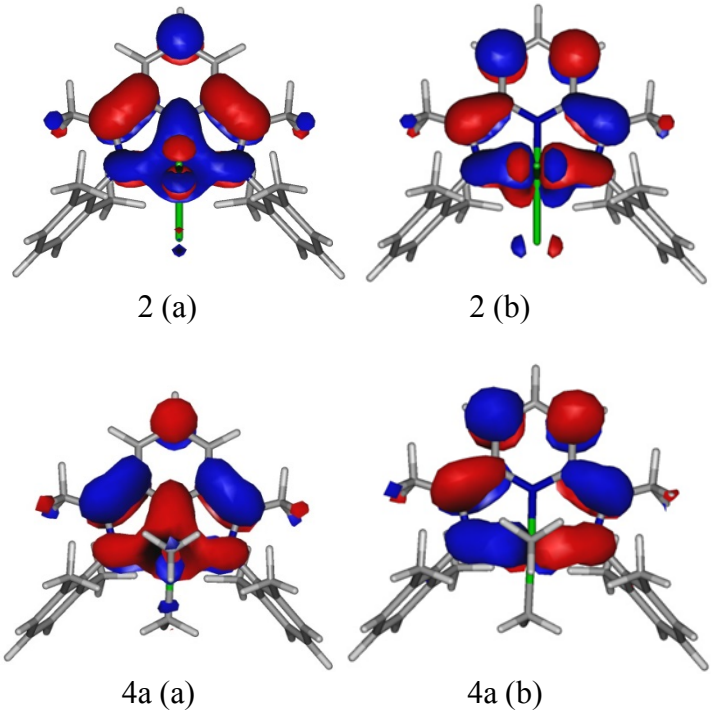


Figure 2.14. (a) HOMO and (b) LUMO orbitals of **2** and **4a**

As shown by X-ray data, theoretical results demonstrate a contraction of $C_{imine}$-$C_{py}$ bonds and an elongation of C=N bonds in the ligand backbone. Analysis of the frontier orbitals indicate that the HOMO of **2** and **4a** are ligand based and located on C-N, Ti-$N_{py}$ and Ti-$N_{imine}$ with a

bonding interaction between the $C_{imine}$-$C_{py}$ and an antibonding interaction between the C−N groups.

The singlet-triplet gaps calculated for **2** and **4a** are 2.02 and 1.30 kcal/mol, respectively. In contrast to **2**, the triplet electronic state of **4a** is calculated to be *lower* in energy than the singlet state at the level of theory used. It is clear from experiment that **4a** prefers a singlet state, but the small singlet-triplet gap we calculate supports an explanation of its $^1$H NMR line broadening based on thermal population of a low-lying triplet state.

## 2.5 Conclusions

True Ti(II) complexes are rare, and Ti(II) is a strong reductant. It is therefore not surprising that in the reported new formally low-valent Ti DIP complexes the diiminopyridine ligand is noninnocent, accepting up to two electrons. It seems complex **1** is perhaps closest to Ti(III)-$L^{(0)}$, while **2**-**4** are probably best regarded as containing Ti(IV)-$L^{(2-)}$. It is at this point not clear to us why further reduction of **1** to **2** also changes the balance between metal-centered and ligand-centered reduction of the *first* electron. The situation is somewhat analogous to the 1-electron reduction of Mn(II)$[L^{(0)}]_2^{2+}$, which produces Mn(III)$[L^{(-)}]_2^{2+}$ (i.e. *oxidation* of the metal centre) However, this Mn case involves a spin state change at the metal, which is not possible for Ti. Calculations and experiment agree in assigning singlet ground states for complexes **2**-**4**, despite the absence of potential antiferromagnetic coupling between metal-centred and ligand-centred electrons. However, singlet-triplet separations are small, and for complex **4a** NMR data indicate a modest thermal population of a triplet excited state.

The mono- and di-alkyl complexes **3** and **4** are surprisingly thermally stable, with both **4a** and **4b** surviving temperatures up to 85 °C in solution. However, alkyl derivatives bearing β-hydrogens could not be isolated, likely due to easy β-elimination.

## 2.6 Experimental Section

*General Considerations*. All air- and moisture-sensitive manipulations were carried out under Argon using standard Schlenk techniques or in an MBraun drybox containing an atmosphere of purified nitrogen. Solvents for air- and moisture-sensitive manipulations were dried and deoxygenated using sodium/benzophenone. Benzene-$d_6$ and toluene-$d_8$ were purchased from Cambridge Isotope Laboratories, distilled from sodium/benzophenone and stored in the drybox.

Pure $TiCl_3(THF)_3$ was isolated from refluxing a mixture of $TiCl_3.AlCl_3$ in tetrahydrofuran.[34] The $^{Et}$DIP ligand was prepared according to a literature procedure.[35]

$^1$H and $^{13}$C NMR spectra were recorded at 25 °C on a Bruker Avance 500 spectrometers. All chemical shifts are reported relative to $SiMe_4$ using $^1$H (residual) and $^{13}$C chemical shifts of the solvent as a secondary standard. $C_6D_6$, 7.16 and 128.06 ppm; $C_6D_5CD_3$, 2.08 and 20.43 ppm.[36] All coupling constants are in Hz. VT-NMR spectra were simulated using gNMR.[37]

Elemental analyses were performed at (1) Canadian Microanalytical Service, Delta, BC, Canada, and at (2) CENTC, University of Rochester, Rochester, NY, USA. In several cases, in particular for compounds containing Ti−C bonds, C analyses were low and irreproducible despite repeated crystallizations and the use of added oxidant for the combustion analysis. We attribute this to partial formation of Ti carbides during combustion.[38] NMR spectra are provided in the Supporting Information as additional proof of purity.

EPR samples of ($^{Et}$DIP)$TiCl_3$ (**1**) in a flame-dried J. Young valve EPR tube were prepared under strictly anaerobic conditions using distilled solvent and recrystallized [$^n$Bu$_4$N]$PF_6$. X-band EPR spectra were recorded on a Bruker EMX spectrometer (Bruker BioSpin) equipped with a He temperature control cryostat system (Oxford Instruments). Simulations of the EPR spectra were performed by iteration of the anisotropic g values and line widths using the EPR simulation program W95EPR developed by Prof. Dr. Frank Neese.[39]

Single crystals suitable for X-ray diffraction were either sealed in glass capillaries or coated with oil in a drybox and then quickly transferred to the goniometer head of a D8 three-circle (equipped with a rotating-anode generator MoKα X-radiation, multilayer optics and an APEX-II CCD area detector) and Bruker D8 QUEST ECO (equipped with MoKα X-ray tubes (λ =0.71 Å)) diffractometers. Preliminary data revealed the crystal system. Data collection was optimized for completeness and redundancy using the APEX3 software suite. The space group was identified, and the data were reduced using the SAINT program[40] and corrected for absorption using SADABS.[41] The structures were solved using direct methods (SHELXS[42]) completed by subsequent Fourier synthesis and refined by full-matrix least-squares procedures (SHELXL[42]).

The XPS spectra were collected on a Kratos Axis Ultra DLD XPS spectrometer in vacuum environment with a base pressure of 10-9 torr. Al Kα (1486.6 eV) monochromatic X-rays at 10 mA emission current and 15 kV anode voltage were used to excite the photoelectrons. Samples were transferred from a nitrogen glove box to the instrument in a sealed container designed to mate with the sample loading arm of the spectrometer so that the samples were not exposed to air/moisture. A co-axial charge neutralizer was utilized to prevent built up of charge on the samples. All spectra were collected with a fixed analyzer transmission mode. Survey scans were collected with a pass-energy of 160 eV and high resolution scans were collected with a pass-energy of 20 eV. Peak fitting of the high resolution XP spectra was performed using CasaXPS software (casaxps.com). All peak positions were normalized with respect to the C 1s peak with a binding energy of 285 eV.

**Computational Details**. For EPR studies, geometry optimizations of ($^{Et}$DIP)TiCl$_3$ (**1**) were carried out with the Turbomole program package[43] coupled to the PQS Baker optimizer[44,45] via the BOpt package,[46] at the b3-lyp[47]/def2-TZVP[48,49] level. The structure was characterized by a vibrational analysis (no imaginary frequencies). EPR parameters[50] were calculated with

the ADF2013[51] program system using the B3LYP functional with the ZORA/TZ2P basis sets supplied with the program (all electron, core double-ζ, valence triple-ζ, double polarized basis set on all atoms), using the coordinates from the X-ray structure or structures optimized in Turbomole as inputs (unrestricted SPINORBIT ZORA COLLINEAR calculations for the SOC corrected HFI tensors and spin polarization corrected g tensors).

EPR parameters were also calculated with ORCA[52] using the B3LYP functional and the def2-TZVP[48-49] basis set (NORI, SOCType 3, SOCFlags 1,2,3,1), again using the X-ray geometry or the geometry obtained by geometry optimization using Turbomole, giving results almost identical with those for ADF. For examination of the SP-TBP path for **4a′**, as well as prediction of NMR data, geometry optimizations for **1′**−**4′** were performed with Turbomole[43] (V6.3) coupled to the PQS Baker optimizer[44,45] at the TPSSh[53]/def TZVP[48] level. Vibrational analyses were used to confirm the nature of the stationary points (no imaginary frequencies). Free energies were obtained by combining electronic energy, enthalpy, and entropy corrections (298 K, entropy scaled by 0.67[54,55]) with dispersion corrections calculated using DFT-D3 (options "-func tpssh -zero").[56] NMR chemical shifts (TPSSh functional, GIAO method;[57,58] IGLO-II basis set[59]) were calculated using Gaussian 09.[60] MO and spin density plots were generated with the program Molden.[61]

**($^{Et}$DIP)TiCl$_3$** (**1**). A 100 mL Schlenk tube was charged with 2.30 g (6.20 mmol) of $TiCl_3(THF)_3$, approximately 30 mL of THF, and a stirrer bar. $^{Et}$DIP (3.96 g, 9.30 mmol) was added, and the reaction mixture was stirred for 12 h, during which the color quickly changed to green. The solid was filtered off and washed three times with 20 mL of THF. The obtained crystals were dried in vacuo, giving 3.23 g of ($^{Et}$DIP)$TiCl_3$ (90%). Suitable single crystals for X-ray studies were obtained by careful layering (1:1) of solutions of $TiCl_3(THF)_3$ and $^{Et}$DIP.

Anal. Calcd for $C_{29}H_{35}N_3Cl_3Ti \cdot C_4H_8O$: C, 60.80; H, 6.65; N, 6.45. Found (1): C, 60.38; H, 7.01; N, 6.28.

**($^{Et}$DIP)TiCl$_2$** (**2**). A 100 mL Schlenk tube was charged with 2.27 g (3.48 mmol) of complex **1**, approximately 30 mL of THF, and a stirrer bar. $KC_8$ (0.47 g, 3.48 mmol) was added, and the reaction mixture was stirred for 3 days. Suspended solid was removed by centrifugation, and the solvent was removed in vacuo. The solid residue was dissolved in a few milliliters of toluene and left at −35 °C to give 1.81 g (95%) of dark green crystals suitable for X-ray crystallography.

Anal. Calcd for $C_{29}H_{35}N_3Cl_2Ti$: C, 63.98; H, 6.48; N, 7.72. Found: C, 63.74; H, 6.85; N, 7.44. $^1$H NMR (500 MHz, toluene-$d_8$): δ 1.21 (12H, t, *J* 7.5, $CH_2CH_3$), 1.79 (6H, s, $CH_3C$=N), 2.4, 2.9 (4H each, m, $CH_2CH_3$), 5.11 (1H, t, *J* 7.5, py 4), 5.99 (2H, d, *J* 8.0, py 3/5), 7.14 (6H, m, Ar). $^{13}$C{$^1$H} NMR (500 MHz, toluene-$d_8$): δ 14.3 ($CH_2CH_3$), 15.0 ($CH_3$C=N), 24.2 ($CH_2CH_3$), 123.9 (py 4), 126.5 (*m*-Ar), 126.9 (py 3), 127.8 (*p*-Ar), 134.9 (*o*-Ar), 142.4, 148.8 (py 2, C=N), 166.6 (*i*-Ar).

**($^{Et}$DIP)TiCl(Me)** (**3a**). A 100 mL Schlenk tube was charged with 0.168 g (0.308 mmol) of **2**, approximately 15 mL of toluene, and a stirrer bar. Solid MeLi (0.01 g, 0.455 mmol) was added, and the reaction mixture was stirred for 3 days. Suspended solids were removed by centrifugation, and the solvent was removed in vacuo. The solid residue was dissolved in a few milliliters of toluene and left to crystallize at −35 °C, producing 0.076 g (47%) of dark green crystals suitable for X-ray crystallography (containing one molecule of toluene of crystallization).

Anal. Calcd for $C_{30}H_{38}N_3ClTi.C_7H_8$, Calcd: C, 72.13; H, 7.52; N, 6.82. Found (1): C, 70.62; H, 7.66; N, 6.77. $^1$H NMR (500 MHz, toluene-$d_8$): δ 0.91 (6H, t, *J* 7.5, $CH_2CH_3$), 1.30 (6H, s,

$CH_3C$=N), 1.36 (6H, t, *J* 7.8, $CH_2CH_3$), 1.9, 2.0 (2H each, m, $CH_2CH_3$), 2.04 (3H, s, Ti-Me), 2.6, 3.1 (2H each, m, $CH_2CH_3$), 5.19 (1H, t, *J* 7.5, py 4), 5.87 (2H, d, *J* 7.5, py 3/5), 6.88 (2H, d, *J* 7.5, *m*-Ar), 7.07 (2H, t, *J* 7.5, *p*-Ar), 7.14 (2H, d, *J* 7.5, *m*-Ar). $^{13}C\{^1H\}$ NMR (500 MHz, toluene-$d_8$): δ 14.3, 14.5 ($CH_2CH_3$), 14.7 ($CH_3C$=N), 23.8, 24.7 ($CH_2CH_3$), 64.8 (Ti-Me), 119.9 (py 4), 126.2, 126.4 (*m*-Ar), 127.1 (*p*-Ar), 128.5 (py 3), 133.1, 137.2 (*o*-Ar), 139.6, 148.0, 160.9 (py 2, C=N, *i*-Ar).

**($^{Et}$DIP)TiCl($CH_2Si(CH_3)_3$)** (**3b**). A 100 mL Schlenk tube was charged with 0.203 g (0.373 mmol) of **2**, 15 mL of toluene, and a stirrer bar. Solid $Me_3SiCH_2Li$ (0.0351 g, 0.373 mmol) was added, and the reaction mixture was stirred for 3 days. Suspended solids were removed by centrifugation, and the solvent was removed in vacuo. The solid residue was dissolved in a few milliliters of diisopropyl ether and layered with pentane. Crystallization at −35 °C gave 0.117 g (52%) of dark green crystals.

Anal. Calcd for $C_{33}H_{46}N_3ClSiTi$: C, 66.49; H, 7.78; N, 7.05. Found (2): C, 67.36; H, 7.39; N, 7.41. $^1H$ NMR (500 MHz, benzene-$d_6$): δ 0.08 (2H, s, Ti-$CH_2$), 0.74 (9H, s, $SiMe_3$), 1.04, 1.32 (6H each, t, *J* 7.5, $CH_2CH_3$), 1.34 (6H, s, $CH_3C$=N), 2.2, 2.3, 2.6, 3.3 (2H each, m, $CH_2CH_3$), 5.29 (1H, t, *J* 7.5, py 4), 5.99 (2H, d, *J* 8, py 3/5), 6.97 (2H, d, *J* 7.5, *m*-Ar), 7.11 (2H, t, *J* 7.5 Hz, *p*-Ar), 7.22 (2H, d, *J* 7.5, *m*-Ar). $^{13}C\{^1H\}$ NMR (500 MHz, benzene-$d_6$): δ 3.3 ($SiMe_3$), 14.0, 14.7 ($CH_2CH_3$), 14.9 ($CH_3C$=N), 23.7, 24.7 ($CH_2CH_3$), 84.1 (Ti-$CH_2$), 119.2 (py 4), 126.1, 126.5, 127.2 (*m*- and *p*-Ar), 128.8 (py 3), 132.7, 137.7 (*o*-Ar), 140.7, 148.6, 161.4 (py 2, C=N, *i*-Ar).

**($^{Et}$DIP)TiCl(Ph)** (**3c**). A 100 mL Schlenk tube was charged with 0.215 g (0.395 mmol) of **2**, 15 mL of toluene, and a stirrer bar. Solid PhLi (0.035 g, 0.416 mmol) was added, and the reaction mixture was stirred for 4 days. Suspended solids were removed by centrifugation,

and the solvent was removed in vacuo. The residue was dissolved in a few milliliters of diisopropyl ether and layered with pentane (1:5). Crystallization at −35 °C gave 0.127 g (55%) of dark green crystals. X-ray quality crystals were obtained from benzene.

Anal. Calcd for $C_{35}H_{40}N_3ClTi$: C, 71.73; H, 6.88; N, 7.17. Found (2): C, 68.25; H, 6.76; N, 6.94. $^1$H NMR (500 MHz, benzene-$d_6$): δ 0.58 (6H, t, *J* 7.5, $CH_2CH_3$), 1.07 (6H, s, $CH_3C$=N), 1.46 (4H, q, *J* 7.5, $CH_2CH_3$), 1.55 (6H, t, *J* 7.8, $CH_2CH_3$), 3.1, 3.8 (2H each, m, $CH_2CH_3$), 4.90 (1H, t, *J* 7.8, py 4), 5.58 (2H, d, *J* 7.5, py 3/5), 6.80 (2H, d, *J* 7.5, *m*-Ar), 7.04 (2H, t, *J* 7.5, *p*-Ar), 7.18 (1H, t, *J* 7.0, *p*-Ph), 7.24 (2H, d, *J* 7.5, *m*-Ar), 7.37 (2H, t, *J* 7.5, *m*-Ph), 8.63 (2H, d, *J* 6.0, *o*-Ph). $^{13}$C{$^1$H} NMR (500 MHz, benzene-$d_6$): δ 13.5, 14.4 ($CH_2CH_3$), 14.5 ($CH_3C$=N), 23.0, 25.1 ($CH_2CH_3$), 120.9 (py 4), 125.8, 126.5 (*m*-Ar), 127.0 (*o*-Ph), 127.2 (*p*-Ar), 127.5 (*m*-Ph), 129.3 (py 3), 130.5 (*p*-Ph), 132.5, 137.7 (*o*-Ar), 141.0, 147.4, 163.3 (py 2, C=N, *i*-Ar), 207.4 (*i*-Ph).

**($^{Et}$DIP)Ti(Me)$_2$** (**4a**). A 100 mL Schlenk tube was charged with 0.548 g (1.01 mmol) of **2**, approximately 15 mL of toluene, and a stirrer bar. Solid MeLi (0.053 g, 2.41 mmol) was added, and the reaction mixture was stirred for 2 days. Suspended solids were removed by centrifugation, and the solvent was removed in vacuo. The solid residue was dissolved in a few milliliters of diethyl ether and crystallized at −35 °C, giving 0.336 g (66%) of dark green crystals.

Anal. Calcd for $C_{31}H_{41}N_3Ti$: C, 73.94; H, 8.21; N, 8.34. Found (1): C, 72.69; H, 8.21; N, 8.17; (2): C, 69.63; H, 7.50; N, 7.95; (2): C, 70.67; H, 7.92; N, 8.21. $^1$H NMR (500 MHz, toluene-$d_8$): δ 1.17 (12 H, t, *J* 7.5, $CH_2CH_3$), 1.38 (6H, s, $Ti(CH_3)_2$), 1.57 (6H, br, $CH_3C$=N), 2.6, 2.9 (4H each, m, $CH_2CH_3$), 4.57 (1H, br t, py 4), 5.08 (2H, br, py 3/5), 7.02 (6H, s, Ar). $^{13}$C{$^1$H} NMR (500 MHz, toluene-$d_8$): δ 12.6 (br, $CH_3C$=N), 14.4 ($CH_2CH_3$), 24.1 ($CH_2CH_3$),

59.8 (br, $Ti(CH_3)_2$) 118.8 (py 4), 126.1 (*m*-Ar), 126.6 (*p*-Ar), 136.9 (*o*-Ar), 144.0 (br), 146.1, 155.5 (v br) (py 2, C=N, *i*-Ph). Py 3 not detected.

**($^{Et}$DIP)Ti($CH_2Si(CH_3)_3$)$_2$** (**4b**). A 100 mL Schlenk tube was charged with 0.201 g (0.370 mmol) of **2**, 15 mL of toluene, and a stirrer bar. $Me_3SiCH_2Li$ (0.070 g, 0.740 mmol) was added, and the reaction mixture was stirred for 3 days. Suspended solids were removed by centrifugation, and the solvent was removed in vacuo. The solid residue was dissolved in a few milliliters of diisopropyl ether and left to crystallize at −35 °C, giving 0.153 g (64%) of dark green crystals.

Anal. Calcd for $C_{37}H_{57}N_3Si_2Ti$: C, 68.59; H, 8.87; N, 6.49. Found (1): C, 68.04; H, 9.18; N, 6.82. $^1$H NMR (500 MHz, toluene-$d_8$): δ 0.10 (18H, br s, $SiMe_3$), 1.21 (12H, t, *J* 7.5, $CH_2CH_3$), 1.32 (6H, s, $CH_3C$=N), 2.5 (4H, m, $CH_2CH_3$), 2.8 (4H, br, $CH_2CH_3$), 5.12 (1H, t, *J* 7.5, py 4), 5.81 (2H, d, *J* 7.5, py 3/5), 7.07 (6H, s, Ar). $TiCH_2$ not observed. $^{13}$C{$^1$H} NMR (500 MHz, toluene-$d_8$): δ 2.8 ($SiMe_3$), 13.9 ($CH_2CH_3$), 14.5 ($CH_3C$=N), 24.2 ($CH_2CH_3$), 80.5 (br, $TiCH_2$), 118.5 (py 4), 126.3 (*m*-Ar), 126.8 (*p*-Ar), 127.8 (py 3), 135.8 (br, *o*-Ar), 142.7, 148.5, 155.8 (py 2, C=N) (*i*-Ar). $^1$H NMR (500 MHz, toluene-$d_8$, 80 °C): δ 0.03 (18H, s, $SiMe_3$), 1.19 (12H, t, *J* 7.3, $CH_2CH_3$), 1.36 (4H, br s, $TiCH_2$), 1.42 (6H, s, $CH_3C$=N), 2.5 (4 H, m, $CH_2CH_3$), 2.7 (4H, $CH_2CH_3$), 5.19 (1H, t, *J* 7.0, py 4), 5.89 (2H, d, *J* 7.0, py 3/5), 7.07 (6H, s, Ar). $^1$H NMR (500 MHz, toluene-$d_8$, −50 °C): δ −0.35 (9H, s, $SiMe_3$), 0.07 (2H, s, $TiCH_2$), 0.85 (9H, s, $SiMe_3$), 1.18 (12H, br s, $CH_2CH_3$ and $CH_3C$=N), 1.28 (6H, br s, $CH_2CH_3$), 2.4 (2H, br m, $CH_2CH_3$), 2.5 (4H, br m, $CH_2CH_3$), 2.82 (2H, s, $TiCH_2$), 3.3 (2H, br, $CH_2CH_3$), 5.02 (1H, t, *J* 7.8, py 4), 5.62 (2H, d, *J* 7.5, py 3/5), 7.1 (6H, m, Ar).

## 2.7 References


1. Boor, J., *Ziegler-Natta Catalysts and Polymerization*. Academic Press, New York: 1979.

2. (a) Zhang, H.; Nomura, K., Living Copolymerization of Ethylene with Styrene Catalyzed by (Cyclopentadienyl)(ketimide)titanium(IV) Complex−MAO Catalyst System. *J. Am. Chem. Soc.* **2005,** *127* (26), 9364-9365; (b) Furuyama, R.; Mitani, M.; Mohri, J.-i.; Mori, R.; Tanaka, H.; Fujita, T., Ethylene/Higher α-Olefin Copolymerization Behavior of Fluorinated Bis(phenoxy−imine)titanium Complexes with Methylalumoxane: Synthesis of New Polyethylene-Based Block Copolymers. *Macromolecules* **2005,** *38* (5), 1546-1552; (c) Chen, Z.; Li, J.-F.; Tao, W.-J.; Sun, X.-L.; Yang, X.-H.; Tang, Y., Copolymerization of Ethylene with Functionalized Olefins by [ONX] Titanium Complexes. *Macromolecules* **2013,** *46* (7), 2870-2875.

3. Tshuva, E. Y.; Goldberg, I.; Kol, M.; Goldschmidt, Z., Living polymerization and block copolymerization of [small alpha]-olefins by an amine bis(phenolate) titanium catalyst. *Chem. Commun.* **2001,** (20), 2120-2121.

4. Duncalf, D. J.; Wade, H. J.; Waterson, C.; Derrick, P. J.; Haddleton, D. M.; McCamley, A., Synthesis and Mechanism of Formation of Syndiotactic Polystyrene Using a (tert-Butylcyclopentadienyl)titanium Complex. *Macromolecules* **1996,** *29* (20), 6399-6403.

5. Frediani, M.; Sémeril, D.; Comucci, A.; Bettucci, L.; Frediani, P.; Rosi, L.; Matt, D.; Toupet, L.; Kaminsky, W., Ultrahigh-Molecular-Weight Polyethylene by Using a Titanium Calix[4]arene Complex with High Thermal Stability under Polymerization Conditions. *Macromol. Chem. Phys.* **2007,** *208* (9), 938-945.

6. Esteruelas, M. A.; López, A. M.; Mateo, A. C.; Oñate, E., New Titanium Complexes Containing a Cyclopentadienyl Ligand with a Pendant Aminoalkyl Substituent: Preparation,

Behavior of the Amino Group, and Catalytic Hydroamination of Alkynes. *Organometallics* **2005,** *24* (21), 5084-5094.

7. Kool, L. B.; Rausch, M. D.; Herberhold, M.; Alt, H. G.; Thewalt, U.; Honold, B., Diamagnetic isocyanide complexes of titanium, zirconium, and hafnium. *Organometallics* **1986,** *5* (12), 2465-2468.

8. Basuli, F.; Huffman, J. C.; Mindiola, D. J., Reactivity at the β-Diketiminate Ligand Nacnac- on Titanium(IV) (Nacnac- = [Ar]NC(CH3)CHC(CH3)N[Ar], Ar = 2,6-[CH(CH3)2]2C6H3). Diimine-alkoxo and Bis-anilido Ligands Stemming from the Nacnac-Skeleton. *Inorg. Chem.* **2003,** *42* (24), 8003-8010.

9. (a) Gielens, E. E. C. G.; Tiesnitsch, J. Y.; Hessen, B.; Teuben, J. H., Titanium Hydrocarbyl Complexes with a Linked Cyclopentadienyl−Alkoxide Ancillary Ligand; Participation of the Ligand in an Unusual Activation of a (Trimethylsilyl)methyl Group. *Organometallics* **1998,** *17* (9), 1652-1654; (b) Christie, S. D. R.; Man, K. W.; Whitby, R. J.; Slawin, A. M. Z., Novel Routes to Bidentate Cyclopentadienyl−Alkoxide Complexes of Titanium: Synthesis of (η5-σ-C5R14CHR2CH2CR3R4O)TiCl2. *Organometallics* **1999,** *18* (3), 348-359.

10. Girolami, G. S.; Wilkinson, G.; Galas, A. M. R.; Thornton-Pett, M.; Hursthouse, M. B., Synthesis and properties of the divalent 1,2-bis(dimethylphosphino)ethane (dmpe) complexes MCl2(dmpe)2 and MMe2(dmpe)2(M = Ti, V, Cr, Mn, or Fe). X-Ray crystal structures of MCl2(dmpe)2(M = Ti, V, or Cr), MnBr2(dmpe)2, TiMe1.3Cl0.7(dmpe)2, and CrMe2(dmpe)2. *J. Chem. Soc., Dalton Trans.* **1985,** (7), 1339-1348.

11. (a) Hitchcock, P. B.; Kerton, F. M.; Lawless, G. A., The Elusive Titanocene. *J. Am. Chem. Soc.* **1998,** *120* (39), 10264-10265; (b) Brintzinger, H.; Bercaw, J. E., Bis(pentamethylcyclopentadienyl)titanium(II). Isolation and reactions with hydrogen, nitrogen, and carbon monoxide. *J. Am. Chem. Soc.* **1971,** *93* (8), 2045-2046.

12. Graham, T. W.; Kickham, J.; Courtenay, S.; Wei, P.; Stephan, D. W., Reduction of Titanium(IV)-Phosphinimide Complexes: Routes to Ti(III) Dimers, Ti(IV)-Metallacycles, and Ti(II) Species. *Organometallics* **2004,** *23* (13), 3309-3318.

13. Hagadorn, J. R.; Arnold, J., Low-Valent Chemistry of Titanium Benzamidinates Leading to New Ti μ-N2, μ-O, Alkyl Derivatives, and the Cyclometalation of TMEDA. *J. Am. Chem. Soc.* **1996,** *118* (4), 893-894.

14. Tondreau, A. M.; Stieber, S. C. E.; Milsmann, C.; Lobkovsky, E.; Weyhermüller, T.; Semproni, S. P.; Chirik, P. J., Oxidation and Reduction of Bis(imino)pyridine Iron Dinitrogen Complexes: Evidence for Formation of a Chelate Trianion. *Inorg. Chem.* **2013,** *52* (2), 635-646.

15. Zhu, D.; Korobkov, I.; Budzelaar, P. H. M., Radical Mechanisms in the Reaction of Organic Halides with Diiminepyridine Cobalt Complexes. *Organometallics* **2012,** *31* (10), 3958-3971.

16. (a) Hoyt, J. M.; Schmidt, V. A.; Tondreau, A. M.; Chirik, P. J., Iron-catalyzed intermolecular [2+2] cycloadditions of unactivated alkenes. *Science* **2015,** *349* (6251), 960-963; (b) Bart, S. C.; Lobkovsky, E.; Chirik, P. J., Preparation and Molecular and Electronic Structures of Iron(0) Dinitrogen and Silane Complexes and Their Application to Catalytic Hydrogenation and Hydrosilation. *J. Am. Chem. Soc.* **2004,** *126* (42), 13794-13807; (c) Tondreau, A. M.; Atienza, C. C. H.; Weller, K. J.; Nye, S. A.; Lewis, K. M.; Delis, J. G. P.; Chirik, P. J., Iron Catalysts for Selective Anti-Markovnikov Alkene Hydrosilylation Using Tertiary Silanes. *Science* **2012,** *335* (6068), 567-570.

17. Vidyaratne, I.; Gambarotta, S.; Korobkov, I.; Budzelaar, P. H. M., Dinitrogen Partial Reduction by Formally Zero- and Divalent Vanadium Complexes Supported by the Bis-iminopyridine System. *Inorg. Chem.* **2005,** *44* (5), 1187-1189.

18. Vidyaratne, I.; Scott, J.; Gambarotta, S.; Budzelaar, P. H. M., Dinitrogen Activation, Partial Reduction, and Formation of Coordinated Imide Promoted by a Chromium Diiminepyridine Complex. *Inorg. Chem.* **2007,** *46* (17), 7040-7049.

19. Russell, S. K.; Bowman, A. C.; Lobkovsky, E.; Wieghardt, K.; Chirik, P. J., Synthesis and Electronic Structure of Reduced Bis(imino)pyridine Manganese Compounds. *Eur. J. Inorg. Chem.* **2012,** *2012* (3), 535-545.

20. Kooistra, T. M.; Knijnenburg, Q.; Smits, J. M. M.; Horton, A. D.; Budzelaar, P. H. M.; Gal, A. W., Olefin Polymerization with [{bis(imino)pyridyl}CoIICl2]: Generation of the Active Species Involves CoI. *Angew. Chem. Int. Ed.* **2001,** *40* (24), 4719-4722.

21. Zhu, D.; Thapa, I.; Korobkov, I.; Gambarotta, S.; Budzelaar, P. H. M., Redox-Active Ligands and Organic Radical Chemistry. *Inorg. Chem.* **2011,** *50* (20), 9879-9887.

22. Calderazzo, F.; Englert, U.; Pampaloni, G.; Santi, R.; Sommazzi, A.; Zinna, M., Bis(arylimino)pyridine derivatives of Group 4 metals: preparation, characterization and activity in ethylene polymerization. *Dalton Trans.* **2005,** (5), 914-922.

23. (a) Hanna, T. E.; Lobkovsky, E.; Chirik, P. J., Dinitrogen Activation by Titanium Sandwich Complexes. *J. Am. Chem. Soc.* **2004,** *126* (45), 14688-14689; (b) Pez, G. P.; Apgar, P.; Crissey, R. K., Reactivity of .mu.-(.eta.1:.eta.5-cyclopentadienyl)-tris(.eta.-cyclopentadienyl)dititanium ([.mu.-(.eta.1:.eta.5-C5H4)](.eta.-C5H5)3Ti2) with dinitrogen. Structure of a titanium complex with a triply coordinated dinitrogen ligand. *J. Am. Chem. Soc.* **1982,** *104* (2), 482-490; (c) Sanner, R. D.; Duggan, D. M.; McKenzie, T. C.; Marsh, R. E.; Bercaw, J. E., Structure and magnetism of .mu.-dinitrogen-bis(bis(pentamethylcyclopentadienyl)titanium(II)), {(.eta.5-C5(CH3)5)2Ti}2N2. *J. Am. Chem. Soc.* **1976,** *98* (26), 8358-8365; (d) Volpin, M. E.; Shur, V. B.; Kudryavtsev, R. V.; Prodayko, L. A., Amine formation in molecular nitrogen fixation: nitrogen insertion into transition metal-carbon bonds. *Chem. Commun.* **1968,** (17), 1038-1040.

24. Fürstner, A.; Bogdanović, B., New Developments in the Chemistry of Low-Valent Titanium. *Angew. Chem. Int. Ed.* **1996,** *35* (21), 2442-2469.

25. Addison, A. W.; Rao, T. N.; Reedijk, J.; van Rijn, J.; Verschoor, G. C., Synthesis, structure, and spectroscopic properties of copper(II) compounds containing nitrogen–sulphur donor ligands; the crystal and molecular structure of aqua[1,7-bis(N-methylbenzimidazol-2′-yl)-2,6-dithiaheptane]copper(II) perchlorate. *J. Chem. Soc., Dalton Trans.* **1984,** (7), 1349-1356.

26. (a) Liu, H.; Jia, X.; Wang, F.; Dai, Q.; Wang, B.; Bi, J.; Zhang, C.; Zhao, L.; Bai, C.; Hu, Y.; Zhang, X., Synthesis of bis(N-arylcarboximidoylchloride)pyridine cobalt(ii) complexes and their catalytic behavior for 1,3-butadiene polymerization. *Dalton Trans.* **2013,** *42* (37), 13723-13732; (b) Kooistra, T. M.; Hekking, Koen F. W.; Knijnenburg, Q.; de Bruin, B.; Budzelaar, Peter H. M.; de Gelder, R.; Smits, Jan M. M.; Gal, Anton W., Cobalt Chloride Complexes of N3 and N4 Donor Ligands. *Eur. J. Inorg. Chem.* **2003,** *2003* (4), 648-655; (c) Cámpora, J.; Naz, A. M.; Palma, P.; Rodríguez-Delgado, A.; Álvarez, E.; Tritto, I.; Boggioni, L., Iron and Cobalt Complexes of 4-Alkyl-2,6-diiminopyridine Ligands: Synthesis and Ethylene Polymerization Catalysis. *Eur. J. Inorg. Chem.* **2008,** *2008* (11), 1871-1879; (d) Britovsek, G. J. P.; Bruce, M.; Gibson, V. C.; Kimberley, B. S.; Maddox, P. J.; Mastroianni, S.; McTavish, S. J.; Redshaw, C.; Solan, G. A.; Strömberg, S.; White, A. J. P.; Williams, D. J., Iron and Cobalt Ethylene Polymerization Catalysts Bearing 2,6-Bis(Imino)Pyridyl Ligands: Synthesis, Structures, and Polymerization Studies. *J. Am. Chem. Soc.* **1999,** *121* (38), 8728-8740; (e) Reardon, D.; Aharonian, G.; Gambarotta, S.; Yap, G. P. A., Mono- and Zerovalent Manganese Alkyl Complexes Supported by the α,α‘-Diiminato Pyridine Ligand: Alkyl Stabilization at the Expense of Catalytic Performance. *Organometallics* **2002,** *21* (5), 786-788.

27. Edema, J. J. H.; Duchateau, R.; Gambarotta, S.; Hynes, R.; Gabe, E., Novel titanium(II) amine complexes L4TiCl2[L = 1/2 N,N,N',N'-tetramethylethylenediamine (TMEDA), 1/2 N,N,N'-trimethylethylenediamine, pyridine, 1/2 2,2'-bipyridine]: synthesis and crystal structure of monomeric trans-(TMEDA)2TiCl2. *Inorg. Chem.* **1991,** *30* (2), 154-156.

28. Jensen, J. A.; Wilson, S. R.; Schultz, A. J.; Girolami, G. S., Divalent titanium chemistry. Synthesis, reactivity, and x-ray and neutron diffraction studies of Ti(BH4)2(dmpe)2 and Ti(CH3)2(dmpe)2. *J. Am. Chem. Soc.* **1987,** *109* (26), 8094-8096.

29. Guérin, F.; McConville, D. H.; Payne, N. C., Conformationally Rigid Diamide Complexes: Synthesis and Structure of Titanium(IV) Alkyl Derivatives. *Organometallics* **1996,** *15* (24), 5085-5089.

30. (a) Siokou, A.; Ntais, S., *Surf. Sci.* **2003,** *540*, 379-388; (b) Magni, E.; Somorjai, G. A., *J. Phys. Chem. B* **1998,** *102*, 8788-8795; (c) Hasebe, K.; Mori, H.; Terano, M., *J. Mol. Catal. A: Chem.* **1997,** *124*, L1-L3.

31. Gonbeau, D.; Guimon, C.; Pfisterguillouzo, G.; Levasseur, A.; Meunier, G.; Dormoy, R., *Surf. Sci.* **1991,** *254*, 81-89.

32. Franzen, H. F.; Umaña, M. X.; McCreary, J. R.; Thorn, R. J., XPS spectra of some transition metal and alkaline earth monochalcogenides. *J. Solid State Chem.* **1976,** *18* (4), 363-368.

33. Le Guennic, B.; Floyd, T.; Galan, B. R.; Autschbach, J.; Keister, J. B., Paramagnetic Effects on the NMR Spectra of “Diamagnetic” Ruthenium(bis-phosphine)(bis-semiquinone) Complexes. *Inorg. Chem.* **2009,** *48* (12), 5504-5511.

34. Jones, N. A.; Liddle, S. T.; Wilson, C.; Arnold, P. L., Titanium(III) Alkoxy-N-heterocyclic Carbenes and a Safe, Low-Cost Route to TiCl3(THF)3. *Organometallics* **2007,** *26* (3), 755-757.

35. Schmidt, R.; Welch, M. B.; Knudsen, R. D.; Gottfried, S.; Alt, H. G., N,N,N-Tridentate iron(II) and vanadium(III) complexes: Part I. Synthesis and characterization. *J. Mol. Catal. A: Chem.* **2004,** *222* (1), 9-15.

36. Fulmer, G. R.; Miller, A. J. M.; Sherden, N. H.; Gottlieb, H. E.; Nudelman, A.; Stoltz, B. M.; Bercaw, J. E.; Goldberg, K. I., NMR Chemical Shifts of Trace Impurities: Common Laboratory Solvents, Organics, and Gases in Deuterated Solvents Relevant to the Organometallic Chemist. *Organometallics* **2010,** *29* (9), 2176-2179.

37. Budzelaar, P. H. M. *gNMR, 5.0.6*, IvorySoft (http://home.cc.umanitoba.ca/~budzelaa/gNMR/gNMR.htmlhttp: home.cc.umanitoba.ca/~budzelaagNMR/gNMR.html): 2006.

38. Stephan, D. W.; Stewart, J. C.; Guérin, F.; Courtenay, S.; Kickham, J.; Hollink, E.; Beddie, C.; Hoskin, A.; Graham, T.; Wei, P.; Spence, R. E. v. H.; Xu, W.; Koch, L.; Gao, X.; Harrison, D. G., An Approach to Catalyst Design: Cyclopentadienyl-Titanium Phosphinimide Complexes in Ethylene Polymerization. *Organometallics* **2003,** *22* (9), 1937-1947.

39. Neese, F., QCPE Bull.: 1995; p. 15.

40. *smart program suite, 6*, Bruker AXS Inc.; Madison, WI.

41. Sheldrick, G. M. *SADABS*, University of Göttingen, Göttingen, Germany.

42. Sheldrick, G. M., *Acta Crystallogr. Sect. A: Found. Crystallogr.* **2008,** *64*, 112-122.

43. *TURBOMOLE, V6.3*, TURBOMOLE GmbH, Karlsruhe, Germany: 2011.

44. Baker, J., An algorithm for the location of transition states. *J. Comput. Chem.* **1986,** *7* (4), 385-395.

45. Baker, J. *PQS, 2.4*, Parallel Quantum Solutions, Fayetteville, AR: 2001.

46. Budzelaar, P. H. M., Geometry optimization using generalized, chemically meaningful constraints. *J. Comput. Chem.* **2007,** *28* (13), 2226-2236.

47. (a) Lee, C. T.; Yang, W. T.; Parr, R. G., Development of the Colle-Salvetti correlation-energy formula into a functional of the electron density. **1988,** *37*, 785-789; (b) Becke, A. D., A new mixing of Hartree–Fock and local density-functional theories. *The Journal of Chemical Physics* **1993,** *98* (2), 1372-1377; (c) Becke, A. D., Density-functional thermochemistry. III. The role of exact exchange. *The Journal of Chemical Physics* **1993,** *98* (7), 5648-5652.

48. Weigend, F.; Häser, M.; Patzelt, H.; Ahlrichs, R., RI-MP2: optimized auxiliary basis sets and demonstration of efficiency. *Chem. Phys. Lett.* **1998,** *294* (1), 143-152.

49. Weigend, F.; Ahlrichs, R., Balanced basis sets of split valence, triple zeta valence and quadruple zeta valence quality for H to Rn: Design and assessment of accuracy. *PCCP* **2005,** *7* (18), 3297-3305.

50. (a) Lenthe, E. v.; Wormer, P. E. S.; Avoird, A. v. d., Density functional calculations of molecular g-tensors in the zero-order regular approximation for relativistic effects. *The Journal of Chemical Physics* **1997,** *107* (7), 2488-2498; (b) Lenthe, E. v.; Avoird, A. v. d.; Wormer, P. E. S., Density functional calculations of molecular hyperfine interactions in the zero order regular approximation for relativistic effects. *The Journal of Chemical Physics* **1998,** *108* (12), 4783-4796.

51. Versluis, L.; Ziegler, T., The determination of molecular structures by density functional theory. The evaluation of analytical energy gradients by numerical integration. *The Journal of Chemical Physics* **1988,** *88* (1), 322-328.

52. Neese, F., The ORCA program system. *Wiley Interdisciplinary Reviews: Computational Molecular Science* **2012,** *2* (1), 73-78.

53. Tao, J.; Perdew, J. P.; Staroverov, V. N.; Scuseria, G. E., Climbing the Density Functional Ladder: Nonempirical Meta–Generalized Gradient Approximation Designed for Molecules and Solids. *Phys. Rev. Lett.* **2003,** *91*, 146401.

54. Raucoules, R.; de Bruin, T.; Raybaud, P.; Adamo, C., Theoretical Unraveling of Selective 1-Butene Oligomerization Catalyzed by Iron−Bis(arylimino)pyridine. *Organometallics* **2009,** *28* (18), 5358-5367.

55. Tobisch, S.; Ziegler, T., Catalytic Oligomerization of Ethylene to Higher Linear α-Olefins Promoted by the Cationic Group 4 [(η5-Cp-(CMe2-bridge)-Ph)MII(ethylene)2]+ (M = Ti, Zr, Hf) Active Catalysts: A Density Functional Investigation of the Influence of the Metal on the Catalytic Activity and Selectivity. *J. Am. Chem. Soc.* **2004,** *126* (29), 9059-9071.

56. Grimme, S.; Antony, J.; Ehrlich, S.; Krieg, H., A consistent and accurate ab initio parametrization of density functional dispersion correction (DFT-D) for the 94 elements H-Pu. *The Journal of Chemical Physics* **2010,** *132* (15), 154104.

57. Ditchfield, R., Self-consistent perturbation theory of diamagnetism. *Mol. Phys.* **1974,** *27* (4), 789-807.

58. Wolinski, K.; Hinton, J. F.; Pulay, P., Efficient implementation of the gauge-independent atomic orbital method for NMR chemical shift calculations. *J. Am. Chem. Soc.* **1990,** *112* (23), 8251-8260.

59. Kutzelnigg, W.; Fleischer, U.; Schindler, M., *The IGLO-Method: Ab Initio Calculation and Interpretation of NMR Chemical Shifts and Magnetic Susceptibilities*. Springer-Verlag: Heidelberg, Germany: 1990; Vol. 23.

60. Frisch, M. J.; Trucks, G. W.; Schlegel, H. B.; Scuseria, G. E.; Cheeseman, J. R.; Scalmani, G.; Barone, V.; Mennucci, B.; Petersson, G. A.; Nakatsuji, H.; Caricato, M.; Li, X.; Hratchian, H. P.; Izmaylov, A. F.; Bloino, J.; Zheng, G.; Sonnenberg, J. L.; Hada, M.; Ehara, M.; Toyota, K.; Fukuda, R.; Hasegawa, J.; Ishida, M.; Nakajima, T.; Honda, Y.; Kitao, O.; Nakai, H.; Vreven, T.; Montgomery, J. A., Jr.; Peralta, J. E.; Ogliaro, F.; Bearpark, M.; Heyd, J. J.; Brothers, E.; Kudin, K. N.; Staroverov, V. N.; Kobayashi, R.; Normand, J.;

Raghavachari, K.; Rendell, A.; Burant, J. C.; Iyengar, S. S.; Tomasi, J.; Cossi, M.; Rega, N.; Millam, J. M.; Klene, M.; Knox, J. E.; Cross, J. B.; Bakken, V.; Adamo, C.; Jaramillo, J.; Gomperts, R.; Stratmann, R. E.; Yazyev, O.; Austin, A. J.; Cammi, R.; Pomelli, C.; Ochterski, J. W.; Martin, R. L.; Morukuma, K.; Zakrzewski, V. G.; Voth, G. A.; Salvador, P.; Dannenberg, J. J.; Dapprich, S.; Daniels, A. D.; Farkas, O.; Foresman, J. B.; Ortiz, J. V.; Ciolowski, J.; Fox, D. J. *Gaussian 09, B.01*, Gaussian, Inc., Wallingford, CT: 2009.

61. Schaftenaar, G.; Noordik, J. H., Molden: a pre- and post-processing program for molecular and electronic structures. *J. Comput. Aided Mol. Des.* **2000,** *14* (2), 123-134.

# 3 Reactivity of Diiminopyridine Ti Complexes

## 3.1 ABSTRACT

The reactivity of formally Ti(II) complexes ($^{Et}$DIP)$TiCl_2$ (**2**) and ($^{Et}$DIP)$TiMe_2$ (**4a**) of the diiminopyridine ligand ($^{Et}$DIP = 2,6-(2,6-$Et_2C_6H_3N$=CMe)$_2C_5H_3N$) towards with potential reductants, oxidants and bases was explored. Reduction of **2** with 2 equivalents of $KC_8$ gave formally $Ti^0$ bis chelate complex ($^{Et}$DIP)$_2$Ti (**5**). Reaction of **2** with 1 equivalent of $OPPh_3$ afforded the simple adduct ($^{Et}$DIP)$TiCl_2(OPPh_3)$ (**6**). Dissolution of **2** in $CHCl_3$ resulted in C-Cl bond cleavage giving ($^{Et}$DIP)$TiCl_3$ (**1**). Treatment of **2** with CO and $CO_2$ produced **1** as the only identifiable Ti-containing product. Reaction of **4a** with 1 equivalent of $(PhHN)_2$ furnished titanium amido/imido complex ($^{Et}$DIP+Me)Ti(NPh)(NHPh) (**7**) containing a methylated DIP ligand. Reaction of **2** with 2.2 equivalents of MeLi led to formation of ($^{Et}$DIP+H/-H)$TiMe_2$ (**8**) (with an H-shifted isomerized ligand) and ($^{Et}$DIP-2H)$TiMe_2$ (**9**) (with a doubly dehydrogenated ligand) as the major and minor products, respectively. Reaction of **2** with (2,6-$Me_2C_6H_3$)NHLi resulted in straightforward substitution to give ($^{Et}$DIP)Ti(NH-2,6-$Me_2C_6H_3)_2$ (**10**). Use of the bulky amide $KN(SiMe_3)_2$ led to DIP ligand dehydrogenation and activation of one $SiMe_3$ C-H bond, affording [($^{Et}$DIP-H)Ti($\kappa^2$-C,N-$CH_2SiMe_2NSiMe_3$)][K($O^iPr_2)_2$] (**11**). Reaction with one equivalent of $KO^tBu$ gave the simple substitution product ($^{Et}$DIP)Ti(Cl)($O^tBu$) (**12**). With two equivalents, ($^{Et}$DIP-2H)Ti($O^tBu)_2$ (**14**) was only a minor product, the major product being ($^{Et}$DIP+H/-H)Ti($O^tBu)_2$ (**13**), a complex of the isomerized ("H-shifted") ligand. For comparison, **1** was reacted with 3 $KO^tBu$ giving **14** and ($^{Et}$DIP-2H)TiCl($O^tBu$) (**15**). Treatment of ($^{Et}$DIP)Ti($CH_2SiMe_3)_2$ (**4b**) with 2 equivalents of

TEMPO yielded doubly dehydrogenated complex ($^{Et}$DIP-2H)Ti($CH_2SiMe_3$)$_2$ (**16**). Complexes **5**, **6**, **7**, **8**, **9**, **10**, **11**, **12**, **13** and **14** are diamagnetic and were characterized by NMR and single-crystal X-ray diffraction. On the basis of spectroscopic data and the C=N and $C_{imine}$–$C_{py}$ bond lengths, a description involving $Ti^{IV}$ and a dianionic ligand seems most appropriate for **5**, **6**, **10** and **12**.

## 3.2 INTRODUCTION

One of the most notable features of DIP ligands (Figure 3.1) is their ability to stabilize main group and transition metals in low formal oxidation states by accepting electrons in their extended π* orbitals.

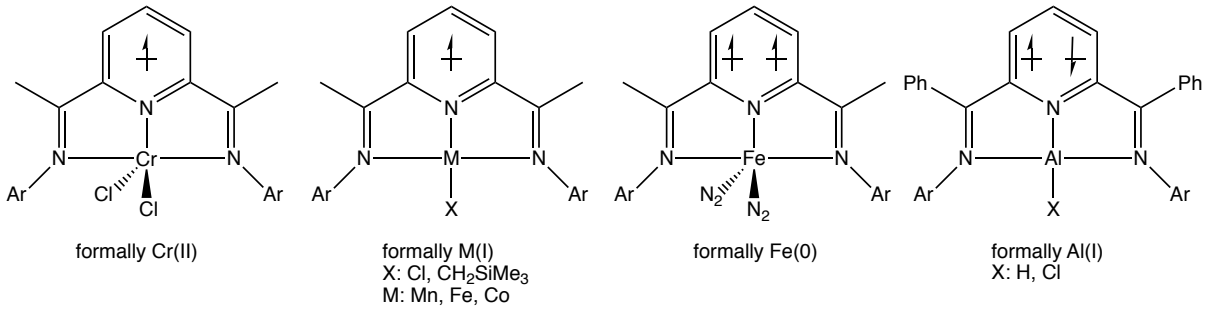


Figure 3.1. Formally low-valent main group and transition metal complexes of DIP

The combined involvement of metal and ligand in reactions of these complexes enables first-row transition metals to undergo 2*e* elementary steps even in cases where the metal alone would likely follow 1*e* paths.[1] There are many examples of the reducing power of the ligand-stored electrons in different applications of low-valent metal complexes of DIP. In one of the earlier reports, it was shown that reduction of a (DIP)$CrCl_2$ complex leads to fixation of dinitrogen, its partial reduction and hydrogenation and eventually to cleavage of the N-N bond giving an amide product.[2] Reduction of a trivalent vanadium complex of DIP to

formally zero and divalent vanadium resulted in formation of end-on dinitrogen complexes with partially reduced dinitrogen molecules, as well.[3] Recently, Chirik *et al*. reported the reactivity of the same DIP complex of vanadium with an end-on bridging dinitrogen in N=N, N-N, O=O and $S_8$ bond cleavages.[4] The cooperativity between the DIP ligand and the metal center makes the small molecule activation achievable. Redox and chemical reactivity of the DIP ligand has also been reported for molybdenum complexes that cleave the N-H bonds of ammonia, aryl hydrazines, and primary and secondary amines.[5] DIP ligands can also undergo dehydrogenation,[3] dimerization[6] and alkylation.[7] Alkyl[8] and H[9] atom migration to the ligand from the metal center have frequently been reported. Moreover, the negatively charged N atoms and electron-rich aromatic rings of the reduced ligand result in a tendency to interact with more than one metal at the same time.[10]

In Chapter 2, the synthesis and investigation of the electronic structure of a series of diiminopyridine Ti complexes were described (Scheme 3.1).[11]

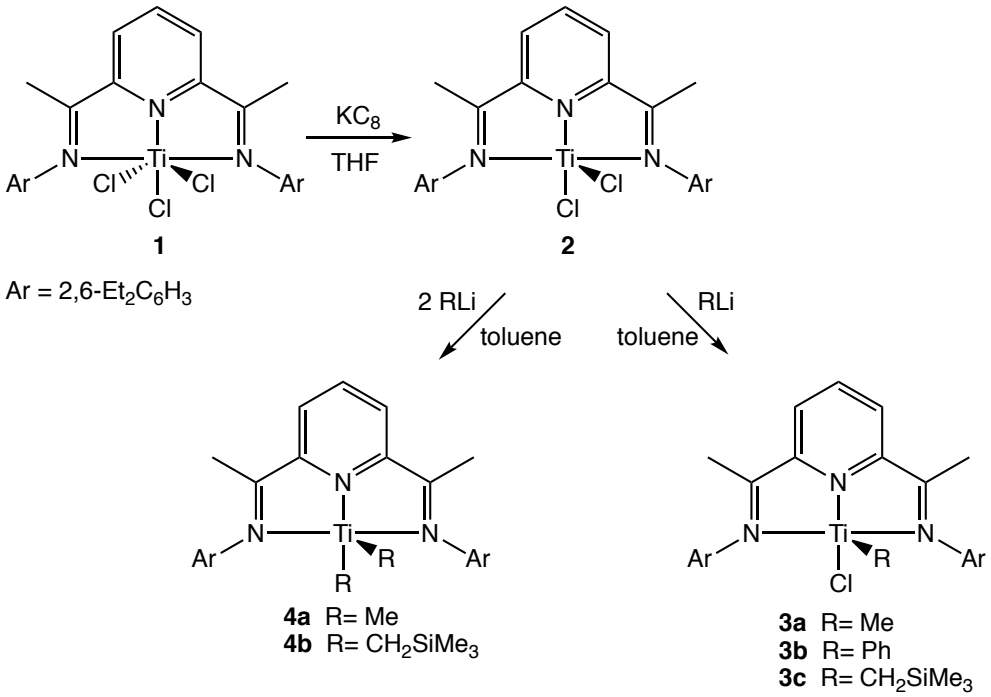


Scheme 3.1. Synthesis of ($^{Et}$DIP)$TiCl_2$ and ($^{Et}$DIP)$TiR_2$

Structural, spectroscopic and computational studies indicated the Ti center of **1** to be $Ti^{III}$, whereas complexes **2** and **4** were proposed to contain $Ti^{IV}$ and a doubly reduced ligand. In this chapter, we explore the reactivity of these complexes, in particular towards potential redox and H atom transfer chemistry.

# 3.3 RESULTS AND DISCUSSION

## 3.3.1 Attempted redox chemistry of 2- 4

Since complex **2** still contains $Ti^{IV}$, we wondered whether further reduction to true low-valent Ti would be possible. However, attempted reduction of **2** with $KC_8$ resulted in disproportionation to ($^{Et}$DIP)$_2$Ti (**5**) and unidentified further products (Scheme 3.2).

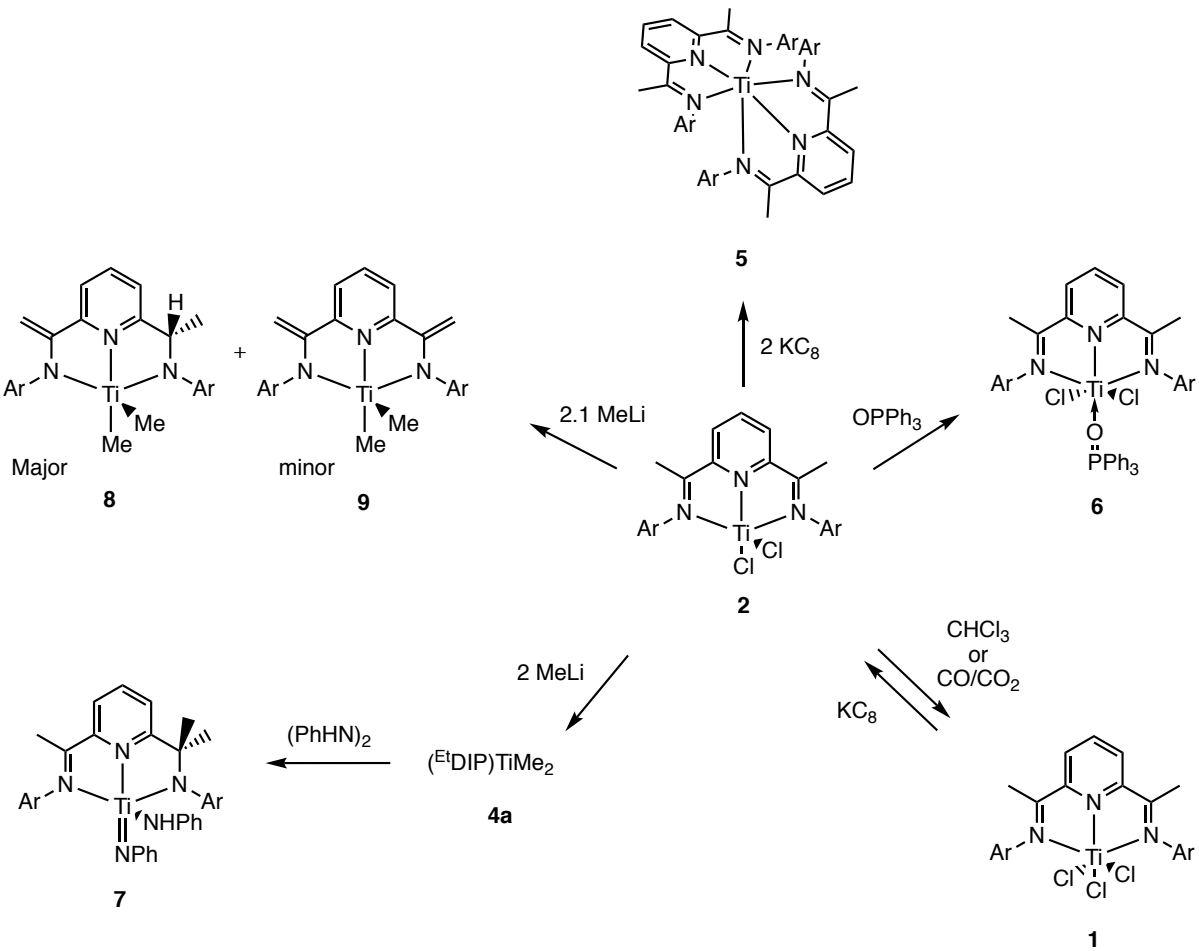


Scheme 3.2. Attempted redox chemistry involving **2** and **4a**

Clean separation of **5** from its contaminants proved impossible, but we managed to obtain a crystal structure of the complex. To the best of our knowledge, **5** is the first example of a bis(DIP) metal complex with bulky 2,6-disubstituted aryl groups (many examples exist containing 2,6-unsubstituted Ar groups at N[12]). Bond lengths within the DIP ligands (vide infra) indicate that both ligands are doubly reduced, implying that the metal is still in the $Ti^{IV}$ oxidation state.

Halide abstraction through C-X cleavage has been reported previously for low-valent complexes of Co[13] and Fe.[14] We briefly explored whether formally $Ti^{II}$ complex **2** displays similar reactivity. It turns out that **2** does not react with $CH_2Cl_2$ but quickly cleaves a C-Cl bond of $CHCl_3$ to produce **1**; this brackets the reducing power of complex **2**.

Titanium forms very strong bonds to oxygen, hence it seemed possible that ($^{Et}$DIP)$TiCl_2$ would reduce $OPPh_3$ to $PPh_3$. However, we only ever observed formation of Lewis acid-base complex **6**. Interestingly, the $^1$H NMR signals of **6** show a temperature dependence similar to that of ($^{Et}$DIP)$TiMe_2$ (**4a**) but with even broader lines, indicating a thermally populated triplet state with a smaller singlet/triplet gap than in **4a**. The room temperature $^1$H NMR spectrum of **6** has the signals of Py *H4*, Py *H3/5* and $OPPh_3$ phenyl groups merged into the baseline, and the resonance of the imine methyl fragments is strongly broadened (C*H*$_3$C=N: 1.52 ppm, linewidth: 0.07 ppm). In a variable temperature (VT) $^1$H NMR study, over the temperature range of -55 to +65 °C, the chemical shifts of py *H4* and C*H*$_3$C=N change by about 0.52 and 1.32 ppm, respectively (Figure 3.2).

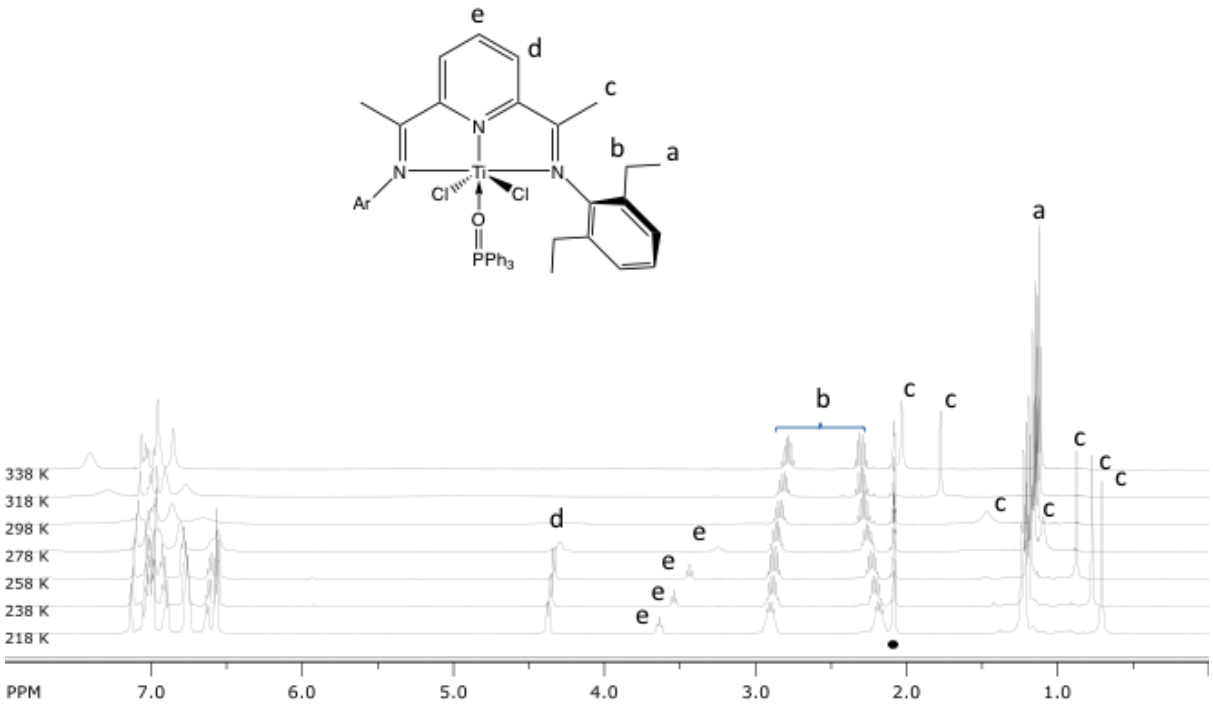


Figure 3.2. VT $^{1}$H NMR (500 MHz) study of **6** in $d_8$-toluene (the black dot indicates solvent)

The py *H3/5* signal appear as a sharp doublet at low temperature and starts to broaden at +5 °C. Upon warming up the solution, it does not undergo any chemical shift change but merges into the baseline around room temperature. The Et group signals are fairly sharp at all temperatures, indicating that little unpaired electron density delocalizes to the ligand Ar groups. They are consistent with effective $C_{2v}$ symmetry even at low temperature, and hence prove that the observed temperature dependence is not due to freezing out of an exchange phenomenon.

Carbon dioxide is another species that could be reduced to interesting products by the electrons stored in the DIP ligand. Potential products include metallaformate (straight 2*e* reduction), oxalate (reductive C-C coupling) and CO (O atom abstraction). Unfortunately, in our hands treatment of solutions of **2** and **3a** in toluene with $CO_2$ gave **1** as the only identifiable product. This must involve some form of disproportionation, possibly involving Ti oxide formation, but we were unable to fully characterize any product other than **1**.

Carbon monoxide is good at stabilizing low oxidation states through backdonation (rather than the full electron transfer typically observed with DIP ligands). Thus, it seemed possible that coordination of CO to **2** would result in a less reduced DIP ligand and a lower spectroscopic oxidation state of Ti (c.f. (DIP)Mn(CO)$_2$Br[15]). Unfortunately, also this reaction simply produced **1** and further unidentifiable products.

The above makes it clear that complex **2** does not have a high tendency to act as a reductant. We next turned to more easily reduced substrates containing weak X-X bonds: $S_8$, ($^t$BuO)$_2$ and (PhHN)$_2$, but even these did not react with **2**. We then focused on complex **4a** which should be both more chemically reactive and more strongly reducing. Indeed, **4a** reacts with (PhHN)$_2$ to give mixed amido/imido Ti$^{IV}$ complex **7**.

Apparently, the reducing power of the two electrons sitting on the ligand plays an important role in this reaction. One possible mechanism starts with dehydrogenation of hydrazobenzene by a Me(Ti) group, followed by migration of the second Me group to the ligand (alkyl migration is a well-known feature of DIP complexes), coordination of the second hydrazobenzene N atom to Ti, and finally reductive cleavage of the N-N bond by the two electrons still residing on the ligand (Scheme 3.3).

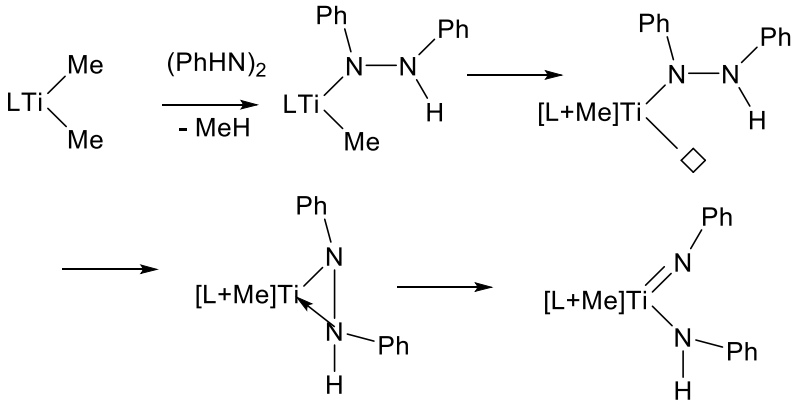


Scheme 3.3. Possible mechanism for formation of **7**

In previous work we reported formation of **4a** from **2** and two equivalents of MeLi.[11] We have now found that with a bit more MeLi (2.1 eq) the main product becomes **8**, in which the coordinated DIP ligand has undergone isomerization (see Scheme 3.2). A small amount of a complex with a doubly dehydrogenated ligand, **9**, is often seen as a by-product. The related $^1$H-NMR spectrum is shown in Figure 3.3.

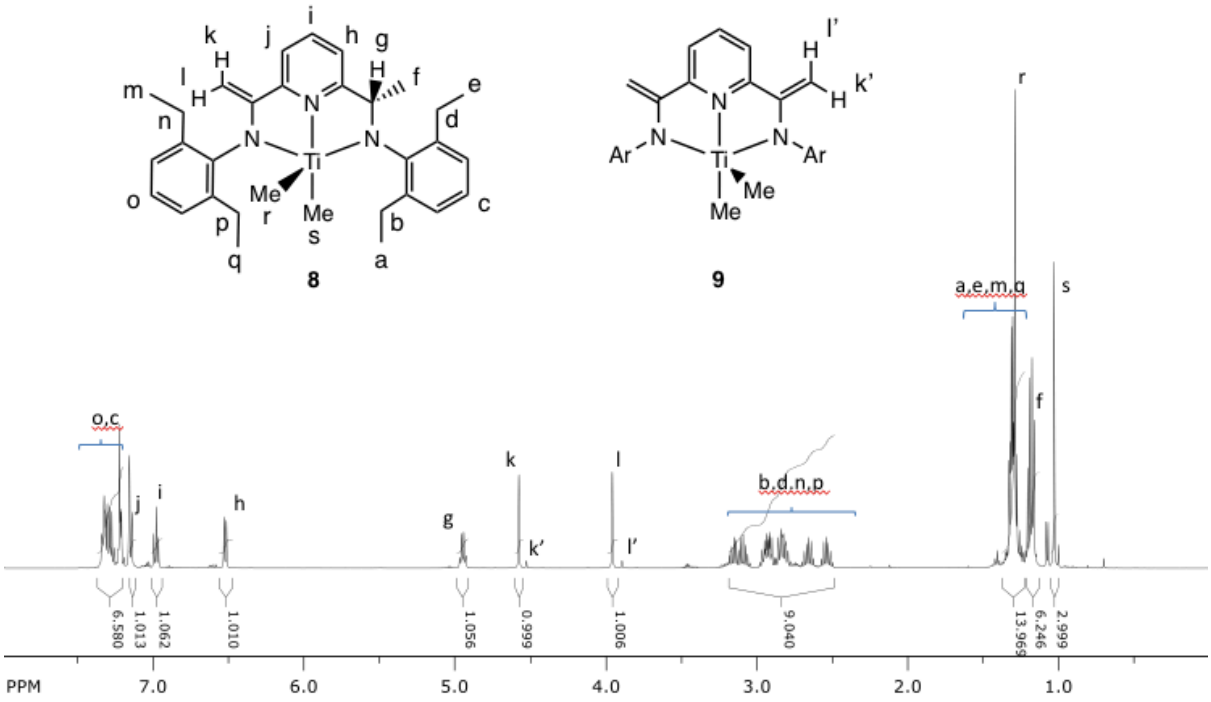


Figure 3.3. $^1$H-NMR (500 MHz) spectrum of **8** in $d_6$-benzene

The reaction is remarkable because the H atom leaving appears to do so as a proton, while the H atom adding to the imine carbon behaves like a hydride. The net effect of the isomerization is that the ligand changes from being noninnocent (formally neutral, but the ligand π* orbitals have accepted two electrons) to a regular bis(amido) ligand, and this presumably provides a driving force.

### 3.3.2 X-ray Structural Characterization of 5-8

The solid-state structure of **5** and **6** are presented in Figure 3.4 and Figure 3.5 and the related bond lengths and structural parameters are collected in Table 3.1.

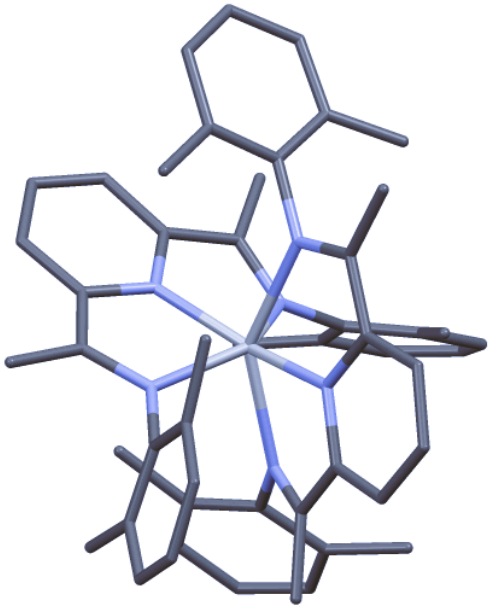

a)

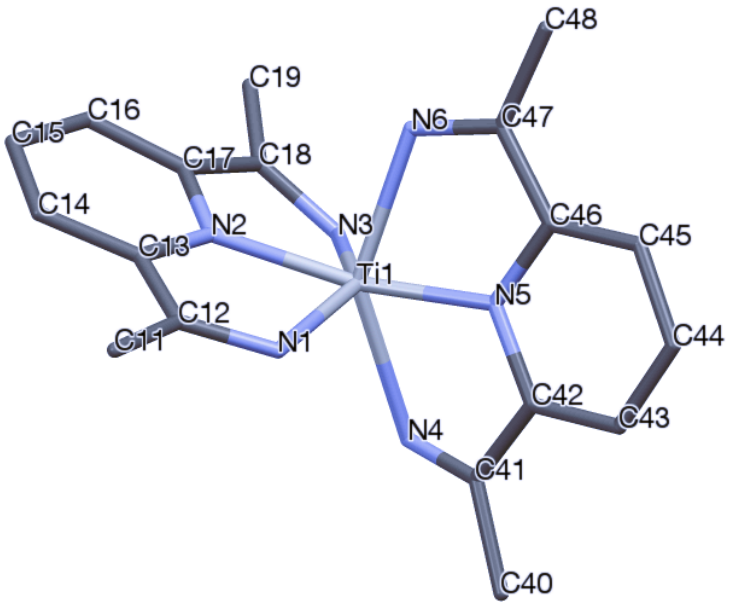


b)

Figure 3.4. a) Molecular structure of **5**. Hydrogens and ethyl $CH_3$ carbons are omitted for clarity. b) Numbered molecular structure of **5**. Aryl rings are omitted for clarity

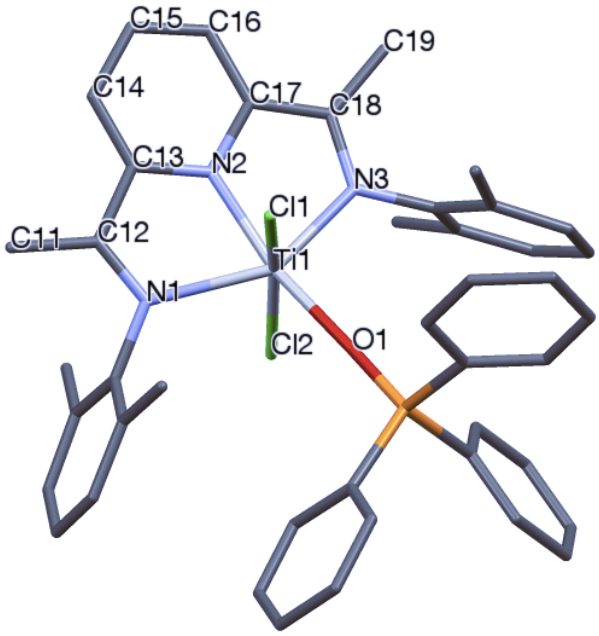


Figure 3.5. Molecular structure of **6**. Hydrogens and ethyl $CH_3$ carbons are omitted for clarity

Table 3.1. Selected bond lengths (Å) for ($^{Et}$DIP)Ti complexes

| | **5** | **6** | **7** | **8** |
|---|---|---|---|---|
| Ti-N1 | 2.190(7) | 2.2557(17) | 2.253(2) | 1.997(4) |
| Ti-N2 | 1.981(7) | 2.0135(17) | 2.176(3) | 2.160(4) |
| Ti-N3 | 2.201(7) | 2.0719(17) | 1.996(3) | 1.979(4) |
| Ti-N4 | 2.219(7) | | 1.750(5) | |
| Ti-N5 | 1.967(7) | | 1.902(5) | |
| Ti-N6 | 2.174(7) | | | |
| Ti-X1 | | 2.4067(6) | | 2.079(5) |
| Ti-X2 | | 2.3839(6) | | 2.093(5) |
| Ti-O1 | | 2.0483(14) | | |
| N1-C12 | 1.343(12) | 1.295(3) | 1.285(4) | 1.400(6) |
| N4-C41 | 1.324(12) | | | |
| C12-C13 | 1.419(14) | 1.454(3) | 1.476(4) | 1.475(8) |
| C41-C42 | 1.435(13) | | | |
| C17-C18 | 1.439(13) | 1.391(3) | 1.507(5) | 1.486(9) |
| C46-C47 | 1.412(13) | | | |
| C18-N3 | 1.346(12) | 1.352(3) | 1.485(4) | 1.422(7) |
| C47-N6 | 1.358(12) | | | |
| C11-C12 | 1.525(14) | 1.504(3) | 1.491(5) | 1.327(8) |
| C40-C41 | 1.507(14) | | | |
| C19-C18 | 1.480(13) | 1.504(3) | 1.533(5) | 1.310(13) |
| C47-C48 | 1.498(14) | | | |
| τ | | | 0.51 | 0.78 |

In both complexes, the geometry around Ti is best described as distorted octahedral and the highest possible symmetries for **5** and **6** are $D_{2d}$ and $C_{2v}$, respectively. In **6**, two chlorine atoms and one $OPPh_3$ molecule have occupied the apical and basal positions, respectively, relative to the (DIP)Ti moiety. In **6**, there is a lot of left-right asymmetry. It is as if one imine arm is nearly dissociated, and also not elongated (C=N: 1.295(3) and 1.352(3) Å). As showed above (see Figure 3.2), this is fluxional in solution and there is no difference between the left and right of the chelate. In **5**, the asymmetry within each DIP ligand is not as severe as that in **6**, but clearly there is a lot of distortion (relative to ideal $D_{2d}$ symmetry) in how the two ligands are oriented relative to each other (∠N2-Ti-N2′: 155.7(3)°). The average Ti-Cl bond lengths (2.39 Å) in **6** is longer than that observed for $Ti^{IV}$-Cl bonds ($Ti^{IV}$-Cl: ~2.31 Å; $Ti^{III}$-Cl: ~2.38 Å; $Ti^{II}$-Cl: ~ 2.4-2.5 Å).[16] There is no indication of dehydrogenation of the imine methyl groups since the $CH_3$-$C_{imine}$ are in the normal range for C-C single bonds (1.502 Å in **5** and 1.504 Å in **6**).

One measure of the degree of asymmetry in these complexes is the left/right root mean square deviation, which we calculate for the whole conjugated system (2×5 bonds) as well as restricted to the imine side arms (2×2 bonds):

$$rmsd5 = \sqrt{\frac{(N2C13-N2C17)^2+(C13C14-C16C17)^2+(C14C15-C15C16)^2+(C12C13-C17C18)^2+(C12N1-C18N3)^2}{5}} \quad (1)$$

$$rmsd2 = \sqrt{\frac{(C12C13-C17C18)^2+(C12N1-C18N3)^2}{2}} \quad (2)$$

The values obtained in this way for **6** (0.048 and 0.060 Å) clearly indicate a major asymmetry in the complex, whereas in highly distorted complex **5** each of the two DIP ligands is somewhat less asymmetric (DIP1: 0.023 and 0.014 Å; DIP2: 0.020 and 0.029 Å). At this point the reasons for the asymmetric ligand binding are unclear, but we note that also

($^{Et}$DIP)TiPhCl showed considerable asymmetry in the solid state.[11] Apparently the energy difference between asymmetric and symmetric binding is small (NMR spectra do not show left/right asymmetry even on strong cooling), and at this point it is uncertain which of the two would be preferred by a single isolated molecule in the gas phase.

The solid-state structure of **7** is shown in Figure 3.6 and the relevant bond lengths are included in Table 3.1.

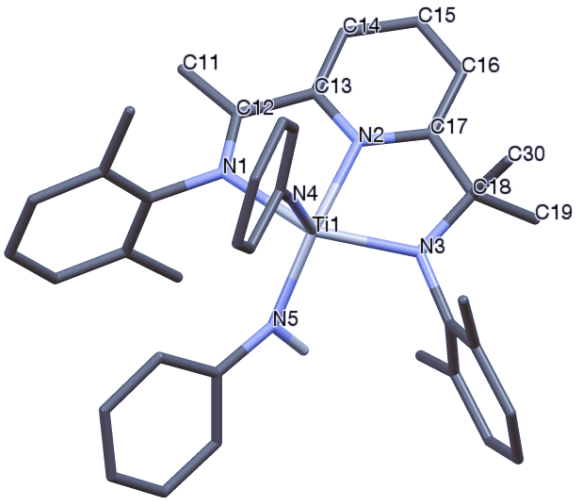


Figure 3.6. Molecular structure of **7**. Hydrogens and ethyl $CH_3$ carbons are omitted for clarity

The complex has a $C_1$ symmetry with one methylated imine fragment. This has made the corresponding C-N dramatically elongated (1.485(4) Å) compared to the intact imine group (1.285(4) Å). Titanium imide and amide bonds are 1.750(5) Å and 1.902(5) Å, respectively, which fall within the range of $Ti^{IV}$=N (1.672-1.757 Å)[17] and $Ti^{IV}$-N (1.868- 2.077 Å)[18] observed before.

In line with its NMR spectrum (see Figure 3.3), the X-ray structure of **8** has a $C_1$ symmetry (Figure 3.7) with a distorted trigonal bipyramidal Ti coordination environment.

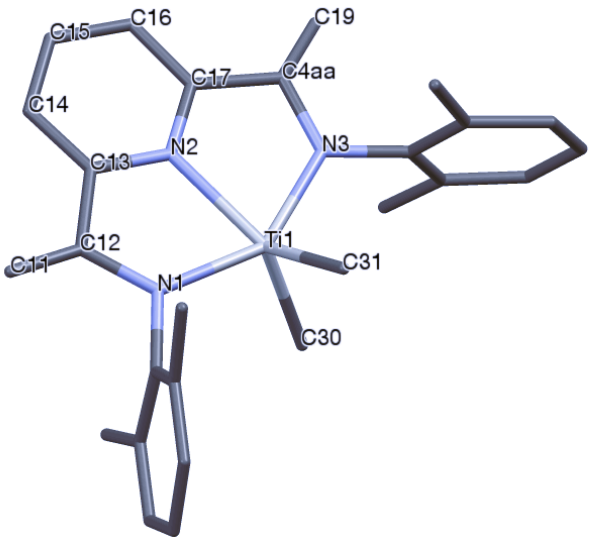


Figure 3.7. Molecular structure of **8**. Hydrogens and ethyl $CH_3$ carbons are omitted for clarity

One of the imine methyls has clearly undergone dehydrogenation ($CH_2$=$C_{imine}$: 1.327(8) Å). The second imine fragment has been "protonated" and the imine methyl group is intact ($CH_3$-$C_{imine}$: 1.468(8) Å). Consequently, both imine groups are strongly elongated indicating two C-N single bonds (1.422(7) and 1.400(6) Å). The sum of the bond angles around the imine carbon bearing the intact methyl group is 340.0°, i.e. considerably less than expected for a planar $sp^2$ carbon (360) and closer to the 328.4° expected for a $sp^3$ hybridized carbon.

It should be noted here that complex **8**, its parent complex **4a** and its doubly dehydrogenated analog **9** probably co-crystallize. Thus, the presence of a small amount of **4a** and/or **9** in the crystal used cannot be excluded, and bond lengths should be treated with caution.

### 3.3.3 Reactions with amides and alkoxides

In $^1$H NMR spectra of solutions of DIP complexes we have frequently observed singlets around 4 ppm, most likely due to dehydrogenated imine groups. Since it was not always clear how such dehydrogenation could have happened, we decided to study in more detail the reactions of **2** and **4** with bases: amides and alkoxides.

Reaction of **2** with 2 equivalents of (2,6-$Me_2C_6H_3$)NHLi in toluene gave **10** (Scheme 3.4).

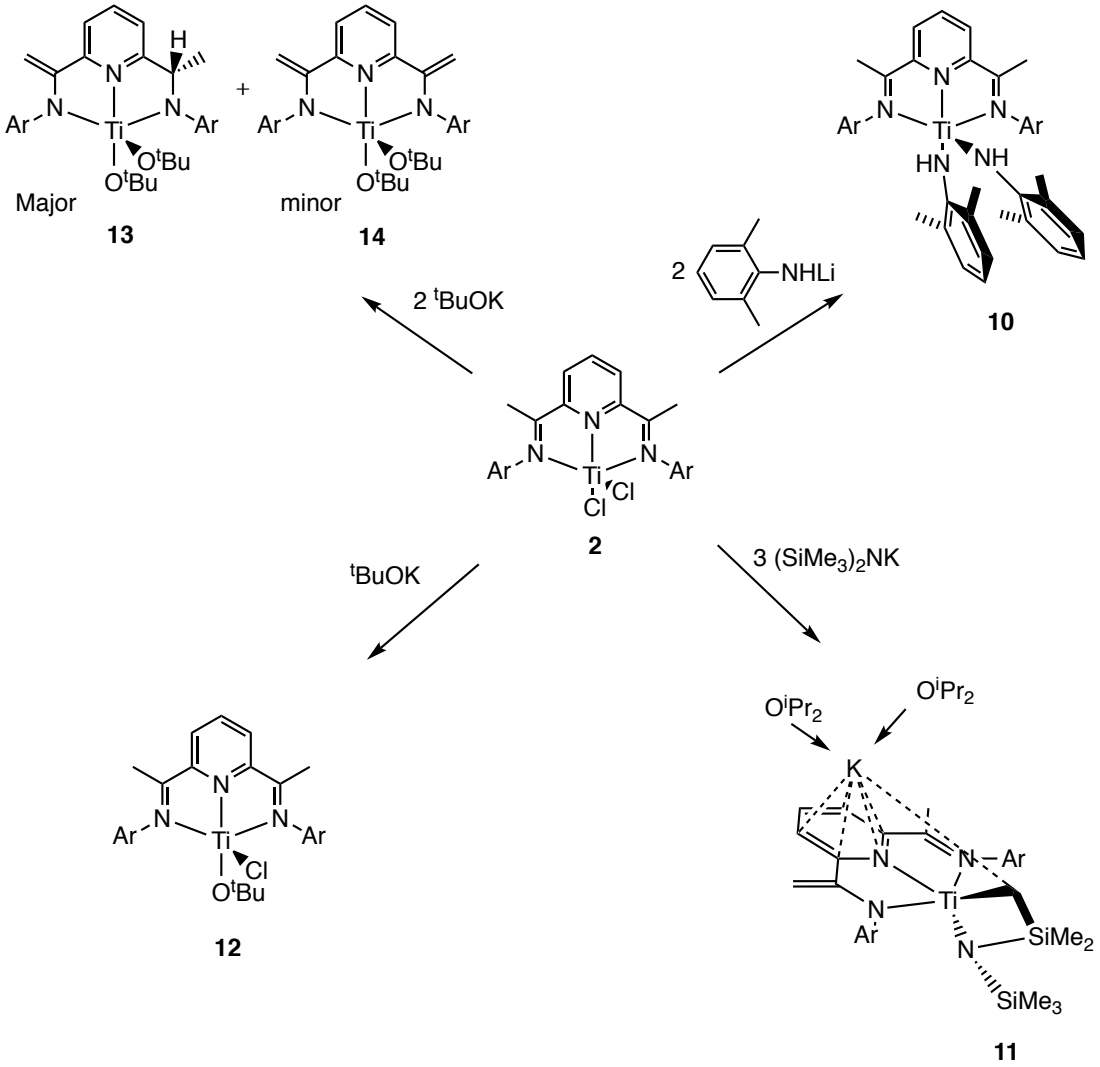


Scheme 3.4. Treatment of **2** with varying size bases

$^1$H NMR spectra of **10** show both sharp and broad signals in the normal 0-10 ppm range. The observation of sharp backbone signals (one doublet of 2H at 5.88 ppm, Py *H3/5*), one triplet of 1H at 4.98 ppm, Py *H4*) and one singlet of 3H at 2.47 ppm, C*H*$_3$C=N)) but broadened side-arm signals suggests slow exchange of apical and equatorial amido groups, similar to the fluxionality observed for **4b**.

Treatment of **2** with 3 equivalents of a bulkier base, KN(SiMe$_3$)$_2$, led to formation of diamagnetic ionic complex **11** (see Scheme 3.4). The $^1$H NMR spectrum of this complex is

consistent with $C_1$ symmetry. The two trimethylsilyl groups at the amido nitrogen are inequivalent. One $SiMe_3$ fragment signal of 9H appear as a singlet at -0.26 ppm, while the other $SiMe_3$ has undergone dehydrogenation, appearing as two doublets of 1H each (diastereotopic hydrogens) at 0.96 and 1.06 ppm (for Ti-C$H_2$) and two singlets of 3H each (diastereotopic methyls) at 0.08 and 0.19 ppm (for N-Si$Me_2$). This type of N(SiMe) C-H activation has numerous precedents; for additional Ti examples see.[19] Three inequivalent pyridine hydrogens (1H each) are found at 5.03, 5.44 and 5.91 ppm. One of the imine methyls is dehydrogenated and appears as two singlets of 1H each at 3.47 and 4.16 ppm. The signal of the intact imine methyl group is found at 1.44 ppm. Based on bond lengths (vide infra) and NMR shifts, the intact mono-imino-pyridine part of the DIP ligand is still accommodating two electrons coming from Ti.[1]

Complex **2** was also reacted with 1 equivalent of $^t$BuOK which furnished **12** (see Scheme 3.4). $^1$H NMR analysis of **12** shows a $C_s$ symmetric compound in solution with sharp resonances indicating a diamagnetic compound. As observed for **2**, the backbone in **10** shows one doublet of 2H at 6.37 ppm (py *H3/5*), one triplet of 1H at 5.59 ppm (py *H4*) and one singlet of 6H at 1.45 ppm (C$H_3$C=N). The signal corresponding to Ti-O$^t$Bu emerges as one singlet of 9H at 0.91 ppm.

Reaction of **2** with two equivalents of $^t$BuOK afforded a mixture of two compounds: **13** (major) and the expected product **14** (minor). Structures were assigned based on (mostly $^1$H) NMR and for **13** on an X-ray structure determination (*vide infra*).

In the $^1$H NMR spectrum, the major product shows two singlets of 1H each at 3.91 and 4.42 ppm for $H_2$C=CN, as well as a quartet of 1H at 5.03 ppm coupled to a doublet of 3H at 1.13 ppm which we ascribe to the $CH_3$CH-N fragment. Complex **13** is a "H-shifted" isomer of **14**:

[1] The noninnocent iminopyridine ligand is able to accept up to two electrons in a low-lying π* orbital.[20]

a hydrogen atom has moved from one imine methyl group to the imine carbon of the other ligand arm, similar to what happened in the reaction of ($^{Et}$DIP)TiCl$_2$ with excess MeLi (vide supra). We will indicate such a modified ligand as in ($^{Et}$DIP+-H)Ti(O$^t$Bu)$_2$. Possible mechanisms for the formation of **13** are discussed below.

For comparison, we also reacted **1** with excess (3 equivalents) of $^t$BuOK. Assuming simple substitution and dehydrogenation, the expected product would be a Ti$^{III}$ complex, but we obtained a mixture of compounds, containing doubly dehydrogenated complexes **14** and **15** with Ti$^{IV}$ centers (Scheme 3.5) as well as free ligand.

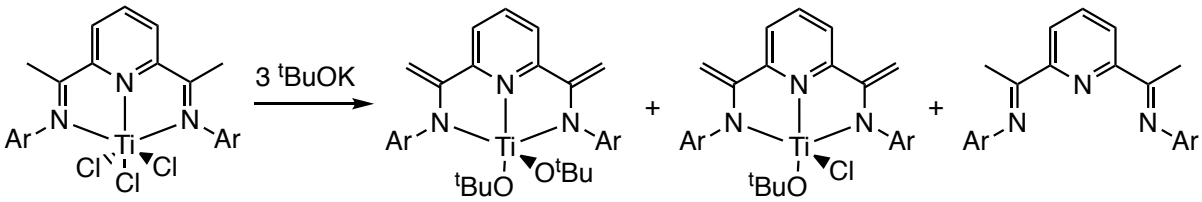


**1** **14** **15**

Scheme 3.5. Reaction of $^t$BuOK with ($^{Et}$DIP)TiCl$_3$

After a recrystallization in ($^i$Pr)$_2$O, pure **15** was obtained. The $^1$H NMR spectrum of **15** shows an effective $C_s$ symmetry. The two characteristic singlets for dehydrogenated DIP ligand in **15** of 2H each appear at 3.75 and 4.39 ppm and the pyridine hydrogens are at 6.94 ppm (for py *H3/5*) and 6.84 ppm (for py *H4*). The signal corresponding to the $^t$BuO ligand appears as a singlet of 9H at 0.64 ppm. The $^1$H NMR spectrum of **14** indicates $C_{2v}$ symmetry with only two multiplets and one triplet for the Et groups (see exp. section).

In view of the above H atom transfer reactions we decided to include TEMPO, a base specifically known for its facile H abstraction chemistry (Scheme 3.6).

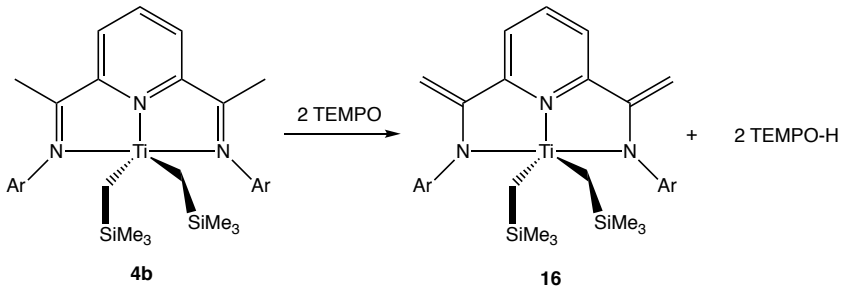


Scheme 3.6. Reaction of **4b** with TEMPO

Treatment of **4b** with two equivalents of TEMPO resulted in clean formation of doubly "dehydrogenated" complex **16**, easily identified by its characteristic $H_2C$=CN singlets at 3.88 and 4.48 ppm.

The $^1$H NMR pattern of **16** is very similar to that of **14**. Comparing to **4b**, the pyridine resonances are downfield shifted (6.89 ppm for py *H4* and 7.02 ppm for *H3/5*) and the $CH_2SMe_3$ groups appear at 2.12 (Ti-C*H*$_2$) and -0.22 (Si*Me*$_3$) ppm (Figure 3.8).

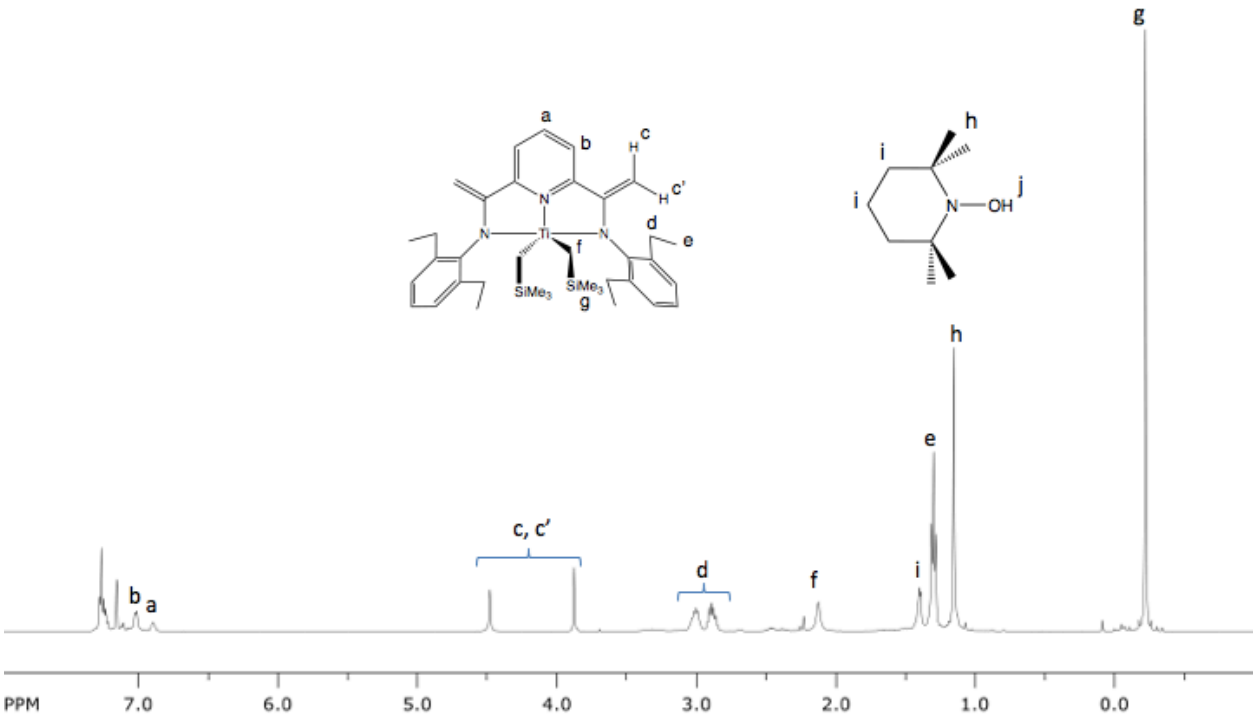


Figure 3.8. $^1$H NMR (500 MHz) spectrum of **16** in $d_6$-benzene

### 3.3.4 X-ray Structural Characterization of 10-14

The solid-state structures of **10** and **12** are shown in Figure 3.9 and Figure 3.10, respectively, and the bond lengths and structural parameters are summarized in Table 3.2.

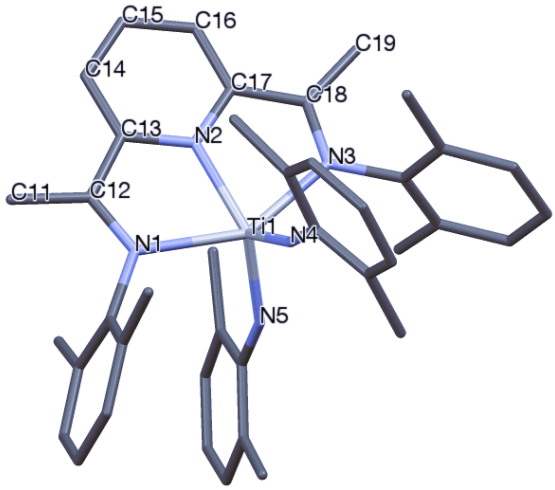


Figure 3.9. Molecular structure of **10**. Hydrogens and ethyl $CH_3$ carbons are omitted for clarity

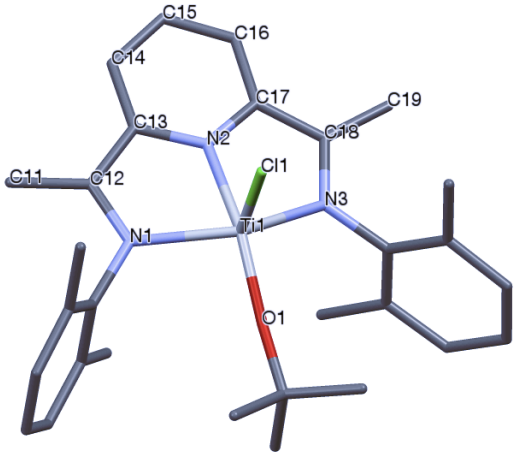


Figure 3.10. Molecular structure of **12**. Hydrogens and ethyl $CH_3$ carbons are omitted for clarity

Table 3.2. Selected bond lengths (Å) for ($^{Et}$DIP)Ti complexes

| | **10** | **11** | **12** | **13** | **14** |
|---|---|---|---|---|---|
| Ti-N1 | 2.187(3) | 2.0384(18) | 2.0716(14) | 2.0074(18) | 2.056(2) |
| Ti-N2 | 2.044(3) | 2.0535(17) | 2.0153(14) | 2.1326(18) | 2.094(2) |
| Ti-N3 | 2.174(2) | 2.0466(18) | 2.0912(14) | 2.0546(17) | 2.048(2) |
| Ti-N4 | 1.809(4) | 1.9726(18) | | | |
| Ti-N5 | 1.913(4) | | | | |
| Ti-Cl1 | | | 2.2965(5) | | |
| Ti-O1 | | | 1.7826(12) | 1.7902(16) | 1.785(2) |
| Ti-O2 | | | | 1.7709(15) | 1.785(2) |
| Ti-C30 | | 2.151(2) | | | |
| C12-N1 | 1.323(4) | 1.395(3) | 1.352(2) | 1.439(3) | 1.380(4) |
| C12-C13 | 1.429(5) | 1.450(3) | 1.414(2) | 1.490(3) | 1.454(4) |
| C17-C18 | 1.427(4) | 1.402(3) | 1.423(3) | 1.468(3) | 1.452(4) |
| C18-N3 | 1.324(4) | 1.400(3) | 1.347(2) | 1.389(3) | 1.384(4) |
| C11-C12 | 1.512(5) | 1.397(3) | 1.490(3) | 1.457(4) | 1.396(5) |
| C18-C19 | 1.497(4) | 1.451(3) | 1.492(2) | 1.369(3) | 1.400(5) |
| τ | 0.67 | 1 | 0.45 | 0.39 | 0.41 |

The geometry around Ti in **10** and **12** is distorted square pyramidal so they could have at most local $C_s$ symmetry. However, the two bulky 2,6-$Me_2$-$C_6H_3$ fragments in **10** are rotated to avoid each other's methyl groups and the Et groups on the N-aryl rings. The Ti-N bond lengths (1.913(4) and 1.809(4) Å) have previously been observed in complexes including $Ti^{IV}$-N bonding (1.804-1.918 Å).[16a] The $^{t}$BuO ligand in **12** has occupied the basal position likely to minimize steric interactions with the Et substituents on the aryl rings. The Ti-Cl1 bond length is in the range observed for $Ti^{IV}$-Cl (~2.31 Å).[16a] In both X-ray structures, as observed in **2**, the C=N bond elongation (to 1.323 Å for **10** and 1.349 Å for **12**) and the

$C_{imine}$-$C_{py}$ bond contraction (1.428 Å for **10** and 1.418 Å for **12**) indicate dianionic DIP ligands. The imine methyl C-C bond lengths in both complexes are normal for C-C single bonds (1.504 Å for **10** and 1.491 Å for **12**), indicating intact methyl groups, in agreement with the $^{1}$H NMR data discussed above.

The X-ray structure of **11** is presented in Figure 3.11 and bond lengths are collected in Table 3.2.

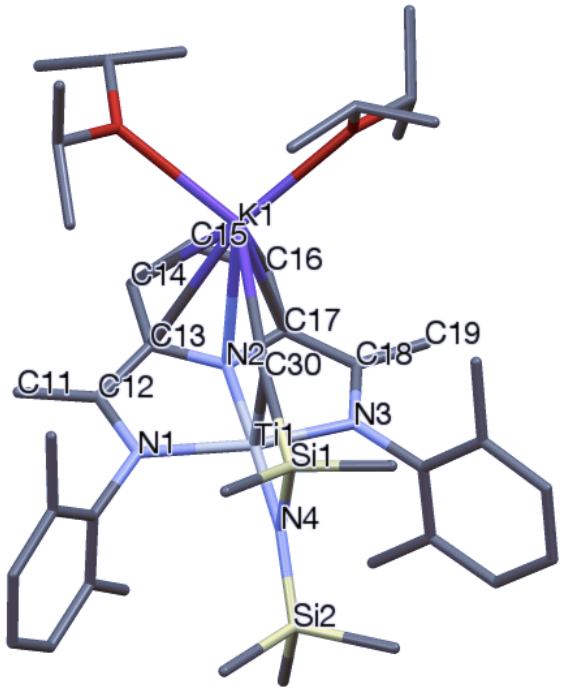


a)

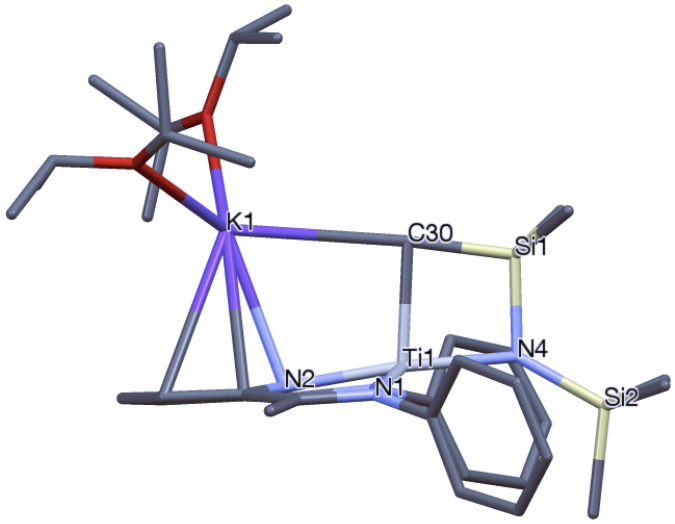


b)

Figure 3.11. Two views of the molecular structure of **11**. Hydrogens and ethyl carbons are omitted for clarity

The complex has a $C_1$ symmetry and the geometry around Ti is best described as distorted square pyramidal. One of the original $(Me_3Si)_2N$ groups, after undergoing dehydrogenation at one of its methyl groups, has formed a four membered titanacycle (Ti-N-Si-C). Based on the bond lengths, one of the imine methyl groups is dehydrogenated (C=C: 1.397(3) Å, C-N (1.395(3) Å); the other imine methyl fragment seems to be intact ($H_3C$-CN: 1.451(3) Å) so the ligand is essentially a monoiminopyridine (IP) moiety. Table 3.3 presents the comparison of the bond lengths of the IP ligand in different oxidation states[20] with the intact part of DIP in **11**.

Table 3.3. Bond length comparison between IP ligand and DIP in **11**

| Ligand | C=N | $C_{imine}$-$C_{py}$ | $C_{py}$-$N_{py}$ | $C_{py}$-$C_3$ |
|---|---|---|---|---|
| IP | 1.284(6) | 1.453(7) | 1.347(6) | 1.391(6) |
| $IP^-$ | 1.354(2) | 1.405(2) | 1.366(2) | 1.412(2) |
| $IP^{2-}$ | 1.414(6) | 1.356(6) | 1.399(6) | 1.437(6) |
| $IP^{2-}$ in **11** | 1.400(3) | 1.402(3) | 1.401(3) | 1.413(3) |

A logical route for formation of **11** starts with dehydrogenation (Scheme 3.7).

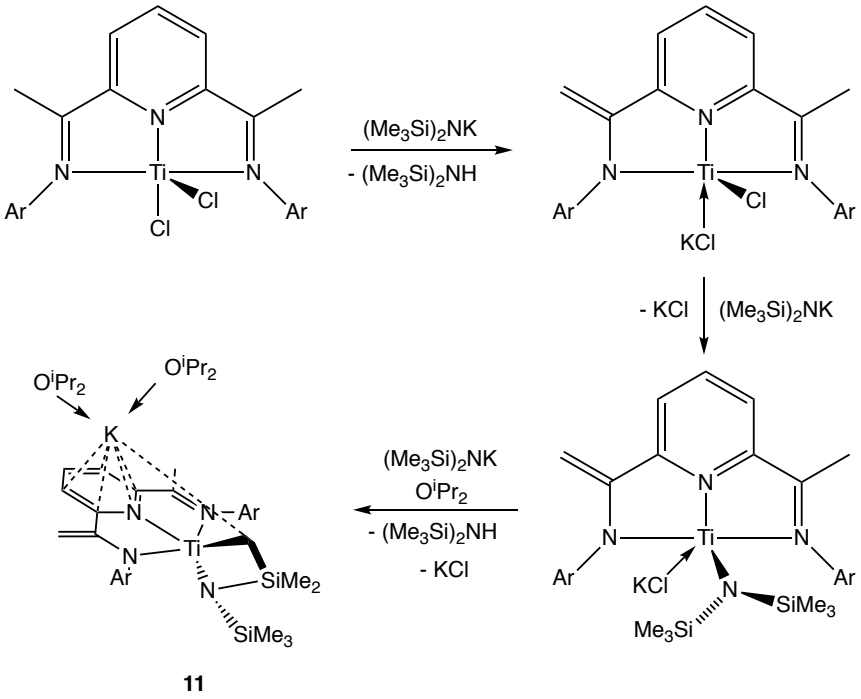


Scheme 3.7. Probable mechanism for formation of **11**

The second equivalent of base then does a metathesis reaction while the third deprotonates one $SiMe_3$ group to fill the apical coordination site. This makes the complex anionic, with $K^+$ as counterion. Recrystallization of the product from $^iPr_2O$ led to replacement of the probable toluene coordinated to K by two $^iPr_2O$ molecules. The potassium ion also interacts with the π system of the DIP pyridine ring and the anionic carbon at Ti.

In the solid-state structure of **13** (Figure 3.12), the geometry around Ti is best described as square pyramidal and the complex has $C_1$ symmetry.

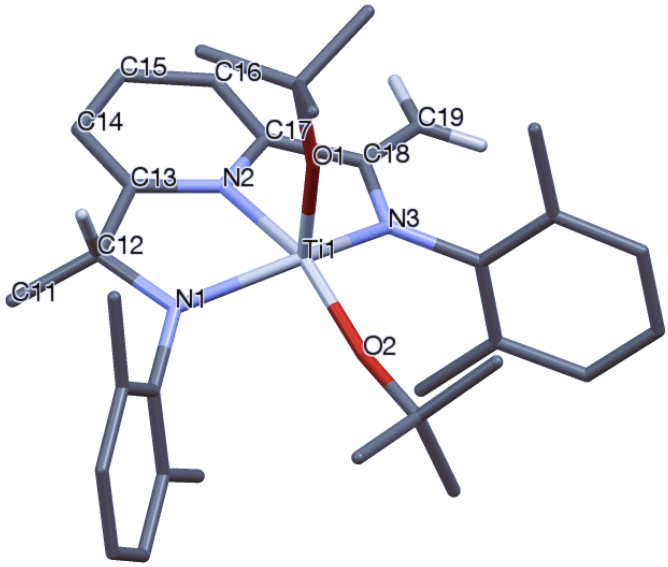


Figure 3.12. Molecular structure of **13**. Hydrogens and ethyl $CH_3$ carbons are omitted for clarity

One of the original imine carbons carries an extra hydrogen atom: the sum of angles around it is 343.0°, close to the ideal $sp^3$ value of 328.4° than the 360° expected for a $sp^2$ carbon; the C-N distance is indicative of a single bond. The other imine methyl group is clearly dehydrogenated (C=C: 1.369(3) Å) and the corresponding C-N bond is elongated (C-N: 1.389(3) Å).

The route by which **13** forms from **2** and $^t$BuOK must involve some form of hydrogen migration, but at this point the mechanism leading to it is unclear. It seems logical to assume that **12** is formed first. This could then undergo a second substitution to give (DIP)Ti($O^t$Bu)$_2$, followed by isomerization to major product **13**, but isomerization might also happen before the second substitution step. Or alternatively, the second equivalent of $^t$BuOK deprotonates the ligand, leading to formation of one molecule of $^t$BuOH interacting with the reducing Ti center; two electrons stored in the DIP π* system are then used to convert the O-bound proton into a hydride which could attack the intact C=N bond (Scheme *3.8*).

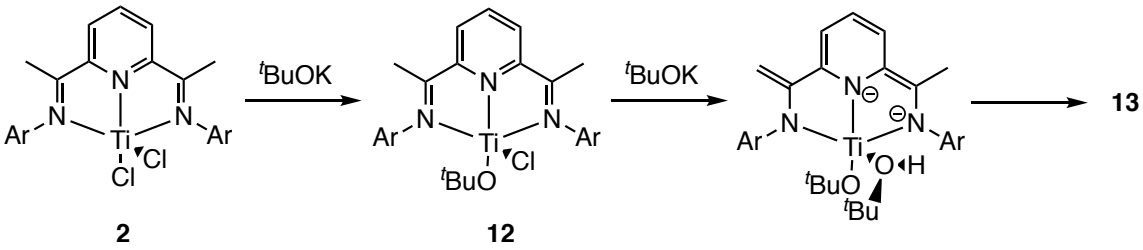


Scheme 3.8. Possible mechanism for formation of **13**

The solid-state structure of **14** is shown in Figure 3.13 and the bond lengths are summarized in Table 3.2.

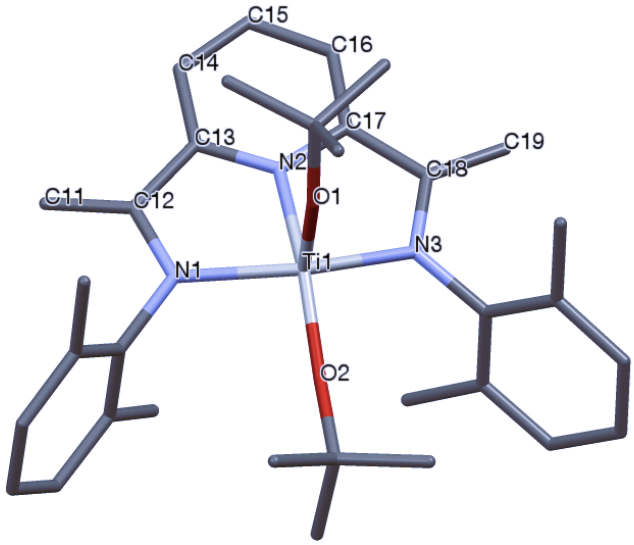


Figure 3.13. Molecular structure of **14**. Hydrogens and ethyl $CH_3$ carbons are omitted for clarity

In agreement with the NMR data which indicated double dehydrogenation, the X-ray bond lengths of **14** indicate two short bonds to the imine "methyl" groups ($H_2C$=CN: 1.400(5) and 1.396(5) Å) and two correspondingly elongated C-N single bonds (1.380(4) and 1.384(4) Å).

## 3.3.5 XPS

X-ray photoelectron spectroscopy is one of the most suitable techniques for assigning the oxidation state of the metal atom. In this work, the three complexes **5**, **6** and **10** with Ti formal oxidation state 2+ were tested by XPS. In Table 3.4, the binding energies for Ti compounds with oxidation states 2+ to 4+ are presented.

Table 3.4. Ti $2p_{3/2}$ Binding energies

| complex | binding energy (eV) |
|---|---|
| **$TiO_2$** | 458.8 |
| **$TiCl_3$** | 457.8 |
| **TiO** | 454.7 |
| **5** | 458.5 |
| **6** | 458.5 |
| **10** | 458.7 |
| **11** | 458.9 |

As shown, the binding energies of **5**, **6** and **10** are 458.5, 458.5 and 458.7 eV, respectively, typical of $Ti^{IV}$ rather than $Ti^{II}$. Also, based on these data, the binding energy of **11**, containing an IP intact ligand accommodating two electrons, indicates the presence of $Ti^{IV}$. These results are thus in good agreement with X-ray data where the oxidation state 4+ was assigned for these complexes based on bond elongations and contractions in the DIP ligand.

## 3.4 Conclusions

In this chapter, it was shown that the two electrons sitting on the ligand are not very "available" for chemical reactions. Attempts to use the reducing power of the electrons in (DIP)$TiCl_2$ in small molecule activation and various bond breaking reactions (e.g. P=O, N-N) were unsuccessful. However, it was demonstrated that there is enough space around Ti to accommodate an incoming Lewis base to form an adduct. The other Ti mono alkyl complexes tested also did not show any of the hoped-for reactivity. Ultimately, the more

reactive (DIP)$TiMe_2$ was found to cleave the N-N bond of hydrazobenzene using the electrons stored in the DIP ligand.

In addition to known ligand-based reactivity (e.g. dimerization, dehydrogenation, alkylation and electron transfer), several examples of a more unusual H-shift isomerization were observed. So far, it is not entirely clear what triggers this isomerization reaction. The presence of a base (and its nature) seems to be an important factor, but a simple base-assisted proton transfer to the imine carbon does not seem likely in view of the $C^{\delta+}=N^{\delta-}$ polarity of the imine group. On the other hand, "umpolung" of $H^+$ (abstracted) to $H^-$ (attacking the imine) by the ligand-stored electrons also does not seem probable given the observed reluctance of these electrons to participate in redox chemistry. Transfer as a hydrogen atom (i.e. radical chemistry) remains a possibility. Further work would be required to settle this issue.

## 3.5 Experimental

*General Considerations*. All air- and moisture-sensitive manipulations were carried out under argon using standard Schlenk techniques or in an MBraun drybox containing an atmosphere of purified nitrogen. Solvents for air- and moisture-sensitive manipulations were dried and deoxygenated using sodium/benzophenone. Benzene-$d_6$ and toluene-$d_8$ were purchased from Cambridge Isotope Laboratories, distilled from sodium/benzophenone, and stored in the drybox. The $^{Et}$DIP ligand was prepared according to a literature procedure.[21]

$^1H$ and $^{13}C$ NMR spectra were recorded at 25 °C (unless noted otherwise) on Bruker Avance 300 and 500 spectrometers. All chemical shifts are reported in ppm relative to $SiMe_4$ using H (residual) and $^{13}C$ chemical shifts of the solvent as a secondary standard[22]: $C_6D_6$, 7.16 and 128.06 ppm; $C_6D_5CD_3$, 2.08 and 20.43 ppm; $C_4D_8O$, 1.72 and 3.58 and 25.31 ppm; $CD_2Cl_2$, 5.32 and 53.84 ppm. All coupling constants are in Hz.

Single crystals suitable for X-ray diffraction were sealed in glass capillaries and transferred to the goniometer head of a D8 three-circle diffractometer (equipped with a rotating-anode Mo Kα generator, multilayer optics, and an APEX-II CCD area detector) or coated with oil in a drybox and then quickly transferred to a Bruker D8 QUEST ECO diffractometer (equipped with a Mo Kα X-ray tube). In the former method, data were collected at room temperature while in the latter method, data were collected at lower temperature. Preliminary data revealed the crystal system. Data collection was optimized for completeness and redundancy using the APEX3 software suite. The space group was identified, and the data were reduced using the SAINT[23] program and corrected for absorption using SADABS.[24] The structures were solved using direct methods (SHELXS[25]) and refined by full-matrix least-squares procedures (SHELXL[25]).

XPS spectra were collected on a Kratos Axis Ultra DLD XPS spectrometer in a vacuum environment with a base pressure of 10−9 Torr. Al Kα (1486.6 eV) monochromatic X-rays at 10 mA emission current and 15 kV anode voltage were used for photoexcitation. Samples were transferred from a nitrogen glovebox to the instrument in a sealed container designed to mate with the sample loading arm of the spectrometer so that the samples were not exposed to air/ moisture. A coaxial charge neutralizer was utilized to prevent buildup of charge on the samples. All spectra were collected with a fixed analyzer transmission mode. Survey scans were collected with a pass energy of 160 eV, and high-resolution scans were collected with a pass energy of 20 eV. Peak fitting of the high-resolution XPS spectra was performed using CasaXPS software (casaxps.com). All peak positions were normalized with respect to the C 1s peak with a binding energy of 285 eV.

**($^{Et}$DIP)$_2$Ti** (**5**). A 100 mL Schlenk tube was charged with 0.15 g (0.275 mmol) of **2**, approximately 30 mL of toluene, and a stirrer bar. $KC_8$ (0.0745 g, 0.551 mmol) was added,

and the reaction mixture was stirred for 24 h. The suspension was passed through celite and dried under a reduced pressure. Then, it was dissolved in 1 mL toluene which was layered by 3 mL of pentane. Cooling to -35 °C produced a few green crystals (0.0055 g, 2.2 %) suitable for X-ray crystallography, mixed with colourless crystals of the free ligand.

**($^{Et}$DIP)TiCl$_2$(OPPh$_3$)** (**6**). A 50 mL Schlenk tube was charged with 0.100 g (0.183 mmol) of **2**, approximately 30 mL of toluene, and a stirrer bar. $OPPh_3$ (0.511 g, 0.183 mmol) was added, and the reaction mixture was stirred for 24 h. After centrifugation, the amount of solvent was reduced to 2 mL and layered with 4 mL of pentane. It was kept undisturbed at –35 °C for a few days to give 0.0649 g (43%) of dark purple-brown crystals.

$^1$H NMR (500 MHz; toluene-$d_8$) at -15 °C: δ 0.87 (6H, s, $CH_3C$=N), 1.19 (12H, t, *J* 7.4, $CH_2CH_3$), 2.22, 2.88 (4H each, m, $CH_2CH_3$), 3.44 (1H, t, *J* 7.8, py 4), 4.33 (2H, d, *J* 7.9, py 3/5), 6.56 (4H, d, *J* 6.8, *m*-Ar), 6.61 (2H, t, *J* 7.4, *p*-Ar), 6.79 (6H, m, $OPPh_3$ *m*-Ar), 6.93 (3H, t, *J* 7.4, $OPPh_3$ *p*-Ar), 6.99-7.04 (6H, m, $OPPh_3$ *o*-Ar). $^{13}$C{$^1$H} NMR (500 MHz; toluene-$d_8$) at -55 °C (partial assignment only): 13.2 ($CH_3C$=N), 14.0 ($CH_2CH_3$), 23.9 ($CH_2CH_3$), 125.3, 128.2, 128.3, 128.4, 129.1, 131.9, 132.9, 133.0, 136.8, 139.7, 145.2, 158.8. $^{31}$P{$^1$H} NMR (toluene-$d_8$) at -55 °C: 43.4

**($^{Et}$DIP+Me)Ti(NPh)(NHPh)** (**7**). A 25 mL Schlenk tube was charged with 0.100 g (0.198 mmol) of **4a** and 5 mL of toluene. $(NHPh)_2$ (0.0366 g, 0.198 mmol) was added, and the reaction mixture was left for 2 days. The amount of solvent was reduced to 1 mL and layered with 3 mL pentane. It was kept undisturbed at −35 °C for a few days to give 0.0236 g (18%) of orange-red crystals suitable for X-ray crystallography.

**($^{Et}$DIP-H/+H)TiMe$_2$** (**8**). A 50 mL Schlenk tube was charged with 0.535 g (0.983 mmol) of **2**, 20 mL of toluene, and a stirrer bar. MeLi (0.045 g, 2.1 mmol) was added, and the reaction mixture was stirred for 72 h. Suspended solids were removed by centrifugation, and the solvent was removed in vacuo. The solid residue was dissolved in 1 mL of toluene which was layered by 4 mL *n*-hexane and left to crystallize at −35 °C, giving 0.235 g (47%) of dark green crystals.

$^1$H NMR (500 MHz; benzene-$d_6$): δ 1.03 (3H, s, Ti-CH$_3$), 1.17 (3H, t, *J* 6.6, C*H*$_3$(H)C-N), 1.19 (3H, t, *J* 7.1, CH$_2$C*H*$_3$), 1.27-1.33 (9H, m, CH$_2$C*H*$_3$), 1.29 (3H, s, Ti-CH$_3$), 2.53, 2.652 (1H each, m, C*H*$_2$CH$_3$), 2.82, 2.92 (2H each, m, C*H*$_2$CH$_3$), 3.09, 3.15 (1H each, m, C*H*$_2$CH$_3$), 3.96, 4.58 (1H each, s, CH$_2$=CN), 4.95 (1H, q, *J* 6.7, CH$_3$(*H*)C-N), 6.52 (1H, d, *J* 7.7, py 3/5), 6.98 (1H, t, *J* 7.8, py 4), 7.15 (1H, d, *J* 7.7, py 3/5), 7.22-7.34 (6H, m, Ar). $^{13}$C{$^1$H} NMR (500 MHz; benzene-$d_6$) (partial assignment only): 15.5, 15.6, 15.6, 15.8 (CH$_2$*C*H$_3$), 21.8 (*C*H$_3$(H)C-N), 24.4, 24.4, 24.5, 24.8 (*C*H$_2$CH$_3$), 66.0, 68.3 (Ti-CH$_3$), 72.1 (CH$_3$(H)*C*-N), 85.2 (*C*H$_2$=CN), 116.9, 118.4 (py 3/5), 126.1, 126.4, 126.6, 126.7, 126.7, 127.1 (*m*- and *p*-Ar), 138.6 (py 4), 140.0, 140.8, 140.9, 141.9 (*o*-Ar), 147.6, 150.1 (py 2, CH2=*C*N), 156.2, 157.2 (*i*-Ar), 167.0 (py 2).

**($^{Et}$DIP)Ti(NH(2,6-Me$_2$-C$_6$H$_3$)$_2$** (**10**). A 50 mL Schlenk tube was charged with 0.100 g (0.183 mmol) of **2**, 20 mL of toluene, and a stirrer bar. LiNH(2,6-Me$_2$-C$_6$H$_3$)$_2$ (0.0467 g, 0.367 mmol) was added, and the reaction mixture was stirred for 24 h. Suspended solids were removed by centrifugation, and the solvent was removed in vacuo. The solid residue was dissolved in 2 mL of diisopropyl ether and left to crystallize at −35 °C, giving 0.095 g (72%) of dark yellow-orange crystals.

$^1$H NMR (500 MHz; benzene-$d_6$) (partial assignment only): δ 0.78 (6H, t, J 7.5, CH$_2$C*H*$_3$), 1.46 (3H, s, NHAr-C*H*$_3$), 1.62 (12H, br, CH$_2$C*H*$_3$, NHAr-C*H*$_3$), 2.34 (6H, s, CH$_3$C=N), 2.50

(4H, m, C*H*$_2$CH$_3$), 2.63 (4H, br, C*H*$_2$CH$_3$), 4.99 (1H, t, *J* 7.6, py 4), 5.88 (2H, d, *J* 7.6, py 3/5), 6.76-7.13 (12H, m, Ar). $^{13}$C{$^1$H} NMR (500 MHz; benzene-$d_6$): 13.5 (CH$_2$*C*H$_3$), 14.0 (NHAr-CH$_3$), 19.3 (*C*H$_3$C=N), 23.6 (*C*H$_2$CH$_3$), 113.7 (py 4), 118.2, 119.9, 125.0, 125.8, 128.0 (*m*- and *p*-Ar), 128.2 (py 3/5), 128.4, 128.9, 138.0, 142.7, 146.9, 151.5, 154.4 (NHAr-*C*H$_3$, *o*-Ar, *i*-Ar, py 2).

**[(EtDIP-H)TiN⌒CH$_2$SiMe$_2$(SiMe$_3$)][K(O$^i$Pr$_2$)$_2$]** (**11**). A 50 mL Schlenk tube was charged with 0.150 g (0.275 mmol) of **2**, 15 mL of toluene, and a stirrer bar. (Me$_3$Si)$_2$NK (0.165 g, 0.827 mmol) was added, and the reaction mixture was stirred for 2 days. Suspended solids were removed by centrifugation, and the solvent was removed in vacuo. The solid residue was dissolved in 2 mL of toluene which was layered by 4 mL of hexane. It was left to crystallize at −35 °C, giving 0.128 g (61%) of brownish crystals.

$^1$H NMR (500 MHZ; toluene-$d_8$): δ -0.27 (9H, s, SiMe$_3$), 0.08, 0.19 (3H each, s, SiMe$_2$), 0.96, 1.09 (1H, each, d, *J* 9.5, Ti-CH$_2$), 1.17 (3H, t, *J* 7.5, CH$_2$C*H*$_3$), 1.35 (3H, t, *J* 7.5, CH$_2$*CH*$_3$), 1.37 (6H, t, *J* 7.5, CH$_2$C*H*$_3$), 1.43 (3H, s, CH$_3$C=N), 2.26, 2.59 (1H each, m, C*H*$_2$CH$_3$), 2.72 (3H, m, C*H*$_2$CH$_3$), 3.09 (2H, m, C*H*$_2$CH$_3$), 3.24 (1H, m. C*H*$_2$CH$_3$), 3.46, 4.15 (1H each, s, H$_2$C=CN), 5.02 (1H, d, *J* 5.3, py 3/5), 5.44 (1H, t, *J* 7.4, py 4), 5.91 (1H, d, *J* 8.8, py 3/5), 7.07-7.20 (6H, m, *m*- and *p*-Ar). $^{13}$C{$^1$H} NMR (500 MHz; toluene-$d_8$): 4.6 (SiMe$_3$), 5.2, 5.6 (SiMe$_2$), 13.1, 13.2, 13.4, 14.7 (CH$_2$*C*H$_3$), 24.3, 24.8, 24.9, 26.0 (*C*H$_2$CH$_3$), 52.8 (Ti-CH$_2$), 65.9, 77.6 (H$_2$*C*=CN), 91.7 (py 3/5), 119.7 (py 4), 120.4 (py 3/5), 122.5, 124.5, 125.2, 125.4, 126.1, 128.3 (*m*- and *p*-Ar), 129.2, 129.6, 136.2, 137.0, 138.4, 138.6, 151.6, 153.2, 155.6, 159.2 (o-Ar, *i*-Ar, H$_3$C-*C*=N, py 2).

**(EtDIP)Ti(Cl)(O$^t$Bu)** (**12**). A 25 mL Schlenk tube was charged with 0.150 g (0.275 mmol) of 2, 15 mL of toluene, and a stirrer bar. $^t$BuOK (0.0309 g, 0.275 mmol) was added, and the

reaction mixture was stirred for 24 h. Suspended solids were removed by centrifugation, and the solvent was removed in vacuo. The solid residue was dissolved in 1 mL of THF which was layered by 3 mL of hexane. It was left to crystallize at −35 °C and gave 0.0548 g (34%) of green crystals. Crystals obtained from an NMR sample in benzene-$d_6$ were used for X-ray crystallography. The structure contained one molecule of benzene-$d_6$ in the unit cell.

$^1$H NMR (500 MHz; benzene-$d_6$): δ 0.91 (9H, s, C(C$H_3$)$_3$), 0.98, 1.2 (6H each, t, *J* 7.5, CH$_2$*CH$_3$*), 1.45 (6H, s, CH$_3$C=N), 2.06, 2.24 2.43, 3.16 (2H each, m, *CH$_2$*CH$_3$), 5.59 (1H, t, *J* 7.6, py 4), 6.37 (2H, d, *J* 7.6, py 3/5), 6.99 (2H, d, *J* 7.6, *m*-Ar), 7.14 (1H, t, *J* 7.6, *p*-Ar), 7.25 (2H, d, *J* 7.6, *m*-Ar). $^{13}$C{$^1$H} NMR (500 MHz; benzene-$d_6$): 13.5, 13.9 (CH$_2$*C*H$_3$), 15.5 (*C*H$_3$C=N), 23.5, 24.6 (*C*H$_2$CH$_3$), 31.4 (C(*C*H$_3$)$_3$), 83.0 (*C*(CH$_3$)$_3$), 120.2 (py 4), 125.8 (*m*-Ar), 126.3 (*m*-Ar), 127.0 (*p*-Ar), 128.3 (py 3/5), 133.0, 137.3, 142.1 (*o*-Ar, CH$_3$*C*=N), 149.8, 162.3 (*i*-Ar, py 2).

**($^{Et}$DIP-H/+H)Ti(O$^t$Bu)$_2$ (13)**. A 50 mL Schlenk tube was charged with 0.100 g (0.183 mmol) of **2**, 15 mL of toluene, and a stirrer bar. KO$^t$Bu (0.0412 g, 0.367 mmol) was added, and the reaction mixture was stirred for 2 days. Suspended solids were removed by centrifugation, and the solvent was removed in vacuo. The solid residue was dissolved in 2 mL of diisopropyl ether and left to crystallize at −35 °C, giving 0.067 g (59%) of orange-brown crystals.

$^1$H NMR (500 MHz; benzene-$d_6$) (partial assignment only): δ 0.73, 0.93 (9H each, s, C(C$H_3$)$_3$), 1.02 (3H, t, *J* 6.0, C*H$_3$*(H)C-N), 1.23, 1.24, 1.25, 1.29 (3H each, t, *J* 7.5, CH$_2$C*H$_3$*), 2.74-2.96 (8H, m, *CH$_2$*CH$_3$), 3.53, 4.33 (1H each, s, CH$_2$=CN), 5.14 (1H, br, CH$_3$(*H*)C-N), 6.74 (1H, d, *J* 7.5, py 3/5), 6.96 (1H, d, *J* 6.1, Ar), 7.02 (1H, t, *J* 7.5, py 4), 7.07 (3H, br, Ar, py 3/5), 7.13 (1H, d, *J* 7.8, *o*-Ar), 7.18 (1H, t, *J* 7.8, *p*-Ar), 7.26 (1H, d, *J* 7.8, *o*-Ar). $^{13}$C{$^1$H} NMR (500 MHz; benzene-$d_6$): 13.6, 13.7, 14.3, 14.5, 14.6, 24.6, 24.7, 25.0, 31.4, 31.5, 32.4,

82.0, 83.2, 84.1, 116.5, 117.5, 124.8, 125.7, 125.9, 126.0, 126.3, 138.3, 139.2, 139.9, 140.0, 141.2, 152.9, 156.0, 157.0, 165.7.

**($^{Et}$DIP-2H)Ti(O$^t$Bu)$_2$** (**14**) and **($^{Et}$DIP-2H)TiCl(O$^t$Bu)** (**15**). A 50 mL Schlenk tube was charged with 0.308 g (0.473 mmol) of **1**, 15 mL of toluene, and a stirrer bar. KO$^t$Bu (0.159 g, 1.42 mmol) was added, and the reaction mixture was stirred for 24 h. Suspended solids were removed by centrifugation, and the solvent was removed in vacuo. The solid residue was dissolved in a 3 mL of diisopropyl ether and left to crystallize at −35 °C, giving 0.104 g (35%) of orange-brown crystals of **14** mixed with free ligand. In a second crystallization attempt, 0.0066 g (2.4%) of pure orange-brown crystals of **15** was obtained.

$^1$H NMR (500 MHz; benzene-$d_6$) (**14**): δ 0.86 (18H, s, C(C*H*$_3$)$_3$), 1.32 (12H, t, *J* 7.5, CH$_2$C*H*$_3$), 2.95 (8H, m, C*H*$_2$CH$_3$), 3.74, 4.40 (2H each, s, CH$_2$=CN), 5.83 (1H, t, *J* 7.5, py 4), 6.70 (2H, d, *J* 7.5, py 3/5), 7.09 (2H, t, *J* 7.9, *p*-Ar), 7.13 (4H, d, *J* 7.9, *m*-Ar). $^{13}$C{$^1$H} NMR (500 MHz; benzene-$d_6$): 14.4 (CH$_2$*C*H$_3$), 25.3 (*C*H$_2$CH$_3$), 31.0 (C(*C*H$_3$)$_3$), 82.8 (*C*H$_2$=CN), 115.8 (py 4), 125.6, 125.7, 126.5 (*m*- and *p*-Ar), (py 3/5), 128.3, 137.1, 140.1, 155.7, 166.8 (*C*(CH$_3$)$_3$, *o*-Ar, py 2, *i*-Ar).

$^1$H NMR (500 MHz; benzene-$d_6$) (**15**): δ 0.64 (9H, s, C(C*H*$_3$)$_3$), 1.15, 1.40 (6H each, t, *J* 7.5, CH$_2$C*H*$_3$), 2.60, 2.72, 3.02, 3.25 (2H each, m, C*H*$_2$CH$_3$), 3.75, 4.39 (2H each, s, CH$_2$=CN), 6.84 (1H, t, *J* 7.7, py 4), 6.94 (2H, d, *J* 7.7, py 3/5), 7.17-7.24 (6H, m, Ar). $^{13}$C{$^1$H} NMR (500 MHz; benzene-$d_6$): 14.1, 14.9 (CH$_2$*C*H$_3$), 24.1, 24.8 (*C*H$_2$CH$_3$), 29.9 (C(*C*H$_3$)$_3$), 85.7 (*C*H$_2$=CN), 117.3 (py 3/5), 125.8, 126.4, 126.6 (*m*- and *p*-Ar), 138.9 (py 4), 128.3 (CH$_2$=*C*N), 137.6 (*C*(CH$_3$)$_3$), 140.2, 150.7 (*o*-Ar), 154.9, 155.9 (*i*-Ar, py 2).

**($^{Et}$DIP-2H)Ti(CH$_2$SiMe$_3$)$_2$** (**16**). A 10 mL vial was charged with 0.0688 g (0.106 mmol) of **4b** and 2 mL of benzene-$d_6$. TEMPO (0.156 g, 0.212 mmol) was added, and the reaction

mixture was left for 15 min. $^{1}$H NMR spectrum of the solution indicated the formation of **16**. The solvent was removed in vacuo. The solid residue was dissolved in 0.5 mL of toluene and layered with 2 mL of pentane. It was left to crystallize at −35 °C, giving 0.045 g (66%) of dark green crystals.

$^{1}$H NMR (500 MHz; benzene-$d_6$) (16): δ -0.22 (18H, s, $SiMe_3$), 1.30 (12H, t, *J* 7.6, $CH_2CH_3$), 2.12 (4H, s, Ti-$CH_2$), 2.89, 3.00 (4H each, m, $CH_2CH_3$), 3.88, 4.48 (2H each, s, $CH_2$=CN), 6.90 (1H, t, *J* 6.5, py 4), 7.02 (2H, d, *J* 6.5, py 3/5), 7.27 (6H, m, Ar). $^{13}$C{$^{1}$H} NMR (500 MHz; benzene-$d_6$): 2.0 ($SiMe_3$), 15.1 ($CH_2CH_3$), 24.5 ($CH_2CH_3$), 86.7 ($CH_2$=CN), 94.7 (Ti-$CH_2$), 117.5 (py 3/5), 126.6, 126.9 (*m*- and *p*-Ar), 139.2 (py 4), 139.5 ($CH_2$=CN), 149.7 (*o*-Ar), 155.9, 156.4 (*i*-Ar, py 2).

## 3.6 References


1. Bart, S. C.; Lobkovsky, E.; Chirik, P. J., Preparation and Molecular and Electronic Structures of Iron(0) Dinitrogen and Silane Complexes and Their Application to Catalytic Hydrogenation and Hydrosilation. *J. Am. Chem. Soc.* **2004,** *126* (42), 13794-13807.

2. Vidyaratne, I.; Scott, J.; Gambarotta, S.; Budzelaar, P. H. M., Dinitrogen Activation, Partial Reduction, and Formation of Coordinated Imide Promoted by a Chromium Diiminepyridine Complex. *Inorg. Chem.* **2007,** *46* (17), 7040-7049.

3. Vidyaratne, I.; Gambarotta, S.; Korobkov, I.; Budzelaar, P. H. M., Dinitrogen Partial Reduction by Formally Zero- and Divalent Vanadium Complexes Supported by the Bis-iminopyridine System. *Inorg. Chem.* **2005,** *44* (5), 1187-1189.

4. (a) Milsmann, C.; Semproni, S. P.; Chirik, P. J., N–N Bond Cleavage of 1,2-Diarylhydrazines and N–H Bond Formation via H-Atom Transfer in Vanadium Complexes Supported by a Redox-Active Ligand. *J. Am. Chem. Soc.* **2014,** *136* (34), 12099-12107; (b) Milsmann, C.; Turner, Z. R.; Semproni, S. P.; Chirik, P. J., Azo N□N Bond Cleavage with a Redox-Active Vanadium Compound Involving Metal–Ligand Cooperativity. *Angew. Chem. Int. Ed.* **2012,** *51* (22), 5386-5390.

5. (a) Margulieux, G. W.; Turner, Z. R.; Chirik, P. J., Synthesis and Ligand Modification Chemistry of a Molybdenum Dinitrogen Complex: Redox and Chemical Activity of a Bis(imino)pyridine Ligand. *Angew. Chem. Int. Ed.* **2014,** *53* (51), 14211-14215; (b) Margulieux, G. W.; Bezdek, M. J.; Turner, Z. R.; Chirik, P. J., Ammonia Activation, H2 Evolution and Nitride Formation from a Molybdenum Complex with a Chemically and Redox Noninnocent Ligand. *J. Am. Chem. Soc.* **2017,** *139* (17), 6110-6113.

6. Sugiyama, H.; Aharonian, G.; Gambarotta, S.; Yap, G. P. A.; Budzelaar, P. H. M., Participation of the α,α‘-Diiminopyridine Ligand System in Reduction of the Metal Center during Alkylation. *J. Am. Chem. Soc.* **2002,** *124* (41), 12268-12274.

7. Scott, J.; Gambarotta, S.; Korobkov, I.; Budzelaar, P. H. M., Metal versus Ligand Alkylation in the Reactivity of the (Bis-iminopyridinato)Fe Catalyst. *J. Am. Chem. Soc.* **2005,** *127* (37), 13019-13029.

8. Sandoval, J. J.; Palma, P.; Álvarez, E.; Cámpora, J.; Rodríguez-Delgado, A., Mechanism of Alkyl Migration in Diorganomagnesium 2,6-Bis(imino)pyridine Complexes: Formation of Grignard-Type Complexes with Square-Planar Mg(II) Centers. *Organometallics* **2016,** *35* (18), 3197-3204.

9. Thompson, E. J.; Berben, L. A., Frontispiece: Electrocatalytic Hydrogen Production by an Aluminum(III) Complex: Ligand-Based Proton and Electron Transfer. *Angew. Chem. Int. Ed.* **2015,** *54* (40), n/a-n/a.

10. (a) Scott, J.; Vidyaratne, I.; Korobkov, I.; Gambarotta, S.; Budzelaar, P. H. M., Multiple Pathways for Dinitrogen Activation during the Reduction of an Fe Bis(iminepyridine) Complex. *Inorg. Chem.* **2008,** *47* (3), 896-911; (b) Scott, J.; Gambarotta, S.; Korobkov, I.; Knijnenburg, Q.; de Bruin, B.; Budzelaar, P. H. M., Formation of a Paramagnetic Al Complex and Extrusion of Fe during the Reaction of (Diiminepyridine)Fe with AlR3 (R = Me, Et). *J. Am. Chem. Soc.* **2005,** *127* (49), 17204-17206.

11. Rahimi, N.; de Bruin, B.; Budzelaar, P. H. M., Balance between Metal and Ligand Reduction in Diiminepyridine Complexes of Ti. *Organometallics* **2017,** *36* (17), 3189-3198.

12. (a) Bowman, A. C.; Milsmann, C.; Bill, E.; Lobkovsky, E.; Weyhermüller, T.; Wieghardt, K.; Chirik, P. J., Reduced N-Alkyl Substituted Bis(imino)pyridine Cobalt Complexes: Molecular and Electronic Structures for Compounds Varying by Three Oxidation States. *Inorg. Chem.* **2010,** *49* (13), 6110-6123; (b) Wile, B. M.; Trovitch, R. J.; Bart, S. C.; Tondreau, A. M.; Lobkovsky, E.; Milsmann, C.; Bill, E.; Wieghardt, K.; Chirik, P. J., Reduction Chemistry of Aryl- and Alkyl-Substituted Bis(imino)pyridine Iron Dihalide Compounds: Molecular and Electronic Structures of [(PDI)2Fe] Derivatives. *Inorg. Chem.*

**2009,** *48* (9), 4190-4200; (c) de Bruin, B.; Bill, E.; Bothe, E.; Weyhermüller, T.; Wieghardt, K., Molecular and Electronic Structures of Bis(pyridine-2,6-diimine)metal Complexes [ML2](PF6)n (n = 0, 1, 2, 3; M = Mn, Fe, Co, Ni, Cu, Zn). *Inorg. Chem.* **2000,** *39* (13), 2936-2947.

13. Zhu, D.; Thapa, I.; Korobkov, I.; Gambarotta, S.; Budzelaar, P. H. M., Redox-Active Ligands and Organic Radical Chemistry. *Inorg. Chem.* **2011,** *50* (20), 9879-9887.

14. Trovitch, R. J.; Lobkovsky, E.; Bouwkamp, M. W.; Chirik, P. J., Carbon−Oxygen Bond Cleavage by Bis(imino)pyridine Iron Compounds: Catalyst Deactivation Pathways and Observation of Acyl C−O Bond Cleavage in Esters. *Organometallics* **2008,** *27* (23), 6264-6278.

15. Stor, G. J.; van der Vis, M.; Stufkens, D. J.; Oskam, A.; Fraanje, J.; Goubitz, K., Coordination of the potentially tridentate ligands 2,6-diacetylpyridine-bis(anil) (dapa) and 2-(2-(2′-methylidenepyridyl) aminoethyl) pyridine (map) in the complexes fac-BrMn(CO)3 L, fac-(CO)5MM′(CO)3L (M, M′= Mn, Re; L = dapa, map) and their photoproducts. The crystal structure of BrMn(CO)2(N,N,N-dapa). *J. Organomet. Chem.* **1994,** *482* (1), 15-29.

16. (a) Graham, T. W.; Kickham, J.; Courtenay, S.; Wei, P.; Stephan, D. W., Reduction of Titanium(IV)-Phosphinimide Complexes: Routes to Ti(III) Dimers, Ti(IV)-Metallacycles, and Ti(II) Species. *Organometallics* **2004,** *23* (13), 3309-3318; (b) Edema, J. J. H.; Duchateau, R.; Gambarotta, S.; Hynes, R.; Gabe, E., Novel titanium(II) amine complexes L4TiCl2[L = 1/2 N,N,N',N'-tetramethylethylenediamine (TMEDA), 1/2 N,N,N'-trimethylethylenediamine, pyridine, 1/2 2,2'-bipyridine]: synthesis and crystal structure of monomeric trans-(TMEDA)2TiCl2. *Inorg. Chem.* **1991,** *30* (2), 154-156; (c) Girolami, G. S.; Wilkinson, G.; Galas, A. M. R.; Thornton-Pett, M.; Hursthouse, M. B., Synthesis and properties of the divalent 1,2-bis(dimethylphosphino)ethane (dmpe) complexes MCl2(dmpe)2 and MMe2(dmpe)2(M = Ti, V, Cr, Mn, or Fe). X-Ray crystal structures of

MCl2(dmpe)2(M = Ti, V, or Cr), MnBr2(dmpe)2, TiMe1.3Cl0.7(dmpe)2, and CrMe2(dmpe)2. *J. Chem. Soc., Dalton Trans.* **1985,** (7), 1339-1348.

17. (a) Dastgir, S.; Lavoie, G. G., Titanium(iv) imido complexes of imine imidazol-2-imine ligands. *Dalton Trans.* **2012,** *41* (32), 9651-9658; (b) Hill, J. E.; Profilet, R. D.; Fanwick, P. E.; Rothwell, I. P., Synthesis, Structure, and Reactivity of Aryloxo(imido)titanium Complexes. *Angew. Chem. Int. Ed.* **1990,** *29* (6), 664-665; (c) Duchateau, R.; Williams, A. J.; Gambarotta, S.; Chiang, M. Y., Carbon-carbon double-bond formation in the intermolecular acetonitrile reductive coupling promoted by a mononuclear titanium(II) compound. Preparation and characterization of two titanium(IV) imido derivatives. *Inorg. Chem.* **1991,** *30* (25), 4863-4866; (d) Adams, N.; Bigmore, H. R.; Blundell, T. L.; Boyd, C. L.; Dubberley, S. R.; Sealey, A. J.; Cowley, A. R.; Skinner, M. E. G.; Mountford, P., New Titanium Imido Synthons: Syntheses and Supramolecular Structures. *Inorg. Chem.* **2005,** *44* (8), 2882-2894; (e) J. Blake, A.; E. Collier, P.; H. Gade, L.; McPartlin, M.; Mountford, P.; Schubart, M.; J. Scowen, I., Highly selective trimerisation of MeNC by a novel titanium imido complex containing a tridentate dianionic ligand. *Chem. Commun.* **1997,** (16), 1555-1556; (f) Selby, J. D.; Manley, C. D.; Feliz, M.; Schwarz, A. D.; Clot, E.; Mountford, P., New ligand platforms for developing the chemistry of the Ti[double bond, length as m-dash]N-NR2 functional group and the insertion of alkynes into the N-N bond of a Ti[double bond, length as m-dash]N-NPh2 ligand. *Chem. Commun.* **2007,** (46), 4937-4939.

18. Paparo, A.; van Kruchten, F. D.; Spaniol, T. P.; Okuda, J., Formate complexes of titanium(iv) supported by a triamido-amine ligand. *Dalton Trans.* **2018,** *47* (10), 3530-3537.

19. Planalp, R. P.; Andersen, R. A., Dialkyl bis[bis(trimethylsilyl)amide] Group IVA compounds. Phosphine-induced transformation of a bridging carbene into a metallacycle.

Crystal structure of zirconium-to-nitrogen-bonded Zr[CH2Si(Me)2NSiMe3]2(Me2PCH2CH2PMe2). *Organometallics* **1983,** *2* (11), 1675-1680.

20. Myers, T. W.; Kazem, N.; Stoll, S.; Britt, R. D.; Shanmugam, M.; Berben, L. A., A Redox Series of Aluminum Complexes: Characterization of Four Oxidation States Including a Ligand Biradical State Stabilized via Exchange Coupling. *J. Am. Chem. Soc.* **2011,** *133* (22), 8662-8672.

21. Schmidt, R.; Welch, M. B.; Knudsen, R. D.; Gottfried, S.; Alt, H. G., N,N,N-Tridentate iron(II) and vanadium(III) complexes: Part I. Synthesis and characterization. *J. Mol. Catal. A: Chem.* **2004,** *222* (1), 9-15.

22. Fulmer, G. R.; Miller, A. J. M.; Sherden, N. H.; Gottlieb, H. E.; Nudelman, A.; Stoltz, B. M.; Bercaw, J. E.; Goldberg, K. I., NMR Chemical Shifts of Trace Impurities: Common Laboratory Solvents, Organics, and Gases in Deuterated Solvents Relevant to the Organometallic Chemist. *Organometallics* **2010,** *29* (9), 2176-2179.

23. *smart program suite, 6*, Bruker AXS Inc.; Madison, WI.

24. Sheldrick, G. M. *SADABS*, University of Göttingen, Göttingen, Germany.

25. Sheldrick, G. M., *Acta Crystallogr. Sect. A: Found. Crystallogr.* **2008,** *64*, 112-122.

# 4 Synthesis and Characterization of Diiminopyridine Zr and Hf Complexes

## 4.1 ABSTRACT

We report on the electronic and chemical noninnocence of the diiminepyridine ligand $^{R}$DIP [(2,6-$R_2$-$C_6H_3N$=CMe)$_2C_5H_3N$] in its Zr and Hf complexes. Reaction of $^{Et}$DIP with $MCl_4$ gave the corresponding complexes ($^{Et}$DIP)$MCl_4$ (M: Zr (**1**); Hf (**2**)) which have a pentagonal bipyramidal seven-coordinate structure. Treatment of **1** with two equivalents of $KC_8$ in THF yielded the expected reduction product ($^{Et}$DIP)$ZrCl_2$(THF) (**3**). The reactions of **1** and **2** with the same amount of $KC_8$ in toluene afforded ($^{Et}$DIP)$MCl_2$ (M: Zr (**4**), Hf (**5**)). Complex **4** proved to be unstable, and on standing partially isomerized through transfer of a hydrogen atom from one imine methyl group to the second imine carbon. Addition of $Et_2O$ to this mixture allowed isolation of pure ($^{Et}$DIP)$ZrCl_2(OEt_2)$ (**4-Et$_2$O**). Alkylation of **5** with two equivalents of $Me_3SiCH_2Li$ or MeMgBr gave the corresponding complexes ($^{Et}$DIP)$HfR_2$ (R: $CH_2SiMe_3$ (**5'**), Me (**5"**). Similar to **4**, complex **5"** underwent isomerization on standing. The formally Zr(II) and Hf(II) complexes **3**, **4**, **4-Et$_2$O**, **5**, **5'** and **5"** show strong upfield $^1$H NMR shifts for the pyridine β and γ protons caused by transfer of negative charge to the ligand. On the basis of this and the C=N and $C_{imine}$–$C_{py}$ bond lengths, a description involving Zr(IV) and Hf(IV) and a dianionic ligand seems most appropriate, and DFT calculations support this interpretation. The analogous reduction of **2** in diethyl ether yielded the complex ($^{Et}$DIP-2H)$HfCl_2(OEt_2)$ (**6**) containing the doubly dehydrogenated $^{Et}$DIP ligand [$^{Et}$DIP-2H = (2,6-$Et_2$-$C_6H_3N$-C=$CH_2$)$_2C_5H_3N$)]. Treatment of **1** and **2** with 1 equivalent of $(Me_3Si)_2NK$ produced complexes of the singly dehydrogenated ligand: ($^{Et}$DIP-H)$MCl_3$ (M = Zr (**7**), Hf (**8**)). Reaction of $^{R}$DIP (R = Me, Et, $^{i}$Pr) with $M(CH_2Ph)_4$ (M = Zr, Hf) resulted in benzyl transfer

to both imine groups, forming complexes [($^{R}$DBAP)M($CH_2Ph)_2$] of the dibenzylated ligand [$^{R}$DBAP = (2,6-$R_2$-$C_6H_3$N-CMe($CH_2Ph$))$_2C_5H_3N$] as a mixture of *rac* ($C_2$ symmetric) and *meso* ($C_s$ symmetric) diastereomers. In several cases the diastereomers could be separated, but heating of either pure diastereomer in solution re-establishes the equilibrium mixture. Reaction of $C_2$-[($^{Et}$DBAP)Zr($CH_2Ph)_2$] with 2 equivalents of TEMPO led to formation of $C_2$-[($^{Et}$DBAP)Zr($CH_2Ph$)(TEMPO)] (**13**) which did not convert into an equilibrium mixture upon heating. Treatment of $^{Et}$DIP with *in situ* formed Hf($CH_2SiMe_3)_4$ gave the bis chelate complex **14** in which each ligand is doubly dehydrogenated.

# 4.2 INTRODUCTION

Diiminopyridines are well-known 6 electron donor noninnocent ligands which can accommodate up to three electrons in their extended π-system[1] (Figure 4.1).

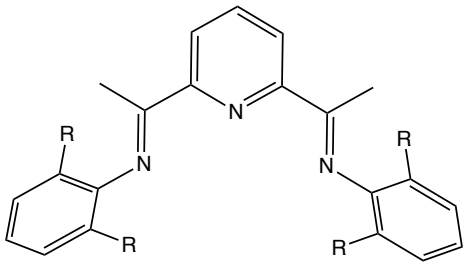


Figure 4.1. $^{R}$DIP ligand

This stabilizes first-row transition metal complexes in low formal oxidation states of the metal atom.[2] Much less work has been done on combinations with heavier transition metals. DIP complexes of Ru, Rh and Ir by Berry[3] and Burger[4], of lanthanides by Gambarotta[5] and of Mo by Chirik[6] have been reported.

One of the remarkable properties of DIP as a redox-active ligand is the possibility of enabling non-noble metals to behave like noble metals: the combination can lead to low-spin states and

$2e^-$ redox reactions.[7] DIP complexes of iron and cobalt have been shown to be competent in various catalytic conversions such as hydrogenation,[8] hydroboration,[9] hydrosilation,[7] cyclization[10] and C-C cross coupling reactions.[11] In addition to functioning as electron reservoirs, DIP complexes undergo extensive and somewhat unpredictable ligand-based reactivity such as dimerization,[12] dehydrogenation[13] and alkylation[14] that create new ligand modifications. In alkylation of the chelate, the destination of the transferred alkyl is highly dependent to the type of alkyl, the metal center and the steric hindrance of the ligand (Figure 4.2).

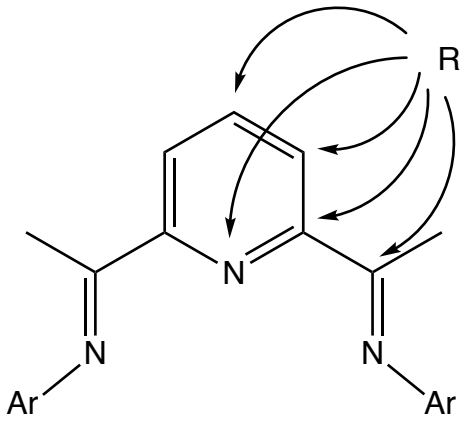


Figure 4.2. Possible alkylation positions in DIP ligand

Several research groups have conducted experiments to explore the chemistry of DIP ligands with main group (Li[15], Mg,[16] Ca,[17] Sr,[17] Ba[17]) and transition metal (e.g. Mn,[18] Fe,[7] Co[2]) alkyls. As shown in Scheme 1.17, it is now believed that the strong π-backdonating character of the ligand weakens the M-C bond. There are a few isolated examples of polyalkyls in which the M-C bonds are stabilized by a ß-silyl group (e.g. (DIP)Mn($CH_2SiMe_3$)$_2$ and (DIP)Fe($CH_2SiMe_3$)$_2$),[18-19] while $MR_n$ fragments without ß-silylated R groups are much less stable. Combinations of the DIP ligand with almost all of the first-row transition metals have been extensively studied (Ti,[20,21] V,[22] Cr,[23] Mn,[18] Fe,[24] Co,[25] Ni,[26] Zn[27]) and the possibly

noninnocent character of the ligand has been investigated. In a previous paper, we reported on noninnocence of the DIP ligand in its Ti complexes.[21] (DIP)$TiCl_3$ was found to contain essentially Ti(III), but formally divalent complexes (DIP)$TiCl_2$ and (DIP)$TiR_2$ were demonstrated to contain a doubly reduced ligand. In this chapter, we describe an extension of this work to the heavier group IV congeners Zr and Hf. Calderazzo already prepared (DIP)$ZrCl_4$ and reported it to have some activity in ethene polymerization on activation with MAO.[20] A 7-coordinate pentagonal bipyramidal structure was proposed based mainly on IR data. We used this as a convenient starting point for the synthesis of formally low-valent Zr and Hf complexes.

## 4.3 RESULTS AND DISCUSSION

Calderazzo reported formation of ($^{R}$DIP)$ZrCl_4$ from $ZrCl_4$ and $^{R}$DIP (R = H, $^{i}$Pr) in toluene at elevated temperatures and proposed the complex to be 7-coordinate. We prepared both ($^{Et}$DIP)$ZrCl_4$ (**1**) and its Hf analog (**2**) in $CH_2Cl_2$ at room temperature, and X-ray structure determinations confirm the 7-coordinate nature of **1** in the solid state. The $^{1}$H NMR spectrum of **1** shows backbone resonances at their "normal" positions: 8.57 ppm for Py *H4*, 8.43 ppm for Py *H3/5* and 2.38 ppm for C*H*$_3$C=N.

While analogous Zr and Hf complexes usually have similar physical properties, we observed that **1** and **2** differ substantially in their solubility in $CH_2Cl_2$. Upon mixing $ZrCl_4$ with $^{Et}$DIP ligand a yellow precipitate formed, while its Hf analog remained in the solution. Yet, the backbone resonances of the ligand in **2** (8.59 ppm for Py *H4*, 8.45 ppm for Py *H3/5* and 2.36 ppm for C*H*$_3$C=N) are very close to those for **1**.

$KC_8$, previously reported to be a clean and convenient reductant for ($^{R}$DIP)Ti complexes, was then reacted with **1** and **2**. These reactions were found to be rather solvent-dependent. Unlike for Ti, we never observed formation of (DIP)$MCl_3$ complexes with either Zr or Hf. The reaction of **1** with 2 equivalents of $KC_8$ in THF gave doubly reduced derivative

($^{Et}$DIP)$ZrCl_2$(THF) (**3**) (Scheme 4.1); when smaller amounts of reductant were employed the result was a mixture of **1** and **3**.

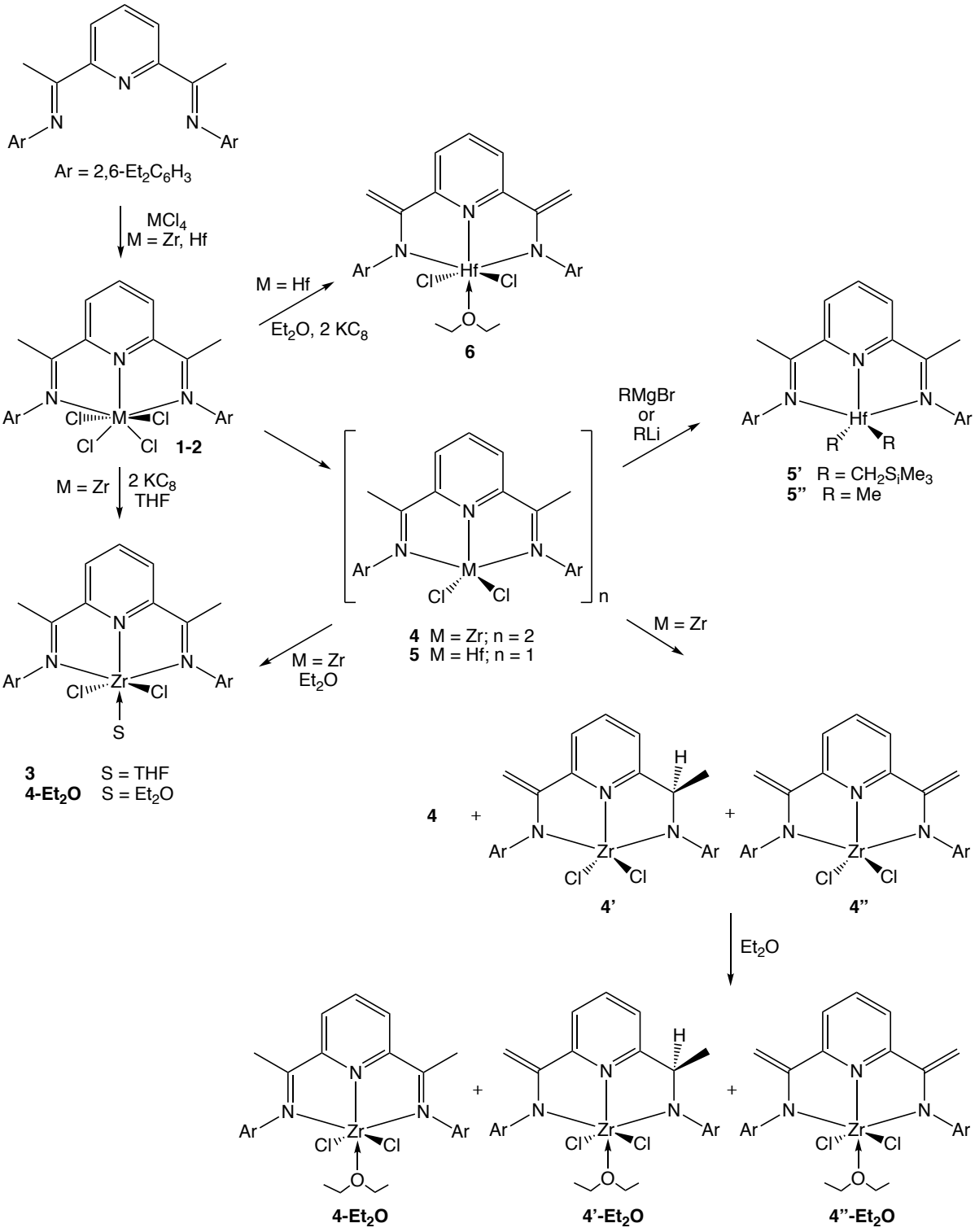


Scheme 4.1. Synthesis of Zr(IV), Hf(IV), Hf(II) and Zr(II) Complexes

Like previously reported Ti complexes with dianionic DIP ligands,[21] $^{1}$H-NMR of **3** showed upfield shifted resonances for the pyridine and imine methyl hydrogens (4.82 ppm for Py *H4*, 5.75 ppm for Py *H3/5* and 1.28 ppm for C*H*$_3$C=N).

When the reduction was carried out in toluene, solvent-free complexes ($^{Et}$DIP)ZrCl$_2$ (**4**) and ($^{Et}$DIP)HfCl$_2$ (**5**) were obtained as brownish/purplish solids. The $^{1}$H NMR spectra of complexes **4** and **5** in toluene-d$_8$ show the same pattern as their Ti counterpart and **3** (effective C$_{2v}$ symmetry). The signals of **4** are strongly broadened at room temperature but those of **5** are much sharper (Figure 4.3).

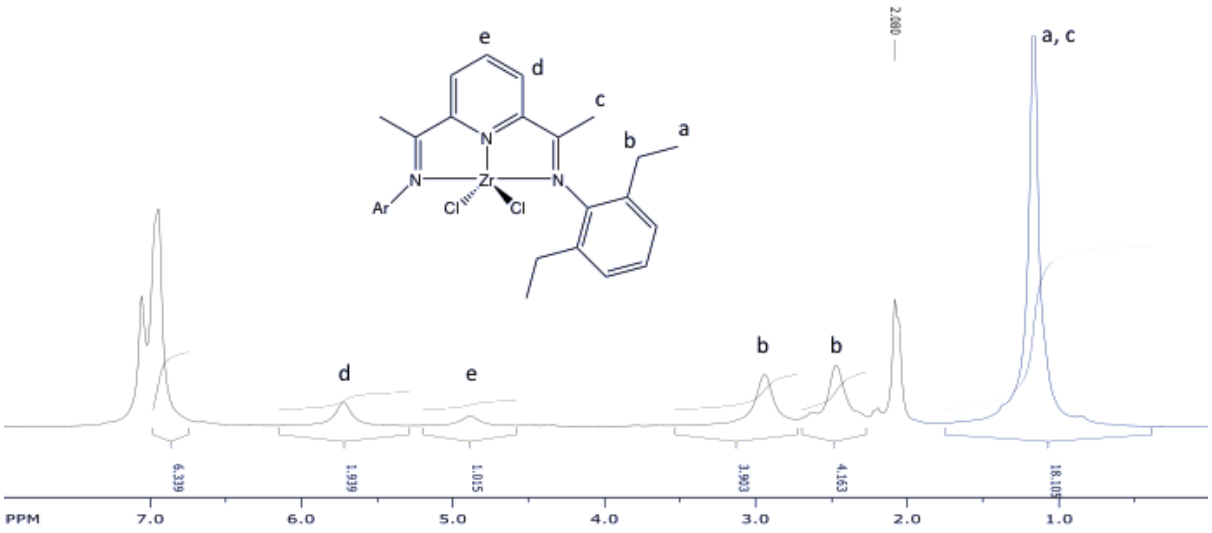


a)

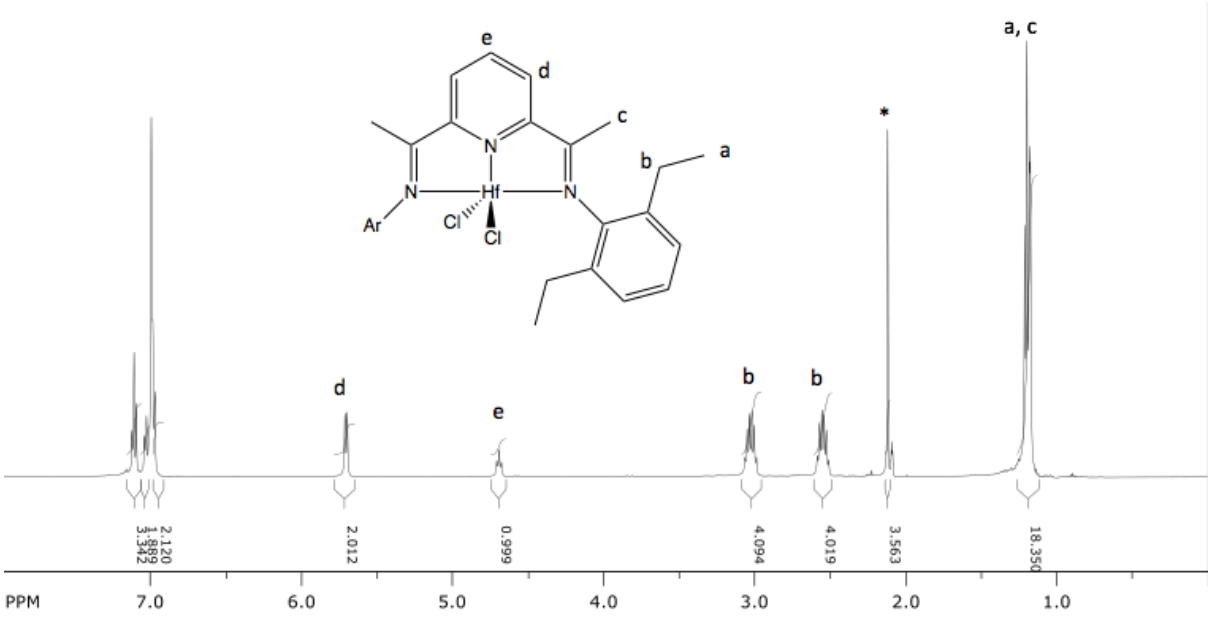


b)

Figure 4.3. $^{1}$H-NMR spectra of a) **4** at 25 °C and b) **5** at -5 °C (in toluene-$d_8$). (*) one molecule of toluene in the crystal lattice of **5**.

As observed in **3**, pyridine hydrogens in **4** and **5** are also shifted upfield (in **4**: 5.00 ppm for Py *H*4 and 5.82 ppm for Py *H*3/5; in **5**: 4.70 ppm for Py *H*4 and 5.71 ppm for Py *H*3/5) and the imine methyls appear as singlets at 2.12 ppm and 1.18, respectively. The Et groups in these complexes appear as two multiplets of 4H each at 2.50 and 2.97 ppm (in **4**) and 2.55 and 3.02 ppm (in **5**) for C$H_2$ and one triplet of 12H at 1.19 ppm (in **4**) and 1.19 (in **5**) for C$H_3$. On cooling the solution of **4**, decoalescence into a much more complicated spectrum was observed. The observed pattern is consistent with $C_1$ symmetry in a frozen-out structure, but even at -55 ºC the signals remain broad (Figure 4.4).

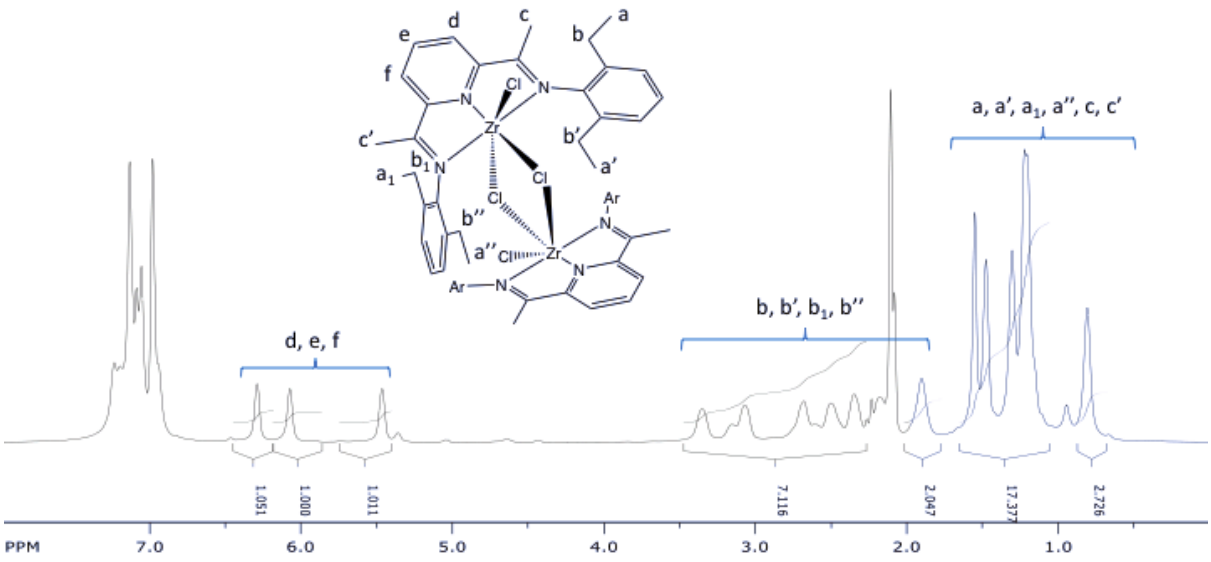


Figure 4.4. $^{1}$H-NMR spectrum of **4** in toluene-$d_8$ at -55 °C. (∗) molecules of toluene in the crystal lattice of **4**

Unexpectedly, the solid-state structure of **4**, which will be discussed later, appeared to be a dimer rather than a monomer like **5**. This suggests that perhaps the observed dynamic behavior in solution may be due to reversible formation of an asymmetric dimer. Surprisingly, cooling the solution of **5** only led to sharper peaks and no decoalescence was observed.

After prolonged reaction times (9 days), **4** was always accompanied by variable amounts of second and third products **4'** and **4"**. In fact, in toluene solution complex **4** slowly rearranges to **4'** and **4"** which give sharp $^{1}$H NMR signals (Figure 4.5).

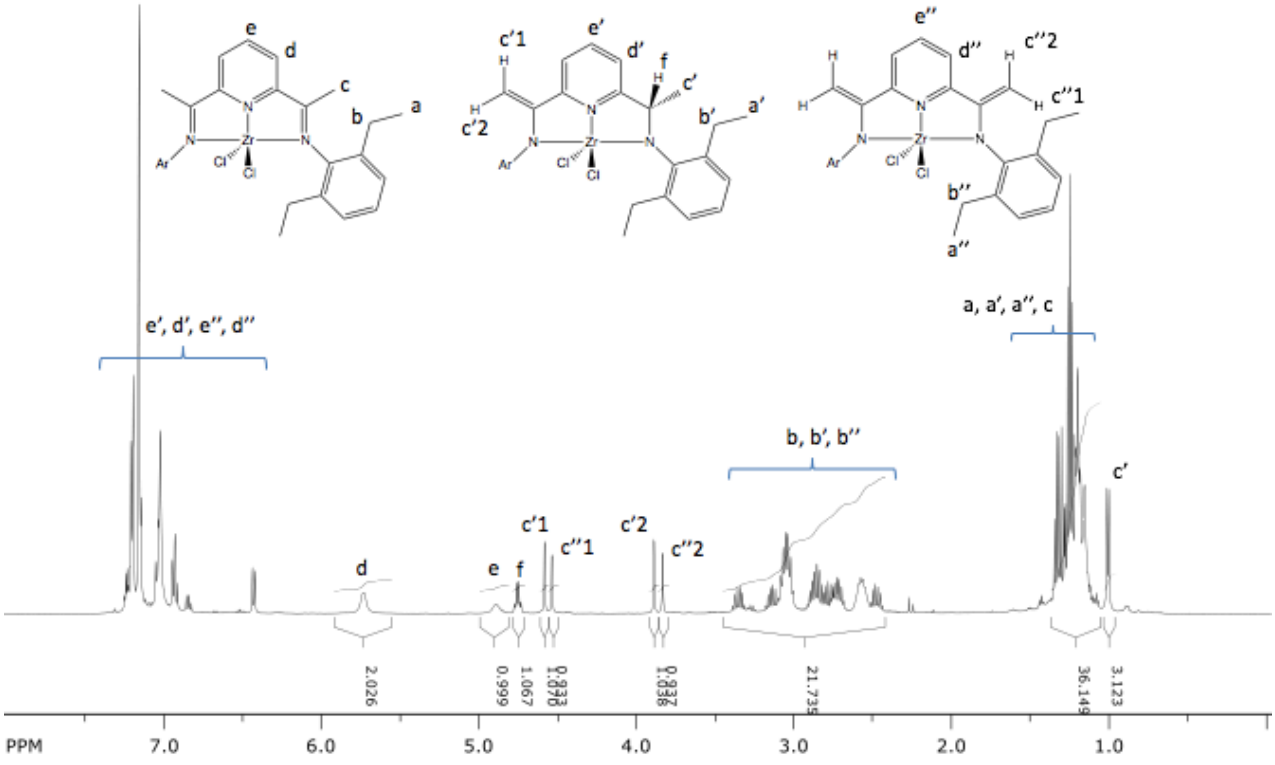


Figure 4.5. $^{1}$H-NMR spectrum of the mixture of **4**, **4'** and **4"** in benzene-$d_6$

Based on its NMR data, **4'** is asymmetric, having four inequivalent ligand Et groups and separately observed pyridine *H*3 and *H*5 signals coupling to the same *H*4 signal. Instead of the expected two imine methyl group singlets of 3H each, we observed two singlets of 1H each at 3.89 and 4.58 ppm (indicative of a dehydrogenated imine methyl group) and in addition a 3H doublet at 1.0 ppm coupling to a 1H quartet at 4.75 ppm. The latter two signals strongly suggest the presence of a $NCHCH_3$ moiety formed by addition of a hydrogen to the imine C=N bond. Thus, **4'** appears to be an isomer of **4** in which one imine methyl H has moved to the imine carbon of the other ligand arm, similar to what was observed for some Ti complexes in the previous chapter. In addition, the spectrum shows two more singlets at 3.83 and 4.54 ppm for **4"** indicative of a doubly dehydrogenated ligand. While there are numerous reports of DIP ligands being chemically modified, including through loss of hydrogens from the $CH_3C$=N groups, the **4** to **4′** hydrogen-shift isomerization presented here has never been

reported in the literature. Its mechanism is not clear at this point. A direct movement of a hydrogen radical from one end of the ligand to the other seems rather unlikely, and the imine methyl groups are too far away from the metal to allow a direct H atom transfer (HAT) from methyl to metal, leaving a "hopping" mechanism and intermolecular HAT as the most plausible alternatives. Addition of 15 mL of diethyl ether to the mixture gave a mixture of the ether adducts **4-Et$_2$O/4'-Et$_2$O/4''-Et$_2$O** (see Scheme 4.1) which crystallized well, but the crystals appear to be co-crystals containing all three compounds. The complex **4-Et$_2$O** can also be obtained upon dissolution of **4** in 5 ml Et$_2$O (see Scheme 4.1).

Alkylation of **5** with 2 equivalents of $Me_3SiCH_2Li$ or MeMgBr resulted in formation of dialkyl complexes **5'** and **5''**, respectively. Like their Ti counterparts, the pyridine hydrogens in **5'** and **5''** are shifted upfield (**5'**: 5.03 ppm for Py *H*4, 6.03 ppm for Py *H*3/5 and 1.44 for $H_3$CCN; **5''**: 4.40 ppm for Py *H*4, 5.30 ppm for Py *H*3/5 and 0.29 for $H_3$CCN) indicating the presence of dianionic DIP ligands. The Et groups appear as one triplet for C$H_3$ at 1.30 in **5'** and 1.27 in **5''** and two multiplets for C$H_2$ at 2.80 and 3.03 in **5'** and 2.66 and 2.84 ppm in **5''** (Figure 4.6).

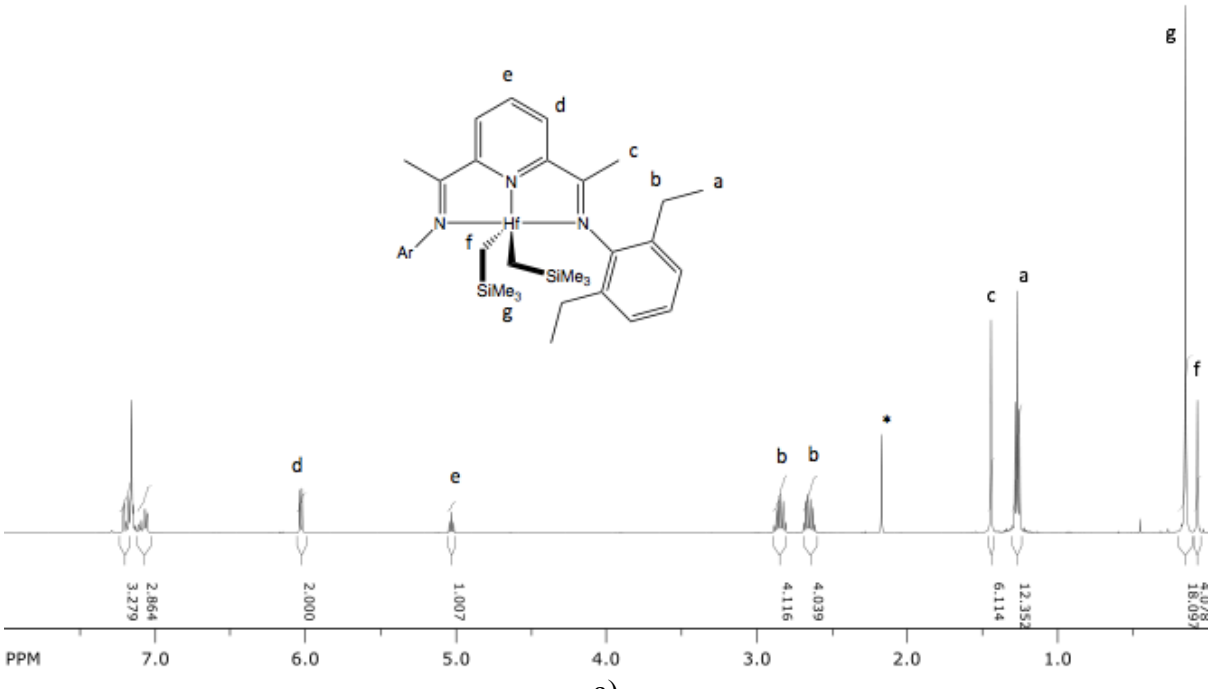


a)

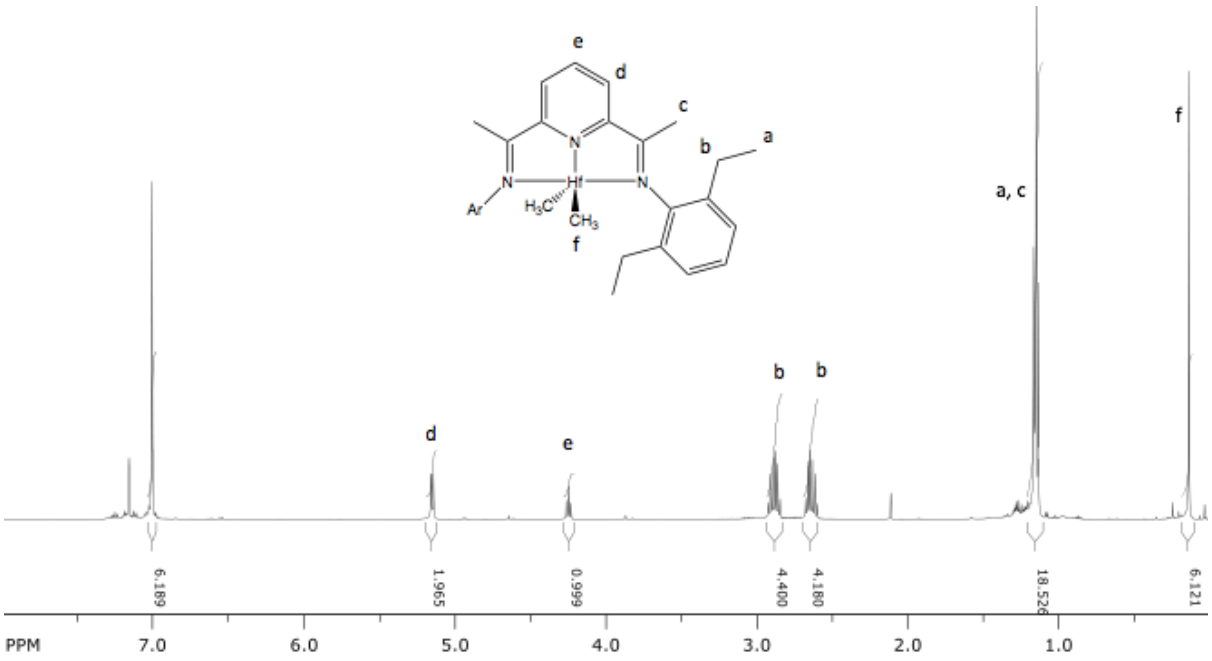


b)

Figure 4.6. $^{1}$H-NMR spectra of a) **5'** and b) **5"** in toluene-$d_8$. (*) toluene solvent peak

As observed in its Ti counterpart, the complex **5"** underwent hydrogen atom migration and loss on standing (Scheme 4.2). The related $^{1}$H-NMR spectrum is presented in Figure 4.7.

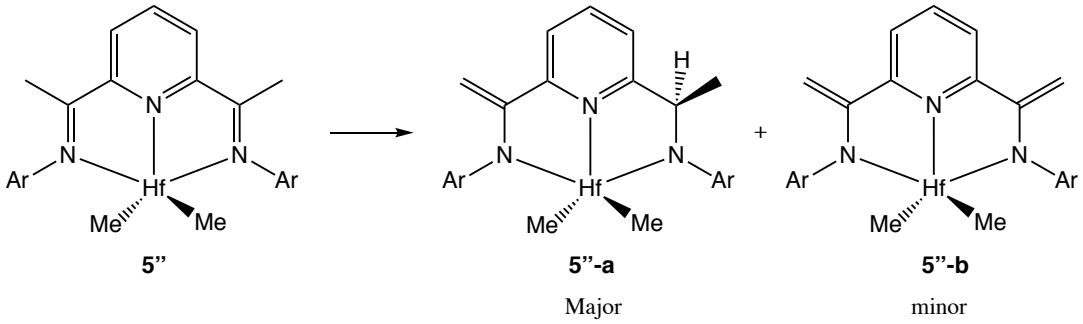


Scheme 4.2. Isomerization of **5"** on standing

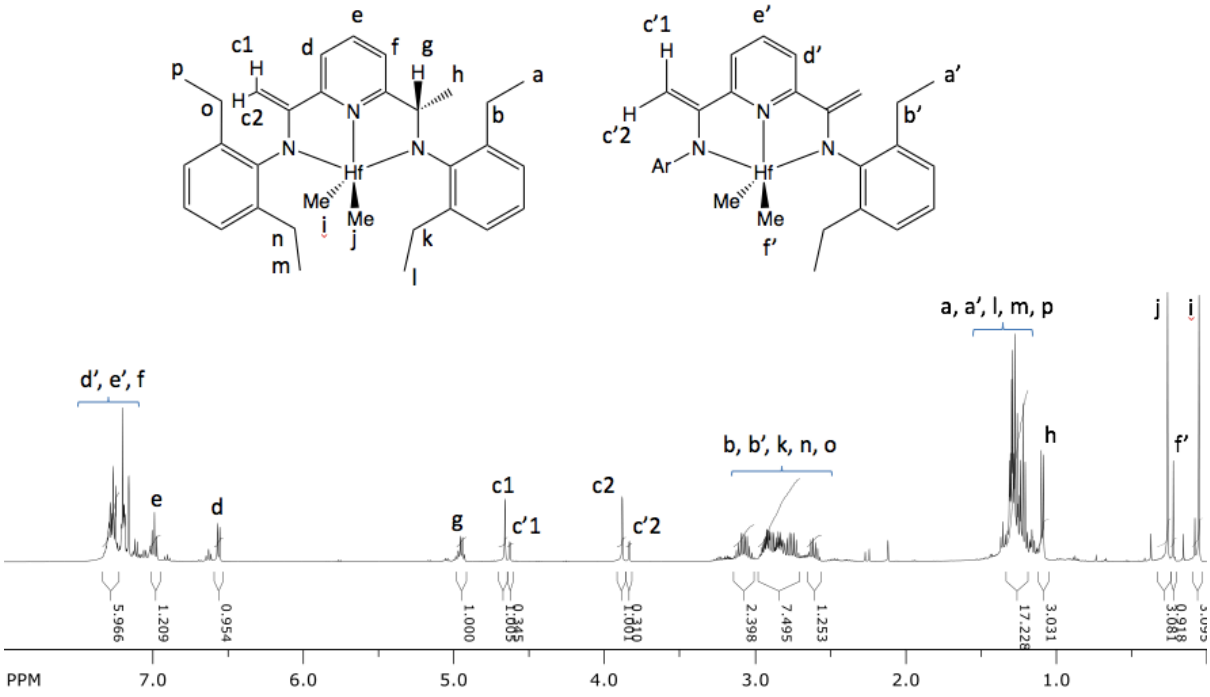


Figure 4.7. $^{1}$H NMR (500 MHz; toluene-$d_8$) spectrum of **5"** after 5 days in solution, showing hydrogen atom migration and loss

Treatment of **2** with two equivalents of $KC_8$ in THF did not result in formation of an identifiable reduced Hf complex but only gave free ligand. A similar reaction carried out in ether resulted in purple/brown ether adduct **6** (see Scheme 4.1), containing a doubly dehydrogenated ligand, which was characterized by single crystal X-ray diffraction.

It appears that the reducing power of the electrons stored in the DIP ligand of **4** and **5** is more available for chemical reactions than in the corresponding Ti complex. For example, treatment of **4** or **5** with $CH_2Cl_2$ results in C-Cl bond cleavage and formation of ($^{Et}$DIP-H)$MCl_3$ (**7** and **8**, Scheme 4.3).

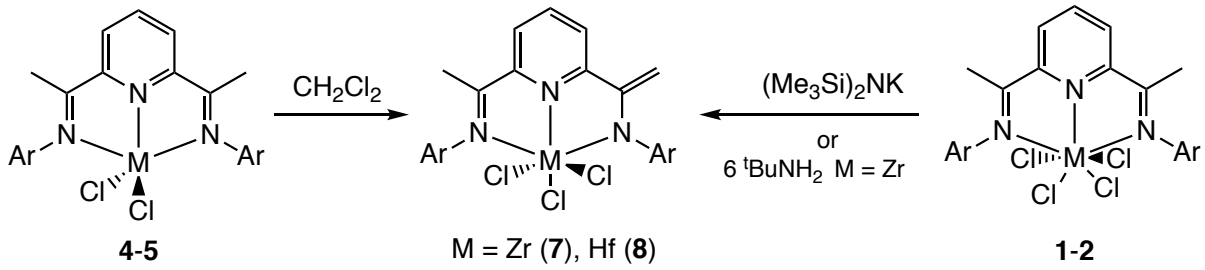


Scheme 4.3. Synthesis of **7** and **8** via C-Cl bond cleavage and bases

The mechanism of this reaction is unclear; one possibility is chlorine atom abstraction by **4** (or **5**), forming a $CH_2Cl$ radical which could then abstract a hydrogen atom from a DIP imine methyl group.

The $^1$H NMR spectrum of **7** suggests a $C_s$-symmetric complex with three inequivalent pyridine signals of 1H each at 8.20, 8.25 and 8.30 ppm, and two singlets of 1H each at 3.65 and 4.95 ppm for C$H_2$=CN. The imine methyl protons appear at 2.39 ppm as a singlet. The reaction of **1** with 1 equivalent of $(Me_3Si)_2NK$ provided independent access to **7**, and a similar reaction using **2** produced ($^{Et}$DIP-H)$HfCl_3$ (**8**). Attempts to generate a zirconium imido complex from **1** using $^t$BuNH$_2$ failed since the amine acted as a base to give **7**.

## 4.3.1 X-ray Structural Characterization

The solid-state structure of **1** is presented in Figure 4.8 and the related bond lengths are collected in Table 4.1.

Table 4.1. Selective bond lengths (Å) for ($^{Et}$DIP)Zr and Hf complexes

| | **1** | **3** | **4** | **4-Et$_2$O** | **4"-Et$_2$O** | **5** | **5'** | **6** |
|---|---|---|---|---|---|---|---|---|
| M-N1 | 2.516(13) | 2.283(2) | 2.165(9) | 2.305(11) | 2.117(5) | 2.192(3) | 2.1825(17) | 2.098(3) |
| M-N2 | 2.373(12) | 2.109(2) | 2.097(7) | 2.114(11) | 2.206(5) | 2.070(3) | 2.1047(17) | 2.252(3) |
| M-N3 | 2.524(13) | 2.162(2) | 2.266(7) | 2.120(11) | 2.203(5) | 2.119(3) | 2.1927(18) | 2.136(3) |
| M-N4 | | | 2.122(10) | | | | | |
| M-N5 | | | 2.098(7) | | | | | |
| M-N6 | | | 2.268(7) | | | | | |
| M-Cl1 | 2.425(4) | 2.4483(13) | 2.426(2) | 2.472(4) | 2.4513(15) | 2.3928(10) | | 2.4519(8) |
| M-Cl2 | 2.438(4) | 2.4825(11) | 2.568(2) | 2.458(3) | 2.4795(16) | 2.3541(11) | | 2.4250(8) |
| M-Cl2 | | | 2.619(2) | | | | | |
| M-Cl3 | 2.453(4) | | 2.424(2) | | | | | |
| M-Cl4 | 2.426(4) | | 2.609(2) | | | | | |
| M-Cl4 | | | 2.574(2) | | | | | |
| M-O1 | | 2.3723(19) | | 2.361(9) | 2.341(4) | | | 2.272(2) |
| M-C30 | | | | | | | 2.208(2) | |
| M-C31 | | | | | | | 2.237(2) | |
| N1-C12 | 1.263(18) | 1.328(3) | 1.353(11) | 1.310(17) | 1.399(8) | 1.343(5) | 1.361(3) | 1.409(5) |
| N4-C40 | | | 1.364(11) | | | | | |
| C12-C13 | 1.48(2) | 1.424(4) | 1.402(12) | 1.449(19) | 1.423(9) | 1.419(5) | 1.395(3) | 1.481(5) |
| C40-C41 | | | 1.402(11) | | | | | |
| C17-C18 | 1.54(3) | 1.388(4) | 1.404(13) | 1.370(19) | 1.455(9) | 1.388(6) | 1.406(3) | 1.474(5) |
| C45-C46 | | | 1.411(13) | | | | | |
| C18-N3 | 1.27(2) | 1.370(3) | 1.348(10) | 1.371(16) | 1.379(8) | 1.387(5) | 1.355(3) | 1.387(4) |
| C46-N6 | | | 1.331(10) | | | | | |
| C11-C12 | 1.52(2) | 1.502(4) | 1.502(13) | 1.497(19) | 1.404(10) | 1.489(5) | 1.495(3) | 1.285(7) |
| C39-C40 | | | 1.484(13) | | | | | |
| C18-C19 | 1.49(2) | 1.501(4) | 1.497(12) | 1.49(2) | 1.397(12) | 1.490(6) | 1.494(3) | 1.343(5) |
| C46-C47 | | | 1.507(12) | | | | | |
| τ | | | | | | 0.38 | 0.37 | |

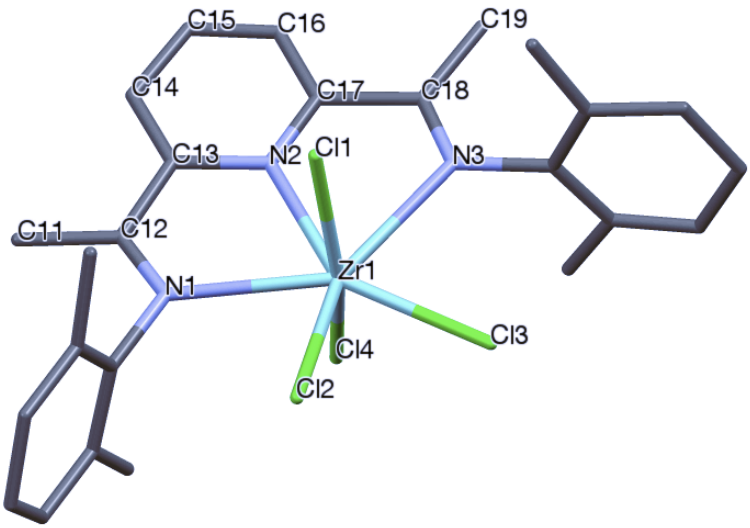


Figure 4.8. Molecular structure of **1** [($^{Et}$DIP)ZrCl$_4$]. Hydrogens and ethyl CH$_3$ carbons are omitted for clarity

Coordination numbers higher than 6 are not very common and are mostly observed for metal ions with relatively large ionic radii, such as early second and third row transition metals, lanthanides and actinides. In addition to the pentagonal bipyramidal geometry observed here, monocapped octahedral and monocapped trigonal prismatic geometries have been reported for seven-coordinate compounds. A pentagonal bipyramidal geometry has frequently been observed in complexes of the type [M(unidentate A)$_5$(unidentate B)$_2$] (e.g. $[Zr(C_6F_5)_5F_2]^{3-}$), ionic salts (e.g. $ZrF_7^{3-}$), and in compounds involving pentadentate macrocyclic ligands in which the sixth and seventh ligands occupy the axial coordination sites. Seven-coordinate compounds containing salen-type ligands also form pentagonal bipyramidal geometries in which one of the coordination sites is normally occupied by a coordinating solvent.[28] According to MO calculations,[29] the pentagonal bipyramidal geometry is more favorable for main-group metal compounds and the other two geometries are more established for transition metal compounds. However, in our complex **1** the DIP ligand is rather rigid, has small bite angles and does not allow much deformation in the plane of the ligand. Also, the two perpendicular N-aryl rings of moderate steric bulk hinder access to the positions above and below the metal center. With these constraints, a pentagonal bipyramidal structure appears to be energetically favoured for **1**.

In **1**, the two apical chlorides are bent back over the DIP ligand (∠N2−Zr−Cl1 = 79.4(3)°, ∠N2−Zr−Cl4 = 79.5(3)°. Such a "bent-back" chloride, which has been observed in ($^{iPr}$DIP)ScCl$_3$,[7] ($^{Et}$DIP)TiCl$_3$,[21] and ($^{iPr}$DIP)TiCl$_3$,[20] is likely due to steric factors. The two equatorial chlorides in **1** are displaced out of the NNN plane by 0.433 Å and 0.310 Å. The C=N and $C_{imine}$-$C_{py}$ bond lengths fall within the range expected for complexes with neutral (innocent) DIP ligands (C=N: 1.266 Å; $C_{imine}$-$C_{py}$: 1.51 Å).

The structures of **3**, **4**, **4-$Et_2O$**, **4"-$Et_2O$**, **5** and **5′** are shown in Figure 4.9, Figure 4.11, Figure 4.12, Figure 4.13 and Figure 4.14, respectively, and the bond lengths and structural parameters are summarized in Table 4.1.

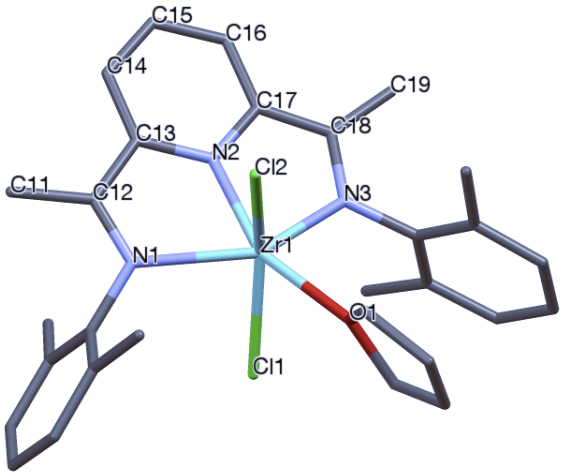


Figure 4.9. Molecular structure of **3** [($^{Et}$DIP)$ZrCl_2$(THF)]. Hydrogens and ethyl $CH_3$ carbons are omitted for clarity

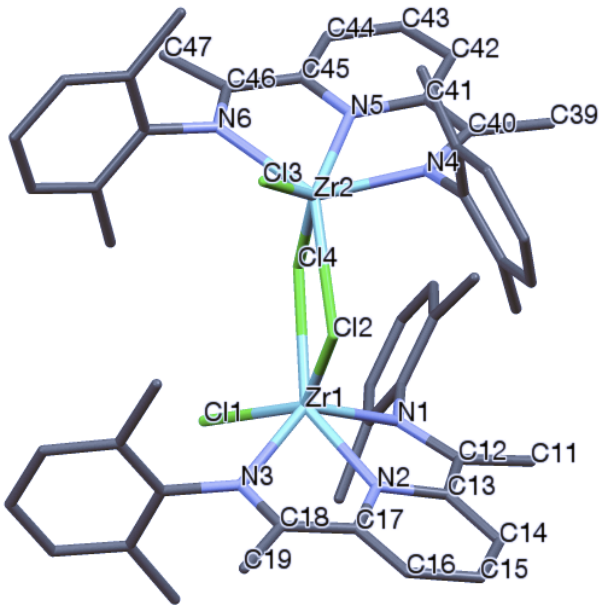


Figure 4.10. Molecular structure of **4** [($^{Et}$DIP)$ZrCl_2$]$_2$. Hydrogens and ethyl $CH_3$ carbons are omitted for clarity. Only one of three crystallographically independent dimeric units shown.

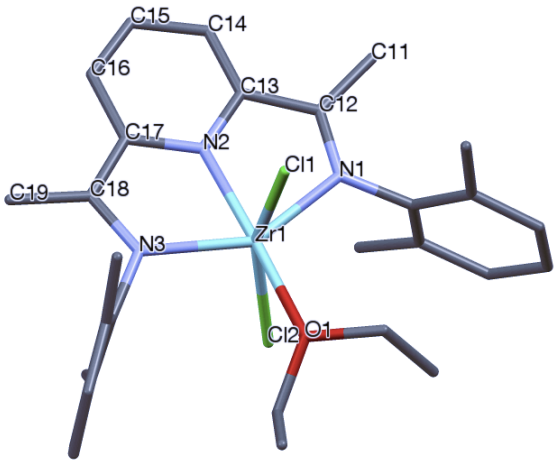


Figure 4.11. Molecular structure of **4-Et$_2$O** [($^{Et}$DIP)ZrCl$_2$(Et$_2$O)]. Hydrogens and ethyl $CH_3$ carbons are omitted for clarity

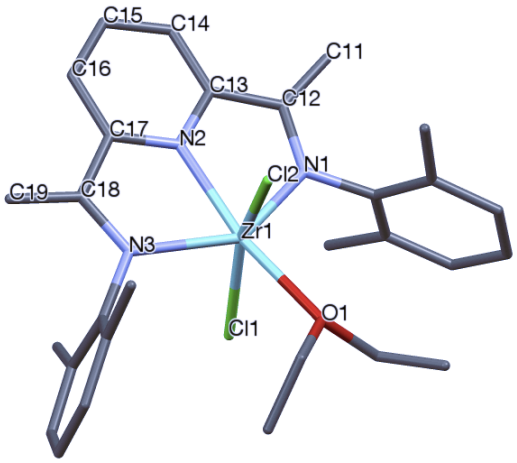


Figure 4.12. Molecular structure of **4"-Et$_2$O** [($^{Et}$DIP-2H)ZrCl$_2$(Et$_2$O)]. Hydrogens and ethyl $CH_3$ carbons are omitted for clarity

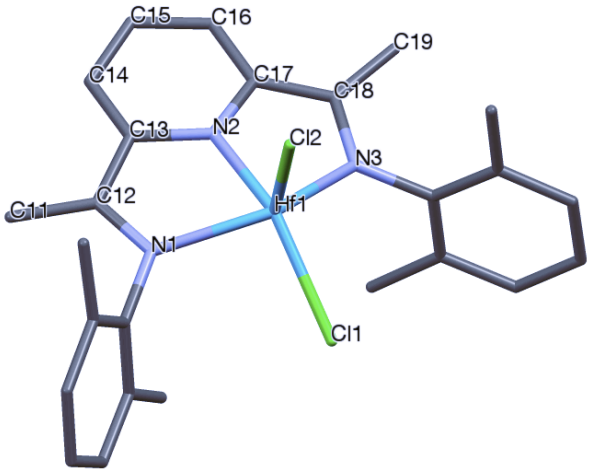


Figure 4.13. Molecular structure of **5** [($^{Et}$DIP)HfCl$_2$]. Hydrogens and ethyl $CH_3$ carbons are omitted for clarity

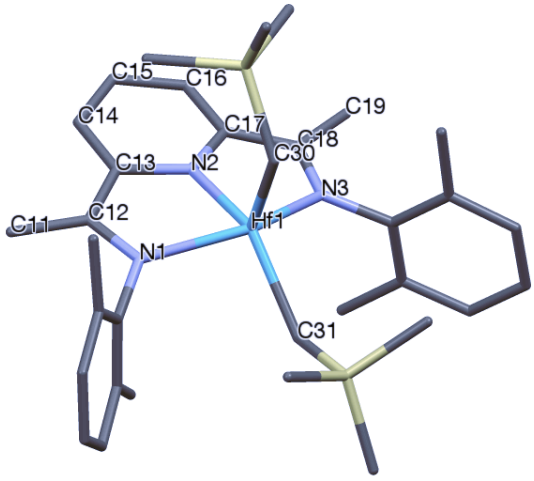


Figure 4.14. Molecular structure of **5"** [($^{Et}$DIP)Hf($CH_2SiMe_3$)$_2$]. Hydrogens and ethyl $CH_3$ carbons are omitted for clarity

In both **3**, dimeric **4**, **4-Et$_2$O** and **4"-Et$_2$O**, the geometry around Zr is best described as distorted octahedral. The highest possible symmetry for these complexes is $C_{2v}$, but we find that one of the chloride atoms (Cl1) and the THF oxygen atom in **3** are deviated about 0.555

and 0.765 Å from the potential mirror plane through Zr1, N2, Cl2, and C31, respectively. The Zr-Cl bond lengths in **3**, **4-Et$_2$O** and **4"-Et$_2$O** are 2.448-2.482, 2.458-2.472 and 2.451-2.479 Å which fall within the range of Zr(IV)-Cl bonds (2.372-2.444 Å).[30] Complex **4** has clearly abnormal bond lengths due to its very distorted and asymmetric structure (Zr-Cl: 2.424-2.619 Å). Generally, electron transfer from metal to ligand π system results in the population of C=N antibonding and $C_{imine}$-$C_{py}$ bonding orbitals. This results in the elongation of the former and contraction of the latter bonds. Like in its Ti counterpart, the bond lengths in **3**, **4** and **4-Et$_2$O** strongly suggest 2e transfer. These elongations and contractions, as well as NMR data indicate the presence of Zr(IV) bound to a dianionic DIP ligand.

Interpretation of the X-ray structure of **4"-Et$_2$O** is more problematic. The $^1$H NMR spectrum of the sample used for crystallization indicated presence of **4-Et$_2$O** and **4′-Et$_2$O**. In the crystal structure of **4"-Et$_2$O** the imine C-C bond distances are clearly too short for single bonds (as in **3**) but too long for double bonds (as in **6**, see below). The most likely explanation is that the specific crystal selected for structure determination was a co-crystal containing **4"-Et$_2$O** together with a substantial amount of **4-Et$_2$O** and/or **4′-Et$_2$O**. We therefore refrain from a detailed discussion of the structure of **4"-Et$_2$O**.

In **5** and **5"**, the geometry around Hf is best described as distorted square pyramidal. The quality of the X-ray structure of **5** is low which makes it difficult to draw conclusions about the noninnocent character of the ligand. Elongation of the C=N bonds (1.343 and 1.387 Å) and contraction of $C_{imine}$-$C_{py}$ bonds (1.419 and 1.388 Å) are much greater than expected for having only two electrons transferred to the ligand. If the two transferred electrons are located at one side of the ligand, the other imine moiety bond lengths should stay closer to the "innocent" situation observed in the neutral form of the DIP ligand (C=N: ~1.28 Å).

In **5"**, as observed in its Ti counterpart, one of the $SiMe_3$ groups is bent over the ligand backbone and the other one is located in between the aryl rings. This is likely to avoid the

bulky Et groups on the aryls. In contrast to **5**, the ligand bond lengths in **5"** unambiguously indicate a doubly reduced chelate (C=N: 1.361 and 1.355 Å; $C_{imine}$-$C_{py}$: 1.395 and 1.406 Å). Single crystals of **6** suitable for X-ray crystallography were obtained by keeping a concentrated $Et_2O$ solution of **6** at -35 °C. The solid-state structure of **6** is shown in Figure 4.15 and the relevant bond lengths are included in Table 4.1.

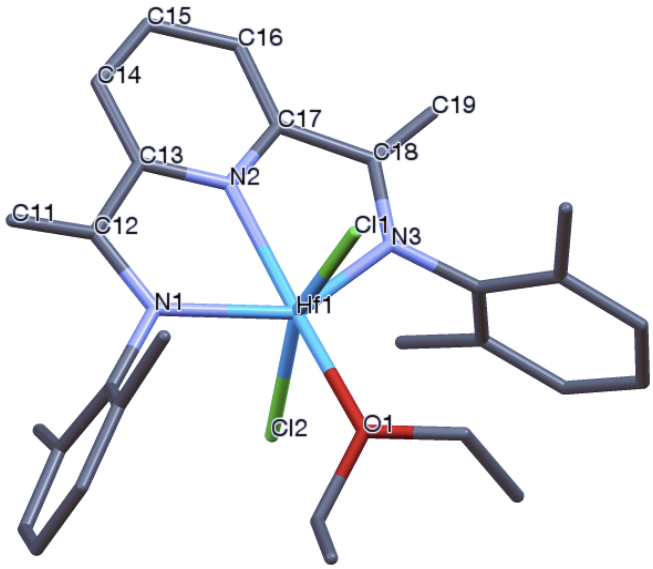


Figure 4.15. Molecular structure of **6** [($^{Et}$DIP-2H)$HfCl_2(Et_2O)$]. Hydrogens and ethyl $CH_3$ carbons are omitted for clarity

The short imine C-C bonds (1.285(7) and 1.343(5) Å) indicate that both imine methyl groups have been dehydrogenated. Consequently, both imine fragments have been converted into amides with real C-N single bonds (1.409(5) and 1.387(4) Å). The $C_{imine}$-$C_{py}$ bonds (1.481(5) and 1.474(5) Å) fall within the expected range for $Csp^2$-$Csp^2$ single bonds.

The solid-state structures of **7** (Figure 4.16) shows a distorted octahedral geometry with three chloride ligands at Zr (Zr-Cl1: 2.4789(16) Å; Zr-Cl2: 2.4410(17) Å; Zr-Cl3: 2.4093(17) Å).

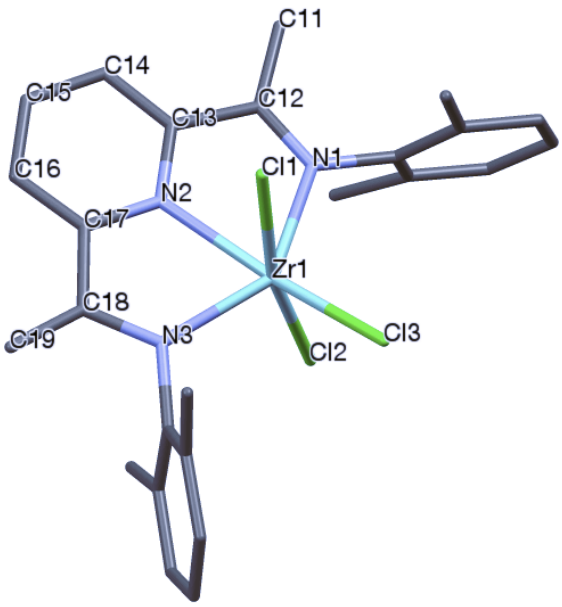


Figure 4.16. Molecular structure of **7** [($^{Et}$DIP-H)ZrCl$_3$]. Hydrogens and ethyl $CH_3$ carbons are omitted for clarity

The ligand backbone is distorted due to dehydrogenation of one of the imine methyl groups ($H_2C$=CN: 1.363(5) Å) and dramatic elongation of the relevant C-N bond (1.386(5) Å).

The solid-state structure of isomorphous **8** is presented in Figure 4.17. Bond lengths of both complexes are summarized in Table 4.2.

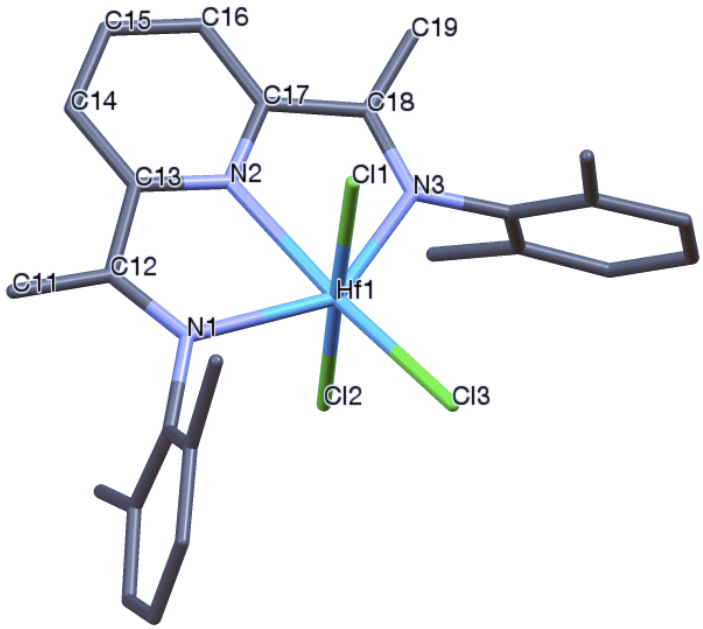


Figure 4.17. Molecular structure of **8** [($^{Et}$DIP-H)HfCl$_3$]. Hydrogens and ethyl CH$_3$ carbons are omitted for clarity

Table 4.2. Selected bond lengths (Å) for (DIP-H)MCl$_3$ complexes

| | **7** | **8** |
|---|---|---|
| M-N1 | 2.324(3) | 2.193(5) |
| M-N2 | 2.298(3) | 2.257(5) |
| M-N3 | 2.114(3) | 2.200(5) |
| M-Cl1 | 2.4787(10) | 2.4427(16) |
| M-Cl2 | 2.4091(10) | 2.3963(17) |
| M-Cl3 | 2.4414(14) | 2.3995(15) |
| N1-C12 | 1.309(5) | 1.345(8) |
| C11-C12 | 1.459(5) | 1.405(10) |
| C12-C13 | 1.479(5) | 1.475(9) |
| C17-C18 | 1.469(5) | 1.468(10) |
| C18-C19 | 1.363(5) | 1.407(10) |
| C18-N3 | 1.386(5) | 1.346(8) |

The bond lengths listed for **8** show much less left-right asymmetry than for **7**, suggesting nearly complete disorder in the position of the C=CH$_2$ group in **8**.

### 4.3.2 Alkyl Migration

Reaction of DIP ligand with various main group metal and transition metal alkyls results in loss of alkyl (presumably as radical) as well as alkylation of the ligand in different positions. Gibson, Cámpora and Budzelaar have studied the reactivity of DIP in combination with different main group metal alkyls ($MR_n$ where M = Li, Mg, Zn, Al; R = Me, Et, Pr, $^{i}$Pr, $^{n}$Bu; n = 1, 2, 3) where the alkyl migrates to the imine carbon, Py-N, -C2 and –C4 positions.[15-16, 31] Hill et al.[17] showed that the use of alkaline-earth metals (Mg, Ca, Sr, Ba) bearing bulky alkyl groups ($CH(SiMe_3)_2$) resulted in a mixture of Py-C3 and –C4 alkylated isomers. These turned out to be thermally unstable at room temperature and finally re-aromatized the pyridine ring by undergoing a dealkylation/dehydrogenation.[17] Based on a comparison of several published studies, one could make a case that the difference in destination of the alkyl at the ligand is mostly determined by the nature of the alkyl group rather than the metal center. The behaviors of $ZnR_2$ (R = benzyl, allyl)[27] and $Mg(Bn)_2(THF)_2$[16] are very similar to their manganese[18] counterpart. In all of those complexes the benzyl or allyl fragment consistently migrates to the Py-C4 position. In the case of the late transition metal alkyls, Fe and Co reacted in two different ways. Reaction of dialkylcobalt with DIP resulted in formation of (DIP)CoR[32] which has a singly reduced ligand, while dialkyliron gave $(DIP)FeR_2$.[19] However, the latter undergoes rearrangement in solution at longer reaction times.

To arrive at a better understanding of DIP-centered reactivity, we reacted tetrabenzyl complexes of zirconium and hafnium with $^{R}$DIP ligands of varying bulk. These reactions all led to formation of novel pyridinediamide complexes via migration of two benzyl groups to the two imine carbons (Scheme 4.4).

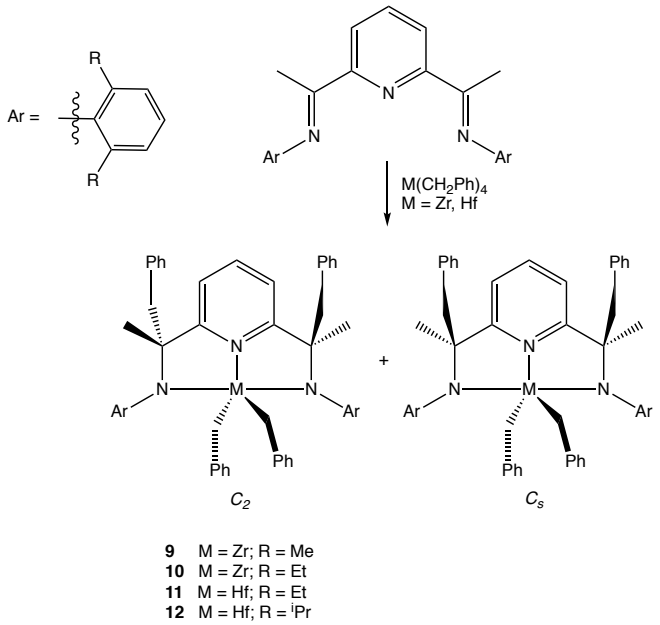


Scheme 4.4. Synthesis of Zr and Hf complexes with a doubly benzylated ligand

This afforded mixture of $C_s$ and $C_2$ isomers in comparable yields. Gratifyingly, the two diastereomers of **9** and **10** could be separated by layering their toluene solution with hexanes at −35 °C. Increasing the steric size of the aryl ring at the imine nitrogen did not affect the destination of the benzyl groups. To the best of our knowledge, only alkylation of a single imine group has been previously observed[17, 31] and the present dibenzylation is new to DIP ligand-centered reactivity, although closely related diamido-pyridine group IV complexes have been prepared via different routes.[33]

The $^1$H NMR spectrum of **10-*C*$_2$** shows four doublets of 2H each at 2.04, 2.59, 2.96 and 3.81 ppm for the four benzylic hydrogens in the molecule which occur as diastereotopic pairs. In contrast, for **10-*C*$_s$**, the benzylic hydrogens at Zr appear as two singlets at 1.45 and 2.35 ppm due to the presence of an effective mirror plane through the metal and the benzylic carbons. The migrated Bn groups of this isomer are still diastereotopic as expected, showing two doublets for 2H each at 3.19 and 3.49 ppm. For each isomer, there are two triplets of 6H each (**10-*C*$_2$**: 1.62 and 1.44 ppm; **10-*C*$_s$**: 1.04 and 1.44 ppm) for the methyl groups of the DIP Et

substituents. Similarly, four multiplets of 2H each (**10-*C*$_2$**: 2.29, 2.49, 3.19 and 3.49 ppm; **10-*C*$_s$**: 2.39, 2.51, 3.31 and 3.46 ppm) appear for the methylene hydrogens in Et groups.

Normally, alkyl migration to pyridine- or imine-N atoms, pyridine-C2 or imine carbon atoms gives a kinetic product. Upon heating the compound, the alkyl migrates to pyridine-C4 position to give the thermodynamic product (which still could undergo further rearrangements such as dimerization,[34] dealkylation[17] of the ligand or rearomatization[18] of the pyridine ring). In contrast to these previously reported alkyl migration examples, heating either of the pure isomer **10-*C*$_2$** and **10-*C*$_s$** in toluene at 100 ºC for 16 h afforded a mixture of isomers with in both cases a 1:4 ratio (**10-*C*$_2$** : **10-*C*$_s$**) (Scheme 4.5). It can be concluded that the $C_s$-symmetry isomer is the thermodynamically slightly more stable product.

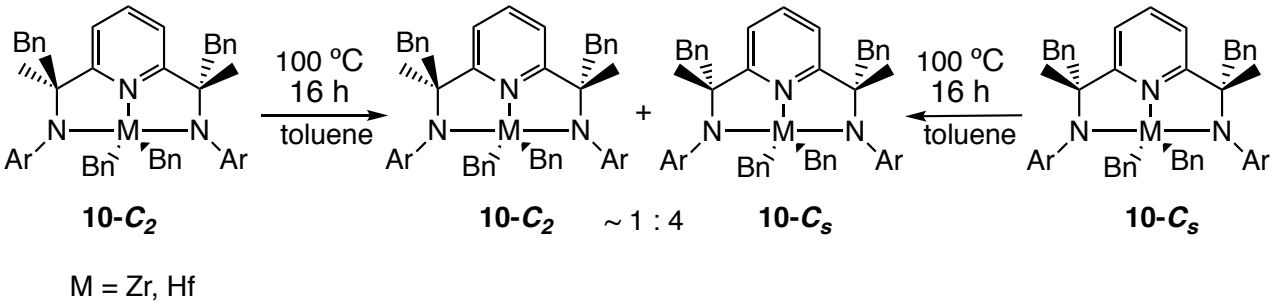


Scheme 4.5. Isomerization of pure isomers over heating

The mechanism of equilibration of **10-*C*$_2$** and **10-*C*$_s$** likely involves radicals, and so we tested for reactivity in the presence of the radical trap TEMPO, which might trap a free Bn radical or abstract a Bn group from either metal or ligand (reaction of TEMPO with an $\alpha$-diimine Zr dibenzyl complex has been reported to result in abstraction of Bn from the ligand[35]). It turned out that TEMPO reacts stoichiometrically (2:1) with **10-*C*$_2$** already at room temperature, producing a complex (**13**) of the TEMPO anion (Scheme 4.6).

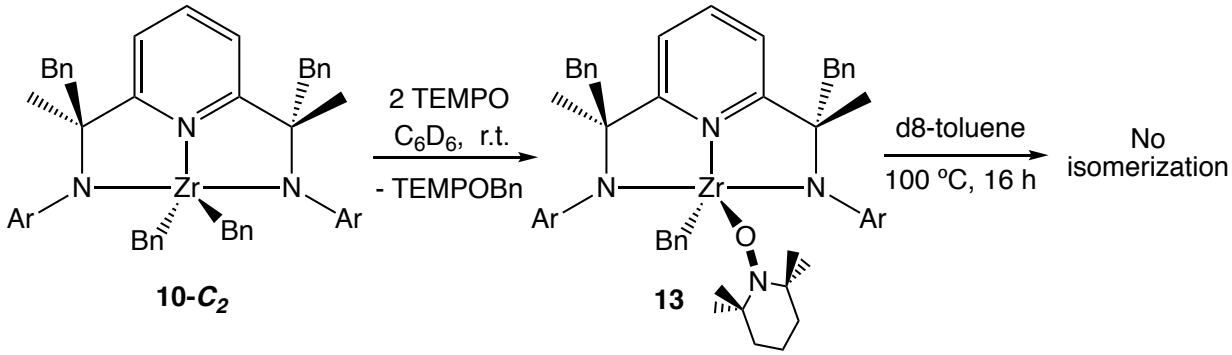


Scheme 4.6. Treatment of **10-*C*$_2$** with 2 equivalents of TEMPO

In contrast to the abovementioned equilibration of **10-*C*$_2$** with **10-*C*$_s$**, heating a solution of **13** under the same condition did not lead to isomerization. Assuming that the isomerization follows a free-radical path, it is remarkable that the TEMPO group apparently blocks this path without undergoing any further reaction.

In addition, the situ formed tetrakis (methylene trimethylsilyl) hafnium was reacted with $^{Et}$DIP ligand (Scheme 4.7).

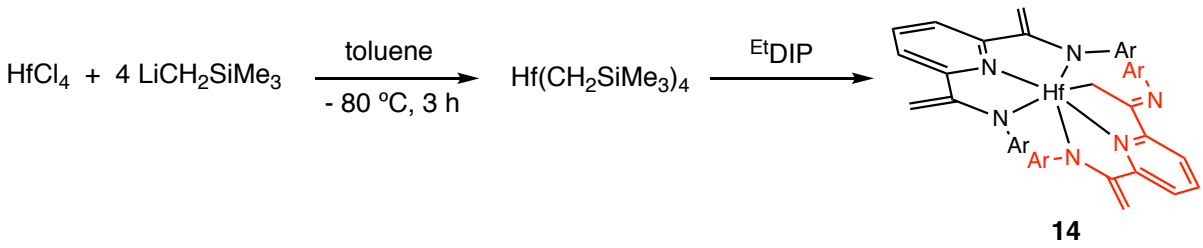


Scheme 4.7. Synthesis of the bis chelate complex **14**

In contrast to the alkyl migrations mentioned above, this led to formation of the bis chelate complex **14**, in which each chelate is doubly dehydrogenated.

The size of the alkyl, the Hf-C bond strength and the less favored formation of $^{\bullet}$R in $Hf(CH_2SiMe_3)_4$ compare to $Hf(CH_2Ph)_4$ could lead to dehydrogenation rather than alkyl migration.

### 4.3.3 X-ray structures of benzyl derivatives.

Table 4.3 presents selected bond lengths and structural parameters of **9-*C*$_s$**, **10-*C*$_s$**, **10-*C*$_2$**, **13** and **14**.

Table 4.3. Selective bond lengths (Å) for ($^R$DBAP)Zr and Hf complexes

| | **9-*C*$_s$** | **10-*C*$_s$** | **10-*C*$_2$** | **13** | **14** |
|---|---|---|---|---|---|
| M-N1 | 2.0910(15) | 2.0966(15) | 2.107(3) | 2.1254(15) | 2.155(6) |
| M-N2 | 2.3340(15) | 2.3273(15) | 2.315(3) | 2.3168(15) | 2.240(5) |
| M-N3 | 2.1229(15) | 2.1193(15) | 2.119(3) | 2.1358(15) | 2.124(5) |
| M-N4 | | | | | 2.172(5) |
| M-N5 | | | | | 2.288(5) |
| M-C44 | 2.3086(18) | 2.2918(19) | 2.304(4) | 2.3000(19) | |
| M-C48 | | | | | 2.281(6) |
| M-C51 | 2.3062(19) | 2.2929(19) | 2.297(4) | | |
| Zr-O1 | | | | 1.9238(13) | |
| N1-C12 | 1.494(2) | 1.493(2) | 1.496(5) | 1.500(2) | |
| C12-C13 | 1.513(3) | 1.517(3) | 1.512(6) | 1.517(3) | |
| C11-C12 | 1.534(3) | 1.526(3) | 1.523(6) | 1.527(3) | 1.357(11) |
| C12-C30 | 1.567(3) | 1.568(3) | 1.563(6) | 1.573(3) | |
| C17-C18 | 1.511(3) | 1.513(3) | 1.504(6) | 1.512(3) | |
| C18-C19 | 1.537(3) | 1.531(3) | 1.530(6) | 1.524(3) | 1.351(11) |
| C40-C41 | | | | | 1.350(10) |
| C18-C37 | 1.572(3) | 1.571(3) | 1.571(6) | 1.568(3) | |
| C18-N3 | 1.488(2) | 1.489(2) | 1.501(5) | 1.490(2) | |
| C47-N6 | | | | | 1.288(9) |
| τ | 0.46 | 0.39 | 0.51 | 0.52 | |

The structure of **9-*C*$_s$**, **10-*C*$_2$**, **10-*C*$_s$** and **13** are shown in Figure 4.18, Figure 4.19, Figure 4.20 and Figure 4.21.

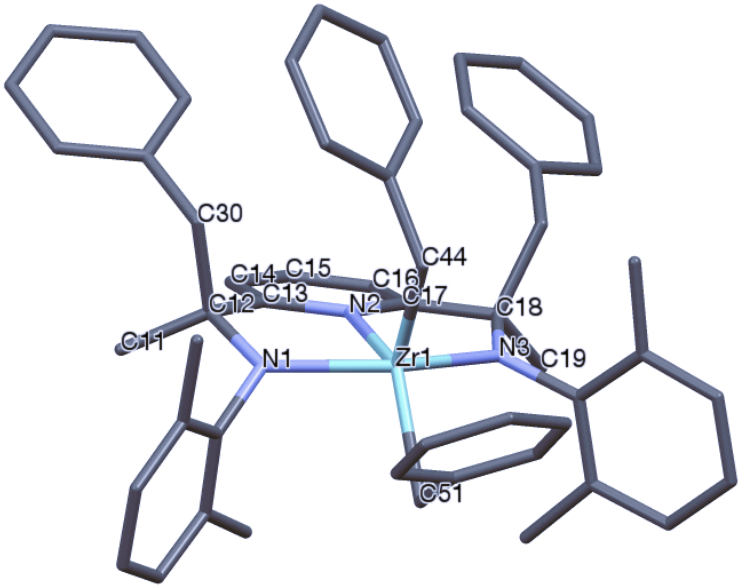


Figure 4.18. Molecular structure of **9-*C*$_s$**. Hydrogens are omitted for clarity

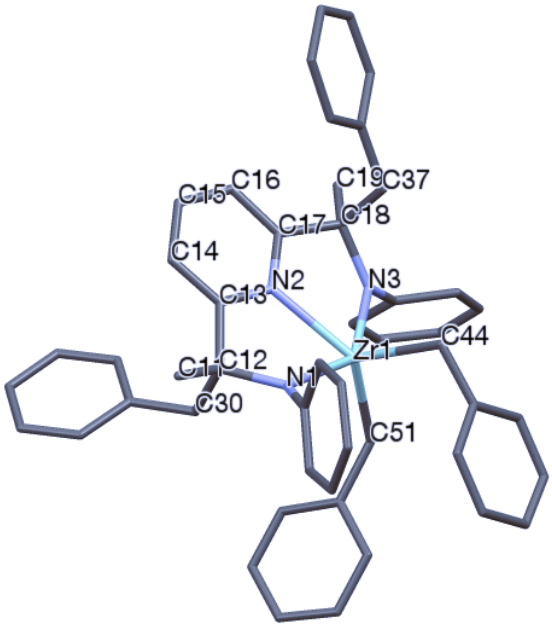


Figure 4.19. Molecular structure of **10-*C*$_2$**. Hydrogens and ethyl carbons are omitted for clarity

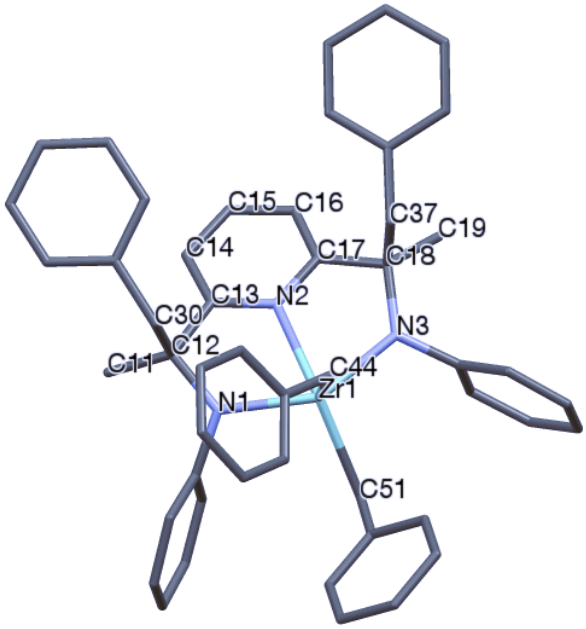


Figure 4.20. Molecular structure of **10-*C*$_s$**. Hydrogens and $CH_3$ carbons are omitted for clarity

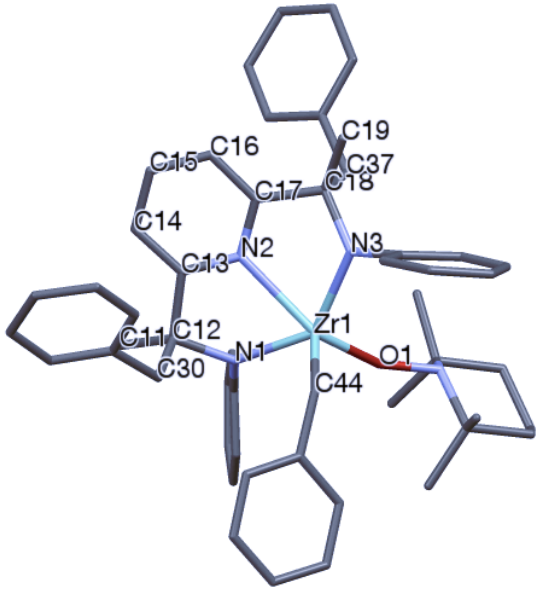


Figure 4.21. Molecular structure of **13**. Hydrogens and ethyl carbons are omitted for clarity

In all complexes, the geometry around Zr is best described as distorted-trigonal-bipyramidal. The C-N bonds are 1.482-1.501 Å, much longer than in the free DIP ligand, and clearly demonstrate the reduction of the ligand. The Zr-C bonds lengths fall within the normal range for Zr(IV)-C bonds (2.25-2.33 Å).[36]

The solid-state structure of **14** is shown in Figure 4.22.

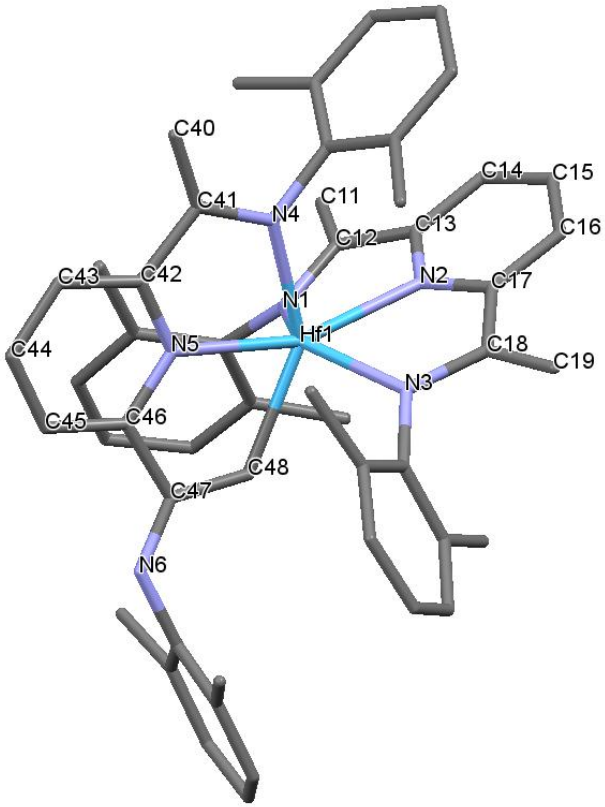


Figure 4.22. Molecular structure of **14**. Hydrogens and ethyl $CH_3$ carbons are omitted for clarity

The geometry around Hf is best described as distorted octahedral. One of the chelates is coordinated to hafnium in N,N,C mode, in which the imine methyl is dehydrogenated and formed a Hf-C bond (2.281(6) Å). The $CH_3$-$C_{imine}$ bonds are 1.357, 1.351, 1.350 Å, evidently show the dehydrogenation of the ligands. Consequently, the C-N bonds are much longer than

in the free DIP ligand (1.395, 1.414 and 1.395 Å). The C=N bond in non-coordinating imine fragment is 1.288, normally observed in the free DIP ligand.

## 4.4 Conclusions

This chapter uncovers interesting similarities and differences between reduced DIP complexes of Ti and Zr/Hf. As for Ti, it is possible to prepare formally divalent DIP complexes of Zr and Hf, and like their Ti counterparts they are best viewed as containing the metal in oxidation state +4, bound to a dianionic DIP ligand. However, the Zr and Hf complexes show increased reactivity. While (DIP)$TiCl_2$ is a very stable complex and stays unchanged in solution, the analogous (DIP)$ZrCl_2$ undergoes hydrogen atom migration or loss on standing, and attempted reduction of (DIP)$HfCl_4$ in $Et_2O$ led instead to direct formation of a doubly dehydrogenated complex. The electrons residing in the π-system of the ligand in (DIP)$ZrCl_2$ appear to be more available for further reactivity, as illustrated by the observed cleavage of a C-Cl bond of $CH_2Cl_2$. We have also uncovered a few unexpected differences between Zr and Hf chemistry. **4** appears to be a dimer which shows a dynamic behavior in solution while its Hf counterpart, **5**, is monomer and appears as sharp signals in solution. The difference in $CH_2Cl_2$ solubility of **1** and **2** is notable, as is the difference in dynamic behaviour of complexes **4** and **5** in solution.

Reaction of $MBn_4$ with $^{R}$DIP does not result in reduction but instead in selective transfer of two Bn groups to the imine carbons of the DIP ligand. Experiments involving separated $C_2$ and $C_s$ isomers indicate that the Bn transfer is reversible. Surprisingly, even prolonged heating does not result in Bn transfer to the pyridine C4 position, which is the final destination in many other DIP alkylation reactions.

## 4.5 Experimental Section

*General Considerations*. All air- and moisture-sensitive manipulations were carried out under argon using standard Schlenk techniques or in an MBraun drybox containing an atmosphere of purified nitrogen. Solvents for air- and moisture-sensitive manipulations were dried and deoxygenated using sodium/benzophenone. Benzene-$d_6$ and toluene-$d_8$ were purchased from Cambridge Isotope Laboratories, distilled from sodium/benzophenone, and stored in the drybox. The $^{Et}$DIP ligand was prepared according to a literature procedure.[37] $^1$H and $^{13}$C NMR spectra were recorded at 25 °C (unless noted otherwise) on Bruker Avance 300 and 500 spectrometers. All chemical shifts are reported in ppm relative to $SiMe_4$ using $^1$H (residual) and $^{13}$C chemical shifts of the solvent as a secondary standard: benzene-$d_6$, 7.16 and 128.06 ppm; toluene-$d_8$, 2.08 and 20.43 ppm; DCM-$d_2$, 5.32 and 53.84 ppm.[38]

Single crystals suitable for X-ray diffraction were either sealed in glass capillaries or coated with oil in a drybox and then quickly transferred to the goniometer head of a D8 three-circle diffractometer (equipped with a rotating-anode Mo Kα generator, multilayer optics, and an APEX-II CCD area detector) or a Bruker D8 QUEST ECO diffractometer (equipped with a Mo Kα X-ray tube). Preliminary data revealed the crystal system. Data collection was optimized for completeness and redundancy using the APEX3 software suite. The space group was identified, and the data were reduced using the SAINT[39] program and corrected for absorption using SADABS.[40] The structures were solved using direct methods (SHELXS[41]) completed by subsequent Fourier synthesis and refined by full-matrix least-squares procedures (SHELXL[41]).

**($^{Et}$DIP)$ZrCl_4$ (1)**. A 100 mL Schlenk tube was charged with 1.06 g (4.56 mmol) of $ZrCl_4$, approximately 30 mL of DCM, and a stirrer bar. $^{Et}$DIP (2.04 g, 4.79 mmol) was added, and

the reaction mixture colour changed quickly to yellow and then the mixture was stirred for another 12 h at room temperature.

The solid was filtered off and washed three times with 20 mL of toluene and 20 mL of hexane. The obtained crystals were dried in vacuo, giving 2.75 g of ($^{Et}$DIP)$ZrCl_4$ (91.6%). Suitable single crystals for X-ray studies were obtained by the interface method (DCM: hexane; 1:1) or by slow evaporation of DCM solvent.

$^1$H NMR (500 MHz; DCM-$d_2$): δ 1.15 (12H, t, *J* 7.5, $CH_2CH_3$), 2.38 (6H, s, $CH_3C$=N), 2.47, 2.80 (4H each, m, $CH_2CH_3$), 7.19 (4H, d, *J* 7.1, *m*-Ar), 7.24 (2H, dd, *J* 9.0/8.6, *p*-Ar), 8.43 (2H, d, *J* 8.0, py 3/5), 8.57 (1H, t, *J* 7.8, py 4).

$^{13}$C{$^1$H} NMR (500 MHz; DCM-$d_2$): δ 14.3 ($CH_2CH_3$), 21.5 ($CH_3$C=N), 24.5 ($CH_2CH_3$), 126.0 (py 4), 126.9 (*m*-Ar), 129.7 (py 3), 129.8 (*p*-Ar), 135.4 (*o*-Ar), 143.7, 149.0 (py 2, C=N), 175.2 (*i*-Ar).

**($^{Et}$DIP)$HfCl_4$** (**2**). A 100 mL Schlenk tube was charged with 1.69 g (5.27 mmol) of $HfCl_4$, approximately 30 mL of DCM, and a stirrer bar. $^{Et}$DIP (2.35 g, 5.54 mmol) was added, and the reaction mixture colour changed quickly to yellow. The mixture was stirred for another 12 h at room temperature. The solvent was removed under reduced pressure and the solid was collected and washed three times with 20 mL of toluene and 20 mL of hexane. The obtained crystals were dried in vacuo, giving 3.68 g of ($^{Et}$DIP)$HfCl_4$ (93.6%). Suitable single crystals for X-ray studies were obtained by interface method (DCM: hexane; 1:1) or by slow evaporation of DCM solvent.

$^1$H NMR (500 MHz; DCM-$d_2$): δ 1.15 (12H, t, *J* 7.5, $CH_2CH_3$), 2.36 (6H, s, $CH_3C$=N), 2.50, 2.80 (4H each, m, $CH_2CH_3$), 7.19 (4H, d, *J* 7.6, *o*-Ar), 7.24 (2H, d, *J* 9.0, *p*-Ar), 8.45 (2H, d, *J* 8.0, py 3/5), 8.59 (1H, t, *J* 8.0, py 4).

$^{13}C\{^{1}H\}$ NMR (500 MHz; DCM-$d_2$): δ 14.3 ($CH_2CH_3$), 21.5 ($CH_3C$=N), 24.5 ($CH_2CH_3$), 126.0 (py 4), 126.9 (*m*-Ar), 130.0 (py 3), 135.6 (*p*-Ar), 144.0 (*o*-Ar), 149.0, 152.3 (py 2, C=N), 175.2 (*i*-Ar).

**($^{Et}$DIP)ZrCl$_2$(THF)** (**3**). A 100 mL Schlenk tube was charged with 0.50 g (0.76 mmol) of complex **1**, approximately 30 mL of THF, and a stirrer bar. $KC_8$ (0.20 g, 1.52 mmol) was added, and the reaction mixture was stirred for 1 day. The resulting purple-brown solution was passed through celite and the solvent was removed in vacuo. The solid residue was dissolved in a few milliliters of THF and layered with hexane (1: 2) and left at −35 °C to give 0.41 g (82%) of dark purple-brown crystals suitable for X-ray crystallography.

$^{1}H$ NMR (500 MHz; THF-$d_8$): δ 1.16 (12H, t, *J* 7.5, $CH_2CH_3$), 1.28 (6H, s, $CH_3C$=N), 1.77 (4H, m, $CH_2$-THF), 2.53, 2.90 (4H each, m, $CH_2CH_3$), 3.60 (4H, m, $CH_2$-THF), 4.82 (1H, t, *J* 7.7, py 4), 5.75 (2H, d, *J* 7.8, py 3/5), 7.00 (6H, s, Ar).

$^{13}C\{^{1}H\}$ NMR (500 MHz; THF-$d_8$): δ 14.2 ($CH_2CH_3$), 14.4 ($CH_3C$=N), 24.9 ($CH_2CH_3$), 26.4, 68.2, 117.8 (py 4), 126.3 (*m*-Ar), 127.0 (py 3), 129.4 (*p*-Ar), 139.4 (*o*-Ar), 143.4, 145.2 (py 2, C=N), 154.3 (*i*-Ar).

**[($^{Et}$DIP)ZrCl$_2$]$_2$** (**4**). A 100 mL Schlenk tube was charged with 0.24 g (0.36 mmol) of complex **1**, approximately 30 mL of toluene, and a stirrer bar. $KC_8$ (0.1 g, 0.73 mmol) was added, and the reaction mixture was stirred for 15 hours. Suspended solid was removed by passing the liquid through celite, and the solvent was removed in vacuo. The solid residue was dissolved in 2 mL of toluene and layered with 6 mL of hexane. It was left at −35 °C to give 0.051 g (24%) of purple-brown crystals.

$^{1}H$ NMR (500 MHz; toluene-$d_8$): δ 1.20 (12H, s, $CH_2CH_3$), 2.12 (6H, s, $CH_3C$=N), 2.48, 2.96 (4H each, br, $CH_2CH_3$), 5.00 (1H, br, py 4), 5.82 (2H, br, py 3/5), 7.08 (6H, s, Ar).

$^{13}C\{^{1}H\}$ NMR (500 MHz; toluene-$d_8$): δ 14.3, 21.4, 25.2, 125.6, 126.3, 127.5, 128.5, 129.3

The broadness of the spectrum results in several expected $^{13}C$ resonances not being observed.

**($^{Et}$DIP)ZrCl$_2$(Et$_2$O)** (**4-Et$_2$O**); **($^{Et}$DIP-H/+H)ZrCl$_2$(Et$_2$O)** (**4'-Et$_2$O**); **($^{Et}$DIP-2H)ZrCl$_2$(Et$_2$O)** (**4''-Et$_2$O**). A 100 mL Schlenk tube was charged with 2.48 g (3.72 mmol) of complex **1**, approximately 30 mL of toluene, and a stirrer bar. $KC_8$ (1.00 g, 7.44 mmol) was added, and the reaction mixture was stirred for 9 days. Suspended solid was removed by passing the liquid through celite, and the solvent was removed in vacuo. The solid residue was dissolved in 15 mL of ether and left at −35 °C to give 0.66 g (27%) of purple-brown crystals suitable for X-ray crystallography.

(partial assignment only):

$^1H$ NMR **(4-Et$_2$O)** (500 MHz; benzene-$d_6$): δ 1.19 (12H, s, $CH_2CH_3$), 2.57, 3.04 (4H each, br, $CH_2CH_3$), 4.89 (1H, br, py 4), 5.73 (2H, br, py 3/5), 7.02 (6H, s, Ar).

**(4'-Et$_2$O)** (500 MHz; benzene-$d_6$): δ 1.00 (3H, d, *J* 6.9, $CH_3$C-N), 1.15-1.34 (12H, m, $CH_2CH_3$), 2.47-3.35 (8H, m, $CH_2CH_3$), 3.89, 4.58 (1H each, s, $CH_2$=CN), 4.75 (1H, q, *J* 6.9, ($CH_3$)*H*C-N), 6.43 (1H, d, *J* 7.6, py 3 or 5), 6.93 (1H, t, *J* 7.9, py 4), 6.93-7.25 (7H, m, py 3 or 5; Ar)

**(4''-Et$_2$O)** (500 MHz; benzene-$d_6$): 1.15-1.34 (12H, m, $CH_2CH_3$), 2.47-3.35 (8H, m, $CH_2CH_3$), 3.83, 4.53 (2H each, s, $CH_2$=CN), 6.84 (1H, t, *J* 8, py 4), 6.93-7.25 (8H, m, py 3/5; Ar).

$^{13}C\{^1H\}$ NMR (500 MHz; benzene-$d_6$): 14.0, 14.3, 15.3, 15.3, 15.5, 21.3, 24.6, 24.9, 24.9, 24.9, 25.0, 25.4, 72.1, 89.3, 89.9, 117.8, 118.3, 119.1, 126.4, 126.8, 126.8, 126.9, 127.3, 127.4, 127.6, 128.0, 128.3, 138.0, 139.2, 139.6, 139.6, 140.5, 141.5, 141.9, 142.1, 142.3, 142.9, 143.3, 154.6, 155.0, 157.1, 157.6, 167.9. (some peaks are missing)

**($^{Et}$DIP)HfCl$_2$** (**5**). A 50 mL Schlenk tube was charged with 1.00 g (1.34 mmol) of complex **2**, approximately 30 mL of toluene, and a stirrer bar. $KC_8$ (0.36 g, 2.68 mmol) was added, and

the reaction mixture was stirred for 33 hours. Suspended solid was removed by passing the liquid through celite, and the solvent was removed in vacuo. The solid residue was dissolved in a few milliliters of toluene and left at −35 °C to give 0.735 g (71.5%) of purple-brown crystals suitable for X-ray crystallography.

$^{1}$H NMR at -5 °C (500 MHz; toluene-$d_8$): δ 1.17 (6H, s, $CH_3C$=N), 1.19 (12H, t, *J* 8.0, $CH_2CH_3$), 2.55, 3.02 (4H each, m, $CH_2CH_3$), 4.70 (1H, t, *J* 7.5, py 4), 5.72 (2H, d, *J* 7.5, py 3/5), 7.03, 7.11 (6H, s, Ar).

$^{13}$C{$^{1}$H} NMR (500 MHz; toluene-$d_8$): δ 13.8 ($CH_2CH_3$), 14.2 ($CH_3C$=N), 21.4 ($CH_3$-toluene), 24.3 ($CH_2CH_3$), 117.2 (py 4), 125.6 (*p*-Ar toluene), 126.2, 127.3 (*m*-Ar toluene), 128.4, 129.2 (*o*-Ar toluene), 131.6 (py 3/5), 137.7 (*i*-Ar toluene), 138.5, 141.8, 144.7 (py 2, C=N), 155.4 (*i*-Ar).

**($^{Et}$DIP)Hf($CH_2SiMe_3$)$_2$ (5')**. A 50 mL Schlenk tube was charged with 0.075 g (0.098 mmol) of complex **5**, approximately 20 mL of toluene, and a stirrer bar. $Me_3SiCH_2Li$ (0.018 g, 0.19 mmol) was added, and the reaction mixture was stirred for 24 hours. Suspended solid was removed by passing the liquid through celite, and the solvent was removed in vacuo. The solid residue was dissolved in a few milliliters of toluene and layered with hexane and left at −35 °C to give 0.062 g (81%) of purple-brown crystals suitable for X-ray crystallography.

$^{1}$H NMR (500 MHz; benzene-$d_6$): δ 0.07 (4H, s, Hf-$CH_2$), 0.15 (18H, s, $SiMe_3$), 1.27 (12H, t, *J* 7.5, $CH_2CH_3$), 1.44 (6H, s, $CH_3C$=N), 2.65, 2.85 (4H each, m, $CH_2CH_3$), 5.03 (1H, t, *J* 7.5, py 4), 6.03 (2H, d, *J* 7.5, py 3/5), 7.06 (2H, d, *J* 7.5, Ar), 7.09 (1H, t, *J* 7.2, Ar), 7.18 (2H, t, *J* 7.2, Ar), 7.21 (1H, s, Ar). $^{13}$C{$^{1}$H} NMR (500 MHz; benzene-$d_6$): δ 3.3 ($SiMe_3$), 14.1 ($CH_2CH_3$), 14.3 ($CH_3C$=N), 24.5 ($CH_2CH_3$), 68.7 (Hf-$CH_2$), 116.6 (py 4), 126.4, 126.6, 130.9 (py 3/5), 144.3, 145.1, 153.6.

**($^{Et}$DIP)HfMe$_2$** (**5"**). A 50 mL Schlenk tube was charged with 0.115 g (0.15 mmol) of complex **5**, approximately 20 mL of toluene, and a stirrer bar. MeMgBr (3M solution in ether) (0.1 mL, 0.30 mmol) was added, and the reaction mixture was stirred for 3 hours. Suspended solid was removed by passing the liquid through celite, and the solvent was removed in vacuo. 0.055 g (58%) of purple-brown solid residue was collected.

$^1$H NMR (500 MHz; benzene-$d_6$): δ 0.14 (6H, s, Hf-CH$_3$), 1.15 (12H, t, *J* 7.5, CH$_2$C*H$_3$*), 1.15 (6H, s, CH$_3$C=N), 2.64, 2.88 (4H each, m, C*H$_2$*CH$_3$), 4.25 (1H, t, *J* 7.7, py 4), 5.15 (2H, d, *J* 7.7, py 3/5), 7.01 (6H, s, Ar). $^{13}$C{$^1$H} NMR (500 MHz; benzene-$d_6$): δ 12.9 (CH$_2$*C*H$_3$), 14.25 (*C*H$_3$C=N), 24.2, (*C*H$_2$CH$_3$), 57.8 (Hf-CH$_3$), 117.2 (py 4), 126.0 (Ar), 126.6 (Ar), 132.4 (py 3/5), 139.6, 141.7, 148.6, 151.8.

**($^{Et}$DIP-2H)HfCl$_2$(Et$_2$O)** (**6**). A 100 mL Schlenk tube was charged with 0.28 g (0.37 mmol) of complex **2**, approximately 30 mL of ether, and a stirrer bar. KC$_8$ (0.10 g, 0.75 mmol) was added, and the reaction mixture was stirred for 5 days. Suspended solid was removed by passing the liquid through celite, and the solvent was removed in vacuo. The solid residue was dissolved in a few milliliters of ether and left at −35 °C to give 0.041 g (15%) of purple-brown crystals suitable for X-ray crystallography.

**($^{Et}$DIP-H)ZrCl$_3$** (**7**). A 100 mL Schlenk tube was charged with 0.1 g (0.15 mmol) of complex **1**, approximately 15 mL of THF, and a stirrer bar. (Me$_3$Si)$_2$NK (0.03 g, 0.15 mmol) was added, and the reaction mixture was stirred for 24 h. Suspended solid was removed by passing the solution through celite, and the solvent was removed in vacuo. The solid residue was washed with 5 mL toluene and 10 mL ether. It was dried and dissolved in 2 mL of THF and layered with hexane (1:2; THF: hexane). It was left untouched at −35 °C to give 0.038 g (41%) of dark red crystals suitable for X-ray crystallography.

$^{1}$H NMR (500 MHz; DCM-$d_2$) (partial assignment only): δ 1.17 (6H, t, *J* 7.5, $CH_2CH_3$), 1.20 (6H, t, *J* 7.0, $CH_2CH_3$), 2.38 (3H, s, $CH_3C$=N), 2.71- 2.91 (8H, m, $CH_2CH_3$), 3.84, 4.99 (1H each, s, $H_2C$=C-N), 7.21-7.34 (6H, m, Ar), 7.97 (1H, d, *J* 7.6, py 3 or 5), 8.96 (1H, d, *J* 8.3, py 3 or 5), 8.21 (1H, t, *J* 8.0, py 4). $^{13}$C{$^{1}$H} NMR (500 MHz; DCM-$d_2$): δ 14.5, 15.0 ($CH_2CH_3$), 19.5 ($CH_3$C=N), 24.9, 25.8 ($CH_2CH_3$), 93.9 ($H_2C$=CN), 125.2, 125.6, 126.4, 127.0, 127.4, 128.2, 128.7, 137.2, 138.9, 141.9, 142.8, 150.8, 154.6, 159.5, 177.7 ($CH_3C$=N).

**($^{Et}$DIP-H)HfCl$_3$** (**8**). A 100 mL Schlenk tube was charged with 0.1 g (0.13 mmol) of complex **2**, approximately 15 mL of THF, and a stirrer bar. $(Me_3Si)_2NK$ (0.027 g, 0.13 mmol) was added, and the reaction mixture was stirred for 24 h. Suspended solid was removed by passing the solution through celite, and the solvent was removed in vacuo. The solid residue was washed with 5 mL toluene and 10 mL ether. It was dried and dissolved in a few milliliters of THF and layered with hexane (1:2; THF: hexane). It was left untouched at −35 °C to give 0.029 g (32%) of dark red crystals suitable for X-ray crystallography.

$^{1}$H NMR (500 MHz; DCM-$d_2$) (partial assignment only): δ 1.17, 1.20 (6H, t, *J* 7.6, $CH_2CH_3$), 2.38 (3H, s, $CH_3C$=N), 2.72- 2.90 (8H, m, $CH_2CH_3$), 3.80, 4.98 (1H each, d, *J* 1.9, $H_2C$=C-N), 7.21 (2H, d, *J* 6.0, *m*-Ar), 7.23 (1H, t, *J* 6.0, *p*-Ar), 7.29 (2H, d, *J* 7.0, *m*-Ar), 7.33 (1H, t, *J* 6.4, *p*-Ar) , 7.98 (1H, d, *J* 7.6, py 3 or 5), 8.14 (1H, d, *J* 8.5, py py 3 or 5), 8.23 (1H, t, *J* 8.0, py 4). $^{13}$C{$^{1}$H} NMR (500 MHz; DCM-$d_2$): δ 14.5, 15.1 ($CH_2CH_3$), 19.7 ($CH_3$C=N), 24.8, 25.8 ($CH_2CH_3$), 95.1 ($H_2C$=CN), 125.5, 125.7, 126.1, 126.9, 127.5, 128.7, 128.7, 137.3, 141.8, 141.9, 142.8, 150.5, 154.2, 159.7, 178.1 ($CH_3C$=N).

**($^{Me}$DBAP)Zr(CH$_2$Ph)$_2$** (**9**). A 100 mL Schlenk tube was charged with 0.40 g (0.88 mmol) of $Zr(CH_2Ph)_4$, approximately 10 mL of toluene, and a stirrer bar. $^{Me}$DIP (0.32 g, 0.88 mmol) was added, and the reaction mixture turned dark red-brown and was stirred for 1 day which afforded a mixture of two isomers $C_2$ and $C_s$. The solvent was reduced to half and the

remnant was layered with hexane (1:3) and left at −35 °C. The first crop of dark crystals turned out to be the $C_2$ isomer. Reducing the amount of solvent to half and layering with hexane (1:3) gave the second crop which was a mixture of $C_2$ : $C_s$ isomers. The 3rd time of the recrystallization gave the $C_s$ isomer. Washing the dark crystals with ether gave 0.31 g (43%) (in total) of purer light yellow crystals suitable for X-ray crystallography.

$^1$H NMR (500 MHz; benzene-$d_6$): 9-$C_2$: δ 1.29 (6H, s, $CH_3$C-N), 1.71, 2.20 (2H each, d, *J* 11.0, Zr-C*H*$_2$Ph), 2.41, 2.64 (6H each, s, *o*-$CH_3$-Ar), 2.77, 3.31 (2H each, d, *J* 13.0, PhC*H*$_2$C-N), 6.02 (2H, d, *J* 7.9, py 3/5), 6.35 (4H, d, *J* 7.5, Zr$CH_2$Ph *o*), 6.44 (4H, d, *J* 7.0, *o*-$CH_2$Ph), 6.68 (1H, t, *J* 7.9, py 4), 6.84 (2H, t, *J* 7.0, Zr$CH_2$Ph *p*), 6.95 (4H, t, *J* 7.5, Zr$CH_2$Ph *m*), 6.99 (4H, t, *J* 7.5, *m*-$CH_2$Ph), 7.04 (2H, d, *J* 7.0, *p*-$CH_2$Ph), 7.09 (2H, t, *J* 7.5, *p*-Ar), 7.18, 7.23 (2H each, d, *J* 7.5, *m*-Ar). $^{13}$C{$^1$H} NMR (500 MHz; benzene-$d_6$): δ 22.9 (*C*$H_3$C-N), 23.2, 23.9 (4 *o*-$CH_3$-Ar), 52.7 (2 *C*$H_2$Ph), 66.6 (2 Zr*C*$H_2$Ph), 77.8 (C-N), 120.6 (py 3/5), 122.1 (Zr$CH_2$Ph *m, p*), 125.8 (*m*-, *p*-Ar), 126.6 (*p*-$CH_2$Ph), 127.7 (*o*-, *m*-$CH_2$Ph), 128.0, 128.3 (Zr$CH_2$Ph *o*), 128.8 (Zr$CH_2$Ph *m, p*), 129.4, 129.8 (*m*-, *p*-Ar), 132.0 (*o*-, *m*-$CH_2$Ph), 136.9 (py 4), 138.6 (Zr$CH_2$Ph *i*), 139.8, 139.9 (*o*-Ar), 146.1 (*i*-$CH_2$Ph), 146.3 (py 2), 168.6 (*i*-Ar).

$^1$H NMR (500 MHz; benzene-$d_6$) (partial assignment only): 9-$C_s$: δ 1.13 (6H, s, $CH_3$C-N), 1.72, 2.06 (2H each, s, Zr-C*H*$_2$Ph), 2.19, 2.81 (6H each, s, o-$CH_3$-Ar), 3.19, 3.33 (2H each, d, *J* 12.7, PhC*H*$_2$C-N), 5.82 (2H, d, *J* 7.8, py 3/5), 6.19 (2H, d, *J* 7.2, Ar), 6.46 (1H, t, *J* 7.8, py 4), 6.54 (2H, d, *J* 2.5, Ar), 6.56 (2H, d, *J* 1.7, Ar), 6.68 (2H, t, *J* 7.3, Ar), 6.88 (2H, d, *J* 7.5, Ar), 6.93 (1H, t, *J* 7.3, Ar), 6.97 (2H, d, *J* 7.5, Ar), 7.01 (2H, t, *J* 7.6, Ar), 7.06- 7.13 (10H, m, Ar), 7.29 (2H, d, *J* 7.3, Ar). $^{13}$C{$^1$H} NMR (500 MHz; benzene-$d_6$): δ 22.4 (*C*$H_3$C-N), 22.7, 22.8 (4 *o*-$CH_3$-Ar), 55.2 (2 Zr-*C*$H_2$Ph), 63.5, 69.6 (2 *C*$H_2$Ph), 77.6 (C-N), 120.4 (py 3/5), 121.8, 123.0, 125.8, 126.5, 127.8, 128.3, 128.6, 129.1, 129.2, 129.2, 129.6, 131.7, 136.6 (py 4), 138.7, 139.3, 140.1, 143.3, 146.7, 148.6, 169.2.

**($^{Et}$DBAP)Zr($CH_2Ph$)$_2$ (10)**. A 100 mL Schlenk tube was charged with 0.40 g (0.88 mmol) of $Zr(CH_2Ph)_4$, approximately 10 mL of toluene, and a stirrer bar. $^{Et}$DIP (0.37 g, 0.88 mmol) was added, and the reaction mixture turned dark red-brown and was stirred for 1 day which afforded a mixture of two isomers $C_2$ and $C_s$. The solvent was reduced to half and the remnant was layered with triple amount of hexane and left at −35 °C. The first crop of dark crystals turned to be the $C_2$ isomer. Reducing the amount of solvent to half and layering with hexane (1:3) gave the second crop which was the mixture of $C_2$ : $C_s$ isomers. The 3$^{rd}$ time of the recrystallization gave the $C_s$ isomer. Washing the dark crystals with ether gave 0.36 g (47%) (in total) of purer light yellow crystals suitable for X-ray crystallography.

$^1$H NMR (500 MHz; benzene-$d_6$) (10-$C_2$): δ 1.06 (6H, t, *J* 7.5, $CH_2CH_3$), 1.12 (6H, s, $CH_3$C-N), 1.44 (6H, t, *J* 7.5, $CH_2CH_3$), 2.04 (2H, d, *J* 11.0, $CH_2$Ph), 2.29, 2.50 (2H each, m, $CH_2CH_3$), 2.59 (2H, d, *J* 11.0, $CH_2$Ph), 2.96 (2H, d, *J* 13.0, Zr-$CH_2$Ph), 3.19, 3.49 (2H each, m, $CH_2CH_3$), 3.80 (2H, d, *J* 13.0, Zr-$CH_2$Ph), 5.99 (2H, d, *J* 7.8, py 3/5), 6.40 (4H, d, *J* 7.6, Zr$CH_2$Ph *o*), 6.50 (4H, d, *J* 7.3, *o*-$CH_2$Ph), 6.71 (1H, t, *J* 7.8, py 4), 6.78 (2H, t, *J* 7.3, Zr$CH_2$Ph *p*), 6.96 (4H, d, *J* 7.25, Zr$CH_2$Ph *m*), 6.99 (4H, d, *J* 6.5, *m*-$CH_2$Ph), 7.02 (2H, t, *J* 7.3, *p*-$CH_2$Ph), 7.13 (2H, d, *J* 7.5, *m*-Ar), 7.24 (2H, t, *J* 7.6, *p*-Ar), 7.41 (2H, d, *J* 7.6, *m*-Ar) .

$^{13}$C{$^1$H} NMR (500 MHz; benzene-$d_6$): 13.3, 16.2 ($CH_2CH_3$), 21.5 ($CH_3$C-N), 25.8, 27.3 ($CH_2CH_3$), 60.0 ($CH_2$Ph), 73.3 (Zr-$CH_2$Ph), 75.3 (C-N), 119.4 (py 3/5), 121.6 (Zr$CH_2$Ph *p*), 125.8 (*m*-Ar), 125.9 (*p*-Ar), 126.9 (*m*-Ar), 127.1 (Zr$CH_2$Ph *o*), 127.3, 128.0, 128.3 (Zr$CH_2$Ph *m*, *m*-$CH_2$Ph, *p*-$CH_2$Ph), 131.3 (*o*-$CH_2$Ph), 137.5 (py 4), 138.0, 142.5 (Zr$CH_2$Ph *i*, *i*-$CH_2$Ph), 144.5, 147.6 (*o*-Ar), 147.9, 170.2 (*i*-Ar, py 2).

$^1$H NMR (500 MHz; benzene-$d_6$) (10-$C_s$): δ 1.08 (6H, s, $CH_3$C-N), 1.08 (6H, t, *J* 7.2, $CH_2CH_3$), 1.50 (6H, t, *J* 7.5, $CH_2CH_3$), 1.69 (2H, s, Zr-$CH_2$Ph), 2.32 (2H, s, Zr-$CH_2$Ph), 2.41, 2.52 (2H each, m, $CH_2CH_3$), 3.26 (2H, d, *J* 13.0, $CH_2$Ph), 3.30 (2H, m, $CH_2CH_3$), 3.53 (2H, d, *J* 13.0, $CH_2$Ph), 3.55 (2H, m, $CH_2CH_3$), 5.86 (2H, d, *J* 7.8, py 3/5), 6.17 (2H, d, *J* 7.4,

$ZrCH_2Ph$ o), 6.42 (1H, t, *J* 7.8, py 4), 6.58 (1H, t, *J* 7.4, $ZrCH_2Ph$ *p*), 6.60 (4H, m, $ZrCH_2Ph$ *m*), 6.93 (2H, t, *J* 7.9, *p*-$CH_2Ph$), 6.95 (1H, t, *J* 7.4, $ZrCH_2Ph$ *p*), 7.03 (2H, d, *J* 7.4, $ZrCH_2Ph$ *o*), 7.08 (4H, d, *J* 6.2, *o*-$CH_2Ph$), 7.10 (4H, t, *J* 7.6, *m*-$CH_2Ph$), 7.17 (2H, d, *J* 6.2, *m*-Ar), 7.25 (2H, t, *J* 7.6, *p*-Ar), 7.45 (2H, d, *J* 7.8, *m*-Ar). $^{13}C\{^1H\}$ NMR (500 MHz; benzene-$d_6$): 13.5, 16.0 ($CH_2CH_3$), 21.6 ($CH_3$C-N), 26.2, 26.5 ($CH_2CH_3$), 57.7 ($CH_2Ph$), 65.7, 74.1 (Zr-$CH_2Ph$), 76.0 (C-N), 119.4 (py 3/5), 121.3 ($ZrCH_2Ph$ *p*), 123.0 ($ZrCH_2Ph$ *p*), 125.8 (*p*-Ar), 126.3 (*o*-$CH_2Ph$), 126.6 (*m*-Ar), 127.2 ($ZrCH_2Ph$ *o*), 128.0 (*p*-$CH_2Ph$), 128.2 (*m*-Ar), 128.3 (*m*-$CH_2Ph$), 129.1 ($ZrCH_2Ph$ o), 129.2, 131.4 ( $ZrCH_2Ph$ *m*), 137.0 (py 4), 138.7, 143.2, 144.0 ($ZrCH_2Ph$ *i*, *i*-$CH_2Ph$), 144.4, 146.6 (*o*-Ar), 149.9, 170.7 (*i*-Ar, py 2).

**($^{Et}$DBAP)Hf($CH_2Ph$)$_2$** (**11**). A 100 mL Schlenk tube was charged with 0.20 g (0.37 mmol) of $Hf(CH_2Ph)_4$, approximately 10 mL of toluene, and a stirrer bar. $^{Et}$DIP (0.15 g, 0.37 mmol) was added, and the reaction mixture turned dark red-brown and was stirred for 1 day which afforded a mixture of two isomers $C_2$ and $C_s$. The solvent was reduced to half and the remnant was layered with triple amount of hexane and left at −35 °C. The first crop of dark crystals turned to be the $C_s$ isomer. Reducing the amount of solvent to half and layering with hexane (1:3) gave the second crop which was the mixture of $C_2$ : $C_s$ isomers. The 3$^{rd}$ time of the recrystallization gave the $C_2$ isomer. Washing the dark crystals with ether gave 0.23 g (63%) (in total) of purer light yellow crystals suitable for X-ray crystallography.

$^1H$ NMR (500 MHz; toluene-$d_8$) (11-$C_2$): δ 1.09 (6H, t, *J* 7.5, $CH_2CH_3$), 1.10 (6H, s, $CH_3$C-N), 1.41 (6H, t, *J* 7.5, $CH_2CH_3$),1.76, 2.20 (2H each, d, *J* 12, $CH_2Ph$), 2.40, 2.6 (2H each, m, $CH_2CH_3$), 2.89 (2H, d, *J* 13, $HfCH_2Ph$), 3.15, 3.45 (2H, m, $CH_2CH_3$), 5.95 (2H, d, *J* 7.8, py 3/5), 6.31 (4H, d, *J* 7.4, $HfCH_2Ph$ *o*), 6.45 (4H, d, *J* 7.4, *o*-$CH_2Ph$), 6.68 (1H, t, *J* 7.8, py 4), 6.70 (2H, t, *J* 7.8, $HfCH_2Ph$ *p*), 6.90- 6.95 (10H, m, $HfCH_2Ph$ *p*, *m*- and *p*-$CH_2Ph$), 7.14 (2H, d, *J* 7.6, *m*-Ar), 7.21 (2H, t, *J* 7.6, *p*-Ar), 7.36 (2H, d, *J* 7.6, *m*-Ar). $^{13}C\{^1H\}$ NMR (500 MHz;

toluene-$d_8$)(partial assignment only): 13.5, 16.0 ($CH_2CH_3$), 22.4 ($CH_3$C-N), 25.9, 27.1 ($CH_2CH_3$), 58.9 ($CH_2$Ph), 75.5 (Hf$CH_2$Ph), 83.8 (C-N), 119.7 (py 3/5), 121.9 (Hf$CH_2$Ph *p*), 125.8 (*m*-Ar), 125.9 (*p*-Ar), 126.8 (*m*-Ar), 127.1 (Hf$CH_2$Ph *o*), 128.2, 128.3 (Hf$CH_2$Ph *m*, *m*-$CH_2$Ph, *p*-$CH_2$Ph), 131.3 (*o*-$CH_2$Ph), 137.0 (py 4), 138.2, 143.1 (Hf$CH_2$Ph *i*, *i*-$CH_2$Ph), 144.7, 147.7 (*o*-Ar), 148.9, 170.1 (*i*-Ar, py 2).

$^1$H NMR (500 MHz; benzene-$d_6$) (11-$C_s$): δ 1.07 (6H, s, $CH_3$C-N), 1.08, 1.48 (6H each, t, *J* 7.5, $CH_2CH_3$), 1.49, 2.38 (2H each, s, Hf$CH_2$Ph), 2.43, 2.55 (2H each, m, $CH_2CH_3$), 2.24 (2H, d, *J* 13.0, Hf$CH_2$Ph), 3.35, 3.50 (2H, m, $CH_2CH_3$), 3.55 (2H, d, *J* 13.0, Hf$CH_2$Ph), 4.85 (2H, d, *J* 7.8, py 3/5), 6.12 (2H, d, *J* 7.5, Hf$CH_2$Ph *o*), 6.42 (1H, t, *J* 7.8, py 4), 6.58 (5H, m, Hf$CH_2$Ph *m*, *p*), 6.84 (1H, t, *J* 7.3, Hf$CH_2$Ph *p*), 6.99 (2H, m, Hf$CH_2$Ph *o*), 6.99 (2H, m, $CH_2$Ph *p*), 7.08 (8H, m, *o*- and *m*-$CH_2$Ph p), 7.19 (2H, d, *J* 7.1, *m*-Ar), 7.26 (2H, t, *J* 7.6, *p*-Ar), 7.46 (2H, d, *J* 7.3, *m*-Ar). $^{13}$C{$^1$H} NMR (500 MHz; benzene-$d_6$): 13.5, 16.1 ($CH_2CH_3$), 22.0 ($CH_3$C-N), 26.0, 26.4 ($CH_2CH_3$), 57.9 ($CH_2$Ph), 76.1, 78.8 (Hf$CH_2$Ph), 83.7 (C-N), 119.6 (py 3/5), 121.8, 121.9 (Hf$CH_2$Ph *p*), 125.8 (*p*-Ar), 126.0 (*o*-$CH_2$Ph), 126.7 (*m*-Ar), 127.2 (Hf$CH_2$Ph *o*), 127.8 (*p*-$CH_2$Ph), 127.9 (*m*-Ar), 128.3 (*m*-$CH_2$Ph), 131.4 (Hf$CH_2$Ph *m*), 137.2 (py 4), 138.6, 143.9, 144.4 (Hf$CH_2$Ph *i*, *i*-$CH_2$Ph), 146.0, 147.2 (*o*-Ar), 149.0, 170.6 (*i*-Ar, py 2).

**($^{i\mathrm{Pr}}$DBAP)Hf($CH_2$Ph)$_2$** (**12**). A 100 mL Schlenk tube was charged with 0.20 g (0.37 mmol) of Hf($CH_2$Ph)$_4$, approximately 10 mL of toluene, and a stirrer bar. $^{i\mathrm{Pr}}$DIP (0.18 g, 0.37 mmol) was added, and the reaction mixture turned dark red-brown and was stirred for 1 day which afforded a mixture of two isomers $C_2$ and $C_s$. The solvent was reduced to half and the remnant was layered with triple amount of hexane and left at −35 °C. The first crop of dark crystals turned to be the $C_2$ isomer. Reducing the amount of solvent to half and layering with hexane (1:3) gave the second crop which was the mixture of $C_2$ : $C_s$ isomers. The $C_s$ isomer

was not isolated. Washing the dark crystals with ether gave 0.04 g (10%) (in total) of purer light beige crystals.

$^1$H NMR (500 MHz; benzene-$d_6$) (12-$C_2$): δ 0.95, 0.99 (6H each, d, *J* 6.7, CH(C$H_3$)$_2$), 1.00 (6H, s, $CH_3$C-N), 1.28, 1.50 (6H each, d, *J* 6.7, CH(C$H_3$)$_2$), 2.10, 2.70 (2H, d, *J* 11, HfC$H_2$Ph), 2.74 (1H, m, C*H*($CH_3$)$_2$), 2.99. 4.05 (2H each, d, *J* 13, $CH_2$Ph), 4.67 (1H, m, C*H*($CH_3$)$_2$), 6.02 (2H, d, *J* 7.7, py 3/5), 6.36 (4H, d, *J* 7.7, HfC$H_2$Ph *o*), 6.49 (4H, d, *J* 7.5, *o*-$CH_2$Ph), 6.75 (1H, t, *J* 7.7, py 4), 6.77 (2H, t, *J* 7.6, HfC$H_2$Ph *p*), 6.97- 7.04 (10H, m, *m*- and *p*-$CH_2$Ph, HfC$H_2$Ph *m*), 7.10 (2H, d, *J* 7.6, *m*-Ar), 7.28 (2H, t, *J* 7.6, *p*-Ar), 7.34 (2H, d, *J* 7.6, *m*-Ar). $^{13}$C{$^1$H} NMR (500 MHz; benzene-$d_6$): 20.8 (*C*$H_3$C-N), 25.2, 25.5, 25.8, 26.4 (CH(*C*$H_3$)$_2$), 28.3, 29.2 (*C*H($CH_3$)$_2$), 62.6 ($CH_2$Ph ), 74.3 (C-N), 87.6 (HfC$H_2$Ph), 119.1 (py 3/5), 121.8 (py 4), 124.9, 125.3 (*m*-Ar), 125.9 (*p*-Ar), 127.1 (HfC$H_2$Ph *o*), 127.3 (*m*- and *p*-$CH_2$Ph, HfC$H_2$Ph *m*), 131.0 (*o*-$CH_2$Ph), 137.4 (HfC$H_2$Ph *p*), 147.3, 147.5 (HfC$H_2$Ph *i*, *i*-$CH_2$Ph), 147.6, 147.8 (*o*-Ar), 149.5, 171.4 (*i*-Ar, py 2).

$^1$H NMR (500 MHz; benzene-$d_6$) (12-$C_s$): δ 1.09 (6H, s, $CH_3$C-N), 1.11, 1.13 (6H each, d, *J* 6.7, CH(C$H_3$)$_2$), 1.41, 1.54 (6H each, d, *J* 6.7, CH(C$H_3$)$_2$), 1.84, 2.90 (2H, s, HfC$H_2$Ph), 2.94 (1H, m, C*H*($CH_3$)$_2$), 3.22. 3.82 (2H each, d, *J* 13, $CH_2$Ph), 4.83 (1H, m, C*H*($CH_3$)$_2$), 5.94 (2H, d, *J* 7.8, py 3/5), 6.18 (Ar), 6.46 (1H, d, *J* 7.8, py 4), 6.54 (Ar), 6.77 (Ar), 6.95- 7.36 (Ar). $^{13}$C{$^1$H} NMR (500 MHz; benzene-$d_6$): 22.9 (*C*$H_3$C-N), 25.6, 25.7, 26.9, 27.8 (CH(*C*$H_3$)$_2$), 28.5, 29.1 (*C*H($CH_3$)$_2$), 59.6 ($CH_2$Ph ), 75.1 (C-N), 82.4, 88.7 (HfC$H_2$Ph), 118.6 (py 3/5), 121.5, 122.2, 125.2, 125.6, 126.1, 126.7, 127.0, 128.0, 128.3, 131.1, 137.5, 137.7, 138.6, 146.7, 148.4, 148.5, 149.1, 147.8, 171.7 (*i*-Ar, py 2).

**($^{Et}$DBAP)Zr($CH_2$Ph)(TEMPO)** (**13**). A 25 mL Schlenk tube was charged with 0.046 g (0.05 mmol) of complex **10-*C*$_2$** in approximately 1 mL of benzene-$d_6$. 2 equivalents of TEMPO (0.016 g, 0.1 mmol) was added, and the solution was left for 5 days. Layering of the benzene

solution with hexane (1:3) led to isolation of 0.042 g (88%) of the pure light yellow crystals suitable for X-ray crystallography.

$^{1}$H NMR (500 MHz; benzene-$d_6$): δ 0.59 (6H, s, $H_3$C-TEMPO), 1.01 (3H, s, $CH_3$C-N), 1.04 (6H, s, $HC_3$-TEMPO), 1.17 (3H, t, *J* 7.5, $CH_2CH_3$), 1.28 (6H, m, $CH_2$-TEMPO), 1.32 (3H, t, *J* 7.5, $CH_2CH_3$), 1.35 (3H, s, $CH_3$C-N), 1.43, 1.46 (3H each, t, J 7.5, $CH_2CH_3$), 2.57 (1H, m, $CH_2CH_3$), 2.67 (1H, d, *J* 11.6, $ZrCH_2Ph$), 2.71 (1H, m, $CH_2CH_3$), 2.75 (1H, d, *J* 11.6, $ZrCH_2Ph$), 2.82 (1H, d, *J* 13, $CH_2Ph$), 2.94 (1H, m, $CH_2CH_3$), 3.14 (1H, m, $CH_2CH_3$), 3.30 (1H, d, *J* 13, $CH_2Ph$), 3.45 (2H, m, $CH_2CH_3$), 3.50, 3.55 (1H each, d, *J* 13, $CH_2Ph$), 3.58 (1H, m, $CH_2CH_3$), 6.03, 6.10 (1H each, d, *J* 7.8, py 3/5), 6.35, 6.48, 6.75 (1H, t, *J* 7.8, py 4), 6.77, 6.93, 6.97- 7.15, 7.24 (1H, t, *J* 7.6, *p*-Ar), 7.29 (1H, d, *J* 7.6, *m*-Ar), 7.38, 7.42 (1H, d, *J* 7.6, *m*-Ar). $^{13}$C{$^{1}$H} NMR (500 MHz; benzene-$d_6$): δ 12.8, 14.5, 15.0, 15.6, 17.2, 21.3, 23.0, 25.5, 26.0, 26.2, 27.4, 40.8, 56.8, 57.1, 60.0, 63.2, 75.2, 76.3, 119.6, 120.3, 121.3, 124.6, 124.9, 125.2, 125.8, 126.2, 126.5, 126.6, 126.9, 127.5, 127.7, 127.8, 128.3, 131.4, 132.0, 136.7, 138.5, 138.8, 141.3, 143.4, 144.0, 144.0, 147.4, 150.6, 150.9, 168.9, 169.5.

**($^{Et}$DIP-2H)$^{NNN}$($^{Et}$DIP-2H)$^{NNC}$Hf** (**14**). A 100 mL Schlenk tube was charged with 0.1 g (0.31 mmol) of HfCl4, approximately 15 mL of toluene, and a stirrer bar. At -80 °C, 0.117 g (1.25 mmol) of $Me_3SiCH_2Li$ was added dropwise in toluene. After 3 hours, 0.133 g (0.31 mmol) of $^{Et}$DIP was added in toluene. The solution turned into dark orange-brown quickly, warmed up to room temperature and stirred for 12 hours. Suspended solid was removed by passing the solution through celite, and the solvent was removed in vacuo. The solid residue was dissolved in 1 mL toluene and layered with 5 mL hexane. It was left untouched at −35 °C to give 0.007 g (2.2%) of dark orange-brown crystals suitable for X-ray crystallography.

$^{1}$H NMR (500 MHz; benzene-$d_6$) (partial assignment only): δ 0.88 (6H, t, *J* 7.2, $CH_2CH_3$), 0.90 (3H, t, *J* 7.5, $CH_2CH_3$), 0.95 (6H, t, *J* 7.5, $CH_2CH_3$), 1.19 (6H, t, *J* 7.5, $CH_2CH_3$), 1.23 (6H, t, *J* 7.5, $CH_2CH_3$), 1.32 (2H, s, $CH_2$=C-N), 1.68, 1.90, 2.25, 2.37, 2.53 (2H, m,

C*H*$_2$CH$_3$), 2.94 (6H, m, C*H*$_2$CH$_3$), 3.67, 4.49 (2H each, s, $H_2C$=C-N), 4.58 (1H, s, $H_2C$=C-N), 6.72-7.09 (15H, m, Ar, py), 7.38, 8.22 (1H each, d, *J* 8.0, py).

## 4.6 References


1. Scott, J.; Vidyaratne, I.; Korobkov, I.; Gambarotta, S.; Budzelaar, P. H. M., Multiple Pathways for Dinitrogen Activation during the Reduction of an Fe Bis(iminepyridine) Complex. *Inorg. Chem.* **2008,** *47* (3), 896-911.

2. Kooistra, T. M.; Knijnenburg, Q.; Smits, J. M. M.; Horton, A. D.; Budzelaar, P. H. M.; Gal, A. W., Olefin Polymerization with [{bis(imino)pyridyl}CoIICl2]: Generation of the Active Species Involves CoI. *Angew. Chem. Int. Ed.* **2001,** *40* (24), 4719-4722.

3. Gallagher, M.; Wieder, N. L.; Dioumaev, V. K.; Carroll, P. J.; Berry, D. H., Low-Valent Ruthenium Complexes of the Non-innocent 2,6-Bis(imino)pyridine Ligand. *Organometallics* **2010,** *29* (3), 591-603.

4. (a) Sieh, D.; Schoffel, J.; Burger, P., Synthesis of a chloro protected iridium nitrido complex. *Dalton Trans.* **2011,** *40* (37), 9512-9524; (b) Sieh, D.; Schlimm, M.; Andernach, L.; Angersbach, F.; Nückel, S.; Schöffel, J.; Šušnjar, N.; Burger, P., Metal–Ligand Electron Transfer in 4d and 5d Group 9 Transition Metal Complexes with Pyridine, Diimine Ligands. *Eur. J. Inorg. Chem.* **2012,** *2012* (3), 444-462; (c) Nückel, S.; Burger, P., Transition Metal Complexes with Sterically Demanding Ligands, 3.1 Synthetic Access to Square-Planar Terdentate Pyridine−Diimine Rhodium(I) and Iridium(I) Methyl Complexes: Successful Detour via Reactive Triflate and Methoxide Complexes. *Organometallics* **2001,** *20* (21), 4345-4359.

5. Sugiyama, H.; Gambarotta, S.; Yap, G. P. A.; Wilson, D. R.; Thiele, S. K. H., Preparation of an Active Neodymium Catalyst for Regioselective Butadiene cis-Polymerization Supported by a Dianionic Modification of the 2,6-Diiminopyridine Ligand. *Organometallics* **2004,** *23* (21), 5054-5061.

6. (a) Margulieux, G. W.; Turner, Z. R.; Chirik, P. J., Synthesis and Ligand Modification Chemistry of a Molybdenum Dinitrogen Complex: Redox and Chemical Activity of a

Bis(imino)pyridine Ligand. *Angew. Chem. Int. Ed.* **2014,** *53* (51), 14211-14215; (b) Margulieux, G. W.; Bezdek, M. J.; Turner, Z. R.; Chirik, P. J., Ammonia Activation, H2 Evolution and Nitride Formation from a Molybdenum Complex with a Chemically and Redox Noninnocent Ligand. *J. Am. Chem. Soc.* **2017,** *139* (17), 6110-6113.

7. Bart, S. C.; Lobkovsky, E.; Chirik, P. J., Preparation and Molecular and Electronic Structures of Iron(0) Dinitrogen and Silane Complexes and Their Application to Catalytic Hydrogenation and Hydrosilation. *J. Am. Chem. Soc.* **2004,** *126* (42), 13794-13807.

8. Monfette, S.; Turner, Z. R.; Semproni, S. P.; Chirik, P. J., Enantiopure C1-Symmetric Bis(imino)pyridine Cobalt Complexes for Asymmetric Alkene Hydrogenation. *J. Am. Chem. Soc.* **2012,** *134* (10), 4561-4564.

9. Obligacion, J. V.; Chirik, P. J., Highly Selective Bis(imino)pyridine Iron-Catalyzed Alkene Hydroboration. *Org. Lett.* **2013,** *15* (11), 2680-2683.

10. Hoyt, J. M.; Schmidt, V. A.; Tondreau, A. M.; Chirik, P. J., Iron-catalyzed intermolecular [2+2] cycloadditions of unactivated alkenes. *Science* **2015,** *349* (6251), 960-963.

11. Bedford, R. B.; Betham, M.; Bruce, D. W.; Davis, S. A.; Frost, R. M.; Hird, M., Iron nanoparticles in the coupling of alkyl halides with aryl Grignard reagents. *Chem. Commun.* **2006,** (13), 1398-1400.

12. Zhu, D.; Thapa, I.; Korobkov, I.; Gambarotta, S.; Budzelaar, P. H. M., Redox-Active Ligands and Organic Radical Chemistry. *Inorg. Chem.* **2011,** *50* (20), 9879-9887.

13. Vidyaratne, I.; Gambarotta, S.; Korobkov, I.; Budzelaar, P. H. M., Dinitrogen Partial Reduction by Formally Zero- and Divalent Vanadium Complexes Supported by the Bis-iminopyridine System. *Inorg. Chem.* **2005,** *44* (5), 1187-1189.

14. Scott, J.; Gambarotta, S.; Korobkov, I.; Budzelaar, P. H. M., Metal versus Ligand Alkylation in the Reactivity of the (Bis-iminopyridinato)Fe Catalyst. *J. Am. Chem. Soc.* **2005,** *127* (37), 13019-13029.

15. Blackmore, I. J.; Gibson, V. C.; Hitchcock, P. B.; Rees, C. W.; Williams, D. J.; White, A. J. P., Pyridine N-Alkylation by Lithium, Magnesium, and Zinc Alkyl Reagents: Synthetic, Structural, and Mechanistic Studies on the Bis(imino)pyridine System. *J. Am. Chem. Soc.* **2005,** *127* (16), 6012-6020.

16. Sandoval, J. J.; Palma, P.; Álvarez, E.; Cámpora, J.; Rodríguez-Delgado, A., Mechanism of Alkyl Migration in Diorganomagnesium 2,6-Bis(imino)pyridine Complexes: Formation of Grignard-Type Complexes with Square-Planar Mg(II) Centers. *Organometallics* **2016,** *35* (18), 3197-3204.

17. Arrowsmith, M.; Hill, M. S.; Kociok-Köhn, G., Dearomatization and C−H Deprotonation with Heavier Group 2 Alkyls: Does Size Matter? *Organometallics* **2010,** *29* (19), 4203-4206.

18. Cámpora, J.; Pérez, C. M.; Rodríguez-Delgado, A.; Naz, A. M.; Palma, P.; Álvarez, E., Selective Alkylation of 2,6-Diiminopyridine Ligands by Dialkylmanganese Reagents: A "One-Pot" Synthetic Methodology. *Organometallics* **2007,** *26* (4), 1104-1107.

19. Cámpora, J.; Naz, A. M.; Palma, P.; Álvarez, E.; Reyes, M. L., 2,6-Diiminopyridine Iron(II) Dialkyl Complexes. Interaction with Aluminum Alkyls and Ethylene Polymerization Catalysis. *Organometallics* **2005,** *24* (21), 4878-4881.

20. Calderazzo, F.; Englert, U.; Pampaloni, G.; Santi, R.; Sommazzi, A.; Zinna, M., Bis(arylimino)pyridine derivatives of Group 4 metals: preparation, characterization and activity in ethylene polymerization. *Dalton Trans.* **2005,** (5), 914-922.

21. Rahimi, N.; de Bruin, B.; Budzelaar, P. H. M., Balance between Metal and Ligand Reduction in Diiminepyridine Complexes of Ti. *Organometallics* **2017,** *36* (17), 3189-3198.

22. Milsmann, C.; Semproni, S. P.; Chirik, P. J., N–N Bond Cleavage of 1,2-Diarylhydrazines and N–H Bond Formation via H-Atom Transfer in Vanadium Complexes Supported by a Redox-Active Ligand. *J. Am. Chem. Soc.* **2014,** *136* (34), 12099-12107.

23. Vidyaratne, I.; Scott, J.; Gambarotta, S.; Budzelaar, P. H. M., Dinitrogen Activation, Partial Reduction, and Formation of Coordinated Imide Promoted by a Chromium Diiminepyridine Complex. *Inorg. Chem.* **2007,** *46* (17), 7040-7049.

24. Bart, S. C.; Lobkovsky, E.; Bill, E.; Chirik, P. J., Synthesis and Hydrogenation of Bis(imino)pyridine Iron Imides. *J. Am. Chem. Soc.* **2006,** *128* (16), 5302-5303.

25. Obligacion, J. V.; Chirik, P. J., Bis(imino)pyridine Cobalt-Catalyzed Alkene Isomerization–Hydroboration: A Strategy for Remote Hydrofunctionalization with Terminal Selectivity. *J. Am. Chem. Soc.* **2013,** *135* (51), 19107-19110.

26. Manuel, T. D.; Rohde, J.-U., Reaction of a Redox-Active Ligand Complex of Nickel with Dioxygen Probes Ligand-Radical Character. *J. Am. Chem. Soc.* **2009,** *131* (43), 15582-15583.

27. Sandoval, J. J.; Palma, P.; Alvarez, E.; Rodriguez-Delgado, A.; Campora, J., Dibenzyl and diallyl 2,6-bisiminopyridinezinc(ii) complexes: selective alkyl migration to the pyridine ring leads to remarkably stable dihydropyridinates. *Chem. Commun.* **2013,** *49* (60), 6791-6793.

28. Zhu, H.; Wang, M.; Ma, C.; Li, B.; Chen, C.; Sun, L., Preparation and structures of 6- and 7-coordinate salen-type zirconium complexes and their catalytic properties for oligomerization of ethylene. *J. Organomet. Chem.* **2005,** *690* (17), 3929-3936.

29. Lin, Z.; Bytheway, I., Stereochemistry of Seven-Coordinate Main Group and d0 Transition Metal Molecules. *Inorg. Chem.* **1996,** *35* (3), 594-603.

30. (a) Matsui, S.; Mitani, M.; Saito, J.; Tohi, Y.; Makio, H.; Matsukawa, N.; Takagi, Y.; Tsuru, K.; Nitabaru, M.; Nakano, T.; Tanaka, H.; Kashiwa, N.; Fujita, T., A Family of

Zirconium Complexes Having Two Phenoxy−Imine Chelate Ligands for Olefin Polymerization. *J. Am. Chem. Soc.* **2001,** *123* (28), 6847-6856; (b) Bott, R. K. J.; Hughes, D. L.; Schormann, M.; Bochmann, M.; Lancaster, S. J., Monocyclopentadienyl phenoxy-imine and phenoxy-amine complexes of titanium and zirconium and their application as catalysts for 1-alkene polymerisation. *J. Organomet. Chem.* **2003,** *665* (1–2), 135-149; (c) Leino, R.; Luttikhedde, H. J. G.; Lehtonen, A.; Ekholm, P.; Näsman, J. H., Synthesis and characterization of ethylene-bridged 1-tert-butyldimethylsiloxy-substituted bis(indenyl) and bis(tetrahydroindenyl)zirconium dichlorides. *J. Organomet. Chem.* **1998,** *558* (1–2), 181-188.

31. Knijnenburg, Q.; Smits, J. M. M.; Budzelaar, P. H. M., Reaction of the Diimine Pyridine Ligand with Aluminum Alkyls: An Unexpectedly Complex Reaction. *Organometallics* **2006,** *25* (4), 1036-1046.

32. Zhu, D.; Janssen, F. F. B. J.; Budzelaar, P. H. M., (Py)2Co(CH2SiMe3)2 As an Easily Accessible Source of "CoR2". *Organometallics* **2010,** *29* (8), 1897-1908.

33. (a) Guérin, F.; McConville, D. H.; Vittal, J. J.; Yap, G. A. P., Synthesis, Structure, and Reactivity of Zirconium Alkyl Complexes Bearing Ancillary Pyridine Diamide Ligands. *Organometallics* **1998,** *17* (23), 5172-5177; (b) Guérin, F.; McConville, D. H.; Vittal, J. J., Synthesis, Structure, and Reactivity of Titanacyclopentadiene Complexes Bearing Ancillary Pyridine Diamide Ligands. *Organometallics* **1997,** *16* (7), 1491-1496; (c) Guérin, F.; McConville, D. H.; Vittal, J. J., Conformationally Rigid Diamide Complexes of Zirconium: Electron Deficient Analogues of Cp2Zr. *Organometallics* **1996,** *15* (26), 5586-5590; (d) Tay, B.-Y.; Wang, C.; Chia, S.-C.; Stubbs, L. P.; Wong, P.-K.; van Meurs, M., Synthesis of Bis(amino)pyridines by the Stepwise Alkylation of Bis(imino)pyridines: An Unexpected and Selective Alkylation of the Aminoiminopyridine by AlMe3. *Organometallics* **2011,** *30* (21), 6028-6033; (e) Ziniuk, Z.; Goldberg, I.; Kol, M., Zirconium complexes of chelating dianionic

bis(pentafluorophenylamido) ligands: synthesis, structure and ethylene polymerisation activity. *Inorg. Chem. Commun.* **1999,** *2* (11), 549-551.

34. Sugiyama, H.; Aharonian, G.; Gambarotta, S.; Yap, G. P. A.; Budzelaar, P. H. M., Participation of the α,α‘-Diiminopyridine Ligand System in Reduction of the Metal Center during Alkylation. *J. Am. Chem. Soc.* **2002,** *124* (41), 12268-12274.

35. De Waele, P.; Jazdzewski, B. A.; Klosin, J.; Murray, R. E.; Theriault, C. N.; Vosejpka, P. C.; Petersen, J. L., Synthesis of Hafnium and Zirconium Imino−Amido Complexes from Bis-imine Ligands. A New Family of Olefin Polymerization Catalysts. *Organometallics* **2007,** *26* (16), 3896-3899.

36. Tshuva, E. Y.; Goldberg, I.; Kol, M.; Goldschmidt, Z., Zirconium Complexes of Amine−Bis(phenolate) Ligands as Catalysts for 1-Hexene Polymerization: Peripheral Structural Parameters Strongly Affect Reactivity. *Organometallics* **2001,** *20* (14), 3017-3028.

37. Schmidt, R.; Welch, M. B.; Knudsen, R. D.; Gottfried, S.; Alt, H. G., N,N,N-Tridentate iron(II) and vanadium(III) complexes: Part I. Synthesis and characterization. *J. Mol. Catal. A: Chem.* **2004,** *222* (1), 9-15.

38. Fulmer, G. R.; Miller, A. J. M.; Sherden, N. H.; Gottlieb, H. E.; Nudelman, A.; Stoltz, B. M.; Bercaw, J. E.; Goldberg, K. I., NMR Chemical Shifts of Trace Impurities: Common Laboratory Solvents, Organics, and Gases in Deuterated Solvents Relevant to the Organometallic Chemist. *Organometallics* **2010,** *29* (9), 2176-2179.

39. *smart program suite, 6*, Bruker AXS Inc.; Madison, WI.

40. Sheldrick, G. M. *SADABS*, University of Göttingen, Göttingen, Germany.

41. Sheldrick, G. M., *Acta Crystallogr. Sect. A: Found. Crystallogr.* **2008,** *64*, 112-122.

# 5 Conclusions and Outlook

## 5.1 Conclusions

In this thesis, the noninnocence of the DIP ligand in combination with group IV metals has been investigated.

(1) A series of ($^{Et}$DIP)M (M: Ti, Zr, Hf) halide and alkyl complexes have been synthesized and the oxidation state of the metal has been characterized using a combination of techniques (NMR, EPR, XRD, XPS and DFT calculations). Based on these, the unpaired electron in the paramagnetic ($^{Et}$DIP)$TiCl_3$ mostly resides in a metal 3*d* orbital. Reduction of this complex led to formation of the diamagnetic complex ($^{Et}$DIP)$TiCl_2$ and the further reduction gave ($^{Et}$DIP)$_2$Ti. The ligand in ($^{Et}$DIP)$TiCl_3$ is neutral, (DIP$^{(0)}$)Ti(III), but in the reduced diamagnetic complexes ($^{Et}$DIP)$TiCl_2$, ($^{Et}$DIP)TiClR, ($^{Et}$DIP)$TiR_2$ and ($^{Et}$DIP)$_2$Ti, it has accepted two electrons and is best regarded as dianionic, (DIP$^{2-}$)Ti(IV). Thus, the *reduction* of ($^{Et}$DIP)$TiCl_3$ to ($^{Et}$DIP)$TiCl_2$ has surprisingly resulted in *oxidation* of Ti(III) to Ti(IV). All the above *formally* Ti(II) complexes are diamagnetic, but $^1$H NMR spectra of ($^{Et}$DIP)$TiMe_2$ suggest the presence of a thermally populated triplet state. Due to their larger radii, Zr and Hf form stable seven-coordinate complexes ($^{Et}$DIP)$MCl_4$. In contrast to Ti, attempted one-electron reduction of these complexes to ($^{Et}$DIP)$MCl_3$ was unsuccessful. Instead, use of two equivalents of reductant gave ($^{Et}$DIP)$MCl_2$ (M: Zr, Hf) containing a doubly reduced DIP ligand, (DIP$^{2-}$)M(IV). The $^1$H-NMR patterns of the three complexes ($^{Et}$DIP)$MCl_2$ (M: Ti, Zr, Hf) look similar, but the signals of the Zr complex are strongly broadened. On cooling, they broaden even more and then decoalesce, indicating formation of a left-right asymmetric species. Solid-state structures of ($^{Et}$DIP)$ZrCl_2$ and ($^{Et}$DIP)$HfCl_2$ showed to be dimer and monomer, respectively. This could very-well explain

the broadening in the Zr complex. In contrast to its Ti counterpart, the $^{1}$H-NMR spectra of the dialkyl hafnium complexes ($^{Et}$DIP)HfR$_2$ (R: Me, $CH_2SiMe_3$) are sharp and do not show any indication of population of a triplet state.

(2) The $^{1}$H NMR spectra of ($^{Et}$DIP)TiMe$_2$, ($^{Et}$DIP)HfMe$_2$ and ($^{Et}$DIP)TiCl$_2$(OPPh$_3$) show relatively "normal" shifts for the pyridine and imine hydrogens, in contrast to the unusual values reported for e.g. ($^{iPr}$DIP)Fe(N$_2$)$_2$ and ($^{Et}$DIP)Co$CH_2SiMe_3$ (Table 5.1).

Table 5.1. (DIP)M chemical shifts at room temperature

| Complex/proton | Imine Me(ppm) | Py H3,5 (ppm) | Py H4 (ppm) |
|---|---|---|---|
| ($^{iPr}$DIP)Fe(N$_2$)$_2$[1] | 13.61 | 10.11 | 2.58 |
| ($^{Et}$DIP)Co($CH_2SiMe_3$)[2] | -1.09 | 7.72 | 10.05 |
| ($^{Et}$DIP)TiMe$_2$ | 1.57 | 5.08 | 4.57 |
| ($^{Et}$DIP)TiCl$_2$(OPPh$_3$)* | 0.88 | 5.99 | 5.11 |

* Chemical shifts were recorded at -15 °C

This most likely indicates a difference in electronic structure but so far, no definitive conclusion has been reached. ($^{Et}$DIP)TiMe$_2$, for which we observe a strongly temperature-dependent spectrum, probably exhibits thermal population of a low-lying triplet state (see above). This may also apply to ($^{iPr}$DIP)Fe(N$_2$)$_2$, although the presence of an N$_2$ dissociation equilibrium complicates matters for this compound. Interestingly, ($^{Et}$DIP)Co$CH_2SiMe_3$ despite its somewhat unusual shifts shows extreme temperature-*independence* of the spectrum, which could be taken as an indication of spin admixture (as opposed to thermal triplet population). However, it for the moment this explanation must remain speculative.

(3) Ti(II) compounds are generally known to be strong reductants. However, ($^{Et}$DIP)TiCl$_2$ showed to be rather unreactive in reducing E-E bonds (E: S, N, O). The compound was reducing enough to cleave a C-Cl bond of $CHCl_3$ but not of $CH_2Cl_2$. With OPPh$_3$ only the simple adduct ($^{Et}$DIP)TiCl$_2$(OPPh$_3$) was formed. Reaction with bulky bases resulted in

formation of different products dependent on the size and the heteroatom of the base. Using the somewhat stronger reductant ($^{Et}$DIP)TiMe$_2$ we did observe one example of N-N cleavage: reaction with hydrazobenzene led to N-N bond cleavage and formation of a Ti imido complex. The formally divalent complexes ($^{Et}$DIP)ZrCl$_2$ and ($^{Et}$DIP)HfCl$_2$ are more reducing than ($^{Et}$DIP)TiCl$_2$ and do react not only with CHCl$_3$ but also with CH$_2$Cl$_2$.

(4) In this work, two new examples of ligand-based reactivity of DIP were observed. Reaction of MBn$_4$ (M: Zr, Hf) with DIP resulted in benzylation of *both* imine carbons, producing a mixture of *rac* ($C_2$ symmetric) and *meso* ($C_s$ symmetric) diastereomers ($^{Et}$DIP+2Bn)MBn$_2$. Interestingly, heating of either pure diastereomer in solution re-establishes the equilibrium mixture but does not lead to the expected benzyl shift (to the pyridine ring) or ligand dehydrogenation, indicating benzyl addition to the imines is reversible and likely involves radicals. In preliminary and incomplete work, we have found that use of *in situ* formed Hf(CH$_2$SiMe$_3$)$_4$ instead of HfBn$_4$ leads to formation of a doubly dehydrogenated bis chelate complex ($^{Et}$DIP-2H)$_2$Hf, in which one of the DIP ligands is coordinated in its N,N,C mode.

In several synthesis attempts and reactivity studies of formally divalent complexes we observed a novel type of isomerization of the coordinated DIP ligand: (apparent) migration of a hydrogen atom from an imine methyl group to the second imine carbon atom. This phenomenon is interesting since the H atom leaving the imine group behaves like a proton, while during addition to the second imine group it acts like a hydride. It appears that this H-shift isomerization can be triggered by bases such as MeLi or $^t$BuOK, but we also observed it

during synthesis of ($^{Et}$DIP)$ZrCl_2$ in which no bases were used.[2] Understanding the mechanism of this unexpected isomerization will require more experimental work.

(5) Finally, a few interesting differences between Zr and Hf should be recalled here. The chemistry of Zr and Hf is usually very similar, as are the physical properties of Zr and Hf compounds. In the present work, we have encountered several examples of clear differences:

Both Zr and Hf complexes of (DIP)$MCl_4$ were made in DCM but with substantial difference in solubility. After formation, the Zr complex precipitated while its Hf counterpart stayed in solution.

Although reduction of (DIP)$ZrCl_4$ in THF formed (DIP)$ZrCl_2$(THF), formation of *formally* Hf(II) complexes in coordinating solvents was found to be problematic.

Interestingly, reduction of (DIP)$ZrCl_4$ in toluene formed the dimer [(DIP)$ZrCl_2$]$_2$, while the similar reaction with (DIP)$HfCl_4$ gave monomeric (DIP)$HfCl_2$. The $^1$H NMR spectra of both (DIP)$MCl_2$ complexes (in toluene) were broad at room temperature. Upon lowering the temperature to -15 °C, the $^1$H NMR of (DIP)$HfCl_2$ became sharp and its splitting patterns appeared. Further cooling to -55 °C produced no changes. However, cooling the [(DIP)$ZrCl_2$]$_2$ sample did not result in peak sharpening. Instead, decoalescence was observed and at -55 °C NMR indicated an asymmetric structure.

## 5.2 Outlook

(1) One of the main goals in synthesizing low-valent DIP complexes of early transition metals has been $N_2$ fixation and reduction[3]. Having this idea in mind, I tried to further reduce

[2] However, the $KC_8$ used as reductant could have contained traces of KOH through reaction with air or water.

($^{Et}$DIP)$TiCl_2$ in an atmosphere of $N_2$. However, this gave only the bis chelate complex ($^{Et}$DIP)$_2$Ti. Also, it has previously been reported that reduction of DIP complexes of early transition metals could lead into dehydrogenation of the imine methyl groups. Dehydrogenation of the ligand, consequently, raises the energies of the π* orbitals and hence decreases its π-acceptor capabilities. In order to avoid formation of the bis chelate complex and dehydrogenation, it might be worth making Ti complexes of the partly modified known[4] ligand $^{iPr}$PhDIP (Figure 5.1).

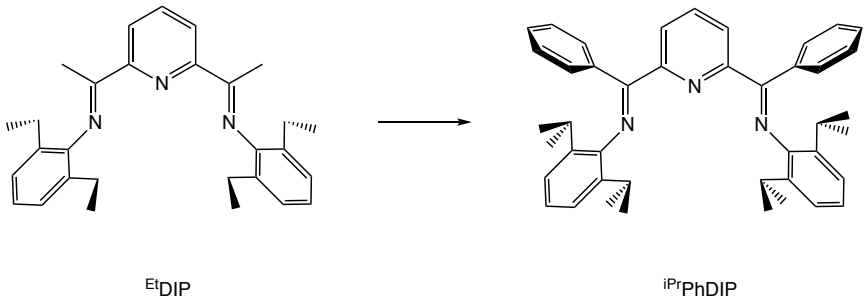


$^{Et}$DIP $^{iPr}$PhDIP

Figure 5.1. Modification of $^{Et}$DIP to $^{iPr}$PhDIP

Replacement of the methyl imines with phenyl groups would avoid ligand dehydrogenation and keep the π-system of the ligand intact. Furthermore, making the aryl rings bulkier could prevent bis chelate formation and result in formation of a dinitrogen (or other small molecules such as CO, $CO_2$) Ti complex. Using ($^{R}$PhDIP) would be useful in cases like ($^{Et}$DIP)$TiMe_2$, ($^{Et}$DIP)$ZrCl_2$ and ($^{Et}$DIP)$HfMe_2$ in which H-shift isomerization happens.

(2) We demonstrated that the reaction of hydroazobenzene (PhHN-NHPh) with ($^{Et}$DIP)$TiMe_2$ leads to activation of the N-N bond which gives a product having a Ti=NPh fragment. Group IV metal complexes containing an M=NR moiety have received great attention in a number of catalytic and biological processes. C-H bond activation[5], insertion[5a, 6], metathesis[7] and [2+2] cycloadditions[5a, 7] are among the applications of group IV metal-

imido complexes. The high reactivity of M(IV)=NR is due to its polarizability which can be controlled via the electronic tuning and modulation of steric hindrance around the metal center. Thus, in a future project, it should be worthwhile to test the reactivity of our Ti(IV)=NPh complex in various organic transformations. Preliminary results showed that ($^{Et}$DIP)TiMe$_2$ is reactive towards reducing PhN=NPh, as well. Now, it might not be unrealistic to expect the dimethyl complex to be reactive in reducing CO and $CO_2$ molecules. In addition, it is suggested to test the reducing power of its heavier counterparts, ($^{Et}$DIP)HfMe$_2$ and ($^{Et}$DIP)MCl$_2$ (M: Zr, Hf) in various bond breaking and reduction reactions (e.g. N-N, N=N, O-O, CO, $CO_2$). The two halide Zr and Hf complexes proved to be able to break the C-Cl bond in $CH_2Cl_2$. Since $CH_2Cl_2$ molecule is a rather stable alkyl halide with reasonably high C-Cl bond energy, these complexes seem to be appropriate reagents for testing in more general C-Cl or even C-F bond activation reactions.

(3) The reaction of MBn$_4$ (M: Zr, Hf) with variations of $^{R}$DIP (R: Me, Et, iPr) resulted in benzyl migration to both imine moieties, forming complexes of dibenzylated ligand as a mixture of *rac* ($C_2$ symmetric) and *meso* ($C_s$ symmetric) diastereomers. While pyridine diamide ligands have been made previously,[8] our double benzylation can be considered as a novel method for making these types of ligands. Hydrolysis of either pure diastereomer and formation of the free pyridine diamine could be useful in synthesizing new pincer-type metal complexes.

(4) Up to date, four main types of the ligand-based reactivity have been classified for DIP: electron reservoir, dimerization, dehydrogenation and alkylation. As mentioned earlier, I have reported a new type of DIP-based reactivity which leads to ligand isomerization accompanied by reduction of both imine groups. This isomerization phenomenon happened in different reactions such as treatment of ($^{Et}$DIP)TiCl$_2$ with 2 $^{t}$BuOK, reduction of

($^{Et}$DIP)$ZrCl_4$ to ($^{Et}$DIP)$ZrCl_2$, treatment of ($^{Et}$DIP)$TiCl_2$ or ($^{Et}$DIP)$HfCl_2$ with 2 MeMgBr. Based on the ratio of the isomerized product to the stoichiometric amount of the reagent used at the beginning, a catalytic process should be involved. At the moment, it is not clear how the isomerization process starts or what the mechanism is. Since, in this process, one H atom is shifted from one imine methyl group to the second imine carbon, reactions in the presence of a catalytic amount of TEMPO, triphenylmethyl radical or triethylsilane with ($^{Et}$DIP)$MMe_2$ (M: Ti, Hf) are suggested.

The isomerization is also interesting for a different reason. Based on general aspects of DIP chemistry, it most likely follows a radical type H atom transfer/H atom abstraction path. This indicates that in the relevant DIP complexes the imine C-H bonds are considerably weakened relative to the free ligand or more standard benzylic/allylic C-H bonds. Metal coordination to the ligand is surely a factor here. Thus, it might be possible to create DIP complexes with highly tunable C-H bond strengths (through variation of the complexed metal fragment), using the complex not for chemical reduction but as a radical source (c.f. the rather toxic tin hydrides). Obviously much more work would be needed to turn this general idea into a practical application.

## 5.3 References


1. Bart, S. C.; Lobkovsky, E.; Chirik, P. J., Preparation and Molecular and Electronic Structures of Iron(0) Dinitrogen and Silane Complexes and Their Application to Catalytic Hydrogenation and Hydrosilation. *J. Am. Chem. Soc.* **2004,** *126* (42), 13794-13807.

2. Kooistra, T. M.; Knijnenburg, Q.; Smits, J. M. M.; Horton, A. D.; Budzelaar, P. H. M.; Gal, A. W., Olefin Polymerization with [{bis(imino)pyridyl}CoIICl2]: Generation of the Active Species Involves CoI. *Angew. Chem. Int. Ed.* **2001,** *40* (24), 4719-4722.

3. (a) Vidyaratne, I.; Gambarotta, S.; Korobkov, I.; Budzelaar, P. H. M., Dinitrogen Partial Reduction by Formally Zero- and Divalent Vanadium Complexes Supported by the Bis-iminopyridine System. *Inorg. Chem.* **2005,** *44* (5), 1187-1189; (b) Vidyaratne, I.; Scott, J.; Gambarotta, S.; Budzelaar, P. H. M., Dinitrogen Activation, Partial Reduction, and Formation of Coordinated Imide Promoted by a Chromium Diiminepyridine Complex. *Inorg. Chem.* **2007,** *46* (17), 7040-7049; (c) Milsmann, C.; Semproni, S. P.; Chirik, P. J., N–N Bond Cleavage of 1,2-Diarylhydrazines and N–H Bond Formation via H-Atom Transfer in Vanadium Complexes Supported by a Redox-Active Ligand. *J. Am. Chem. Soc.* **2014,** *136* (34), 12099-12107; (d) Margulieux, G. W.; Turner, Z. R.; Chirik, P. J., Synthesis and Ligand Modification Chemistry of a Molybdenum Dinitrogen Complex: Redox and Chemical Activity of a Bis(imino)pyridine Ligand. *Angew. Chem. Int. Ed.* **2014,** *53* (51), 14211-14215.

4. Smit, T. M.; Tomov, A. K.; Gibson, V. C.; White, A. J. P.; Williams, D. J., Dramatic Effect of Heteroatom Backbone Substituents on the Ethylene Polymerization Behavior of Bis(imino)pyridine Iron Catalysts. *Inorg. Chem.* **2004,** *43* (21), 6511-6512.

5. (a) Hazari, N.; Mountford, P., Reactions and Applications of Titanium Imido Complexes. *Acc. Chem. Res.* **2005,** *38* (11), 839-849; (b) Duncan, A. P.; Bergman, R. G., Selective transformations of organic compounds by imidozirconocene complexes. *The Chemical Record* **2002,** *2* (6), 431-445.

6. Guiducci, A. E.; Cowley, A. R.; Skinner, M. E. G.; Mountford, P., Novel double substrate insertion versus isocyanate extrusion in reactions of imidotitanium complexes with CO2: critical dependence on imido N-substituents. *J. Chem. Soc., Dalton Trans.* **2001,** (9), 1392-1394.

7. Gade*, L. H.; Mountford*, P., New transition metal imido chemistry with diamido-donor ligands. *Coord. Chem. Rev.* **2001,** *216-217*, 65-97.

8. (a) Guérin, F.; McConville, D. H.; Vittal, J. J.; Yap, G. A. P., Synthesis, Structure, and Reactivity of Zirconium Alkyl Complexes Bearing Ancillary Pyridine Diamide Ligands. *Organometallics* **1998,** *17* (23), 5172-5177; (b) Guérin, F.; McConville, D. H.; Vittal, J. J., Synthesis, Structure, and Reactivity of Titanacyclopentadiene Complexes Bearing Ancillary Pyridine Diamide Ligands. *Organometallics* **1997,** *16* (7), 1491-1496; (c) Guérin, F.; McConville, D. H.; Vittal, J. J., Conformationally Rigid Diamide Complexes of Zirconium: Electron Deficient Analogues of Cp2Zr. *Organometallics* **1996,** *15* (26), 5586-5590.

# 6 Supporting Information

All NMR and XPS spectra and CIF files were collected in one supporting information file and was submitted to MSpace separately.